Oxygen Dependent Biocatalytic Processes

Pedersen, Asbjørn Toftgaard; Woodley, John; Krühne, Ulrich

Publication date:
2017

Document Version
Peer reviewed version

Oxygen Dependent Biocatalytic Processes

Asbjørn Toftgaard Pedersen

Ph.D. Thesis

July 2017

DTU Chemical Engineering
Department of Chemical and Biochemical Engineering

Abstract

Enzyme catalysts have the potential to improve both the process economics and the environmental profile of many oxidation reactions especially in the fine- and specialty-chemical industry, due to their exquisite ability to perform stereo-, regio- and chemo-selective oxidations at ambient temperature and pressure. A significant number of enzymes carrying out redox reactions (oxidoreductases) requiring molecular oxygen as an electron acceptor – those termed oxidases, monooxygenases and dioxygenases. These enzymes catalyze a range of industrially relevant reactions, such as oxidation of alcohols to aldehydes and ketones, oxyfunctionalization of C-H bonds, and epoxidation of C-C double bonds.

Although oxygen dependent biocatalysis offers many possibilities, there are numerous challenges to be overcome before an enzyme can be implemented in an industrial process. These challenges requires the combined effort of protein engineering (i.e. modification of the amino acids sequence to improve activity, stability and selectivity) and reaction engineering (i.e. modification of reaction conditions to increase the yield and productivity) to be solved. The most important reaction engineering challenge is the requirement for oxygen, because the transfer of oxygen from the gas-phase (typically air) to the aqueous phase, where the reaction takes place, is notoriously slow due to the low aqueous solubility of oxygen at ambient conditions. Therefore, vigorous agitation and aeration is required to create a large interfacial area for mass transfer, which is not only expensive but also sets a limit to the maximum productivity of the reactor. The oxygen transfer problem is further complicated by gas-liquid interface induced enzyme deactivation, large dependency of the catalytic rate on the oxygen concentration in solution and stripping of volatile organic compounds from the reaction mixture.

In this thesis, the supply of oxygen and the implications on the biocatalyst performance are studied. The important kinetics of the reaction between enzyme and oxygen are described in detail. In fact, it is found that most enzymes operate far below their potential maximum catalytic rate at industrially relevant oxygen concentrations. Detailed knowledge of the enzyme kinetics are therefore required in order to determine the best operating conditions and design oxygen supply to minimize processing costs. This is enabled by the development of the tube-in-tube reactor (TiTR) setup, capable of performing fully automated kinetic characterization of oxygen dependent enzymes - at oxygen concentrations allowing full saturation of the enzyme. The development of the TiTR enables us to characterize a range of enzyme variants developed through protein engineering. This not only exemplifies the importance of knowing the full enzyme kinetics when choosing an enzyme variant for further development, but also that it is in fact possible to change the oxygen reactivity of an enzyme through substitution of amino acid residues.

Resume

Enzymers evne til at katalysere bl.a. oxidationsreaktioner med en uovertruffen regio- stereo- og kemisk selektivitet ved lave temperaturer og tryk, gør dem i stand til potentielt at forbedre både økonomien og miljøprofilen for kemiske processer. En stor del af de enzymer der katalyserer redoxreaktioner (oxidoreduktaser) kræver molekylært oxygen som elektronacceptor – disse benævnes oxidaser, monooxygenaser, og dioxygenaser. Disse typer af enzymer katalyserer en lang række reaktioner med stort potentiale i den kemiske industri, eksempelvis oxidering af alkoholer til aldehyder og ketoner, selektiv hydroxylering, samt epoxidering af C-C dobbeltbindinger.

Oxygen krævende biokatalyse rummer mange muligheder, men der er også en række udfordringer der skal løses før et enzym kan implementeres i en industrielproces. For at løse disse udfordringer kræves en kombineret og koordineret indsats, for på den ene side af modificere enzymstrukturen så enzymet bliver mere aktivt, selektivt, og/eller stabilt, og på den anden side optimere procesbetingelserne for at opnå det maksimale udbytte samt den højeste mulige produktivitet. Den vigtigste procestekniske udfordring er at levere oxygen til reaktionen, da overførsel af oxygen fra en gasfase (typisk luft) til en vandigfase er notorisk langsom på grund af den lave opløselighed af oxygen i vand ved atmosfæriske betingelser. For at overføre tilstrækkeligt kræves derfor kraftig omrøring og beluftning for at generere et stort areal tilgængeligt for massetransport. Overførsel af oxygen er derfor ikke blot dyrt, men sætter også en begrænsning for den maksimale produktivitet der kan opnås i reaktoren. Problemet bliver yderligere kompliceret ved at mange enzymer bliver inaktiveret af gas-væske grænseflader, at den katalytiske hastighed typisk er næsten direkte proportional med oxygenkoncentrationen og at flygtige stoffer nemt strippes ud af reaktionsblandingen.

I denne afhandling bliver tilførslen af oxygen og dennes indflydelse på biokatalysatoren og reaktionen studeret i detaljer. Betydningen af kinetikken for enzymers reaktion med oxygen har længe været overset i den videnskabelige litteratur. Dette på trods af, at de fleste enzymer ved industrielle oxygenkoncentrationer opererer langt under deres maksimale katalytiske hastighed. Et detaljeret kendskab til enzymets kinetik er derfor nødvendigt for at bestemme de bedste reaktionsbetingelser og designe oxygenoverførsels metoder således at produktionsomkostningerne minimeres. Dette løses ved udviklingen af rør-i-rør reaktoren (TiTR), præsenteret i denne afhandling, der gør det muligt at bestemme enzymkinetik fuldt automatiseret og ved høje oxygenkoncentrationer så fuld mætning af enzymet forekommer. Udviklingen af TiTR gør det muligt for os at karakteriserer en række varianter af det samme enzym udviklet gennem proteinmodificering. Dette viser betydningen af at kende den fulde enzymkinetik når man udvælger den bedste variant, samt at det er muligt at ændre på oxygenreaktiviteten gennem ændringer i aminosyresekvensen.

Preface

This thesis was prepared at the Process and Systems Engineering Center (PROSYS), Department of Chemical and Biochemical Engineering, Technical University of Denmark in partial fulfillment of the requirements for a Ph.D. degree in Engineering. The work presented was performed in the period from April 2014 to July 2017, and was supervised by Professor John M. Woodley.

The work was partly funded by the Technical University of Denmark and the European Union's Seventh Framework Programme for Research and Innovation under Grant Agreement n^{o} 613849 supporting the project BIOOX. The European Project, and the project meetings around Europe, has led to many interesting scientific discussions and enabled several collaborations. A special thank you goes to Professor Nicholas Turner and Dr. William Birmingham at the University of Manchester, Professor Bernhard Hauer and Sara Hoffmann at the University of Stuttgart, and Dr. Michael Breuer at BASF SE.

I would like to thank my Supervisor and Mentor John for giving me the opportunity to work in a field of research I truly love and for his constant support and valuable input. In addition, I would like to thank Gustav for your always constructive inputs and being a great co-worker on BIOOX. Thank you all former and present colleagues at PROSYS for making the long days at DTU enjoyable. I would especially like to thank my office mates through the years (Rolf, Jason, Francesco, and Leander) and the members of the lunch club (Christian, Søren, Mafalda, Ricardo, Morten, Franz, and Ulrich), it has been a true pleasure.

Last, but not least, I am grateful to my girlfriend Signe and our son Lauge for their support and encouragements. Without you, I would never have succeeded.

Kgs. Lyngby, July 12th, 2017

Asbjørn Toftgaard Pedersen

Contents

Nomenclature

Roman letters

Bo	Bodenstein number	-
C_i	concentration	M
C_i^{sat}	concentration at saturation	M
d	diameter	m
D	diffusion coefficient	$m^2\ s^{-1}$
D	Taylor's dispersion coefficient	$m^2\ s^{-1}$
E'^0	standard electrode potential	V
emf	electromotive force	V
F	Farrydays' constant	$C\ mol^{-1}$
H	Henry's constant	Pa
I	ionic strength	M
k	rate constant	s^{-1}
k_{cat}/K_M	bimolecular rate constant or specificity constant	$s^{-1}\ M^{-1}$
k_d	deactivation rate constant	s^{-1}
K_{eq}	equilibrium constant	-
K_I	inhibition constant	M
k_La	volumetric mass transfer coefficient	h^{-1}
K_M	Michaelis constant	M
K_u	protein unfolding equilibrium constant	-
K_{vle}	vapor-liquid equilibrium constant	-
M_w	molecular weight	$g\ mol^{-1}$
n	number of electrons	-
OTR	oxygen transfer rate	$mol\ m^{-3}\ h^{-1}$
P	pressure	Pa
$\mathbf{P_i^{sat}}$	partial pressure at saturation	Pa
P/V	power input per reactor volume	$W\ m^{-3}$
q	volumetric flow rate	$m^3\ s^{-1}$
r	reaction rate	$mol\ L^{-1}\ s^{-1}$
R	ideal gas constant	$Pa\ m^3\ mol^{-1}\ K^{-1}$
t	time	s
T	temperature	K
$t_{½}$	protein half-life	s
T_b	boiling point	K
T_m	protein melting temperature	K
v	linear velocity	$m\ s^{-1}$
V	volume	m^3

v_s	superficial gas velocity	m s^{-1}
vvm	volume gas per volume reactor per minute	min^{-1}
x	liquid phase mol fraction	-
y	gas phase mol fraction	-
$Y_{x,atp}$	yield coefficient of biomass from ATP	-

Greek letters

α	slope of linear ramp	-
β	geometry parameter	-
ΔG_f	Gibbs free energy of formation	J mol^{-1}
ΔG_r	Gibbs free energy of reaction	J mol^{-1}
ΔG_u	Gibbs free energy of protein unfolding	J mol^{-1}
η_{enz}	enzyme utilization efficiency	-
λ	wavelength	nm
μ	viscosity	Pa s
ν	stoichiometric number of reactants	-
τ	residence time	s

Abbreviations

ABE	acetone-butanol-ethanol
ABTS	2,2’-azino-bis(3-ethylbenzothiazoline-6-sulfonic acid)
ATP	adenosine triphosphate
Atm	atmospheric pressure
B_{12}	vitamin B_{12}
BCA	bicinchoninic acid assay
CAPEX	capital expenditures
CFE	cell-free extract
CRISPR	clustered regularly interspaced short palindromic repeats
DFF	2,5-diformylfuran
DO	dissolved oxygen
DNA	deoxyribonucleic acid
EC	enzyme commission number
FFCA	5-formyl-2-carboxylic acid
GlyGly	diglycine
GOase	galactose oxidase
GOx	glucose oxidase
HMF	5-hydroxymethylfurfural
HRP	horseradish peroxidase
IR	infrared
ISPR	*in situ* product removal
MOPS	3-(N-morpholino)propanesulfonic acid

NADH	nicotinamide adenine dinucleotide
NaPi	sodium phosphate
NEM	N-ethylmorpholine
OPEX	operating expenditures
PCR	polymerase chain reaction
PDMS	polydimethylsilxoane
PLS	partial least square
PTFE	polytetrafluoroethylene
PTMSP	poly(1-trimethylsilyl-1-propyne)
SDS	sodium dodecyl sulfate
S.I.	supporting information
TiTR	tube-in-tube reactor
UV/Vis	ultraviolet/visible light

Chapter 1

Introduction

1.1 Background

The application of enzymes for catalyzing synthetically useful chemical reactions can potentially lead to reductions in energy consumption, hazardous waste generation, required reaction steps, as well as improvements in reaction yields and process economics. These advantages are realizable due to the exquisite regio-, stereo-, and chemoselectivity obtainable with a carefully selected or engineered enzyme catalyst and the possibility to obtain high catalytic rates even at ambient temperature and atmospheric pressure [1]. This has led to significant public and private investments in the development and implementation of biocatalysis for chemical synthesis.

Therefore, the field of biocatalysis is in continual development. Novel enzymes, and the reactions they catalyze, are constantly being identified in Nature, and through the application of protein engineering and directed evolution the activity, stability and selectivity is improved and changed to fit the conditions experienced in industrial chemistry, which typically are far from those experienced in natural environments [2,3]. The possibilities and development times are constantly improving, facilitated by the ever decreasing cost of DNA synthesis, novel genetic tools (e.g. CRISPR/Cas9), high-throughput screening methods, computational enzyme design, and expanding knowledge of structure-function relationship of enzymes. Today, it is even possible to engineer enzymes to catalyze reactions never experienced in nature [4], such as the recent examples of carbon-silicon bond formation using an engineered variant of cytochrome c (Figure 1.1A) and the construction of artificial metalloenzymes for e.g. cyclopropanation (Figure 1.1B). However, there are also vast possibilities for identifying novel enzymes in nature, such as the recent examples of a reductive aminase (Figure 1.1C) and an acyltranferase catalyzing the well known Friedel-Craft acylation (Figure 1.1D) (well known in conventional organic chemistry).

Despite the fact that biocatalysis has been applied in various forms for several decades and seem to offer endless possibilities, it is still not yet a standard tool for most organic and industrial chemists. This is most likely due to the substantial effort still required to find, develop, and/or engineer an enzyme to the extent that makes its use in an organic synthesis

meaningful and competitive. However, in recent years specialty enzyme producers have tried to change this by making large screening kits available at a low cost, thus enabling fast identification of a suitable enzyme for a given chemical transformation to avoid extensive protein and reaction engineering at a very early stage [9].

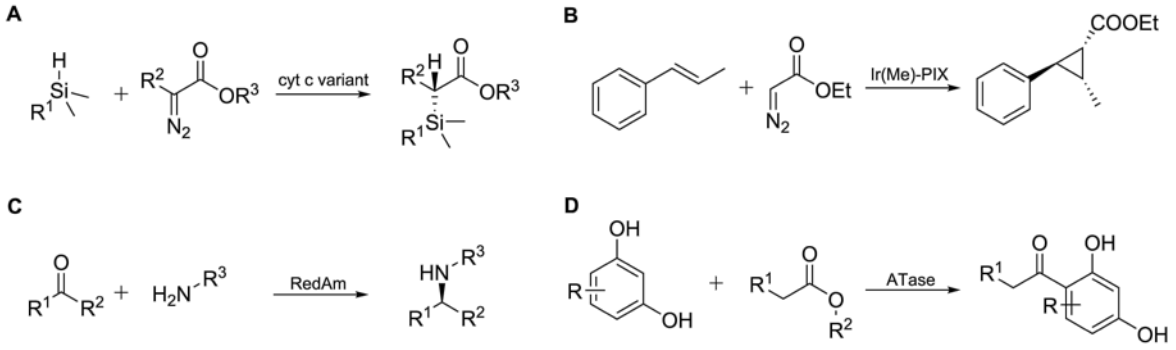

Figure 1.1. Recent examples of novel enzyme catalyzed reactions developed through protein engineering, insertion of a non-natural co-factor, or discovered in nature. A. Carbon-silicon bond formation not known to nature catalyzed by a cytochrome c (cyt c) variant [5]**. B. Cyclopropanation using myoglobin containing a non-natural iridium methyl phorphyrin IX (Ir(Me)-PIX) cofactor**[6]**. C. Newly discovered reductive aminase (RedAm) catalyzing the synthesis of chiral amines** [7]**. D. Recently reported acyltransferase (ATase) catalyzing the Friedel-Crafts acylation of phenols** [8]**.**

Despite the limited adoption by organic chemists, there are several hundred examples of successfully implemented biocatalytic processes, although most of the success stories are limited to the pharma- and specialty-chemical industries where the cost of product is one or two orders of magnitude above those found for the larger volume fine- and bulk-chemicals [10,11]. Thus, the most prominent examples of industrial application are found in the pharmaceutical industry, where especially stereoselective reduction of ketones using alcohol dehydrogenases and stereoselective amination using transaminase often have been used in commercial synthesis (Figure 1.2) [9,12]. However, there are also success stories for lower value, higher volume chemicals, such as the application of nitrile hydratase for the synthesis of acrylamide from acrylonitrile (Figure 1.2C), the production of biodiesel using lipase [13,14], and the isomerization of glucose to fructose using xylose isomerase for the production of high-fructose corn syrup [15]. Nevertheless, a broader implementation of biocatalysis for the production of bulk and fine chemicals has still not happened, despite many promises made by academics and companies developing enzymes. On the one hand, biocatalysis will never, and should never, completely replace homogenous and heterogeneous catalysis in the chemical industry, as there are many areas where traditional chemistry excel with high yields and productivities. On the other hand, as the chemical industry transforms towards increased integration of sustainable feedstocks, enzyme catalysis should obtain a more prominent industrial position in the endeavors to avoid complete decomposition of biomass (e.g. using gasification) to fit it into existing value chains, but rather selective modification of the already present chemical functionalities to fit the needs of consumer products. In either case, there are still significant efforts to be made to develop biocatalysts and biocatalytic processes

to fit the requirements of the modern chemical manufacturing in terms of yield, product concentration, and productivity.

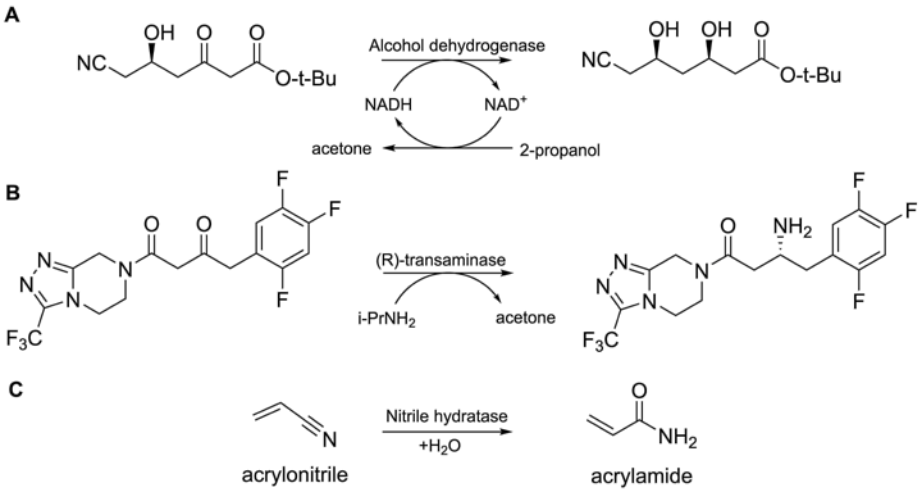

Figure 1.2. Examples of successfully implemented biocatalytic processes. A. Synthesis of a chiral alcohol intermediate in the production of atorvastatin (Lipitor®) developed by Pfizer [16]**. B. Synthesis of chiral amine in the last step of sitagliptin (Januvia®) synthesis developed by Merck/Codexis** [17]**. C. Bulk-scale (>650 kton/yr) biocatalytic production of acrylamide using immobilized nitrile hydratase developed by Mitsubishi Rayon.**

As academic biochemical engineers our job is to develop novel reaction and process engineering concepts to enable the broader adoption of biocatalysis in the chemical industry. This includes novel tools for characterizing enzymes, techniques to increase volumetric productivities, yields, and final product concentrations, and ways of dealing with difficult substrates and products, such as poorly water-soluble substrates or volatile products. Furthermore, we are required to develop the multitude of novel reactions and enzymes supplied by protein engineers to a stage and scale where industrial implementation is no longer a far-fetched dream, but actually realizable within the effort and timeframe possible in an industrial setting.

1.2 Oxygen dependent biocatalysis

Oxidation reactions are a very important chemical transformation in organic chemistry. In the bulk chemical industry oxidations are often carried out using molecular oxygen as the electron acceptor in efficient catalytic processes. However, in the synthesis of fine, specialty and pharma-chemicals the reactions are dominated by non-catalytic reactions requiring stoichiometric amount of oxidants and organic solvents, often halogenated. The reactions are seldom stereo-, regio-, or chemoselective thus leading to the requirement for multiple protection and deprotection steps, giving low reaction yields and generating vast amounts of chemical waste. Implementation of enzymes to perform oxidation reactions therefore represents a large potential for improving the yields, reducing the waste generation, and avoiding hazardous chemical transformations in industrial scale oxidation reactions.

Oxidation reactions are catalyzed by the class of enzymes named oxidoreductases (Enzyme Class 1). This class of enzymes includes a broad range of enzymes including dehydrogenases, oxidases, oxygenases, peroxidases and peroxygenases. Of those, dehydrogenases catalyze reductions and oxidations using cofactors, such as NADH, as electron donors/acceptors, peroxidases and peroxygenases use hydrogen peroxide as the electron acceptor, while oxidases and oxygenases accept molecular oxygen as the electron acceptor. The work presented in this thesis focuses on enzymes requiring molecular oxygen as a substrate because these represent a diverse set of enzymes catalyzing many industrially relevant reactions, while sharing a range of reaction and process engineering challenges.

Oxygen dependent enzymes catalyze many chemical transformations useful in organic chemistry, such as the selective oxidation of primary and secondary alcohols to aldehydes and ketones by alcohol oxidases, the oxidation of amines to imines by amine oxidases, oxyfunctionalization of non-activated C-H bonds by cytochrome P450 monooxygenases, epoxidation of double bonds by monooxygenases, among others. Figure 1.3 lists a range of example reactions catalyzed by oxygen dependent enzymes.

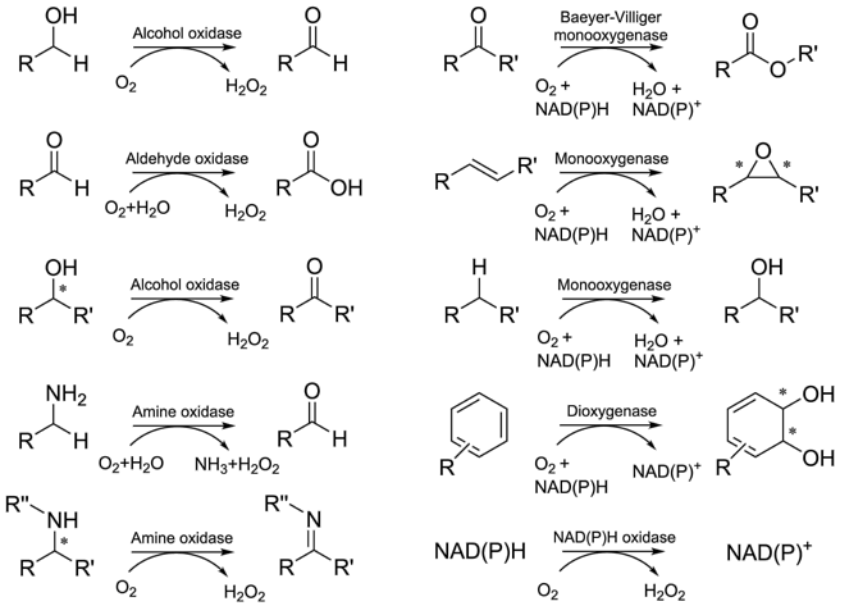

Figure 1.3. Examples of enzyme catalysed reactions requiring molecular oxygen.

The oxidation of alcohols to aldehydes and ketones represents an important application of biocatalytic oxidation reactions in particularly for production of flavors and fragrances, as carbonyl compounds are an essential part of many pleasant scents and tastes. Examples include benzaldehyde (bitter almond), cinnamaldehyde (cinnamon), octanal (citrus), 2-heptanone (banana), ionones (rose), and vanillin (vanilla) [18,19]. Furthermore, carbonyl compounds may act as pheromones useful to influence insect behavior, or they may be further functionalized, e.g. using transaminase or aldolase, and thus acts as intermediates in larger synthetic routes e.g. for pharmaceuticals or in the selective modification of naturally occurring polymers [20–22]. The oxyfunctionalizations possible with mono- and dioxygenases represent a particularly interesting route to chiral alcohols, especially since hydroxylation of

non-activated C-H bonds is something today not possible with traditional organic chemistry without oxidizing many more functional groups than intended. Selective hydroxylation could open-up for completely new synthetic routes and products, such as α,ω-functionalized fatty acid for the synthesis of novel performance polymers and musk scents [23–25]. Enzymes selectively oxidizing one stereoisomer (such as alcohol or amine oxidases) are also often applied in deracemization reactions together with a reducing enzyme or chemical reductant [26].

In general, oxidoreductases are amongst the most widely applied enzymes in industrial chemistry [27]. However, it is primarily dehydrogenases applied for the stereoselective reduction of ketones to chiral secondary alcohols, as previously mentioned [28,29]. Oxygen dependent enzymes are in general not as widely applied, although there are some examples such as the application of amino acid oxidase for deracemization of an amino acid in the synthesis of an antidiabetic, and the oxidation of lactose to lactobionic acid that is used as a food additive (Figure 1.4). Other examples also exist, however, these are often naturally occurring microbes, e.g. carrying out a hydroxylation, where the active enzyme(s) is not necessarily known or applications where the oxidative enzymes, e.g. a cytrochrome P450 monooxygenase, are parts of entire recombinant pathways, such as in the synthesis of the malaria drug Artemisinin from glucose [30].

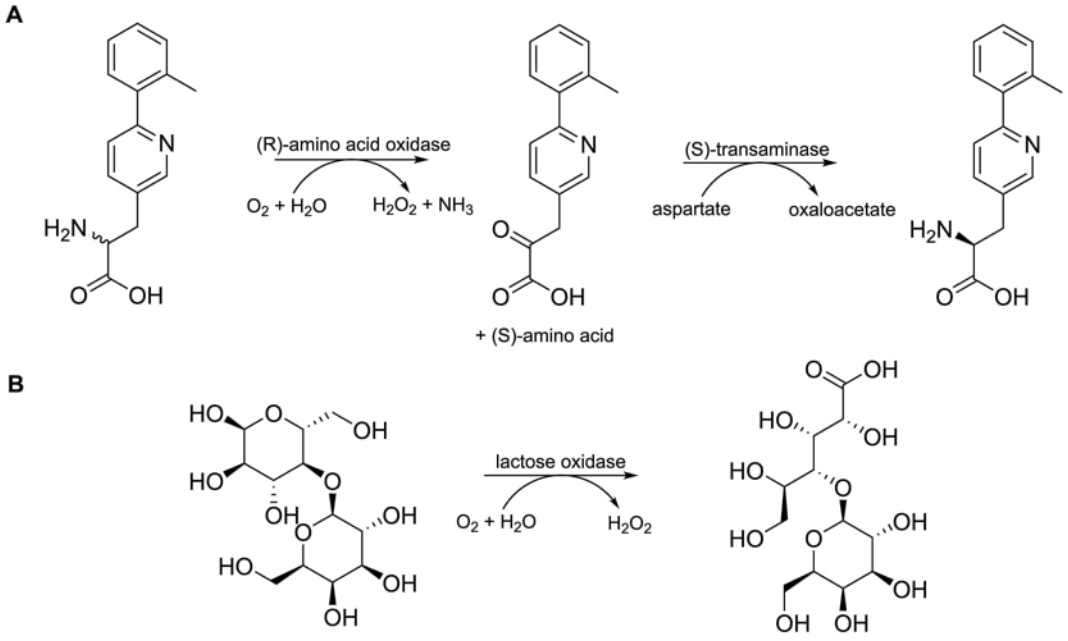

Figure 1.4. Examples of oxygen dependent enzymes applied in industrial scale synthesis. A. Deracemization of racemic amino acid using (R)-amino acid oxidase applied in the synthesis of an antidiabetic drug by Bristol-Myers Squibb [31]**. B. Oxidation of lactose to lactobionic acid that are used as a food additive** [32]**.**

The lacking implementation of oxygen dependent enzymes for industrial chemistry could well be caused by the unique challenges when developing oxygen dependent enzyme processes. The challenges include the ability to supply of oxygen to the reaction without dam-

aging enzymes unstable in the presence of gas-liquid interfaces or stripping out volatile products, and the low solubility of oxygen in water often causing enzymes to be limited by the amount of oxygen available. In this thesis, some of the challenges for oxygen dependent enzymes will be addressed and possible solutions presented.

1.2.1 Studied enzyme systems

The work that has led to the results presented in this thesis has been focused on the application of two oxygen dependent enzymes, the carbohydrate oxidases: glucose oxidase and galactose oxidase. The two enzymes are briefly described below.

Glucose oxidase

Glucose oxidase (EC 1.1.3.4, GOx) is a flavin-dependent oxidase that in Nature catalyzes the oxidation of glucose to gluconolactone, that spontaneously hydrolyse to gluconic acid, while reducing molecular oxygen to hydrogen peroxide (Figure 1.5). The synthetic potential of GOx is limited, although the enzyme is widely used as a technical enzyme in the food industry and for glucose sensors [33]. Nevertheless, GOx is a very useful enzyme as a model system in the development of reaction engineering concepts for oxygen dependent enzymes, because the enzyme is well characterized, reasonably stable, and does not experience product inhibition due to the spontaneous hydrolysis of the product [34]. However, the production of acids necessitate pH control via titration or by the addition of buffer.

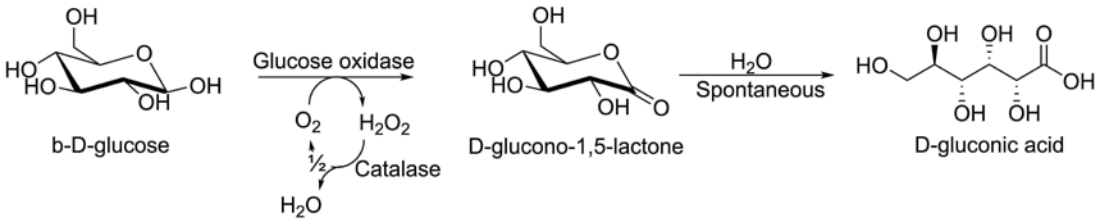

Figure 1.5. The oxidation of glucose to glucono-1,5-lactone by glucose oxidase. The lactone spontaneous hydrolyze to the acid at neutral and alkaline pH.

Galactose oxidase

Galactose oxidase (EC 1.1.3.9, GOase) is a copper containing oxidase that in nature catalyzes the oxidation of the C6-OH of galactose to the corresponding aldehyde. The two-electron oxidation by GOase relies on a remarkable tyrosine radical in the active site, which has been the topic of many scientific publications since its discovery [35,36]. Besides the natural reaction, GOase can catalyze the oxidation of a range of primary alcohols such as benzyl alcohol and dihydroxyacetone [35,37]. A recent reported alcohol oxidase, very closely related to GOase, has expanded the natural substrate scope to various linear aliphatic primary alcohols, such as 1-hexanol and 1-heptanol, and diols, such as 1,3-propanediol [38]. Furthermore, the substrate specificity of GOase has successfully been changed through protein engineering to accommodate the oxidation of other primary alcohols such as other mono-saccharides and aryl alcohols [39–43]. Interestingly, GOase has also been engineered to stereoselectively oxidize secondary aryl alcohols, such as 1-phenylethanol, thus allowing its use in deracemization reactions [42].

In the work presented in this thesis, GOase is used for the oxidation of two primary alcohols, benzyl alcohol and 5-hydroxymethylfurfural (HMF) (Figure 1.6). The oxidation of benzyl alcohol to benzaldehyde is used as a model system for the investigation of the potential reaction and process engineering challenges experienced when applying GOase as an industrial biocatalyst (Chapter 6). Benzaldehyde in itself has little commercial value, but the reaction serves the purpose of having many of the challenges experienced by commercially more relevant reactions. The second reaction, the oxidation of HMF to 2,5-diformylfuran (DFF) is of commercial interest, as HMF is considered a future biomass-derived platform chemical and DFF a potential starting material for the synthesis of monomers [44,45]. This reaction is used for studying the effect of mutations on the reactivity of GOase with oxygen (Chapter 7).

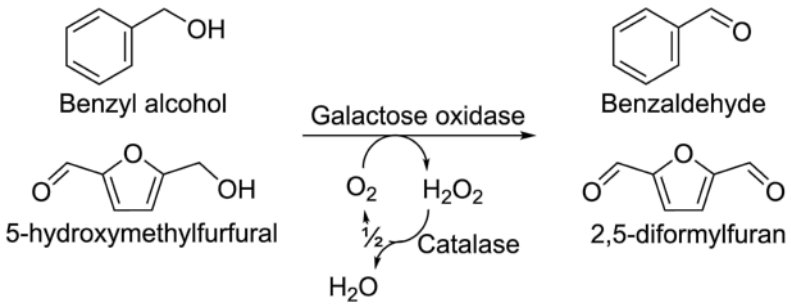

Figure 1.6. Galactose oxidase catalyzed oxidation of benzyl alcohol and 5-hydroxymethylfurfural to the respective aldehydes.

1.3 Scope

The overall aim of this research project was to develop and apply reactions engineering principles to biocatalytic oxidation reactions in order to advance their implementation, especially in the fine- and specialty-chemical industries and to demonstrate the potential of biocatalytic oxidations beyond the test-tube. A large part of this thesis was focused on studying the influence of the concentration of oxygen in solution on a biocatalytic process. This was studied both from the perspective of supplying oxygen to the reaction and from the perspective of the enzyme that in many cases requires a remarkably high concentration to function at the highest possible catalytic rates. The latter, lead to the endeavor to develop a new method for measuring enzyme kinetics of oxygen dependent enzymes as this turned out to be extremely time and material consuming using existing techniques. Finally, the reaction engineering challenges of an example biocatalytic oxidation system were studied and addressed.

1.4 Thesis outline

The thesis consists of ten chapters briefly outlines below:

Chapter 1 gives an introduction to industrial biocatalysis in general and oxygen dependent biocatalysis in particular

Chapter 2 describes the reaction and process engineering challenges specific to oxygen dependent enzyme catalysis.

Chapter 3 presents a techno-economic comparison of oxygen supply methods relevant to oxidative biocatalysis

Chapter 4 discusses the importance of the Michaelis constant for oxygen when developing and optimizing oxygen dependent enzyme processes.

Chapter 5 describes the development and validation of a microfluidic tool enabling fast and autonomous kinetic characterization of oxygen dependent enzymes. This chapter is based on Paper I.

Chapter 6 describes the process challenges involved in galactose oxidase catalyzed oxidation of alcohols. The chapter focus on the oxidation of benzyl alcohol to benzaldehyde. This chapter is based on Paper III.

Chapter 7 illustrates how the tool can be applied to identify galactose oxidase variants with increased oxygen reactivity

Chapter 8 provides a general discussion of the most important findings presented in the thesis

Chapter 9 concludes the thesis while Chapter 10 gives directions for future research objectives and developments.

1.5 Scientific publications

1.5.1 Publications included in thesis

The following three accepted scientific publications have resulted from the work conducted during the Ph.D. studies. Published manuscripts are provided in Appendix A.

Paper I: Ringborg RH*, **Toftgaard Pedersen A***, Woodley JM. 2017. Automated determination of oxygen-dependent enzyme kinetics in a tube-in-tube flow reactor, ChemCatChem, Accepted, DOI: 10.1002/cctc.201700811

*These authors contributed equally to this work

Paper II: **Toftgaard Pedersen A**, de Carvalho TM, Sutherland E, Rehn G, Ashe R, Woodley JM. 2017. Characterization of a Continuous Agitated Cell Reactor for Oxygen Dependent Biocatalysis, Biotechnology and Bioengineering 114(6):1222-1230

Paper III: **Toftgaard Pedersen A**, Birmingham WR, Rehn G, Charnock SJ, Turner NJ, Woodley JM. 2015. Process Requirements of Galactose Oxidase Catalyzed Oxidation of Alcohols, Organic Process Research and Development 19(11):1580-1589

1.5.2 Other publications

The following accepted scientific publication and conference article have also resulted from the work performed during the Ph.D. studies, but are not included as part of this thesis.

Rehn G, **Toftgaard Pedersen A**, Woodley JM. 2016. Application of NAD(P)H oxidase for cofactor regeneration in dehydrogenase catalyzed oxidations, Journal of Molecular Catalysis B: Enzymatic 134:331-339

Toftgaard Pedersen A, Rehn G, Woodley JM. 2015. Oxygen transfer rates and requirements in oxidative biocatalysis, Computer Aided Chemical Engineering 37:2111-2116

1.6 Reference

[1] Woodley JM, **2008**. New opportunities for biocatalysis: making pharmaceutical processes greener, Trends Biotechnol. 26(6):321–327.

[2] Bommarius AS, **2015**. Biocatalysis: A Status Report, Annu. Rev. Chem. Biomol. Eng. 6(1):319–345.

[3] Bommarius AS, Blum JK, Abrahamson MJ, **2011**. Status of protein engineering for biocatalysts: How to design an industrially useful biocatalyst, Curr. Opin. Chem. Biol. 15(2):194–200.

[4] Hammer SC, Knight AM, Arnold FH, **2017**. Design and Evolution of Enzymes for Non-natural Chemistry, Curr. Opin. Green Sustain. Chem. 10.1016/j.ppees.2016.11.003.

[5] Kan SBJ, Lewis RD, Chen K, Arnold FH, **2016**. Directed evolution of cytochrome c for carbon–silicon bond formation: Bringing silicon to life, Science. 354(6315):1048–1051.

[6] Key HM, Dydio P, Clark DS, Hartwig JF, **2016**. Abiological catalysis by artificial haem proteins containing noble metals in place of iron, Nature. 534(7608):534–537.

[7] Aleku GA, France SP, Man H, Mangas-Sanchez J, Montgomery SL, Sharma M, Leipold F, Hussain S, Grogan G, Turner NJ, **2017**. A reductive aminase from Aspergillus oryzae, Nat. Chem. :

[8] Schmidt NG, Pavkov-keller T, Richter N, Wiltschi B, Gruber K, Kroutil W, **2017**. Biocatalytic Friedel–Crafts Acylation and Fries Reaction, Angew. Chem. Int. Ed. 201703270:7615–7619.

[9] Reetz MT, **2013**. Biocatalysis in organic chemistry and biotechnology: Past, present, and future, J. Am. Chem. Soc. 135(34):12480–12496.

[10] Choi J-M, Han S-S, Kim H-S, **2015**. Industrial applications of enzyme biocatalysis: Current status and future aspects, Biotechnol. Adv. 33:1443–1454.

[11] Gröger H, Asano Y, Bornscheuer UT, Ogawa J, **2012**. Development of biocatalytic processes in japan and germany: From research synergies to industrial applications, Chem. - An Asian J. 7(6):1138–1153.

[12] Bornscheuer UT, Huisman GW, Kazlauskas RJ, Lutz S, Moore JC, Robins K, **2012**. Engineering the third wave of biocatalysis, Nature. 485(7397):185–94.

[13] Nielsen PM, Brask J, Fjerbaek L, **2008**. Enzymatic biodiesel production: Technical and economical considerations, Eur. J. Lipid Sci. Technol. 110(8):692–700.

[14] Toftgaard Pedersen A, Nordblad M, Nielsen PM, Woodley JM, **2014**. Batch production of FAEE-biodiesel using a liquid lipase formulation, J. Mol. Catal. B Enzym. 105:89–94.

[15] Pedersen S, Industrial Aspects of Immobilized Glucose Isomerase, in: Ind. Appl. Immobil. Biocatal., **1993**, Marcel dekker, INC., New York: pp. 185–208.

[16] Sutton PW, Adams JP, Archer I, Auriol D, Avi M, Branneby C, Collis AJ, Dumas B,

Eckrich T, Fotheringham I, ter Halle R, Hanlon S, Hansen M, Holt-Tiffin KE, Howard RM, Huisman GW, Iding H, Kiewel K, Kittelmann M, et al., Biocatalysis in the Fine Chemical and Pharmaceutical Industries, in: J. Whittall, P.W. Sutton (Eds.), Pract. Methods Biocatal. Biotransformations 2, **2012**, John Wiley & Sons, Ltd., New York: pp. 1–59.

[17] Savile CK, Janey JM, Mundorff EC, Moore JC, Tam S, Jarvis WR, Colbeck JC, Krebber A, Fleitz FJ, Brands J, Devine PN, Huisman GW, Hughes GJ, **2010**. Biocatalytic asymmetric synthesis of chiral amines from ketones applied to sitagliptin manufacture., Science. 329(5989):305–9.

[18] Berger RG, **2009**. Biotechnology of flavours-the next generation, Biotechnol. Lett. 31(11):1651–1659.

[19] Berger RG, **2015**. Biotechnology as a source of natural volatile flavours, Curr. Opin. Food Sci. 1:38–43.

[20] Kunjapur AM, Prather KLJ, **2015**. Microbial engineering for aldehyde synthesis, Appl. Environ. Microbiol. 81(6):1892–1901.

[21] Mikkonen KS, Parikka K, Suuronen J-P, Ghafar A, Serimaa R, Tenkanen M, **2014**. Enzymatic oxidation as a potential new route to produce polysaccharide aerogels., RSC Adv. 4(23):11884–11892.

[22] Liu XC, Dordick JS, **1999**. Sugar-containing polyamines prepared using galactose oxidase coupled with chemical reduction, J. Am. Chem. Soc. 121(2):466–467.

[23] Liu C, Liu F, Cai J, Xie W, Long TE, Turner SR, Lyons A, Gross RA, **2011**. Polymers from fatty acids: poly(ω-hydroxyl tetradecanoic acid) synthesis and physico-mechanical studies., Biomacromolecules. 12(9):3291–8.

[24] Huf S, Krügener S, Hirth T, Rupp S, Zibek S, **2011**. Biotechnological synthesis of long-chain dicarboxylic acids as building blocks for polymers, Eur. J. Lipid Sci. Technol. 113(5):548–561.

[25] Schaffer S, Haas T, **2014**. Biocatalytic and fermentative production of alpha,omega-bifunctional polymer precursors, Org. Process Res. Dev. 18:752–766.

[26] Wohlgemuth R, **2010**. Asymmetric biocatalysis with microbial enzymes and cells, Curr. Opin. Microbiol. 13(3):283–292.

[27] Straathof A, Panke S, Schmid A, **2002**. The production of fine chemicals by biotransformations, Curr. Opin. Biotechnol. :548–556.

[28] Moore JC, Pollard DJ, Kosjek B, Devine PN, **2007**. Advances in the Enzymatic Reduction of Ketones Background : Whole Cell Bioreductions, Acc. Chem. Res. 40(12):1412–1419.

[29] De Wildeman SMA, Sonke T, Schoemaker HE, May O, **2007**. Biocatalytic reductions: From lab curiosity to “first choice,” Acc. Chem. Res. 40(12):1260–1266.

[30] Paddon CJ, Westfall PJ, Pitera DJ, Benjamin K, Fisher K, McPhee D, Leavell MD, Tai A, Main A, Eng D, Polichuk DR, Teoh KH, Reed DW, Treynor T, Lenihan J, Jiang H, Fleck M, Bajad S, Dang G, et al., **2013**. High-level semi-synthetic production

of the potent antimalarial artemisinin, Nature. 496(7446):528–532.

[31] Chen Y, Goldberg SL, Hanson RL, Parker WL, Gill I, Tully TP, Montana MA, Goswami A, Patel RN, **2011**. Enzymatic preparation of an (S)-amino acid from a racemic amino acid, Org. Process Res. Dev. 15(1):241–248.

[32] Hua L, Nordkvist M, Nielsen PM, Villadsen J, **2007**. Scale-up of enzymatic production of lactobionic acid using the rotary jet head system, Biotechnol. Bioeng. 97(4):842–849.

[33] Wong CM, Wong KH, Chen XD, **2008**. Glucose oxidase: Natural occurrence, function, properties and industrial applications, Appl. Microbiol. Biotechnol. 78(6):927–938.

[34] Gibson QH, Swoboda BEP, Massey V, **1964**. Kinetics and Mechanism of Action of Glucose Oxidase, J. Biol. Chem. 239(11):3927–3934.

[35] Whittaker MM, Whittaker JW, **2001**. Catalytic reaction profile for alcohol oxidation by galactose oxidase, Biochemistry. 40(24):7140–7148.

[36] Lee Y-K, Whittaker MM, Whittaker JW, **2008**. The Electronic Structure of the Cys-Tyr• Free Radical in Galactose Oxidase Determined by EPR Spectroscopy., Biochemistry. 47(25):6637–6649.

[37] Siebum A, van Wijk A, Schoevaart R, Kieboom T, **2006**. Galactose oxidase and alcohol oxidase: Scope and limitations for the enzymatic synthesis of aldehydes, J. Mol. Catal. B Enzym. 41(3–4):141–145.

[38] Yin DT, Urresti S, Lafond M, Johnston EM, Derikvand F, Ciano L, Berrin J-G, Henrissat B, Walton PH, Davies GJ, Brumer H, **2015**. Structure-function characterization reveals new catalytic diversity in the galactose oxidase and glyoxal oxidase family, Nat. Commun. 6:10197.

[39] Deacon SE, Mahmoud K, Spooner RK, Firbank SJ, Knowles PF, Phillips SE V, McPherson MJ, **2004**. Enhanced fructose oxidase activity in a galactose oxidase variant, ChemBioChem. 5(7):972–979.

[40] Sun L, Bulter T, Alcalde M, Petrounia IP, Arnold FH, **2002**. Modification of galactose oxidase to introduce glucose 6-oxidase activity, ChemBioChem. 3(8):781–783.

[41] Staniland S, Yuan B, Gimenez-Agullo N, Marcelli T, Willies SC, Grainger DM, Turner NJ, Clayden J, **2014**. Enzymatic Desymmetrising Redox Reactions for the Asymmetric Synthesis of Biaryl Atropisomers., Chem. - A Eur. J. 20(41):13084–13088.

[42] Escalettes F, Turner NJ, **2008**. Directed evolution of galactose oxidase: generation of enantioselective secondary alcohol oxidases, ChemBioChem. 9(6):857–60.

[43] Sun L, Petrounia IP, Yagasaki M, Bandara G, Arnold FH, **2001**. Expression and stabilization of galactose oxidase in Escherichia coli by directed evolution, Protein Eng. 14(9):699–704.

[44] Xiang T, Liu X, Yi P, Guo M, Chen Y, Wesdemiotis C, Xu J, Pang Y, **2013**. Schiff base polymers derived from 2,5-diformylfuran, Polym. Int. 62(10):1517–1523.

[45] Qin Y-Z, Li Y-M, Zong M-H, Wu H, Li N, **2015**. Enzyme-catalyzed selective oxidation of 5-hydroxymethylfurfural (HMF) and separation of HMF and 2,5-diformylfuran using deep eutectic solvents, Green Chem. 17(7):3718–3722.

Chapter 2

Reaction engineering aspects of oxygen dependent biocatalysis

2.1 Introduction

A multitude of reaction and process challenges arise when transferring biocatalytic reactions from the test tube through bench and pilot scale to industrial scale reactors. Typically, these challenges are very different from those experienced with 'traditional' chemistry, because of the inherent differences, since biocatalysis is conducted at ambient temperatures, at atmospheric pressures and at dilute concentrations compared to those typically experienced in organic chemistry. Therefore, an entire new reaction engineering toolbox is required to develop industrial scale biocatalytic processes, although the physical phenomena governing the reactions are the same. Scientists have been developing and expanding this toolbox during the last 50-60 years and applying it to a range of different reactions with industrial success. In the following chapter, the aspects of biocatalytic reaction engineering relevant to biocatalytic oxidations will be presented and discussed.

Although, some believe protein engineering solves most, if not all, weaknesses of biocatalysis [1], it will never solve inherent thermodynamic limitations of a reaction system, such as an unfavorable chemical equilibrium, poor solubility of oxygen in water, and evaporation of volatile compounds. Furthermore, we believe reaction and process engineering can present solutions that could make further expensive (and slow) protein optimization obsolete once the enzyme has reached certain thresholds for activity and stability. This includes methods of removing an inhibitory product or ways of increasing the oxygen concentration in solution to improve the performance of an oxygen dependent enzyme. All in all, process and protein engineering go hand-in-hand when developing a biocatalytic process and close interaction between the two disciplines is required to reduce the development time and cost.

2.2 Biocatalyst format

Enzymes are produced by fermentation of microorganisms overexpressing a gene encoding for the desired protein, after which the enzymes are purified and formulated to an extent suitable for the intended application. For synthetic purposes, the three primary biocatalyst

formats are free, soluble enzymes (or permeabilized whole cells), immobilized enzymes, and metabolically active whole-cells (either resting or growing). The preferred biocatalyst format depends on the stability of enzyme, the requirement to co-factors, the ability of substrates to cross the cell membrane, among others [2]. If applying an enzyme that is stable outside the cell environment that does not require cofactors difficult to regenerate, free enzymes (or permeabilized whole cells to save on purification) are preferred. In some cases, enzymes immobilized on porous carriers, or by cross-linking, will be beneficial, this is especially relevant for very stable enzymes because this allows easy recycling of the catalyst [3]. However, there are also downsides such as increased cost and lower specific activity [4,5]. Whole-cell biocatalysts are primarily applied when free or immobilized are not possible, most often because of poor enzyme stability outside the cell or because the enzyme requires a cofactor/co-substrate not easily recycled without the cell machinery, such as ATP or B_{12}. Although whole-cells are cheaper than free enzyme due to simpler purification, they add complexity to the process because they require a carbon source (and nitrogen source for growing whole-cells) from which energy for the cell machinery is produced, and potentially a range of by-products (mainly organic acids) that can complicate downstream processing. Thus, in general, whole-cell biocatalysts are cheaper upstream but are more expensive downstream and vice versa for free enzymes.

For oxygen dependent biocatalysis, both whole-cells and free enzymes are widely applied. Whereas, only few examples of immobilized enzymes for synthetic application are reported in the scientific literature [6–9]. This is mainly because immobilized enzymes adds a third phase to the air/liquid reaction system of oxygen dependent enzymes, thus further complicating efficient oxygen transfer to the active site. Although whole-cells are widely applied for oxygen dependent biocatalysis, especially for many mono- and dioxygenases [10,11], it is not a focus of this thesis. The remainder of the chapter will therefore be focused on free enzymes. Nevertheless, a section will highlight the main differences when working with whole-cell systems.

2.3 Biocatalytic process metrics

In early stage bioprocess development, it is often advantageous to have a set of key process metrics and target values to evaluate the feasibility of industrial implementation [12–14]. Although useful, these target values should be applied with care, if a detailed economic assessment of the process has not been performed, because the values will change significantly from reaction to reaction, from product to product, and from enzyme to enzyme. Table 2.1 gives an overview of typical metrics for a process employing a free enzyme and one employing a whole-cell system. The two sets of metrics are based on a reaction in a fine chemical process. The requirements to the biocatalyst yield of a whole-cell process is lower primarily because whole-cells are cheaper to produce on a basis of biocatalyst weight. The difference between the numbers stemming from the protein expression level, for which 12.5% (w/w) of the total dry cell weight is reasonable for an optimized expression system [5,13]. Furthermore, the values for the whole-cell system is taken for a cytochrome P450 process, which typically performs chemistry very difficult to do using existing methods, and

thus the reaction represent a greater value because many synthetic steps can be circumvented by applying the enzyme catalyzed reaction. In any case, the values help to put discussions of process performance into perspective.

Table 2.1. Target process metrics for a typical free enzyme and whole-cell system for the production of a fine chemical.

Metric	Free enzyme system[a]	Whole-cell system[b]
Volumetric productivity [$g_{product}$ L^{-1} h^{-1}]	20-40	2
Product concentration [$g_{product}$ L^{-1}]	100-200[c]	20[c]
Biocatalyst yield [$g_{product}$ $(g_{biocatalyst})^{-1}$]	10^2-10^3	10
Reaction yield [mol mol^{-1}]	>90%	>90%

[a] Adapted from [14], values are based on crude enzyme. [b] Adapted from [13] for a cytochrome P450 process. [c] The difference is not representative for all free and whole-cell processes, as the whole-cell process used here represent a particularly difficult and valuable transformation. For a directly comparable reaction, the required product concentration would be the same, as it determines the downstream processing costs.

2.4 Thermodynamic equilibrium

An unfavorable thermodynamic equilibrium is a problem often encountered in chemical synthesis in general, and also in many industrially relevant biocatalytic transformations, e.g. the transamination between an amine and a carbonyl catalyzed by transaminase [15]. The equilibrium of a reaction is determined by the thermodynamic properties of the reaction species and the reaction conditions. Therefore, process constraints caused by reaction equilibrium cannot be solved using protein engineering, but have to be alleviated using process and reaction engineering tools. This could be shifting an unfavorable equilibrium by removing a reaction product using *in situ* product removal [16,17].

For redox reactions, the reaction equilibrium is most easily accessed by considering the reduction potential of the individual half reactions, as the feasibility of a reaction comprising two half reactions easily can be calculated. The reduction potentials, and the Gibbs free energies, are for biochemical reactions often calculated at 'standard biological conditions' meaning that all reactants are at standard conditions ([reactants] = 1 M, T = 298 K) except for the pH which is at 7 ($[H^+] = 10^{-7}$). Also, in biochemical thermodynamics reactants that are present in different ionic forms are considered one species, e.g. phosphate which will be a mix of ionic species depending of pH. These facts are very important when obtaining and comparing thermodynamic data from different tables [18]. The standard electrode potential and its relation to the Gibbs free energy of formation is given by Eq. 2.1:

$$E'^0 = \frac{-\sum \nu_i' \Delta G_{f,i}'^0}{nF} \qquad \text{Eq. 2.1}$$

Where ν_i' is the stoichiometric numbers of reactants, F is the Faraday constant (96485 C mol^{-1}), and n is the number of electrons involved in the half-reaction.

Based on the reduction potential of the half reactions the *electromotive force, emf*, can be calculated (Eq. 2.2). The emf is a direct measure of the ability of a reaction to happen (at standard conditions), if it is positive the forward reaction will be favorable, and vice versa.

The Gibbs free energy of reaction can be calculated from the emf using Nernst equation (Eq. 2.3), from which the apparent equilibrium constant (K'_{eq}) follows (Eq. 2.4):

$$emf = E'^{0}_{f} - E'^{0}_{b} \quad \text{Eq. 2.2}$$

$$-\Delta G'^{0}_{r} = nF\ emf \quad \text{Eq. 2.3}$$

$$\Delta G'_{r} = \Delta G'^{0}_{r} + RTln\left(K'_{eq}\right) = 0 \quad \text{Eq. 2.4}$$

Where E'^{0}_{f} and E'^{0}_{b} refers to the 'forward' and 'backwards' reduction reactions, 'backwards' reaction referring to the half reaction for the substrate being oxidized. R is the ideal gas constant and T is the temperature.

Table 2.2 gives an overview of the reduction potentials of various half-reactions relevant to oxidative biocatalysis. In general, aldehydes display negative reduction potentials and therefore the corresponding alcohols readily undergoes oxidation (from a thermodynamic perspective). In cases where the reduction potential is close to zero or positive, the large reduction potentials of oxygen reduction to hydrogen peroxide or water drives the reaction.

Table 2.2. Reduction potentials of various relevant redox reactions. The reduction potentials were calculated from $\Delta G'^{0}_{r}$ for the individual half reactions.

Reductive half-reaction	**E'^{0} vs. NHE, pH 7, 25 °C, I=0 M**	**Reference**
Reduction of oxygen		
$O_2 + 2e^- + 2H^+ \rightarrow H_2O_2$	+281 mV	[19]
$O_2 + 4e^- + 4H^+ \rightarrow 2\ H_2O$	+815 mV	[19]
Reduction of aldehydes and ketones		
Acetaldehyde + $2e^- + 2H^+ \rightarrow$ ethanol	-193 mV	[20]
Acetone + $2e^- + 2H^+ \rightarrow$ 2-propanol	-282 mV	[20]
Butanal + $2e^- + 2H^+ \rightarrow$ 1-butanol	-197 mV	[20]
Benzaldehyde + $2e^- + 2H^+ \rightarrow$ Benzyl alcohol	-218 mV	[21] *Estimated*
Dihydroxyacetone + 2e- + 2H+ → glycerol	-180 mV	[20]
Glucono-1,5-lactone + $2e^- + 2H^+ \rightarrow$ glucose	-363 mV	[20]
Xylulose + $2e^- + 2H^+ \rightarrow$ xylose	+22.5 mV	[20]
Reduction of alcohols		
Methanol + $2e^- + 2H^+ \rightarrow$ methane + H_2O	+84.5 mV	[20]
Reduction of co-factors		
$NAD^+ + 2e^- + H^+ \rightarrow$ NADH	-324 mV	[20]
$NADP^+ + 2e^- + H^+ \rightarrow$ NADPH	-342 mV	[20]

From the reduction potentials, it is clear that oxidation reactions using oxygen as electron acceptor is very favorable. As an example, the emf for the oxidation of glucose to gluconо-1,5-lactone (catalyzed by glucose oxidase) is 644 mV, corresponding to an apparent equilibrium constant of $5.8 \cdot 10^{21}$. In other words, the oxidation will in practice be unidirectional.

Monooxygenase reactions that besides oxygen also requires reduced co-factor, typically in the form of NAD(P)H, is an interesting case because the total reaction in principal can be divided into three half reactions (in reality it is more likely two half reactions, each a mix of the three stated below [22]). An example is the oxidation of methane to methanol by methane monooxygenase, which constitutes of the following three half-reactions. Despite the positive potential of the methanol reduction, there are plenty of free energy released in the reduction of oxygen and oxidation of NADPH to drive the reaction:

$$CH_4 + H_2O \rightarrow CH_3OH + 2e^- + 2H^+$$
$$NADPH \rightarrow NADP^+ + H^+ + 2e^-$$
$$O_2 + 4H^+ + 4e^- \rightarrow 2H_2O$$
$$CH_4 + NADPH + O_2 + H+ \rightarrow CH_3OH + NADP^+ + H_2O \qquad emf = 944\ mV$$

It is clear from the above analysis that the equilibrium of oxygen dependent oxidation reactions are not an issue requiring attention when developing processes, the equilibrium will be fully displaced towards the products. However, this does not mean that the reactions proceed instantaneously. The high activation energy barrier of especially the first electron transfer to oxygen means that very efficient catalysts are required for the reactions to happen at industrially relevant rates.

2.5 Oxygen supply

Oxygen supply is perhaps the most important reaction engineering challenge for oxygen dependent biocatalysis, because the transfer of oxygen from air (or pure oxygen) to an aqueous solution is notoriously slow. This means that the rate of oxygen dependent biotechnological reactions (e.g. aerobic fermentations) typically is limited by the oxygen transfer rate that can be obtained in the aerated stirred tank reactor, where the reactions most often take place [23].

Transfer of oxygen from an air bubble to a liquid solution is typically described by the Whitman two-film theory (Figure 2.1), which assumes a stagnant layer on both the gas and liquid side where diffusion governs the transport of oxygen. The diffusion of oxygen through the gas phase is fast (and the thickness of the stagnant layer negligible), thus the diffusion through the stagnant liquid layers governs the transport. The driving force for oxygen transfer is therefore taken as the difference between the concentration at the gas-liquid interface (the oxygen saturation concentration) and the bulk concentration of oxygen. The reason for the slow oxygen transfer is therefore found in the low solubility of oxygen in aqueous media (267 µM in water using air, 25 °C, atm.) and thus a low driving force for oxygen transfer. The oxygen transfer rate (OTR) is determined by the mass transfer coefficient through the

liquid film, the area available to mass transfer and the driving force for oxygen transfer (Eq. 2.5).

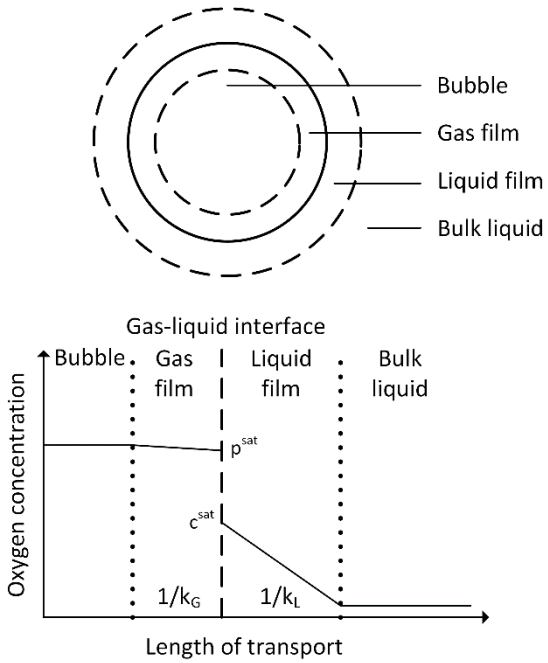

Figure 2.1. Transfer of oxygen from a gas bubble to the bulk liquid where it is consumed by reaction. k_G and k_L refers to the mass transfer coefficient in the gas and liquid film, respectively. The primary resistance to oxygen transfer will be in the liquid film layer.

The turbulent flow and constant bubble breakup and coalescence in an aerated stirred tank makes determination of the interfacial area difficult if not impossible. Thus, the mass transfer coefficient and the interfacial area is combined into one empirical constant, the volumetric mass transfer coefficient, k_La. k_La is a complex function of energy dissipated to the medium, gas hold up, and medium rheology. Typically, empirical power-law correlations are employed to correlate k_La with the power input per unit volume (P/V), the superficial gas velocity (vs) and the liquid viscosity (μ) [23].

$$OTR = k_L a(P/V, v_s, \mu)\left(C_{O_2}^{sat} - C_{O_2}\right) \quad \text{Eq. 2.5}$$

The oxygen transfer rate in an agitated reactor is limited by the amount of agitation power and air possible to supply to the reactor within the mechanical limits of the equipment. At large scale (> 100 m^3) the maximum obtainable k_La is around 500 h^{-1} [24,25], however, this values is very dependent on the media rheology. Very viscous reactions, e.g. at the end of a filamentous fungi fermentations typically have much lower k_La values [26]. A k_La of 500 h^{-1} corresponds to maximum oxygen transfer rate of 100 mmol L^{-1} h^{-1} assuming operation at a driving force corresponding to 80% of air saturation. For the production of a small organic molecule (M_w = 100 g mol^{-1}), this is equivalent to a maximum volumetric productivity of 20 g L^{-1} h^{-1} assuming a reaction catalyzed by an oxidase producing two mol of product per mol of oxygen consumed. Thus, the oxygen transfer equipment has to be pushed to its limits in order for an oxidase catalyzed process to reach the typical productivity requirements.

The difficulties involved in transferring oxygen from air to an aqueous solution result in a substantial energy consumption for compression of air and for the vigorous agitation required. Thus the cost of oxygen transfer might add substantially to the final production cost, depending on the value of the product [27]. The high cost of oxygen transfer has led researchers to investigate alternatives to the bubbled stirred reactor and the bubble column typically applied for industrial scale oxygen dependent reactions. Furthermore, specifically for enzymatic processes, the instability of enzymes in presence of gas-liquid interfaces has encouraged the development of aeration processes where there is no direct contact between air and the liquid reaction mixture.

For biocatalytic purposes, the potential alternative supply method to the bubble aerated stirred tank are pressurization of the reactor headspace to increase the driving force, using enriched air or pure oxygen for sparging, applying membrane aeration, or supplying chemically bound oxygen in the form of hydrogen peroxide, that is decomposed by catalase in the reaction medium (Figure 2.2). These supply methods may not only turn out to be cheaper, but they could also serve to reduce gas-liquid interfacial enzyme deactivation. Additionally, oxygen supply methods employing higher pressure or reduced aeration rate help to avoid problems of volatile reaction species, which can be very difficult to recover from the off-gas. The choice of oxygen supply method is compared in more detail in Chapter 3.

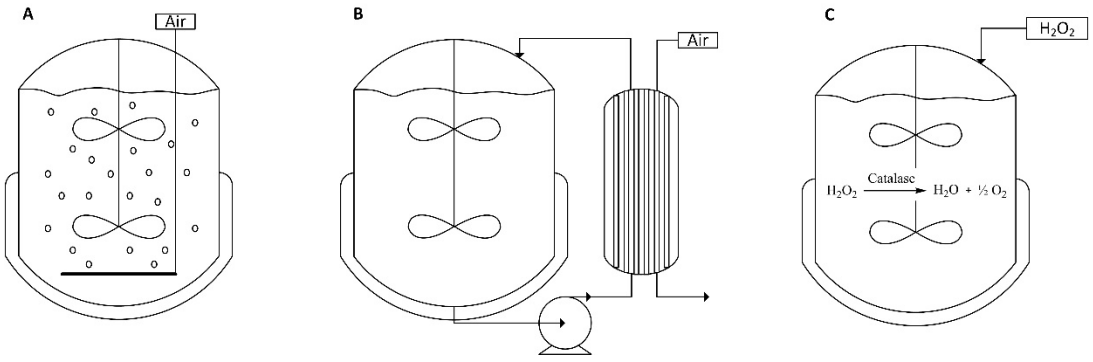

Figure 2.2. Oxygen supply methods available to oxidative biocatalysis. A) Bubble aeration in a stirred tank, B) membrane aeration where oxygen is delivered through a membrane (could also be placed inside the stirred tank), C) hydrogen peroxide decomposition by catalase to generate oxygen *in situ*.

2.6 Stability

Ensuring the biocatalyst stability at process conditions is essential for reaching the volumetric and biocatalyst productivity required for a sustainable process. The activity and specificity of enzymes are dependent on their quaternary and tertiary structure and any mechanism that leads to disruption or changes in these can cause the enzyme to change and/or lose activity and specificity. It is generally recognized, that the loss of protein structure and function is initiated by unfolding of the protein (denaturation), leaving it more susceptible to chemical modification or aggregation leading to inactivation. Denaturation can in most cases be considered as reversible, since the unfolded polypeptide can refold thereby regaining activity

when the cause of denaturation is removed. The denaturation is therefore considered as an equilibrium between the correctly folded active form and the unfolded inactive form. The position of this equilibrium is influenced by temperature, pH, ionic strength, and denaturing agents such as urea. Protein denaturation exposes amino acids otherwise buried within the tertiary structure making these more prone to undergo chemical reaction including proteolysis (thermally or by protease), deamidation, oxidation, racemization, and hydrolysis. Modifications to the amino acids change the polarity, hydrogen bonding, and/or disulfide bridging, which makes correct refolding impossible and hence inactivating the enzyme. Furthermore, unfolded proteins readily aggregate, which also results in inactivation and potentially precipitation of the protein.

Resistance to denaturation is generally referred to as thermodynamic stability due to the chemical equilibrium between the unfolded and native protein, while resistance to time dependent, irreversible inactivation processes are referred to as kinetic stability (Figure 2.3). Because many inactivation reactions acts on the unfolded protein, the kinetic stability is dependent on the fraction of protein being in the unfolded state, i.e. the thermodynamic stability. The thermodynamic stability can be quantified by measuring the Gibbs free energy of unfolding for the protein (ΔG_u) or more commonly the melting temperature of the protein, T_m, the temperature at which half of the protein is in the unfolded state. The denaturation process is in reality a combination of multiple unfolding states, but typically, only one melting temperature can be determined. The kinetic stability is best described by a deactivation rate constant, k_d, which often is measured as an observed rate constant, i.e. a combination of multiple intrinsic deactivation reactions and unfolding equilibria (Figure 2.3). Often the inactivation process follows first order kinetics, thus enabling the calculation of an enzyme half-life ($t_{½}$).

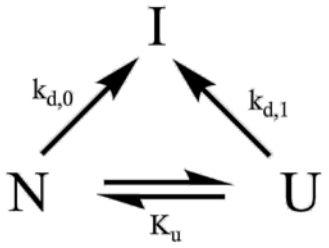

Figure 2.3. Protein denaturation (thermodynamic equilibrium) and inactivation (irreversible). N: Native protein, U: Unfolded protein, and I: Inactive protein.

From a process engineering perspective both thermodynamic and kinetic stability are important when choosing e.g. operating temperature, since neither the unfolded nor the inactivated protein retains any enzyme activity. Nevertheless, the kinetic stability will be the most important parameter, since this determines the operational stability of the enzyme and hence directly influences the overall productivity of the process. It is crucial to design a process that not only maximizes enzyme activity but also stability. To do so numerous factors that influence the stability of proteins have to be taken into account. Table 2.3 lists the most important factors and processes that may cause protein denaturation and inactivation. The

list of influencing factors is long and it will in most cases not be possible to investigate and control all. However, it is important to consider all factors when investigating enzyme stability, since the key factor(s) will vary depending on the specific enzyme and overall process.

Table 2.3. Factors and processes influencing protein denaturation. Based on [28–31].

Factor	Process
Temperature	Denaturation (reversible) that often leads to irreversible aggregation. Most chemical modifications (e.g. deamidation) increase with temperature.
pH	Protonation/deprotonation of amino acid side-chains. pH affects chemical reactions such as deamidation.
Ionic strength	Salts may facilitate aggregation in some cases but in others act stabilizing
Water activity	Lowering the water activity shifts the denaturation equilibrium to the left
Metals	Metals catalyze oxidation reactions
Solvent	Removal of essential surface bound water molecules leading to denaturation
Surfactants	Binds to exposed hydrophobic domains leading to denaturation
Oxidants	Oxidation of amino acid side-chains (Cys, Met, Trp, His, Tyr)
Chelating agents	Removes protein bound metal ions
Interfaces	Surface adsorption and interfacial stress resulting in denaturation
Protein concentration	High concentration increase aggregation upon denaturation
Proteolytic activity	Peptide bond breakage

The above mentioned deactivation processes are relevant for all biocatalytic applications using free enzymes and has been reviewed in detail in several well written scientific publications [28,32,33]. The obvious way of limiting enzyme deactivation is to avoid chemical denaturants, temperatures at or close to the melting temperature, extreme pH values, etc. However, often one would like to operate at conditions not guaranteeing optimal enzyme stability, e.g. at increased temperatures to increase reaction rate or in presence of a co-solvent to increase solubility of substrates and products. In such cases protein engineering, immobilization on solid carriers, and to some extend reaction medium engineering is the available options for enzyme stabilization. These methods will not be considered in more detail for enzymes in general, as they have been reviewed extensively elsewhere[33–37].

For oxygen dependent biocatalysis using free enzymes most, if not all, of the above-mentioned factors influencing inactivation is important. However, three factors are of specific importantance, and to some extend unique, for oxygen dependent enzymes, namely, unfolding and deactivation at gas-liquid interfaces, oxidation of amino acid side-chains, and deactivation caused by reactive aldehyde species.

Gas-liquid interfaces

Presence of gas-liquid interfaces is almost inevitable in a reactor used for carrying out an oxygen dependent biocatalytic reaction as oxygen typically is supplied by bubbling the reaction solution with air or pure oxygen. Air is hydrophobic, so proteins tend to unfold and expose their hydrophobic core (effectively decreasing ΔG_u), when put in contact with an air-liquid interface [38–40]. As explained above, denatured proteins readily undergoes irreversible deactivation via aggregation, oxidation of amino acid residue etc. The rate of unfolding is enhanced by shear effects, such as those experienced in stirred reactors or pumps, although sheer effects alone has little effect on protein stability [41]. Therefore, gas-liquid interfaces, especially in combination with high sheer forces, tend to increase deactivation rates of enzymes. However, the effect is not universal, but very dependent on the enzyme, some enzymes such as formate dehydrogenase [42], cellobiose dehydrogenase [43] and styrene monooxygenase [44], are very sensitive to gas-liquid interfaces, while others are almost unaffected, e.g. galactose oxidase [45].

Avoiding interfaces is the obvious way to overcome interfacial enzyme deactivation. Although interfaces cannot be avoided completely, gas-liquid interfaces can be minimized e.g. by applying membrane aeration. This has successfully been applied for a range of enzymes unstable in presence of gas-liquid interfaces [46–48], however, the implementation of membrane aeration in an industrial biocatalytic process has yet to be demonstrated. Improving the stability of proteins in presence of gas-liquid interfaces has shown to be difficult, judged by the number of examples in the scientific literature. However, general methods of protein stabilization (that increase ΔG_u) should prove useful, as the initial step of interfacial inactivation is unfolding. Therefore, immobilization tend to improve the interfacial stability [49,50]. Alternatives include substitution of amino acids prone to oxidation [42] and by addition of surface active agents [51]. The latter, can be difficult to apply in a biocatalytic reactor because surface active agents also change (often decrease) oxygen transfer, typically are required in relative high concentrations and potentially complicates downstream processing, and thus adds to the final cost of the chemical transformation. The exception being anti-foam agents, which also may alter enzyme deactivation rates. The best way of avoiding air-liquid interfacial enzyme deactivation is therefore most likely protein engineering approaches to increase the thermodynamic and kinetic stability, and potentially by applying alternative oxygen supply methods such as membrane aeration, if such prove to economical and technical feasible at scale.

Oxidation of amino acid side-chains

Oxidizing agents present in the reaction medium may oxidize accessible amino acid residues, especially methionine and cysteine, on a protein surface, in the protein interior upon denaturation, or in the active site. This typically disturbs the tertiary structure or makes essential amino acids unable to partake in the catalytic action, and thus leads to irreversible inactivation [52]. Typical oxidation agents include hydrogen peroxide and superoxide, generated as a co-product from oxidase catalyzed oxidations (only H_2O_2) or as a by-product due to improper electron transport, as known from the uncoupling experienced during the catalytic

cycle of cytochrome P450 monooxygenases [13,53,54]. However, dissolved oxygen may also oxidize surface amino acid (especially in presence of metal ions) and thus lead to deactivation [52,55].

Hydrogen peroxide is routinely scavenged from the reaction medium using catalase. Similarly superoxide may be scavenged using superoxide dismutase, although this is seldom applied in biocatalytic reactions even though it recently was shown to have a significant effect on the stability of a Baeyer-Villiger monooxygenase [56]. Molecular oxygen, on the other hand, cannot be avoided in the reaction medium, as it is required as a substrate. In cases where oxidation of amino acid residues pose a problem engineers can resort to immobilization of the enzyme or attempt to substitute methionine and cysteine residues prone to oxidation. Both approaches have proven to successfully stabilize enzymes prone to oxidative damage by reactive oxygen species [55,57–59].

Aldehydes

Oxidation reaction often involve aldehydes either as the product from the oxidation of primary alcohols or as the substrate for further oxidation to the carboxylic acid. Aldehydes are generally very reactive molecules, since they readily partake in nucleophilic additions. Therefore, aldehydes react with protein amino acid residues containing nucleophilic groups, such as amino groups. Besides the terminal amino group of proteins, proteins are also prone to aldehyde addition reactions with the amino acid side chains, such as the sulfhydryl group of cysteine, the ε-amino group of lysine, the imidazole group of histidine, and to some extend the guanidinium group of arginine [60,61]. Especially lysine residues on the protein surface or in the active site are prone to aldehyde modifications via a Shiff's base addition (Figure 2.4), while the other amino acid residues typically requires conjugated aldehydes to react, such as 4-hydroxynonenal generated during lipid oxidation or the aldol condensation product of acetaldehyde [61–63]. Protein-aldehyde reactions are also well known from the widely applied protein cross-linking reaction using the dialdehyde glutaraldehyde [64].

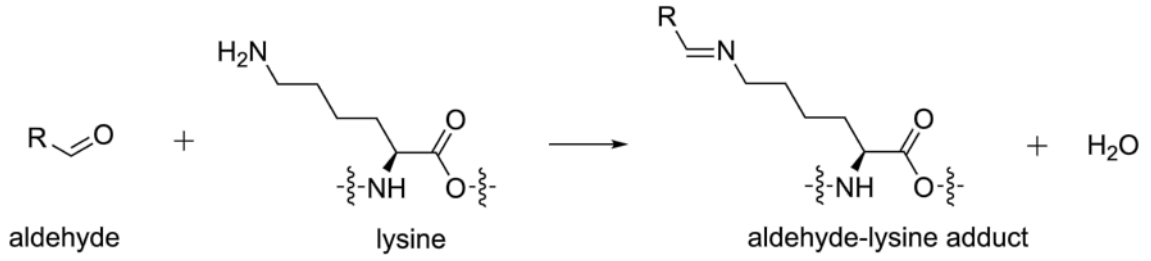

Figure 2.4. Shift base addition of the ε-amino group of lysine to an aldehyde to form an imine.

Aldehyde addition to amino acids side chains do not necessarily deactivate an enzyme, e.g. immobilized enzymes. Obviously, enzyme activity is lost or reduced in cases where the addition happens at a residue taking part in the catalytic action (although lysine rarely is present in the active site) or if the addition adduct block the substrate entrance to the active site. However, modification of amino acid residues on the protein surface may also lead to enzyme deactivation by distorting the quaternary and tertiary structure [65].

Stability of a biocatalyst to aldehydes is a problem often encountered, for example for lipase catalyzed kinetic resolution [62,63], aldolase catalyzed aldol reactions [66,67], benzaldehyde lyase catalyzed C-C bond formation [68], and transketolase catalyzed C-C bond formation [69]. Problems of aldehyde deactivation may to some extend be alleviated by immobilization or by exchanging amino acid residues prone to aldehyde reactions with less reactive amino acids [63,70,71]. There are also examples of the use of directed evolution and *in silico* prediction of stabilization mutation, that have shown to improve the stability in presence of aldehydes [66,67]. Interestingly, no amino acid residues prone to aldehyde modifications were substituted using these approaches, instead the mutations increased the rigidity of the enzyme structure and thus also the stability in presence of aldehydes.

The process engineering solution to aldehyde instability is naturally to feed the aldehyde as it is consumed, in cases where an aldehyde is a substrate, and to remove the aldehyde as it is formed using *in situ* product removal (ISPR), in cases where an aldehyde is formed as a product. ISPR options include extraction of the aldehyde in a two-phase system, crystallization of the aldehyde, and adsorption of the aldehyde onto resins. Eventually, cascade systems can be utilized to convert the aldehyde into a less reactive specie. However, this is only applicable in cases where the aldehyde itself is not the desired end-product.

2.7 Stripping of volatile compounds

The large requirement to oxygen means that oxygen dependent biocatalytic processes requires aeration rates of up to two vvm (volumes of air per volume of reactor per minute). Volatile compounds will at such aeration rates be stripped from the liquid reaction media relatively fast. Even compounds with high boiling points will be stripped from an aqueous solution to a significant extend if their solubility is low (e.g. styrene [72] and perillene [73]). Products of biocatalytic oxidations are often organic molecules that are relatively volatile compounds with low aqueous solubility, such as aldehydes and lactones especially interesting for the flavors and fragrances industry. Loss of product due to evaporation is therefore an important parameter when designing an oxygen dependent biocatalytic process.

In aerated stirred reactors, the gas-phase is well dispersed in the liquid phase and the contact area between the two phases is large. In most cases, it can therefore safely be assumed that the off-gas leaving the reactor is in equilibrium with the liquid phase. The vapor-liquid equilibrium of a compound, i.e. the ratio between the mole fraction in the gas and liquid phase (y_i and x_i, respectively), is described by the equilibrium constant, K_{vle} (Eq. 2.6). Describing the vapor-liquid equilibrium is not straightforward for non-ideal systems. To do so activity coefficient models such as UNIQUAC or NRTL are required, which take interactions between system components into account. However, for dilute solutions of a small molecule (as many solution in biocatalysis are), the much simpler Henry's Law (Eq. 2.7) can be used to estimate the equilibrium constant, when an experimentally determined proportionality constant (H_i) is known. For most compounds, the Henry's Law constant as a function of

temperature can be found in thermodynamic databases. Similarly, when the liquid mole fraction of a compound is close to one, Raoult's Law (Eq. 2.8) can be used to determine the equilibrium constant based on the pure component vapor pressure of the compound (P^{sat}).

$$K_{vle,i} = \frac{y_i}{x_i} \quad \text{Eq. 2.6}$$

$$K_{vle,i} = \frac{H_i}{P} \quad \text{Eq. 2.7}$$

$$K_{vle,i} = \frac{P_i^{sat}}{P} \quad \text{Eq. 2.8}$$

As mentioned above, significant stripping of a compound in solution can occur despite a high boiling point and thus low vapor pressure. An example is the oxidation of benzyl alcohol (T_b, 205 °C) to benzaldehyde (T_b, 179 °C), where the substrate does not evaporate at all from the solution, whereas the product is stripped from the solution to a significant extend [45]. The main reasons for this is the large difference in solubility between the two compounds (42.9 g L^{-1} [74] and 6.6 g L^{-1} [75], respectively), due the ability of benzyl alcohol to form hydrogen bonds whereas benzaldehyde cannot. Figure 2.5 shows the stripping of benzaldehyde from water at a typical aeration rate in a stirred reactor and the good agreement with Henry's law. Additionally, the figure shows the stripping rate at three different benzaldehyde concentrations. At a concentration of 50 mM, the rate of stripping is 3 mmol L^{-1} h^{-1}, which at typical industrial production rates (100 mmol L^{-1} h^{-1}) corresponds to a loss of 3%, which increase with both temperature and product concentration. The high aeration rate and low concentration of benzaldehyde in the off-gas makes recovery of the product difficult, because simple condensation is not an option. Even if the off-gas is cooled to 0 °C, something that is not easy due to the poor heat transfer coefficient of air and the high airflow rate, only 7.5% of the lost benzaldehyde can be recovered. Although a 3% loss is not detrimental to every process, it is a loss that is worthwhile minimizing when designing the process. Furthermore, the loss can easily be significantly higher for other compounds more volatile than benzaldehyde.

Avoiding stripping of a volatile substrate or product, such as benzaldehyde, is thus of significant importance in order to ensure the best possible yield. Stripping can be limited by choosing an oxygen supply method that reduces the aeration rate by increasing the driving force available for oxygen transfer, such as pure oxygen sparging or increased reactor headspace pressure. Furthermore, by increasing the headspace pressure the mole fraction in the gas phase at equilibrium is reduced thus decreasing the rate of evaporation. Alternatively, the concentration of the volatile component in the aqueous phase can be reduced by introducing an organic phase with high affinity for the compound. However, the solvent must be chosen with care, because many solvents traditionally applied in biocatalytic reaction are in themselves volatile and thus easily lost, see below.

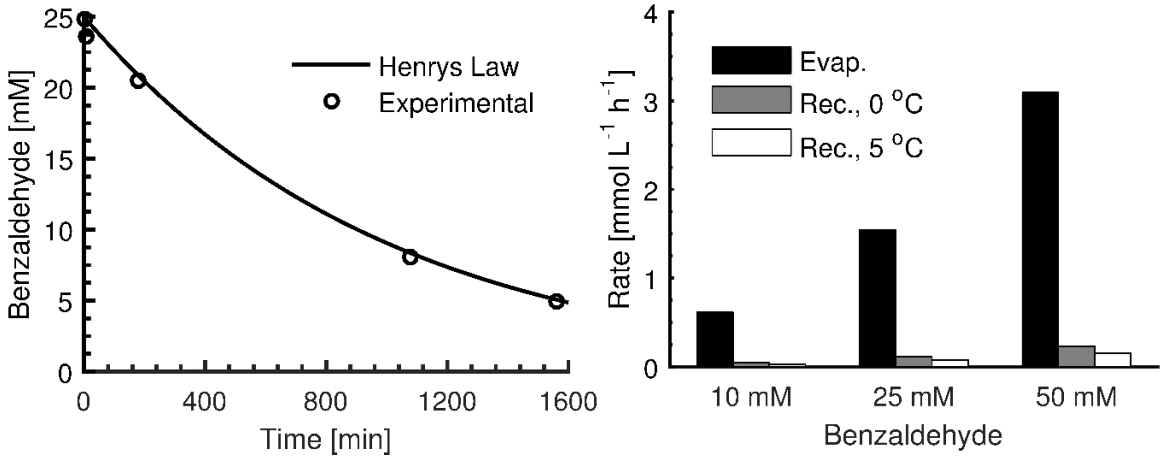

Figure 2.5. Stripping and condensation of benzaldehyde from water at 25 °C at an aeration rate of 1 vvm. Left: Experimental benzaldehyde stripping and comparison with Henry's law. Right: Evaporation rate at different benzaldehyde concentrations and corresponding recovery (condensation) rates if off-gas is cooled to 0 °C or 5 °C.

Utilizing a difference between the volatility of a substrate and product is an obvious way of removing the product as it is formed, in cases where the product inhibits, or otherwise limits, the reaction. However, as exemplified above, this is only in cases where 1) the rate of removal is high enough and 2) in cases where it is possible to recover the product from the off-gas, unless the compound being removed is a byproduct of little value [16,76]. Nevertheless, for products showing higher volatility, stripping is definitely an option for ISPR as these also will be easier to remove from the off-gas using condensation. Alternatively, the volatile compound could be recovered from the off-gas using solvent extraction or adsorption onto solid resins with high affinity for the product. In practice, it will not be possible to recover all product from the off-gas. Therefore, it is frequently suggested to recirculate the gas used for stripping after some product has been recovered, this principle has often been applied with success in e.g. the acetone-butanol-ethanol (ABE) fermentation [77]. This works well for anaerobic processes as the ABE fermentation, where stripping gas serves no other purpose than removing the desired compounds. In aerobic processes, oxygen is constantly consumed from the gas phase and thus needs to be replenished by purging from the gas and feeding air or oxygen. In such cases, it is particularly tempting to use pure oxygen for aeration to avoid having to recirculate and purge inert nitrogen. However, the safety concern of mixing a gaseous organic molecule in pure oxygen will make the hazards at large scale unmanageable. The above mentioned challenges when applying gas stripping for ISPR in combination with oxygen dependent reactions is probably one reason for the limited numbers of examples in the scientific literature [72,78].

Safe operation of an aerated bioprocess containing volatile organic compounds is indeed an important topic, especially as the scale, and thus the risks, is increased. Stripping of a compound like benzaldehyde does not pose a safety problem because of the very low gas-phase concentration. However, in biocatalytic oxidation reactions a secondary organic solvent is often applied to extract the formed product, supply a substrate, and/or simplify downstream

processing [79,80]. In such cases, the explosive atmosphere potentially formed when applying a low boiling solvent, e.g. ethyl acetate (T_b, 77.1 °C), is a serious risk that needs to be avoided through safe operation of the process [81,82]. An explosive atmosphere can be avoided ensuring that the oxygen concentration in the exhaust gas never increases beyond the oxygen limit concentration or keeping the concentration of a flammable compound in the gas phase below the lower explosion limit, e.g. by increasing the headspace pressure above a critical pressure or operating at a temperature below the flashpoint. Alternative, solvents with higher boiling points, and thus higher flashpoints, can be applied, although this makes downstream processing problematic if the product is high boiling, since distillation is very energy intensive. Another alternative is to avoid direct contact of the organic solvent with the aeration gas, by extracting the desired compound into the organic solvent through a suitable membrane [83].

2.8 Whole-cell processes

Whole-cell oxygen dependent processes share many of the challenges of free enzyme systems discussed above, such as the difficulties of supplying sufficient oxygen and loss of substrate or product due to volatility. However, there are also several differences between the systems, which are briefly discussed below.

Whole-cell biocatalysts can either be growing (i.e. combined biomass and product production) or in a resting state where the cells are still alive and metabolically active, but unable to grow due a limitation in one or more nutrients, typically nitrogen. In resting cell biocatalysis, as opposed to growing cell biocatalysis, the biocatalytic reaction is uncoupled from the growth, and thus enabling individual optimization of the reaction conditions for both the growth and the biocatalytic reaction. Both resting and growing cells requires a carbon source for generation energy required for cell maintenance (and growth). Furthermore, the cells require oxygen not only as a substrate for the enzymatic oxidation but also for the oxidative phosphorylation to generate ATP. As growing cells require carbon and energy for growth, they require significantly more oxygen than resting cells. The expected volumetric productivity of whole-cells biocatalytic processes are therefore lower than for free enzymes, because a large part of the limited supply of oxygen is consumed in the cell metabolism [84]. The oxygen consumption increase, and thus oxygen available for the biocatalytic reaction decrease, with increasing growth rate. Selecting an appropriate growth rate, preferably as low as possible, is therefore important to avoid oxygen limitations [85]. The difference in oxygen consumption rate and thus maximum productivity is illustrated in Figure 2.6. Additionally, it must be noted that the high oxygen affinity of the electron transport chain means that all oxygen will be directed there in case of limitations, thus a low oxygen concentration will stop the biocatalytic reaction in a cell before growth rate is decreased [10,84].

With the above described potential oxygen limitation in whole cell catalyzed bioprocesses in mind, it is important to choose a host organism, which not only express the desired protein sufficiently well but also requires as little maintenance energy as possible in the stressful environment of a biocatalytic reactor [88]. Additionally, the general tolerance of the host

organism towards the substrate and product (and an organic solvent in cases where this is required) is important, since the viability of the cell machinery is a prerequisite for biocatalytic activity [89]. Gas-liquid interface facilitated deactivation of enzymes are avoided when applying whole-cells, but even though the enzymes are situated in their natural cellular environment, significant destabilization by reactive oxygen species or aldehyde products can occur.

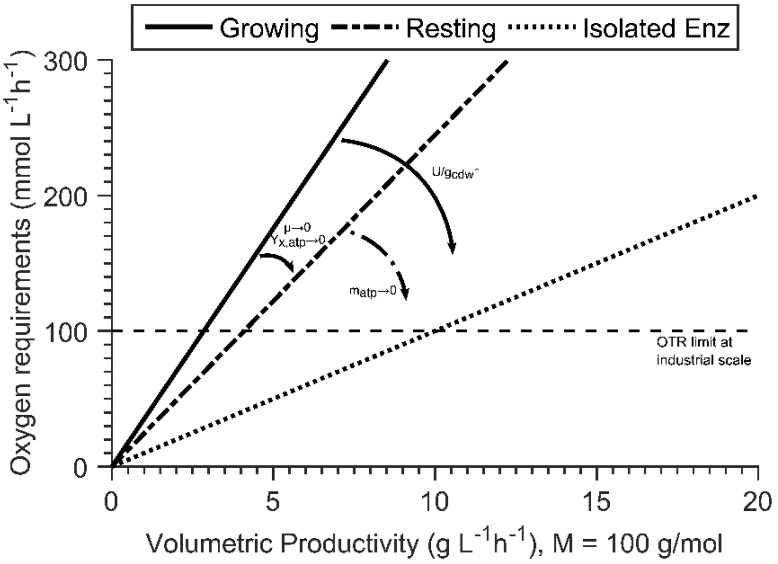

Figure 2.6. Oxygen requirements of different types of biocatalysts carrying out a monooxygenase reaction. The calculations are based on E. coli with an enzyme activity of 50 µmol min^{-1} g_{cdw}^{-1} and using standard values for the yield coefficients and maintenance requirements [86,87] . The growing cell is growing at a specific growth rate of 0.2 h^{-1}. Figure adapted from [85].

2.9 Concluding remarks

Besides the specific challenges listed above, the reaction and process engineering challenges experienced for biocatalytic reactions in general also apply to oxygen dependent enzymes, such as inhibition by substrates or products, decreased enzyme stability in presence of solvents, poorly water soluble substrates, requirements to efficient regeneration of co-factors, tuning of reaction conditions to fit multiple enzymes, etc. [90].

The successful development of an oxygen dependent biocatalytic process requires the combined effort of protein and process engineers. Where protein engineers address problems of activity, selectivity, inhibition, and stability, process engineers tune reaction conditions, apply *in situ* product removal, employ substrate feeding schemes, and choose suitable oxygen supply methods to alleviate problems not possible to solve using protein engineering due to technical or economic constraints. The development requires close contact between protein and process engineers to determine the targets of enzyme engineering efforts, and more importantly making sure the enzyme selected for further process development lives up to a set of minimum targets. These targets most ensure that there is a sufficient thermodynamic driv-

ing force available for implementing process and reaction engineering solutions, e.g. sufficient aldehyde tolerance to allow for an aqueous concentration that can drive an ISPR method.

2.10 References

[1] Bornscheuer UT, Huisman GW, Kazlauskas RJ, Lutz S, Moore JC, Robins K, **2012**. Engineering the third wave of biocatalysis, Nature. 485(7397):185–94.

[2] Woodley JM, **2006**. Choice of biocatalyst form for scalable processes, Biochem. Soc. Trans. 34(2):301–303.

[3] Sheldon RA, **2007**. Enzyme immobilization: The quest for optimum performance, Adv. Synth. Catal. 349(8–9):1289–1307.

[4] Cao L, van Langen L, Sheldon RA, **2003**. Immobilised enzymes: Carrier-bound or carrier-free?, Curr. Opin. Biotechnol. 14(4):387–394.

[5] Tufvesson P, Lima-Ramos J, Nordblad M, Woodley JM, **2011**. Guidelines and cost analysis for catalyst production in biocatalytic processes, Org. Process Res. Dev. 15(1):266–274.

[6] Bolivar JM, Schelch S, Pfeiffer M, Nidetzky B, **2016**. Intensifying the O2-dependent heterogeneous biocatalysis: superoxygenation of solid support from H2O2 by a catalase tailor-made for effective immobilization, J. Mol. Catal. B Enzym. 134:302–309.

[7] Morthensen ST, Meyer AS, Jørgensen H, Pinelo M, **2017**. Significance of membrane bioreactor design on the biocatalytic performance of glucose oxidase and catalase: Free vs. immobilized enzyme systems, Biochem. Eng. J. 117:41–47.

[8] Messing RA, **1974**. Simultaneously immobilized glucose oxidase and catalase in controlled-pore titania, Biotechnol. Bioeng. 16(7):897–908.

[9] Bao J, Furumoto K, Fukunaga K, Nakao K, **2001**. A kinetic study on air oxidation of glucose catalyzed by immobilized glucose oxidase for production of calcium gluconate, Biochem. Eng. J. 8(2):91–102.

[10] Duetz WA, Beilen JB Van, Witholt B, **2001**. Using proteins in their natural environment: potential and limitations of microbial whole-cell hydroxylations in applied biocatalysis, Curr. Opin. Biotechnol. 12(4):419–425.

[11] Schrewe M, Julsing MK, Bühler B, Schmid A, **2013**. Whole-cell biocatalysis for selective and productive C-O functional group introduction and modification, Chem. Soc. Rev. 42(15):6346–77.

[12] Lima-Ramos J, Tufvesson P, Woodley JM, **2014**. Application of environmental and economic metrics to guide the development of biocatalytic processes, Green Process. Synth. 3(3):195–213.

[13] Lundemo MT, Woodley JM, **2015**. Guidelines for development and implementation of biocatalytic P450 processes, Appl. Microbiol. Biotechnol. 99(6):2465–2483.

[14] Tufvesson P, Lima-Ramos J, Haque NA, Gernaey KV, Woodley JM, **2013**. Advances in the process development of biocatalytic processes, Org. Process Res. Dev. 17(10):1233–1238.

[15] Tufvesson P, Jensen JS, Kroutil W, Woodley JM, **2012**. Experimental determination of thermodynamic equilibrium in biocatalytic transamination, Biotechnol. Bioeng.

109(8):2159–2162.

[16] Tufvesson P, Bach C, Woodley JM, **2014**. A model to assess the feasibility of shifting reaction equilibrium by acetone removal in the transamination of ketones using 2-propylamine, Biotechnol. Bioeng. 111(2):309–319.

[17] Woodley JM, **2017**. Bioprocess intensification for the effective production of chemical products, Comput. Chem. Eng. 10.1016/j.compchemeng.2017.01.015.

[18] Alberty RA, **1998**. Calculation of Standard Transformed Formation Properties of Biochemical Reactants and Standard Apparent Reduction Potentials of Half Reactions, Arch. Biochem. Biophys. 358(1):25–39.

[19] Valentine JS, Dioxygen Reactions, in: I. Bertini, H.B. Gray, S.J. Lippard, J.S. Valentine (Eds.), Bioinorg. Chem., **1994**, University Science Books, Mill Valley, CA: pp. 313–523.

[20] Alberty RA, **2000**. Calculating apparent equilibrium constants of enzyme-catalyzed reactions at pH 7, Biochem. Educ. 28(1):12–17.

[21] Flamholz A, Noor E, Bar-Even A, Milo R, **2012**. EQuilibrator - The biochemical thermodynamics calculator, Nucleic Acids Res. 40:770–775.

[22] Alberty RA, **2001**. Standard Apparent Reduction Potentials for Biochemical Half Reactions as a Function of pH and Ionic Strength, Arch. Biochem. Biophys. 389(1):94–109.

[23] Garcia-Ochoa F, Gomez E, **2009**. Bioreactor scale-up and oxygen transfer rate in microbial processes: an overview., Biotechnol. Adv. 27(2):153–76.

[24] Villadsen J, Nielsen J, Lidén G, Bioreaction Engineering Principles, 3rd ed., **2011**, Springer Science+Business Media, New York.

[25] Noorman H, Scale-Up and Scale-Down, in: J. Villadsen (Ed.), Fundam. Bioeng., **2016**, Wiley-VCH Verlag GmbH & Co. KGaA, Weinheim: pp. 463–498.

[26] Albaek MO, Gernaey KV, Hansen MS, Stocks SM, **2012**. Evaluation of the energy efficiency of enzyme fermentation by mechanistic modeling, Biotechnol. Bioeng. 109(4):950–961.

[27] Grotkjær T, Commercial Development of Fermentation Processes, in: J. Villadsen (Ed.), Fundam. Bioeng., **2016**, Wiley-VCH Verlag GmbH & Co. KGaA, Weinheim: pp. 499–545.

[28] Iyer PV, Ananthanarayan L, **2008**. Enzyme stability and stabilization—Aqueous and non-aqueous environment, Process Biochem. 43(10):1019–1032.

[29] Fágáin CÓ, **1995**. Understanding and increasing protein stability, Biochim. Biophys. Acta. 1252:1–14.

[30] Misset O, Dijk A van, Diagnosing the inactivating process of enzymes, in: A. Ballesteros, F. Plou, J. Iborra, P. Halling (Eds.), Stab. Stab. Biocatal. Prog. Biotechnol. Vol. 15, **1998**, Elsevier Science B.V., Amsterdam: pp. 3–18.

[31] Manning MC, Chou DK, Murphy BM, Payne RW, Katayama DS, **2010**. Stability of

protein pharmaceuticals: an update, Pharm. Res. 27(4):544–75.

[32] Polizzi KM, Bommarius AS, Broering JM, Chaparro-Riggers JF, **2007**. Stability of biocatalysts, Curr. Opin. Chem. Biol. 11(2):220–5.

[33] Bommarius AS, Paye MF, **2013**. Stabilizing biocatalysts, Chem. Soc. Rev. 42(15):6534–65.

[34] Eijsink VGH, Gåseidnes S, Borchert T V, van den Burg B, **2005**. Directed evolution of enzyme stability, Biomol. Eng. 22(1–3):21–30.

[35] Mateo C, Palomo JM, Fernandez-Lorente G, Guisan JM, Fernandez-Lafuente R, **2007**. Improvement of enzyme activity, stability and selectivity via immobilization techniques, Enzyme Microb. Technol. 40(6):1451–1463.

[36] Stepankova V, Bidmanova S, Koudelakova T, Prokop Z, Chaloupkova R, Damborsky J, **2013**. Strategies for stabilization of enzymes in organic solvents, ACS Catal. 3(12):2823–2836.

[37] Eijsink VGH, Bjørk A, Gåseidnes S, Sirevåg R, Synstad B, Burg B Van Den, Vriend G, **2004**. Rational engineering of enzyme stability, J. Biotechnol. 113(1–3):105–120.

[38] Thomas CR, Geer D, **2011**. Effects of shear on proteins in solution, Biotechnol. Lett. 33(3):443–56.

[39] Wiesbauer J, Prassl R, Nidetzky B, **2013**. Renewal of the air-water interface as a critical system parameter of protein stability: Aggregation of the human growth hormone and its prevention by surface-active compounds, Langmuir. 29(49):15240–15250.

[40] Perriman AW, Henderson MJ, Holt SA, White JW, **2007**. Effect of the air-water interface on the stability of b-lactoglobulin, J. Phys. Chem. B. 111(48):13527–13537.

[41] Maa YF, Hsu CC, **1997**. Protein denaturation by combined effect of shear and air-liquid interface, Biotechnol. Bioeng. 54(6):503–12.

[42] Bommarius AS, Karau A, **2005**. Deactivation of Formate Dehydrogenase (FDH) in solution and at gas-liquid interfaces, Biotechnol. Prog. 21(6):1663–1672.

[43] Ludwig R, Ozga M, Zámocky M, Peterbauer C, Kulbe KD, Haltrich D, **2004**. Continuous Enzymatic Regeneration of Electron Acceptors Used by Flavoenzymes: Cellobiose Dehydrogenase-Catalyzed Production of Lactobionic Acid as an Example, Biocatal. Biotransformation. 22(2):97–104.

[44] Hofstetter K, Lutz J, Lang I, Witholt B, Schmid A, **2004**. Coupling of biocatalytic asymmetric epoxidation with NADH regeneration in organic-aqueous emulsions, Angew. Chemie - Int. Ed. 43(16):2163–2166.

[45] Toftgaard Pedersen A, Birmingham WR, Rehn G, Charnock SJ, Turner NJ, Woodley JM, **2015**. Process Requirements of Galactose Oxidase Catalyzed Oxidation of Alcohols, Org. Process Res. Dev. 19(11):1580–1589.

[46] Van Hecke W, Ludwig R, Dewulf J, Auly M, Messiaen T, Haltrich D, Van Langenhove H, **2009**. Bubble-free oxygenation of a bi-enzymatic system: effect on

biocatalyst stability, Biotechnol. Bioeng. 102(1):122–31.

[47] Van Hecke W, Haltrich D, Frahm B, Brod H, Dewulf J, Van Langenhove H, Ludwig R, **2011**. A biocatalytic cascade reaction sensitive to the gas–liquid interface: Modeling and upscaling in a dynamic membrane aeration reactor, J. Mol. Catal. B Enzym. 68(2):154–161.

[48] Rissom S, Schwarz-Linek U, Vogel M, Tishkov VI, Kragl U, **1997**. Synthesis of chiral e-lactones in a two-enzyme system of cyclohexanone mono-oxygenase and formate dehydrogenase with integrated bubble-free aeration, Tetrahedron Asymmetry. 8(15):2523–2526.

[49] Betancor L, Fuentes M, Dellamora-Ortiz G, López-Gallego F, Hidalgo A, Alonso-Morales N, Mateo C, Guisán JM, Fernández-Lafuente R, **2005**. Dextran aldehyde coating of glucose oxidase immobilized on magnetic nanoparticles prevents its inactivation by gas bubbles, J. Mol. Catal. B Enzym. 32(3):97–101.

[50] Bolivar JM, Wilson L, Ferrarotti SA, Guisán JM, Fernández-Lafuente R, Mateo C, **2006**. Improvement of the stability of alcohol dehydrogenase by covalent immobilization on glyoxyl-agarose, J. Biotechnol. 125(1):85–94.

[51] Kim MH, Lee SB, Ryu DDY, Reese ET, **1982**. Surface deactivation of cellulase and its prevention, Enzyme Microb. Technol. 4(2):99–103.

[52] Saville BA, Persi S, **1992**. The Effect of Oxygen Upon the Kinetics of Enzyme Inactivation: In vitro Investigations Using Glutamine Synthetase, Can. J. Chem. Eng. 70(6):1143–1148.

[53] Bernhardt R, **2006**. Cytochromes P450 as versatile biocatalysts, J. Biotechnol. 124(1):128–145.

[54] Imlay JA, **2013**. The molecular mechanisms and physiological consequences of oxidative stress: lessons from a model bacterium, Nat. Rev. Microbiol. 11(7):443–454.

[55] Brocklebank S, Woodley JM, Lilly MD, **1999**. Immobilised transketolase for carbon-carbon bond synthesis: Biocatalyst stability, J. Mol. Catal. - B Enzym. 7(1–4):223–231.

[56] Goncalves L, Kracher D, Milker S, Rudroff F, Fink MJ, Ludwig R, Bommarius A, Mihovilovic M, **2017**. Mutagenesis-Independent, Stabilization of Class B Flavin Monooxygenases in Operation, Adv. Synth. Catal. 359(12):2121–2131.

[57] Kim YH, Berry AH, Spencer DS, Stites WE, **2001**. Comparing the effect on protein stability of methionine oxidation versus mutagenesis: steps toward engineering oxidative resistance in proteins, Protein Eng. 14(5):343–347.

[58] Slavica A, Dib I, Nidetzky B, **2005**. Single-site oxidation, cysteine 108 to cysteine sulfinic acid, in D-amino acid oxidase from Trigonopsis variabilis and its structural and functional consequences, Appl. Environ. Microbiol. 71(12):8061–8068.

[59] Oh K-H, Nam S-H, Kim H-S, **2002**. Improvement of oxidative and thermostability of N-carbamyl-d-amino Acid amidohydrolase by directed evolution, Protein Eng. 15(8):689–95.

[60] Nicholls R, de Jersey J, Worrall S, Wilce P, **1992**. Modification of proteins and other biological molecules by acetaldehyde: Adduct structure and functional significance, Int. J. Biochem. 24(12):1899–1906.

[61] Bolgar MS, Gaskell SJ, **1996**. Determination of the sites of 4-hydroxy-2-nonenal adduction to protein by electrospray tandem mass spectrometry, Anal. Chem. 68(14):2325–2330.

[62] Franken B, Eggert T, Jaeger KE, Pohl M, **2011**. Mechanism of acetaldehyde-induced deactivation of microbial lipases, BMC Biochem. 12:10.

[63] Di Lorenzo M, Hidalgo A, Molina R, Hermoso JA, Pirozzi D, Bornscheuer UT, **2007**. Enhancement of the stability of a prolipase from Rhizopus oryzae toward aldehydes by saturation mutagenesis, Appl. Environ. Microbiol. 73(22):7291–7299.

[64] Migneault I, Dartiguenave C, Bertrand MJ, Waldron KC, **2004**. Glutaraldehyde: Behavior in aqueous solution, reaction with proteins, and application to enzyme crosslinking, Biotechniques. 37(5):790–802.

[65] Weber HK, Zuegg J, Faber K, Pleiss J, **1997**. Molecular reasons for lipase-sensitivity against acetaldehyde, J. Mol. Catal. - B Enzym. 3(1–4):131–138.

[66] Jennewein S, Schürmann M, Wolberg M, Hilker I, Luiten R, Wubbolts M, Mink D, **2006**. Directed evolution of an industrial biocatalyst: 2-deoxy-d-ribose 5-phosphate aldolase, Biotechnol. J. 1(5):537–548.

[67] Fei H, Xu G, Wu JP, Yang LR, **2015**. Improving the acetaldehyde tolerance of DERAsep by enhancing the rigidity of its protein structure, J. Mol. Catal. B Enzym. 116:148–152.

[68] Mikolajek R, Spiess AC, Pohl M, Lamare S, Büchs J, **2007**. An activity, stability and selectivity comparison of propioin synthesis by thiamine diphosphate-dependent enzymes in a solid/gas bioreactor, ChemBioChem. 8(9):1063–1070.

[69] Mitra RK, Woodley JM, Lilly MD, **1998**. Escherichia coli transketolase-catalyzed carbon-carbon bond formation: Biotransformation characterization for reactor evaluation and selection, Enzyme Microb. Technol. 22(1):64–70.

[70] Nara TY, Togashi H, Ono S, Egami M, Sekikawa C, Suzuki YH, Masuda I, Ogawa J, Horinouchi N, Shimizu S, Mizukami F, Tsunoda T, **2011**. Improvement of aldehyde tolerance and sequential aldol condensation activity of deoxyriboaldolase via immobilization on interparticle pore type mesoporous silica, J. Mol. Catal. B Enzym. 68(2):181–186.

[71] Kaga H, Siegmund B, Neufellner E, Faber K, Paltauf F, **1994**. Stabilization of Candida lipase against acetaldehyde by adsorption onto celite, Biotechnol. Tech. 8(6):369–374.

[72] McKenna R, Moya L, McDaniel M, Nielsen DR, **2014**. Comparing in situ removal strategies for improving styrene bioproduction, Bioprocess Biosyst. Eng. 38(1):165–174.

[73] Krings U, Berger RG, **2008**. In situ recovery of the aroma compound perillene from stirred-tank cultured Pleurotus ostreatus using gas stripping and adsorption on

polystyrene., Biotechnol. Lett. 30(8):1347–51.

[74] Banerjee S, **1984**. Solubility of Organic Mixtures in Water, Environ. Sci. Technol. 18(8):587–591.

[75] Mitchell A, Wan L, Bjaastad S, **1964**. The solubility of benzene in water, J. Pharm. Pharmacol. :632–633.

[76] Schroer K, Tacha E, Lütz S, **2007**. Process intensification for substrate-coupled whole cell ketone reduction by in situ acetone removal, Org. Process Res. Dev. 11(5):836–841.

[77] Xue C, Zhao J, Liu F, Lu C, Yang ST, Bai FW, **2013**. Two-stage in situ gas stripping for enhanced butanol fermentation and energy-saving product recovery, Bioresour. Technol. 135:396–402.

[78] Rodriguez GM, Atsumi S, **2012**. Isobutyraldehyde production from Escherichia coli by removing aldehyde reductase activity, Microb. Cell Fact. 11(1):90.

[79] Freeman A, Woodley JM, Lilly MD, **1993**. In situ product removal as a tool for bioprocessing, Nat. Biotechnol. 11(9):1007–1012.

[80] Bühler B, Schmid A, **2004**. Process implementation aspects for biocatalytic hydrocarbon oxyfunctionalization, J. Biotechnol. 113(1–3):183–210.

[81] Schmid A, Kollmer A, Sonnleitner B, Witholt B, **1999**. Development of equipment and procedures for the safe operation of aerobic bacterial bioprocesses in the presence of bulk amounts of flammable organic solvents, Bioprocess Eng. 20(2):91–100.

[82] Schmid A, Kollmer A, Mathys RG, Witholt B, **1998**. Developments toward large-scale bacterial bioprocesses in the presence of bulk amounts of organic solvents, Extremophiles. 2(3):249–256.

[83] Molinari F, Aragozzini F, Cabral JMS, Prazeres DMF, **1997**. Continuous production of isovaleraldehyde through extractive bioconversion in a hollow-fiber membrane bioreactor, Enzyme Microb. Technol. 20(8):604–611.

[84] Baldwin CVF, Woodley JM, **2006**. On Oxygen Limitation in a Whole Cell Biocatalytic Baeyer-Villiger Oxidation Process, Biotechnol. Bioeng. 95(3):362–369.

[85] Toftgaard Pedersen A, Rehn G, Woodley JM, **2015**. Oxygen transfer rates and requirements in oxidative biocatalysis, Comput. Aided Chem. Eng. 37:2111–2116.

[86] Ingraham JL, Maaløe O, Neidhardt FC, Growth of the bacterial cell, **1983**, Sinauer Associates Inc., Sunderland, MA, U.S.A.

[87] Varma A, Palsson B, **1994**. Stoichiometric flux balance models quantitatively predict growth and metabolic by-product secretion in wild-type Escherichia coli W3110., Appl. Environ. Microbiol. 60(10):3724–3731.

[88] Kuhn D, Fritzsch FSO, Zhang X, Wendisch VF, Blank LM, Bühler B, Schmid A, **2013**. Subtoxic product levels limit the epoxidation capacity of recombinant E. coli by increasing microbial energy demands., J. Biotechnol. 163(2):194–203.

[89] Kadisch M, Julsing MK, Schrewe M, Jehmlich N, Scheer B, von Bergen M, Schmid

A, Bühler B, **2017**. Maximization of cell viability rather than biocatalyst activity improves whole-cell w-oxyfunctionalization performance, Biotechnol. Bioeng. 114(4):874–884.

[90] Lima-Ramos J, Neto W, Woodley JM, **2014**. Engineering of biocatalysts and biocatalytic processes, Top. Catal. 57(5):301–320.

Chapter 3

A techno-economic comparison of oxygen supply methods for oxidative biocatalysis

This chapter is intended for later publication. The Supporting Information can be found in Appendix A.

3.1 Abstract

Oxygen supply to fermentations has been a widely studied field of research for many decades. With the recent developments within oxidative biocatalysis the supply of oxygen to biocatalytic reactions have never been more important. Although biocatalytic oxidations and aerobic fermentations share many similarities, a number of differences are critical when evaluating oxygen supply methods, such as instability of certain enzymes in the presence of gas-liquid interfaces. To circumvent the problems associated with the traditional method of supplying oxygen via bubble aeration of stirred tanks, a number of alternative oxygen supply methods have been proposed in the scientific literature. In this paper, the most promising alternatives are evaluated based on their technical feasibility and cost, and compared to traditional methods of supplying oxygen via bubble aeration of stirred tanks. The methods investigated comprise enriched air aeration and pressurization of stirred tanks, membrane aeration with a submerged and an external membrane configuration, and *in situ* oxygen generation by hydrogen peroxide decomposition.

3.2 Introduction

In the recent years biocatalytic oxidations have gained significant interest for reactions such as oxidation of alcohols, aldehydes and amines, epoxidation of C-C double bonds, hydroxylation of C-H bonds, and Baeyer-Villiger oxidation [1–3]. Common to all these reactions are that they require a stoichiometric amount of oxidant, which for most practical applications is molecular oxygen. Conventionally, oxygen has been supplied to oxygen dependent reactions by passing air through the liquid reaction medium, as with submerged fermentation processes [4]. Unfortunately, the solubility of oxygen in aqueous media is very low (0.267 mM in water at ambient conditions), which greatly limits the driving force available for oxygen transfer. Therefore, the supply of oxygen often limits the maximum rate of oxygen dependent biocatalytic reactions [5,6] .

Oxygen supply problems have been studied extensively in the scientific literature on aerobic fermentation processes. The primary reason for this is that oxygen supply is one of the main cost drivers, besides the cost of substrate, for highly intensified fermentation processes, e.g. microbial fermentations [7]. High intensity fermentations are all performed in stirred tank reactors or bubble columns using air (and in a few cases using oxygen enriched air) to supply oxygen. Alternative oxygen supply methods are typically only considered for low intensity processes where the conventional methods limit the performance of the process, for example in mammalian cell cultures where bubbling and intensive stirring can cause loss of cell viability, which can be solved by applying gentle aeration to the reactor through membranes [8].

Biocatalytic oxidation reactions are very similar in nature to aerobic fermentation processes, although there are a number of important differences. First, the concentration of biocatalyst (either in the form of resting, but metabolically active, whole-cells or free enzymes), and thereby the oxygen consumption rate, can be chosen independently to match the required productivity and the rate of upstream and downstream processes. This means that the oxygen requirement is almost constant throughout the reaction, unlike fermentations were the consumption will increase with time due to the increased biomass concentration.

Secondly, enzymes in solution can be readily deactivated by the conditions experienced in a bubble aerated stirred tank [9]. Oxidizing agents present in the medium, such as oxygen or hydrogen peroxide, may damage the enzyme by oxidizing amino acid residues, especially methionine and cysteine, on the surface or interior of the enzyme whereby the enzyme structure is disturbed or catalytically active amino acids modified, thus leading to enzyme deactivation [10,11]. There exist several examples in the literature showing how oxidation of surface amino acids can be circumvented by exchanging the amino acids prone to oxidation using protein engineering, especially in cases where the hydrogen peroxide is required as a substrate for the enzyme [12,13]. In addition to oxidation of amino acids residues, free enzymes in solution can be very sensitive to gas-liquid interfaces to which they adhere and unfold, eventually causing the enzymes to aggregate and thereby deactivate [14–17]. Improving the stability in presence of gas-liquid interfaces have shown to be difficult although

sometimes possible using immobilization, surface active agents and to some extent protein engineering [10,14,17,18]. Enzyme deactivation by gas-liquid interfaces is typically accompanied by excessive foaming. Foaming is not unknown in fermentations where it is dealt with using anti-foam solutions. However, the process of enzyme deactivation at the gas-liquid interface cannot always be avoided by adding anti-foam solutions, which might even contribute to further biocatalyst deactivation [19].

Thirdly, the substrates and products in biocatalytic oxidations are typically small organic molecules, which are rarely part of the primary metabolism of typical microorganisms. Often these compounds are hydrophobic, with a low aqueous solubility and are frequently volatile. The slow gas-liquid transfer of oxygen means that large volumetric air flow rates are required to create a sufficient gas-liquid interface. Typically, up to two volumes of air per volume of reaction mixture per minute (vvm) is required. At such aeration rates, even compounds with low volatility evaporate to an extent that may significantly reduce the product yield and therefore cannot be ignored (e.g. benzaldehyde [20]). Furthermore, the mole fraction of such compounds in the off-gas will be very low, which makes recovery from the off-gas by condensation ineffective.

Fourthly, carbon dioxide is not produced, or to a limited extent from metabolism when applying whole-cells, in most biocatalytic oxidations. Removal of CO_2 from the media is therefore not a concern as it is during aerobic fermentations, especially when operating under elevated pressure [21].

The oxygen consumption rate in biocatalytic processes is determined by the concentration of biocatalyst present. Unlike fermentations, where the vast majority of supplied oxygen are spend by the cells for generating energy via oxidative phosphorylation, biocatalytic reactions use the supplied oxygen directly to oxidize the substrate. This result in productivities for biocatalytic oxidations of up to 10-40 kg m^{-3} h^{-1} opposed to 2-5 kg m^{-3} h^{-1}, which is considered the minimum requirement for industrial implementation. As an example, a biocatalytic oxidation process producing a 100 g mol^{-1} product at a rate of 20 kg m^{-3} h^{-1} using an oxidase will require an oxygen supply rate of 100 mol m^{-3} h^{-1}. Such oxygen transfer rate is typically close to the limit of most industrial stirred bioreactor using air for aeration [22].

3.2.1 Technology options

Bubble aeration in stirred tanks result in a number of downsides in terms of limited oxygen transfer rates, destabilization of some enzyme due to gas-liquid interfaces and loss of volatile compounds via evaporation. Combined with the relative high cost of aeration, this creates a significant incentive to consider and develop alternative oxygen supply methods, which has the potential to reduce the cost of aeration, increase oxygen transfer rates, avoid a direct gas-liquid interface, or reduce the volumetric flow rate of gas through the reactor. Several alternative oxygen supply methods have been described in the scientific literature. This paper focuses on the most promising alternatives to the traditional stirred tank reactor, namely sparging of stirred tanks with enriched air, pressurization of stirred reactors to moderate lev-

els, membrane aeration with the membrane module submerged in the reactor or as an external module with media recirculation, and generation of oxygen *in situ* by decomposition of hydrogen peroxide (Figure 3.1). Other oxygen supply methods exist, such as novel agitated reactors [23], oxygen vectors to promote oxygen transfer [24], dynamic membrane aeration [8], and microbubble aeration [25]. These technologies are not considered here since they are deemed too far from application in industrial biocatalysis. Furthermore, bubble columns and airlift reactors will not be considered because the cost of oxygen transfer for these technologies typically are very similar to the cost for stirred tank reactors, especially at the modest maximum scale considered in this paper (100 m^3) [26].

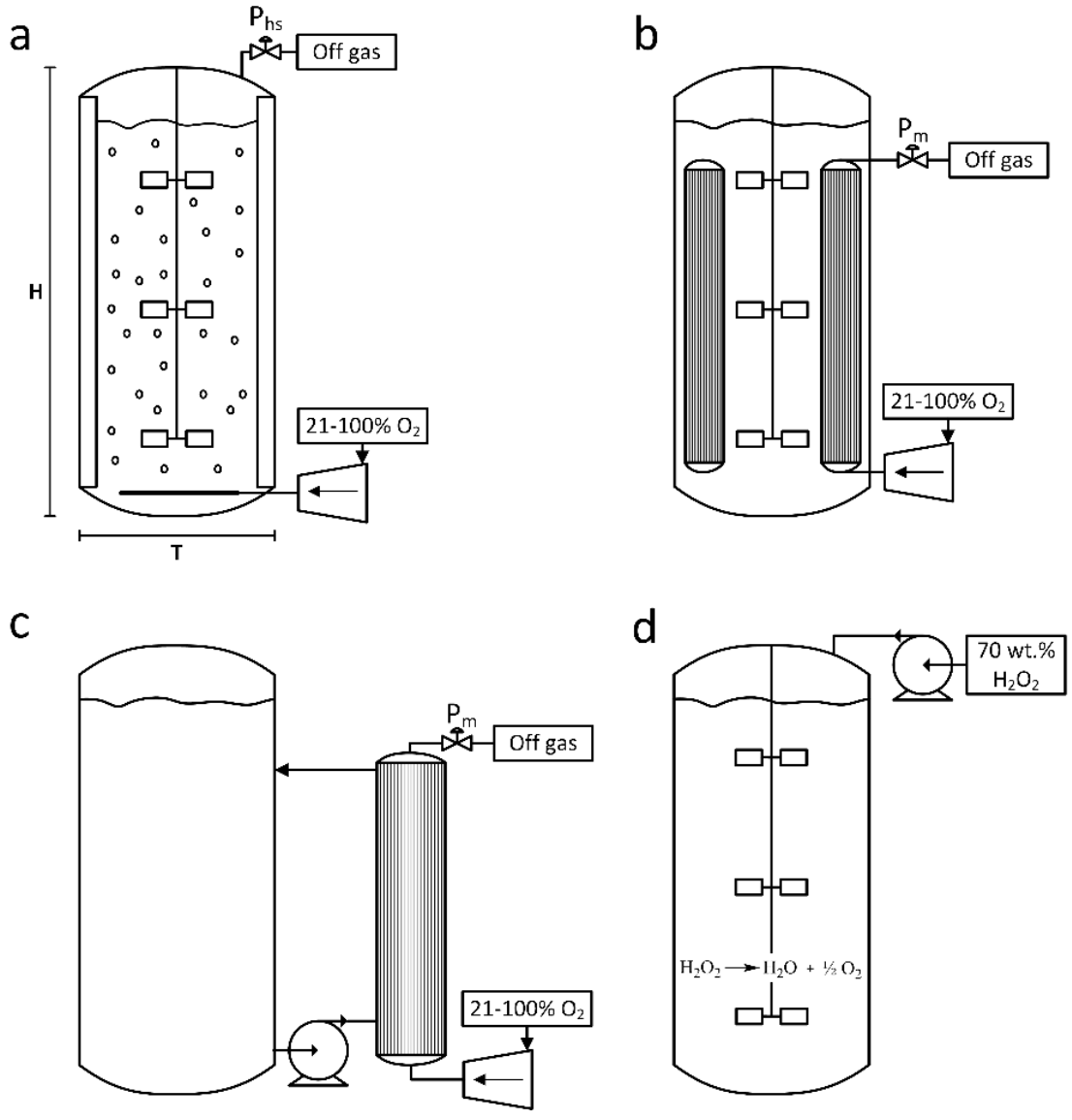

Figure 3.1. Investigated oxygen supply methods. a) stirred tank reactor (STR) with possibility of sparging enriched air and increasing headspace pressure. b) membrane reactor with submerged membrane modules (SMR). c) membrane reactor with external membrane module (EMR). d) generation of oxygen by decomposition of hydrogen peroxide by catalase

Enriched air sparging and pressurization of stirred reactors
Enriched air sparging and pressurized operation of bubbled stirred tanks are both obvious ways of increasing the oxygen transfer rate that have gained significant interesting [27–29], as the increased partial pressure of oxygen in the sparging gas increase the driving force for oxygen transfer. Both types of operation have the potential to limit the evaporation of volatile compounds. At increased headspace pressures, the effect comes from a combination of a reduction in molar fraction in the gas phase to match the vapor pressure of the volatile solute and reduced aeration rate to supply a given amount of oxygen due to the increase driving force for oxygen transfer. For enriched air sparging, only the latter effect helps to reduce evaporation.

Although both methods effectively increase the oxygen transfer rate, implementation in industrial bioprocesses are limited. Typically a slight overpressure is applied in most large-scale fermentations to decrease the risk of contamination, while enriched air applications are limited to very high cell density fermentations [30–32]. A reason for the limited implementation is the increased cost of equipment as well as compressor operation in the case of pressurized reactors and the cost of pure oxygen in the case of enriched air applications [28,32].

Membrane aeration
Membrane aeration offers the possibility to supply oxygen without exposing enzymes to a gas-liquid interface, thus avoiding deactivation of interface sensitive enzymes [15]. Furthermore, membrane aeration may also decrease evaporation of volatile compounds due the ability to pressurize the gas-side of the membrane. The technology has primarily been studied for application in wastewater treatment [33–35], but laboratory examples for biocatalytic reactions also exist [15,36,37]. Membrane aeration typically applies membranes in the form of hollow fibers with the liquid to be aerated flowing either in the fiber lumen or the shell side of the membrane. The hollow fibers can be arranged in two configurations: as a submerged membrane module inside a stirred reactor or as an external membrane module through which the reaction media is circulated. The external membrane module enables simplified scale-up and enhancement of oxygen transfer rates in existing equipment, due to the modular nature of the membrane modules. On the other hand, external membrane aeration requires large circulation rates though the membrane module, which need significant power input and might induce enzyme damage depending on the type of pump applied [16]. Although gaining significant interest, membrane aeration (and membrane contacting in general) is still an area of membrane technology yet to be fully commercialized [38].

Hydrogen peroxide decomposition
An interesting approach to overcome the limited mass transfer rate of oxygen to an aqueous solution is to supply chemically bound oxygen in the form of hydrogen peroxide. By applying the enzyme catalase, hydrogen peroxide can be decomposed to water and oxygen. Since catalase is already present in many biocatalytic oxidations due to the formation of hydrogen peroxide as a by-product during the oxidation, the additional enzyme requirement will be low. The method has limited applicability in fermentations, since sufficient removal of CO_2

cannot be sustained due to the lack of gas sparging, unless the hydrogen peroxide feeding is used as a supplement to sparged aeration [39]. However, for biocatalytic oxidations, where stripping of CO_2 is not required, the method has been demonstrated successfully [40,41]. Hydrogen peroxide enables a supply of oxygen decoupled from the concentration of oxygen in solution (up to the solubility limit of pure oxygen where bubbles start to form). Hence, a biocatalytic process can be operated at oxygen concentrations not economically possible when using oxygen supplied from a gas phase. This is especially important for enzymes with a Michaelis constant for oxygen close to (or above) the solubility of oxygen in water at atmospheric conditions [20]. Immobilized enzymes are typically not an option for oxidation reactions due to the difficulty of supplying oxygen in a solid-liquid-gas system. However, by co-immobilizing catalase and an oxygen dependent enzyme it has recently been shown that oxygen can be generated from supplied hydrogen peroxide in the close vicinity of the oxygen consuming enzyme, thereby locally increasing the oxygen concentration to high levels resulting in faster catalysis [42].

Hydrogen peroxide is a strong oxidant, has a large energy content and an unstable nature. Safe handling at industrial scale requires an aqueous concentration below 70% (w/w) [43]. The decomposition of hydrogen peroxide is an exothermic reaction (ΔH_r: 100.4 kJ mol^{-1} [44]), oxygen supply via decomposition of hydrogen peroxide will therefore increase requirements for cooling of the reaction medium to keep the temperature at the desired level. Thus, heat removal capacity could potentially set a limit to the maximum oxygen transfer rate achievable, especially at large scale. Problems with oxidation of amino acids on the surface of enzymes inevitable become more important when supplying oxygen via hydrogen peroxide decomposition [41]. In particularly as the scale of operation increases, insufficient mixing can create zones of high concentrations of hydrogen peroxide, which potentially can inactive the enzymes present. Thus, the need for designing enzymes robust towards oxidation agents still prevails [45].

Recently, it has also been shown that other oxygen containing compounds such chlorite (ClO_2^-) can be applied together with an appropriate enzyme such as chlorite dismutase for the generation of oxygen [46]. Such compounds might alleviate some of the drawbacks of hydrogen peroxide decomposition, although the system has not been demonstrated at scales larger than a few milliliters.

The above described technologies are often mentioned in various scientific publications as ways to reduce the cost of oxygen transfer, increase oxygen transfer rates or improve process performance. However, such statements are rarely backed-up by cost estimations and direct technical feasibility comparisons. The aim of this study is to provide such a comparison for the most promising oxygen supply methods for biocatalytic oxidations and benchmark these against the conventional stirred tank reactor. The uncertainties associated with early-stage cost estimations and their impact on the cost of oxygen supply are evaluated using Monte Carlo based sensitivity analysis to give the most realistic prediction of the cost of transferring oxygen using the evaluated technologies. To the authors' knowledge, this is the first example

in the scientific literature of a direct economic comparison of alternative oxygen supply methods.

Table 3.1. Advantages and disadvantages of the investigated oxygen supply methods.

Technology	**Advantages**	**Disadvantages**
Bubble aeration of stirred tank	• Well known technology	• Gas-liquid interface • Limited oxygen transfer capabilities
- ***Pressurized***	• Increased driving force for oxygen transfer • Potentially limit evaporation of volatile compounds	• Additional compression and reactor cost
- ***Enriched air***	• Increased driving force for oxygen transfer • Potentially limit evaporation of volatile compounds due to decreased aeration rate at same oxygen transfer rate	• Cost of pure oxygen
Submerged membrane aeration	• No gas-liquid interface • Reduce foaming issues	• The membrane introduce an additional barrier to oxygen transfer • Cost of membrane material
External membrane aeration	• No gas-liquid interface • Simplified scale-up • Possible to increase oxygen supply rate at a later stage by installation of additional membrane modules.	• The membrane introduce an additional barrier to oxygen transfer • Cost of membrane material • Requires high circulation rates through the membrane module • Potential damage of biocatalyst in recirculation pump
H_2O_2 decomposition	• No gas-liquid interface • Reduce foaming issues • Oxygen transfer rate decoupled from oxygen concentration • Direct control of oxygen supply rate • Almost unlimited oxygen supply rate	• Potential damage of biocatalyst by locally high H_2O_2 concentrations due to imperfect mixing • Risk of bubble formation and loss of oxygen due to local oversaturation • Cost of H_2O_2 • Increased cooling requirement due to heat of reaction

3.3 Results and discussion

The results presented are the overall results of the study, for a more detailed analysis of the results see Section 4 and 5 of the Supporting Information (S.I.).

3.3.1 Bubble aeration of stirred reactor

The cost of oxygen transfer when applying bubble aeration of stirred reactors was found to be largely driven by the capital expenses and fixed operating cost (Figure 3.3). The variable operating costs (i.e. cost of electricity for agitation and compression) only accounts for small part of the total cost, for example 13% of the cost of oxygen transfer for a 100 m^3 unpressurized stirred tank reactor using air for aeration (Figure 3.2). This correlates well with the sensitivity analysis, which found that the uncertainty on the capital cost estimation and the volumetric mass transfer coefficient explains the largest part of the uncertainty on the prediction of cost of oxygen transfer. When applying pure oxygen for sparging, the large uncertainty on the cost of oxygen also had a significant influence. Other parameters, such as agitator and compressor efficiency and cost of electricity, only had a minimal impact on uncertainty of the predicted cost.

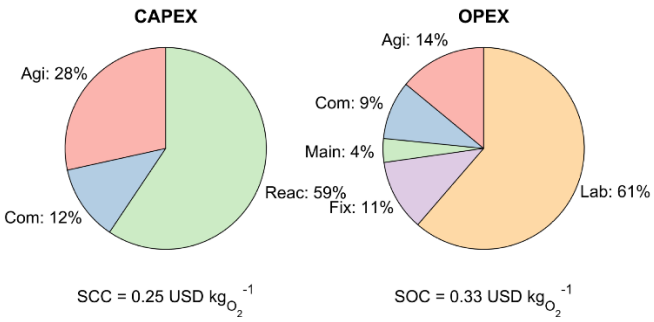

Figure 3.2. Cost distribution for bubble aeration of a stirred tank operated at an oxygen transfer rate of 50 mol m^{-3} h^{-1}. Agi: Agitation, Com: Compression, Reac: Reactor, Main: Maintenance, Fix: Fixed operating costs, Lab: Labor, SCC: specific capital cost, SOC: specific operating cost. See S.I. for cost distributions for other investigated technologies.

The effect of enriched air sparging and pressurization on the total cost of oxygen supply was investigated (A.14-A.15). It was found that neither increased headspace pressure nor enriched air sparging resulted in a significant reduction in the specific oxygen transfer cost. Increasing the headspace pressure could at best result in a cost decrease of a few percent with an optimum pressure of around two bars, depending on the oxygen transfer rate. For enriched air sparging, the decrease in capital cost due to decreased compression and agitation requirements was cancelled out by the increased operating costs due to the consumption of pure oxygen. Partially enriching air with pure oxygen resulted in a higher cost of oxygen transfer than when using pure oxygen for sparging, since the benefit of a high partial pressure of oxygen throughout the reactor is not realized when sparging with partially enriched air.

Problems with evaporation of volatile compounds can potentially be alleviated by increasing the headspace pressure or sparging with enriched air. For an oxygen transfer rate of 50 mol m^{-3} h^{-1} in a 100 m^3 reactor, the aeration required when sparging with air and operating at atmospheric pressure, sparging with air and operating at 10 bar, and sparging with oxygen

at atmospheric conditions are 0.21, 0.13, and 0.03 $Nm^3\ m^{-3}\ min^{-1}$, respectively. In terms of rate of evaporation, this corresponds to a reduction of 16 and 7 times for pressurization to 10 bars and pure oxygen sparging, respectivelym when assuming that the gas leaving the reactor is saturated with the volatile compound. Although not reducing the cost of oxygen supply, pressurization or pure oxygen sparging could be used to decrease the evaporation rate of volatile compounds and increase the maximum oxygen transfer beyond the limit using air sparging ($\approx$ 300 mol $m^{-3}\ h^{-1}$ based on the current assumptions).

3.3.2 Membrane aeration

Both submerged and external membrane aeration has a significantly higher cost of aeration compared to stirred tank reactor technology (Figure 3.3). The high cost is primarily related to the membrane cost, which for operation at atmospheric headspace pressure using air accounts for 74% and 49% of the total cost for submerged and external membrane aeration, respectively (Figure 2, A.4 and A.7). For external membrane aeration, the electricity cost of recirculating the liquid is the second biggest contributor to the total cost of oxygen transfer, accounting for 26% of the cost. The above observations were confirmed in the sensitivity analysis which showed that the cost of the membrane and the mass transfer coefficient through the membrane are the most important parameters for the uncertainty on the predicted cost of oxygen transfer for both the submerged and external membrane configuration. Although, the uncertainty on the capital cost estimation also becomes important when operating the reactor and membrane module under pressure.

The options to decrease the cost contribution from the membrane are limited to increasing the driving force for oxygen transfer by pressurizing the reactor and membrane module or applying pure oxygen in the membrane fibers. Additionally, an increased operating pressure also decrease the amount of media that needs to be recirculated through the external membrane module, since more oxygen can be solubilized in the media due to the higher pressure. The optimal pressure is very dependent on the oxygen transfer rate required, as an example the optimal pressure is 10 bar for the submerged membrane configuration at an oxygen transfer rate of 50 mol $m^{-3}\ h^{-1}$, while it is 41 bar at an oxygen transfer rate of 200 mol $m^{-3}\ h^{-1}$ (Figure A.18). Therefore, a pressure of 25 bar was chosen for the overall comparison (Figure 3.3-3.5). Interestingly, the benefit increasing headspace pressure depends on the scale of operation. At 10 m^3 scale the capital cost contribution dominates the total cost of oxygen supply. Therefore, the increase in reactor cost as pressure is increased is not outweighed by the decrease in membrane and pumping cost as it is the case for a 100 m^3 reactor (Figure 3.3).

The maximum oxygen transfer for membrane aeration depends on membrane configuration. For the submerged membrane module the maximum transfer rate is bounded by the membrane area that physically can fit into the reactor, which for unpressurized reactor operation and applying air results in a maximum oxygen transfer rate of 60 mol $m^{-3}\ h^{-1}$. When applying pure oxygen inside the membrane fibers, the maximum oxygen transfer rate is increased to 220 mol $m^{-3}\ h^{-1}$, while the maximum is beyond the investigated range when applying both

25 bar of pressure and pure oxygen. For external membrane aeration, the oxygen transfer rate is limited by the recirculation rate through the external module, which is limited to 10 reactor volumes per hour. This corresponds to a maximum 150 and 690 mol m^{-3} h^{-1} for unpressurized reactor operation, using air and pure oxygen, respectively. When pressurized the reactor and module to 25 bar the maximum oxygen transfer rate is beyond the investigated range.

3.3.3 Hydrogen peroxide decomposition

In situ oxygen generation by hydrogen peroxide decomposition is costly relative to the other technologies, due to the cost of hydrogen peroxide (700-1200 USD MT^{-1}[43]). This correspond to a cost of oxygen supply in the range of 1.5-2.35 USD kg_{O2}^{-1}, only covering the cost of H_2O_2 and not capital or other operating expenses. This translates into high operating costs compared to the other investigated technologies, whereas the capital cost are very low since no aeration and only modest agitation is required. The importance of the cost of hydrogen peroxide is also obvious from the sensitivity analysis, where the uncertainty on the cost of hydrogen peroxide can describe 71% of the variance in total cost of oxygen supply (Figure A.25). Other cost, such as cost of catalase and hydrogen peroxide tolerance of the biocatalyst, only constitutes a minor part of the total cost and are therefore less important when explaining the uncertainty on the cost of oxygen supply. Overall, the total cost of supply oxygen is higher than for most of the other investigated methods.

3.3.4 Economic comparison

Figure 3.3 compares the cost of oxygen transfer for the investigated technologies at an oxygen transfer rate of 50 mol m^{-3} h^{-1} for medium and large scale operation. A significant part of the cost of oxygen is related to fixed OPEX, which in this case includes cost of labor, especially at 10 m^3 scale. This is due to the smaller scale that has a higher specific CAPEX, which the fixed OPEX is calculated based on, and a higher specific labor cost due to a lower total oxygen transfer because of the smaller reactor volume.

Intuitively, the cost of transferring oxygen in stirred tanks would increase with increasing oxygen transfer rate due to the relationship between the volumetric oxygen transfer coefficient and the power input and superficial space velocity. Although this is true for the cost of aeration and agitation [21], it is not so when accounting for the capital and fixed operating costs. The specific total cost of oxygen transfer in fact decrease with increasing oxygen transfer rate (Figure 3.4). This is because the capital cost can be spread across a larger total oxygen supply, thereby decreasing the specific capital cost. The operational costs not including labor and fixed OPEX increase with increasing oxygen transfer rate for stirred tank aeration (Figure 3.5), as one would expect. Interestingly, the operational costs do not change significantly when increasing the scale from 10 m^3 to 100 m^3, although the oxygen transfer rate typically are reported to increase with increasing scale due to a higher superficial gas velocity at otherwise comparable conditions [56]. However, such effects are minor when increasing the scale from 10 m^3 to 100 m^3, and therefore not directly visible given the uncertainties.

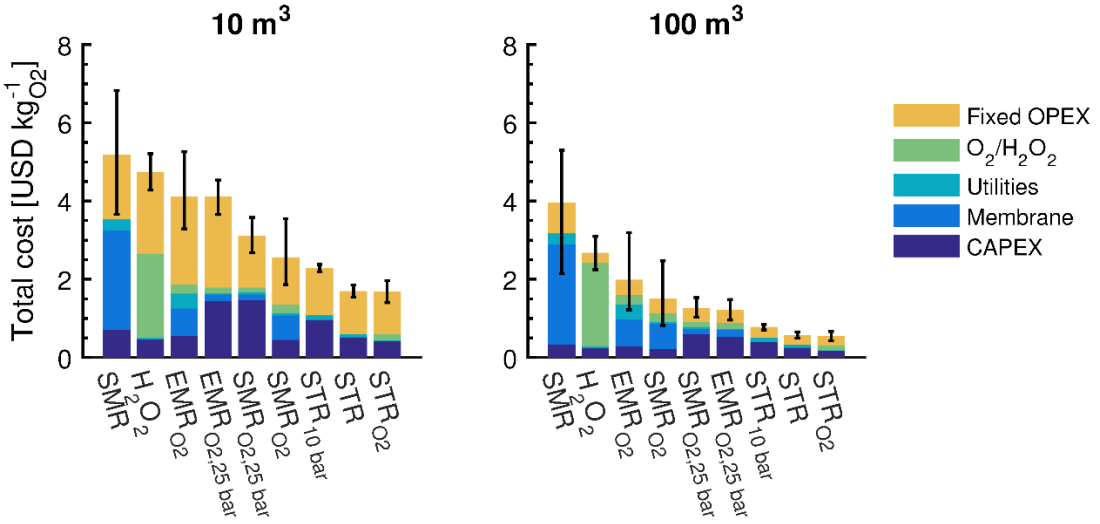

Figure 3.3. Specific cost of oxygen transfer for the compared technologies at an oxygen supply rate of 50 mol m^{-3} h^{-1}. STR: Stirred tank reactor, SMR: Submerged membrane reactor, EMR: External membrane reactor, H_2O_2: hydrogen peroxide decomposition by catalase, O2: pure oxygen supply, xx bar: headspace pressure of reactor.

The comparison shows that the alternative oxygen supply methods considered, in general cannot reduce the cost of oxygen transfer compared to the stirred tank reactor technology. The difference between the investigated technologies depends on the scale of operation. At medium scale operation (10 m^3) the relative difference between bubble aeration in a stirred tank reactor and the alternative oxygen supply methods are smaller than at the larger scale, where the economics of scale are more beneficial for the stirred tank reactor. This is primarily due to the membrane cost, which is not dependent in the scale of operation, and operational costs domination the total cost of oxygen supply for hydrogen peroxide decomposition. Pressurization of the reactor headspace significantly reduces the cost of aeration when using membrane technology, and, at 10 m^3 scale, even to levels comparable with the stirred tank reactor technology. However, it should be noted that there could be additional cost associated with increasing the pressure of the membrane module and reactor not accounted for in analysis, especially when increasing the pressure beyond 5-10 bars, as no examples of such have been reported.

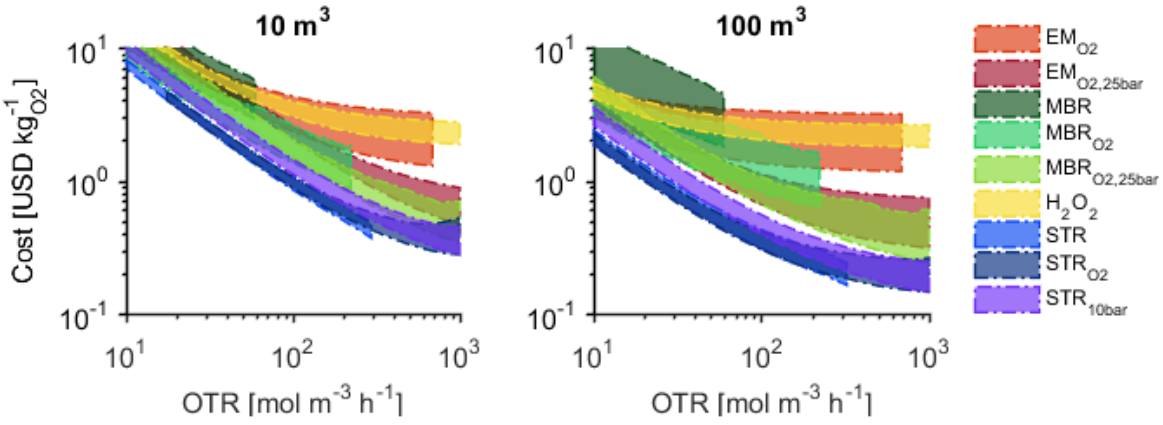

Figure 3.4. Total cost of oxygen transfer as a function of oxygen transfer rate for the investigated technologies. The area represents the uncertainty on the cost estimation represented as the 10th to the 90th percentile.

The analysis presented in this paper focuses on construction of a new plant. However, for biotechnology in general, and biocatalysis in particular, production is often established in existing equipment being retrofitted for the specific application. A comparison of total cost may therefore not be useful, since this covers a range of costs already depreciated and therefore not relevant when retrofitting existing equipment. A direct comparison of the total cost of retrofitting is difficult, since this will change depending on the existing equipment. Therefore, the operating costs, excluding cost of labor and fixed OPEX, have been compared in Figure 3.5, as this gives the best comparison when evaluating retrofitting options, although there can be significant differences in capital costs associated with the technologies. In general, it can be noted that the pressurized membrane technologies potentially can result in comparable operating costs to those expected for stirred tank reactors.

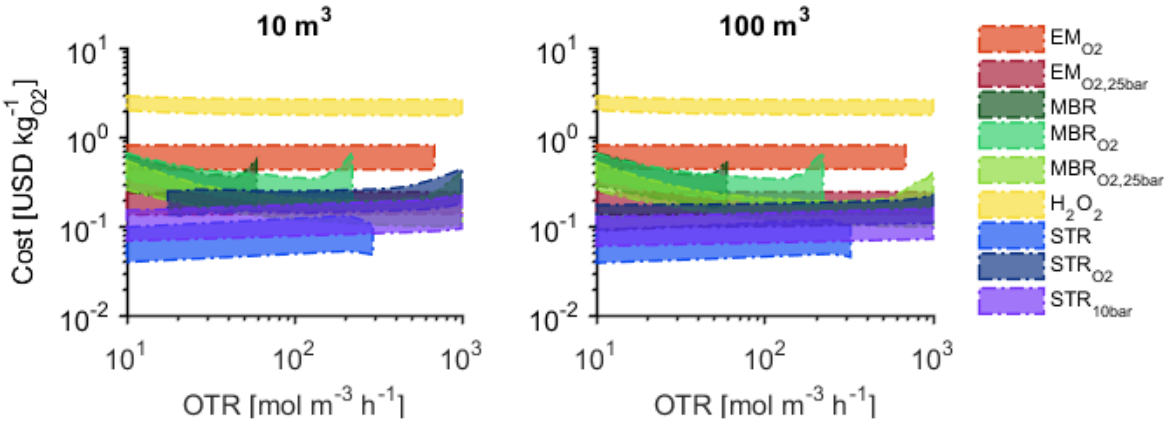

Figure 3.5. Specific operating cost (not including labor and capital related expenses) as a function of oxygen transfer rate for the investigated technoliges. The area represents the uncertainty on the cost estimation represented as the 10th to the 90th percentile.

The cost of oxygen transfer has to be put in context of the value of the product being produced. For a typical small organic molecule (MW 100 g mol^{-1}) oxidized using an oxidase, which requires ½ mol of oxygen per mol of product, the oxygen requirement is 0.16 kg_{O2} $kg_{product}^{-1}$. At a scale of 100 m^3 and an oxygen transfer rate of 50 mol m^{-3} h^{-1}, this corresponds to a cost contribution from oxygen supply to the final processing cost of 0.1 USD $kg_{product}^{-1}$ for bubble aeration in a stirred tank. For the alternative oxygen supply methods, the cost contribution from oxygen supply is up 6.9 times higher. Typically, large scale biocatalytic production (>100 m^3) implies a large volume chemical in the cost range of specialty (≈ 5 USD $kg_{product}^{-1}$) or bulk chemicals (≈ 1 USD $kg_{product}^{-1}$) [55]. For a single oxidation step, the contribution from substrate cost is typically high, meaning that the allowable processing cost is low. Thus, a contribution of 0.1 USD $kg_{product}^{-1}$ from aeration will be significant, even when considering that this cost also covers the cost of the reactor and that the cost contribution for bubble aeration is reduced with increasing productivity, e.g. 0.06 USD $kg_{product}^{-1}$ at an oxygen transfer rate of 100 mol m^{-3} h^{-1}. This means that alternative oxygen supply methods, e.g. applying membrane aeration to improve the stability of the biocatalyst, is not an option at this scale.

For a smaller scale production in a 10 m^3 vessel, the cost contribution from aeration corresponds to 0.3 USD $kg_{product}^{-1}$ when applying bubble aeration at an oxygen transfer rate of 50 mol m^{-3} h^{-1}. At this scale, the value of the products produced typically are higher, e.g. fine- or pharma-chemicals with product costs of >15 USD kg^{-1} and >100 USD kg^{-1}, respectively [55]. The higher product cost means that the contribution from oxygen supply will be insignificant. Application of alternative oxygen supply methods is therefore a possibility at this scale, giving process engineers the possibility to optimize the conditions to maximize enzyme stability, reduce evaporation of volatile reaction species and maximum enzyme utilization.

The above analysis compares the cost of oxygen transfer without including economic effects from elimination or reduction of the current shortcomings of the unpressurized bubble aeration in stirred reactors. Quantification of cost savings from reduced evaporation of volatile compounds or reduced enzyme deactivation rate is difficult, and has to be evaluated on case-by-case basis. However, the above analysis gives an overview of the costs associated with choosing an alternative oxygen supply method, in case such method can alleviate problems experienced during process development. In these cases, the increased cost of oxygen supply has to be compared with the cost of alternative methods of circumventing the problems, e.g. engineering of the biocatalyst to alleviate gas-liquid sensitivity problems or capturing of volatile compounds from the off-gas using condensation.

3.4 Conclusions

Bubble aerated stirred tank reactors have been used for conducting aerobic bioprocesses for decades, although often criticized for being expensive and inefficient. In this analysis, alternative oxygen supply methods for biocatalytic oxidations were compared with the traditional stirred tank reactor in terms of technical feasibility and cost of oxygen transfer. The investigated supply methods covered pressurized and enriched air aeration in stirred tanks, submerged membrane aeration, external membrane aeration, and *in situ* oxygen generation by decomposition of hydrogen peroxide. It was found that the investigated alternative oxygen supply methods in general cannot deliver oxygen more cost effectively than traditional bubble aeration. Consequently, there is no real alternative to bubble aeration when producing a specialty or bulk chemical at very large scale (>100 m^3). However, for the production of higher value chemicals at smaller scale (10 m^3) the cost contribution from oxygen supply is insignificant, meaning that alternative oxygen supply is a possible alternative in cases where they could improve process performance, e.g. by increasing the stability of the applied enzyme.

3.5 Methods

The investigated oxygen transfer methods are compared on a basis of cost per amount of oxygen transferred to the liquid reaction media (USD $kg_{O_2}^{-1}$). The operational and capital expenses were calculated using generally accepted methods [47,48]. All cost calculations, equipment sizing and Monte Carlo simulations were performed in MATLAB (MathWorks, Natick, MA, USA).

3.5.1 Basic assumptions

The cost of oxygen transfer was calculated based on operating expenses, e.g. compression and agitation costs, and capital expenses, which takes into account the bioreactor itself and important auxiliary equipment such as compressor, membrane modules, etc. The most important exception was that cooling was not included in the cost analysis, as this in general will be the same for the investigated technologies. The exception being oxygen generation by hydrogen peroxide decomposition, where the reaction generates additional heat. However, the additional cost related to the cooling will be low compared to other operational costs, but could eventually limit the maximum scale of operation.

The cost of oxygen transfer is highly dependent on the rate of oxygen transfer. This is not only because of a higher specific energy requirement at high oxygen transfer rates, but also because the capital costs can be divided into larger amounts of transferred oxygen at high transfer rates, i.e. the specific capital cost per transferred kg of oxygen will be lower at a high oxygen transfer rate [21]. The oxygen transfer rate was varied from 10 to 1000 $mol/m^3/h$, corresponding to typical slow reaction and a highly intensified process, although the latter would be difficult to obtain in practice for many enzymes due to other process constraints.

Aerobic fermentations are conducted in bioreactors of up to several hundred cubic meters for bulk scale production. Although biocatalytic oxidations are not implemented in the industry to the same extent as fermentations, the size of reactors required are substantial to obtain the economic benefits of scale. However, as for fermentations, biocatalytic oxidations may also be applied in smaller, more specialized, production where reactor sizes of only few cubic meters are required (e.g. in pharmaceutical production). The cost of oxygen transfer will be highly dependent on the scale of production, therefore two reactor volumes were considered in the analysis, a small production scale with a liquid filling volume of 10 m^3 and a large production scale with a filling volume of 100 m^3.

The dissolved oxygen (DO) concentration directly affects the driving force for oxygen transfer in all oxygen supply methods except the hydrogen peroxide/catalase system. On the other hand, the DO also affects the specific reaction rate (i.e. $kg_{product}\ kg_{enzyme}^{-1}\ h^{-1}$) since the Michaelis constant for oxygen (K_{MO}) typically is close to or above the solubility of oxygen in water at ambient conditions [20]. This means that at low DO the enzyme will be used inefficiently (i.e. more enzyme is required) while the oxygen transfer is very efficient, and vice versa. The optimal DO in terms of total cost will depend on the enzyme cost and activity.

For the sake of simplicity, a constant DO of 20% of air saturation (25 °C, 1 atm) was assumed, corresponding to a concentration of 54 µM O_2.

3.5.2 Capital and operating expenses

The total capital expenditure (CAPEX), including both working capital and direct and indirect costs, was estimated based on the total equipment cost multiplied with the Lang Factor, which for a fluid processing plant is 5 [47]. The cost of individual equipment was based on publicly available data sources, scaled using power relationships, and updated to 2015 price levels using the Chemical Engineering Plant Cost Index (CEPCI). The CAPEX was calculated on a basis of the amount of oxygen transferred to the reaction medium by assuming an amortization over 10 years, an operating time of 5840 hours per year (16 h batch times, 1 batch per day), and an interest rate of 7%. See Supporting Information (S.I.) for a detailed list of equipment costs, assumptions and cost calculations.

The operating expenditure (OPEX) covers the cost of raw materials, utilities, labor, maintenance, and fixed costs (insurance, taxes, etc.). Raw material and utility requirements were obtained from the sizing of equipment. Labor costs were calculated based on the assumption that 1 worker is required per large scale bioreactor (100 m^3) and 0.5 worker is required per small scale bioreactor (10 m^3). Maintenance and fixed costs were taken as 5% and 15% of the capital cost, respectively [47]. See S.I. for a complete list of values used to calculate OPEX.

3.5.3 Sensitivity analysis

Typically, early stage CAPEX estimations are subject to uncertainties of ±30% [47], while the uncertainties in OPEX estimates are dependent on the equipment size estimates and costs of materials and labor. Sensitivity analyses were conducted for each oxygen supply method to evaluate the importance of the uncertainty on the input parameters on the estimated cost of oxygen transfer [49]. Monte Carlo simulations were applied to estimate the output uncertainty, and Latin Hypercube Sampling was used to obtain 500 samples from uniformly distributed uncertainties on the input parameters. The key parameters change depending on the oxygen supply method, Table 3.2 gives the input parameters considered in the analysis and the uncertainties for each of the technologies investigated.

The maximum oxygen transfer that can be sustained by a given technology varies with the parameters changed in the uncertainty analysis. The oxygen transfer rate was said to be achievable if more than 25% of the Monte Carlo simulations returned a feasible solution.

Table 3.2. Key parameters and uncertainties for each of the oxygen supply technologies.

Parameter	Unit	Base value	Uncertainty range	Reference
General parameters				
Capital cost index[a,b]	-	1	0.7-1.3	[47]
Electricity	USD kWh^{-1}	0.13	0.06-0.17	[50]
Aerated Stirred tank reactor				
Volumetric mass transfer coefficient index[b]	-	1	0.7-1.3	[51]
Compressor efficiency	-	0.7	0.6-0.8	[47]
Agitator efficiency	-	0.75	0.65-0.85	[47]
Pure oxygen	USD MT^{-1}	80	50-110	[31,52]
Submerged membrane aeration				
Membrane	USD m^{-2}	160	60-260	[38,53,54]
Mixing	kW m^{-3}	0.5	0.25-0.75	*Estimation*
Mass transfer coefficient	mol h^{-1} bar^{-1} m^{-2}	0.2	0.05-0.3	[34]
Compressor efficiency	-	0.7	0.6-0.8	[47]
Agitator efficiency	-	0.75	0.65-0.85	[47]
Pure oxygen	USD MT^{-1}	80	50-110	[31,52]
External membrane aeration				
Membrane	USD m^{-2}	160	60-260	[38,53,54]
Mass transfer coefficient	mol h^{-1} bar^{-1} m^{-2}	0.2	0.05-0.3	[34]
Pressure drop	Bar	3	2-4	*Estimation*
Compressor efficiency	-	0.7	0.6-0.8	[47]
Pump efficiency	-	0.7	0.6-0.8	[47]
Pure oxygen	USD MT^{-1}	80	50-110	[31,52]
Hydrogen peroxide decomposition				
H_2O_2 (100 wt.% basis)	USD MT^{-1}	950	700-1200	[43]
Mixing	kW m^{-3}	0.5	0.25-0.75	*Estimation*
Biocatalyst H_2O_2 tolerance	mol m^{-3}	1	0.2-2	[20]
Agitator efficiency	-	0.75	0.65-0.85	[47]
Catalase	USD kg^{-1}	625	250-1000	[55]

[a] Not including membrane cost. [b] Index to change the total capital cost and overall volumetric mass transfer coefficient.

3.6 References

[1] Hollmann F, Arends IWCE, Buehler K, Schallmey A, Bühler B, **2011**. Enzyme-mediated oxidations for the chemist, Green Chem. 13(2):226.

[2] Turner NJ, **2011**. Enantioselective oxidation of C-O and C-N bonds using oxidases., Chem. Rev. 111(7):4073–87.

[3] Holtmann D, Fraaije MW, Arends IWCE, Opperman J, Hollmann F, **2014**. The taming of oxygen : biocatalytic oxyfunctionalisations, Chem. Commun. 50:13180–13200.

[4] Garcia-Ochoa F, Gomez E, **2009**. Bioreactor scale-up and oxygen transfer rate in microbial processes: an overview., Biotechnol. Adv. 27(2):153–76.

[5] Baldwin CVF, Woodley JM, **2006**. On Oxygen Limitation in a Whole Cell Biocatalytic Baeyer-Villiger Oxidation Process, Biotechnol. Bioeng. 95(3):362–369.

[6] Pilone MS, Pollegioni L, **2002**. D-amino acid oxidase as an industrial biocatalyst, Biocatal. Biotransformation. 20(3):145–159.

[7] Grotkjær T, Commercial Development of Fermentation Processes, in: J. Villadsen (Ed.), Fundam. Bioeng., **2016**, Wiley-VCH Verlag GmbH & Co. KGaA, Weinheim: pp. 499–545.

[8] Frahm B, Brod H, Langer U, **2009**. Improving bioreactor cultivation conditions for sensitive cell lines by dynamic membrane aeration, Cytotechnology. 59(1):17–30.

[9] Bommarius AS, Paye MF, **2013**. Stabilizing biocatalysts., Chem. Soc. Rev. 42(15):6534–65.

[10] Brocklebank S, Woodley JM, Lilly MD, **1999**. Immobilised transketolase for carbon-carbon bond synthesis: Biocatalyst stability, J. Mol. Catal. - B Enzym. 7(1–4):223–231.

[11] Saville BA, Persi S, **1992**. The Effect of Oxygen Upon the Kinetics of Enzyme Inactivation : In vitro Investigations Using Glutamine Synthetase, Can. J. Chem. Eng. 70(6):1143–1148.

[12] Slavica A, Dib I, Nidetzky B, **2005**. Single-site oxidation, cysteine 108 to cysteine sulfinic acid, in D-amino acid oxidase from Trigonopsis variabilis and its structural and functional consequences, Appl. Environ. Microbiol. 71(12):8061–8068.

[13] Oh K-H, Nam S-H, Kim H-S, **2002**. Improvement of oxidative and thermostability of N-carbamyl-d-amino Acid amidohydrolase by directed evolution., Protein Eng. 15(8):689–95.

[14] Bommarius AS, Karau A, **2005**. Deactivation of Formate Dehydrogenase (FDH) in solution and at gas-liquid interfaces, Biotechnol. Prog. 21(6):1663–1672.

[15] Van Hecke W, Haltrich D, Frahm B, Brod H, Dewulf J, Van Langenhove H, Ludwig R, **2011**. A biocatalytic cascade reaction sensitive to the gas–liquid interface: Modeling and upscaling in a dynamic membrane aeration reactor, J. Mol. Catal. B Enzym. 68(2):154–161.

[16] Thomas CR, Geer D, **2011**. Effects of shear on proteins in solution., Biotechnol. Lett. 33(3):443–56.

[17] Wiesbauer J, Prassl R, Nidetzky B, **2013**. Renewal of the air-water interface as a critical system parameter of protein stability: Aggregation of the human growth hormone and its prevention by surface-active compounds, Langmuir. 29(49):15240–15250.

[18] Betancor L, Fuentes M, Dellamora-Ortiz G, López-Gallego F, Hidalgo A, Alonso-Morales N, Mateo C, Guisán JM, Fernández-Lafuente R, **2005**. Dextran aldehyde coating of glucose oxidase immobilized on magnetic nanoparticles prevents its inactivation by gas bubbles, J. Mol. Catal. B Enzym. 32(3):97–101.

[19] Lee BS, Kim EK, **2004**. Lipopeptide production from Bacillus sp. GB16 using a novel oxygenation method, Enzyme Microb. Technol. 35(6–7):639–647.

[20] Toftgaard Pedersen A, Birmingham WR, Rehn G, Charnock SJ, Turner NJ, Woodley JM, **2015**. Process Requirements of Galactose Oxidase Catalyzed Oxidation of Alcohols, Org. Process Res. Dev. 19(11):1580–1589.

[21] Albaek MO, Gernaey K V., Hansen MS, Stocks SM, **2012**. Evaluation of the energy efficiency of enzyme fermentation by mechanistic modeling, Biotechnol. Bioeng. 109(4):950–961.

[22] Charles M, **1985**. Fermentation scale-up: Problems and possibilities, Trends Biotechnol. 3(6):134–139.

[23] Toftgaard Pedersen A, Carvalho T, Sutherland E, Rehn G, Ashe R, Woodley JM, **2017**. Characterisation of a continous agitated cell reactor for oxygen dependent biocatalysis, Biotechnol. Bioeng. 114(6):1222–1230.

[24] Rols J., Condoret J., Fonade C, Goma G, **1990**. Mecanism of enhanced oxygen transfer in fermentation using emulsified oxygen-vectors, Biotechnol. Bioeng. 35(4):427–435.

[25] Weber J, Agblevor FA, **2005**. Microbubble fermentation of Trichoderma reesei for cellulase production, Process Biochem. 40(2):669–676.

[26] Albaek MO, Evaluation of the efficiency of alternative enzyme production technologies, Technical University of Denmark, **2012**.

[27] Kreyenschulte D, Emde F, Regestein L, Büchs J, **2016**. Computational minimization of the specific energy demand of large-scale aerobic fermentation processes based on small-scale data, Chem. Eng. Sci. 153:270–283.

[28] Knoll A, Maier B, Tscherrig H, Büchs J, **2005**. The Oxygen Mass Transfer , Carbon Dioxide Inhibition , Heat Removal , and the Energy and Cost Efficiencies of High Pressure Fermentation, Adv. Biochem. Eng. / Biotechnol. 92:77–99.

[29] Jansen MLA, van Gulik WM, **2014**. Towards large scale fermentative production of succinic acid, Curr. Opin. Biotechnol. 30:190–197.

[30] Follonier S, Panke S, Zinn M, **2012**. Pressure to kill or pressure to boost: A review on the various effects and applications of hydrostatic pressure in bacterial biotechnology,

Appl. Microbiol. Biotechnol. 93(5):1805–1815.

[31] Häusler EBG, van der Wielen LAM, Straathof AJJ, **2016**. Evaluation of gas supply configurations for microbial product formation involving multiple gaseous substrates, Bioresour. Bioprocess. 3(1):18.

[32] Lara AR, Knabben I, Regestein L, Sassi J, Caspeta L, Ramírez OT, Büchs J, **2011**. Comparison of oxygen enriched air vs. pressure cultivations to increase oxygen transfer and to scale-up plasmid DNA production fermentations, Eng. Life Sci. 11(4):382–386.

[33] Voss MA, Ahmed T, Semmens MJ, **1999**. Long-Term Performance of Parallel-Flow, Bubbleless, Hollow-Fiber-Membrane Aerators, Water Environ. Res. 71(1):23–30.

[34] Li J, Zhu L-P, Xu Y-Y, Zhu B-K, **2010**. Oxygen transfer characteristics of hydrophilic treated polypropylene hollow fiber membranes for bubbleless aeration, J. Memb. Sci. 362(1–2):47–57.

[35] Brindle K, Stephenson T, Semmens MJ, **1998**. Nitrification and oxygen utilisation in a membrane aeration bioreactor, J. Memb. Sci. 144(1–2):197–209.

[36] Van Hecke W, Ludwig R, Dewulf J, Auly M, Messiaen T, Haltrich D, Van Langenhove H, **2009**. Bubble-free oxygenation of a bi-enzymatic system: effect on biocatalyst stability., Biotechnol. Bioeng. 102(1):122–31.

[37] Rissom S, Schwarz-Linek U, Vogel M, Tishkov VI, Kragl U, **1997**. Synthesis of chiral e-lactones in a two-enzyme system of cyclohexanone mono-oxygenase and formate dehydrogenase with integrated bubble-free aeration, Tetrahedron Asymmetry. 8(15):2523–2526.

[38] Baker RW, Membrane Technology and Applications, 3rd ed., **2012**, John Wiley & Sons, Ltd., Chichester.

[39] Sonnleitner B, Hahnemann U, **1997**. Robust oxygen supply by controlled addition of hydrogen peroxide to microbial cultures, Bioprocess Eng. 17(4):215–219.

[40] Morthensen ST, Meyer AS, Jørgensen H, Pinelo M, **2017**. Significance of membrane bioreactor design on the biocatalytic performance of glucose oxidase and catalase: Free vs. immobilized enzyme systems, Biochem. Eng. J. 117:41–47.

[41] Schneider K, Dorscheid S, Witte K, Giffhorn F, Heinzle E, **2012**. Controlled feeding of hydrogen peroxide as oxygen source improves production of 5-ketofructose from L-sorbose using engineered pyranose 2-oxidase from Peniophora gigantea., Biotechnol. Bioeng. 109(11):2941–5.

[42] Bolivar JM, Schelch S, Pfeiffer M, Nidetzky B, **2016**. Intensifying the O2-dependent heterogeneous biocatalysis: superoxygenation of solid support from H2O2 by a catalase tailor-made for effective immobilization, J. Mol. Catal. B Enzym. 134:302–309.

[43] Ciriminna R, Albanese L, Meneguzzo F, Pagliaro M, **2016**. Hydrogen Peroxide: A Key Chemical for Tomorrow's Sustainable Development, ChemSusChem. 9:3374–3381.

[44] Nelson DP, Kiesow LA, **1972**. Enthalpy of decomposition of hydrogen peroxide by catalase at 25 C (with molar extinction coefficients of H2O2 solutions in the UV), Anal. Biochem. 49(2):474–478.

[45] Kim YH, Berry AH, Spencer DS, Stites WE, **2001**. Comparing the effect on protein stability of methionine oxidation versus mutagenesis: steps toward engineering oxidative resistance in proteins., Protein Eng. 14(5):343–347.

[46] Hofbauer S, Schaffner I, Furtmüller PG, Obinger C, **2014**. Chlorite dismutases - a heme enzyme family for use in bioremediation and generation of molecular oxygen, Biotechnol. J. 9(4):461–473.

[47] Peters MS, Timmerhaus KD, West RE, Plant Design and Economics for Chemical Engineers, 5th ed., **2003**, McGraw-Hill Education, New York.

[48] Biegler LT, Grossmann IE, Westerberg AW, Systematic Methods of Chemical Process Design, **1999**, Prentice Hall PTR, Upper Saddle River, N.J.

[49] Sin G, Gernaey K V, Lantz AE, **2009**. Good modelling practice (GMoP) for PAT applications: Propagation of input uncertainty and sensitivity analysis, Biotechnol. Prog. 25:1043–1053.

[50] Eurostat, Eurostat**2015**. http://ec.europa.eu/eurostat (accessed March 14, 2017).

[51] Van't Riet K, **1979**. Review of Measuring Methods and Results in Nonviscous Gas-Liquid Mass Transfer in Stirred Vessels, Ind. Eng. Chem. Process Des. Dev. 18(3):357–364.

[52] Kirschner MJ, Oxygen, in: Ullmann's Encycl. Ind. Chem., **2000**, Wiley-VCH Verlag GmbH & Co. KGaA, Weinheim: pp. 317–635.

[53] Fletcher H, Mackley T, Judd S, **2007**. The cost of a package plant membrane bioreactor, Water Res. 41(12):2627–2635.

[54] Judd S, The MBR Book: Principles and applications of membrane bioreactors for water and wastewater treatment, 2nd ed., **2011**, Butterworth-Heinemann, Oxford.

[55] Tufvesson P, Lima-Ramos J, Nordblad M, Woodley JM, **2011**. Guidelines and cost analysis for catalyst production in biocatalytic processes, Org. Process Res. Dev. 15(1):266–274.

[56] Nienow AW, Hunt G, Buckland BC, **1994**. A fluid dynamic study of the retrofitting of large agitated bioreactors: Turbulent flow, Biotechnol. Bioeng. 44(10):1177–1185.

Chapter 4

The Michaelis constant for oxygen: A perspective on the importance for oxygen dependent biocatalysis

The following chapter is intended for later publication.

4.1 Abstract

Oxygen dependent biocatalysis has gained significant interest for a range of industrially relevant oxidation reactions. Protein engineering has enabled the development of novel enzyme activities and improvement of existing ones. However, typically the focus has been on showing improved performance in simple assays at a single oxygen concentration, with no emphasis on the ability of the enzyme to function under low oxygen conditions. This paper highlights the importance of the oxygen reactivity of enzymes, which becomes important at industrial scale due to the low operating concentration of oxygen in solution caused by the requirement for a driving force for oxygen transfer and the low solubility of oxygen in aqueous media at atmospheric conditions. Finally, the possibilities to alleviate this inherent oxygen limitation of many industrially relevant enzymes through process and protein engineering are discussed.

4.2 Introduction

Biocatalytic redox reactions are gaining significant interest in the synthetic chemistry due to their potential implementation in industrial chemistry, more specific for the synthesis of pharmaceutical, fine and specialty chemicals [1,2]. A significant fraction of industrially relevant redox enzymes are dependent on molecular oxygen as the electron acceptor, such as oxidases, monooxygenases, and dioxygenases. These types of enzymes catalyze a range of industrially interesting reactions, such as oxidation of alcohols to aldehydes and ketones, hydroxylation of non-activated C-H bonds, epoxidation of C=C double-bonds, and Baeyer-Villiger oxidations to name a few [3,4].

Although oxygen is a natural substrate for these enzymes and its reactivity with industrially relevant enzymes generally is high, the low solubility of oxygen in water often means that the availability of oxygen limits the catalytic rate [5,6]. This is further complicated by the requirement for a driving force to transfer oxygen (i.e. the difference between the oxygen concentration in solution and the saturation concentration) from the air to the reaction medium, which in practice means that a process needs to be operated at an oxygen concentration much below the solubility limit.

When protein engineering is used to develop novel enzyme activities, or improving existing ones, the focus is naturally on the enzymes ability to catalyze the target reaction. However, in order that an enzyme can function in an industrial setting, its other traits in the form of its inhibition profile, reactivity with co-substrates and stability, need to be evolved to suit conditions experienced in an industrial reactor [7–9]. For oxygen dependent enzymes, especially the reactivity of the enzyme with oxygen becomes important in an industrial setting where enzymes needs to function at low oxygen concentrations.

In this paper, we investigate the general kinetic traits of oxygen dependent enzymes, and describe how these influence the process operation and performance. Finally, we discuss the possibility to develop enzymes with higher oxygen reactivity that are better suited for industrial applications.

4.3 Micro- and macro-kinetic constants

The catalytic action of enzymes has been studied for decades, and many models for enzymatic reactions have been developed, starting with the single substrate, single product model initially proposed by Michaelis and Menten (1913) [10,11]. The Michaelis-Menten model has been extended to enzymes catalyzing the conversion of one or more substrates into one or more products, including inhibitory actions by either substrates, products or external reagents. Enzymes catalyzing the oxidation of a ‘primary’ substrate using molecular oxygen as electron acceptor (such as oxidases) can typically be described using the common two-substrate, two-product enzymatic models; the Ordered bi bi and the Ping-pong bi bi model (Figure 4.1). In some cases, the Random bi bi mechanism is required, where the binding of substrates and leaving of products from the ternary complex do not follow a specific order.

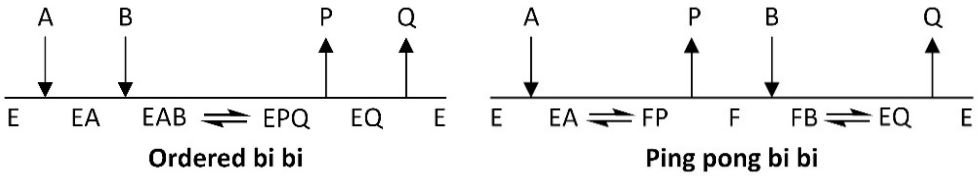

Figure 4.1. Cleland representation of the two most common models for two-substrate, two-product enzyme reactions. A and B represent substrates, while P and Q represent products.

Many oxygen dependent enzymes require more than two substrates, e.g. monooxygenases requiring NAD(P)H besides oxygen, or have more than two products. In such cases, more sophisticated models are required, but typically it is possible to derive Michaelis-Menten type rate expressions [12].

Many industrially relevant oxidases follow the Ping-pong bi bi mechanism, where the 'primary' substrate (i.e. substrate to be oxidized) reacts with the oxidized form of the enzyme, after which the oxidized substrate leaves to obtain a reduced enzyme form that reacts with oxygen to produce hydrogen peroxide and regenerate the oxidized enzyme (Figure 4.2). For oxygen dependent enzymes, only the forward reactions are considered, partly because of the relatively large amount of free energy released upon reduction of oxygen to hydrogen peroxide (E_0 of +281 mV, ΔG_r of -54.2 kJ mol^{-1} [13]) and partly because hydrogen peroxide in most cases is decomposed using catalase to avoid enzyme deactivation. The enzyme mechanism can therefore be divided into a reductive half-reaction where the enzyme is reduced by the 'primary' substrate and an oxidative half-reaction where the enzyme is oxidized by oxygen. In the following, the Ping-pong bi bi system is used as an example to discuss the meaning of the macro-kinetic parameters of the enzymatic rate expression.

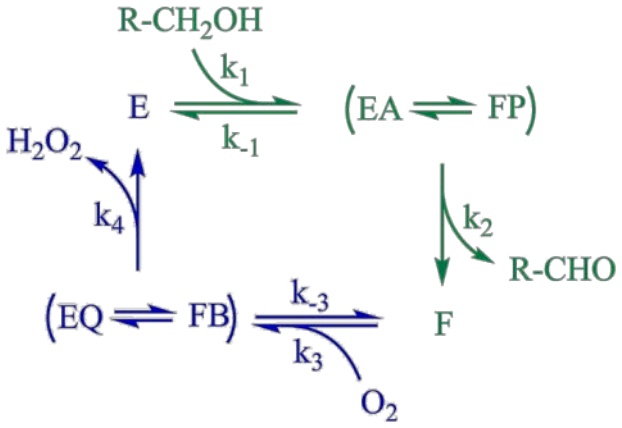

Figure 4.2. Catalytic cycle for an enzyme following the Ping-pong bi bi mechanism illustrated with the oxidation of an alcohol to an aldehyde with subsequent reduction of molecular oxygen to hydrogen peroxide. The reaction is practically irreversible due to the free energy of oxygen reduction and because hydrogen peroxide is decomposed using catalase. The green part of the cycle is referred to as the reductive half-reaction, while the blue part is referred to as the oxidative half-reaction. E: oxidized enzyme, F: reduced enzyme, EA/FB: Enzyme-Substrate complex, FP/EQ: Enzyme-Product complex.

The enzymatic rate expression can relatively easily be derived for a simple enzymatic mechanism such as the Ping-pong bi bi, for which the expression is given in Eq. 4.1.

$$\frac{\mathrm{r}}{C_{ET}} = \frac{\mathrm{k_{cat}}\, C_S C_O}{C_S C_O + \mathrm{K_{MO}} C_S + \mathrm{K_{MS}} C_O} \qquad \text{Eq. 4.1}$$

Where k_{cat} is the rate constant, K_{MO} the Michaelis constant for oxygen, K_{MS} the Michaelis constant for the 'primary' substrate, and C_S, C_O, and C_{ET} represents the concentration of substrate, oxygen and enzyme, respectively. The parameters of the rates expression are typically referred to as 'macro-kinetic' constants because they are functions of the 'micro-kinetic' constants, i.e. the rate constants of the underlying reactions. Eq. 4.2-4.4 show the relationship between the macro- and micro-kinetic constants when derived using the steady-state assumption and the King-Altman approach.

$$k_{cat} = \frac{k_2 k_4}{k_2 + k_4} \qquad \text{Eq. 4.2}$$

$$K_{MS} = \frac{k_{-1} + k_2}{k_1} \frac{k_4}{k_2 + k_4} \qquad \text{Eq. 4.3}$$

$$K_{MO} = \frac{k_{-3} + k_4}{k_3} \frac{k_2}{k_2 + k_4} \qquad \text{Eq. 4.4}$$

The macro-kinetic constants of the Ping-pong bi bi rate expression have the same physical meaning as the parameters of the original Michaelis-Menten equation. The rate constant, k_{cat}, represents the maximum velocity of the enzyme upon full saturation with both substrates ($V_{max} = k_{cat} \cdot C_{ET}$), and the Michaelis constants the concentration of the substrate at which half the maximum velocity is obtained, given that the enzyme is fully saturated with the other substrate.

The resemblance to the classical Michaelis-Menten equation is also seen in the relationship between the macro- and micro-kinetic constants. The rate constant is given by the ratio of the product of the two catalytic rate constants (k_2 and k_4) to the sum of the same two rate constants (Eq. 4.2). In other words, the maximum velocity is a function of the rate of each half-reaction. If one is much faster than the other, the maximum velocity will be given solely by the rate of the limiting half-reaction. The Michaelis constants are a combination of the dissociation constants for the enzyme-substrate complex (i.e. how the single substrate Michaelis constant is defined) and the ratio of the catalytic rate constant of the opposite half-reaction to the sum of the rate constants for the two half-reactions. For example, if the catalytic rate of the reductive half-reaction (i.e. the oxidation of the 'primary' substrate) is increased without the same relative increase of the oxidative catalytic rate, the Michaelis constant for oxygen increases because a higher oxygen concentration is required to match the increased rate of the reductive half-reaction. This in general means that fast enzymes also have relative high Michaelis constants for oxygen, unless the affinity for oxygen has been significantly enhanced.

Determination of macro-kinetic constants is typically done via measurements of initial rates at varying concentrations of both substrates. For oxygen dependent enzymes this can be

challenging, because of the difficulty of controlling the dissolved oxygen concentration at micro-liter scale [14]. Many researchers therefore tend to only consider the kinetic constants associated with the 'primary' substrate, and doing so at a single oxygen concentration, typically that obtained by air saturation under atmospheric conditions. In such cases the apparent kinetic parameters are obtained, which are a function of the true parameters and the oxygen concentration at the experimental conditions (Eq. 4.5-4.6). Kinetic constants for the 'primary' substrate determined at a single oxygen concentration are typically underestimated, since many enzymes have K_{MO} values close to or above the solubility of oxygen in water (see below). Interestingly, the bimolecular rate constant (k_{cat}/K_{MS}), which typically is used to compare the ability of enzymes to catalyze a given reaction, is independent of the oxygen concentration because the oxygen dependent terms of the apparent values cancel out. Thus, bimolecular rate constants recorded in traditional assays are valid.

$$k_{cat}^{app} = \frac{k_{cat}}{1 + \frac{K_{MO}}{C_O}} \quad \text{Eq. 4.5}$$

$$K_{MS}^{app} = \frac{K_{MS}}{1 + \frac{K_{MO}}{C_O}} \quad \text{Eq. 4.6}$$

4.4 Typical oxygen reactivity of enzymes

In the scientific literature, the reaction of enzymes with oxygen has been mostly studied when elucidating enzyme mechanisms and investigating key cellular processes, such as respiration [15–17]. However, documenting kinetic constants describing the oxygen reactivity is not standard procedure when working with oxygen dependent enzymes for synthetic applications, most likely due to the challenges involved in determining these parameters using existing equipment. Therefore, the availability of full Michaelis-Menten data (i.e. k_{cat}, K_{MS}, K_{MO}), and not apparent values, is rather limited. Nevertheless, the BRENDA database [18] was mined for available Michaelis constants for oxygen and corresponding bimolecular rate constants (k_{cat}/K_{MO}) in order to investigate the general oxygen reactivity of enzymes (Figure 4.3).

As previously mentioned, the solubility of oxygen in water is low at atmospheric conditions (268 μM, 25 ˚C, 1 atm.). Interestingly, a large fraction (28%) of the documented Michaelis constants for oxygen lie at or above the solubility limit, with a median of the distribution at 110 μM. This is surprising, because at first glance, the relatively high K_{MO} and physiologically relevant oxygen concentrations (i.e. those below the oxygen saturation concentration) will results in a strong evolutionary pressure towards enzymes reacting faster with oxygen, assuming that faster enzymes are beneficial for the organism. However, when considering the apparent values for K_{MO} at typical concentrations of intra- and extracellular 'primary' substrates (i.e. the substrates to be oxidized) the picture is different. As an example glucose oxidase, which in nature acts as a producer of hydrogen peroxide used in the breakdown of lignin or as an antibacterial agent, has a true K_{MS} of 110 mM and a K_{MO} of 0.48 mM (from *A. niger*) [19,20]. However, in its natural environment, the enzyme will never experience

glucose concentrations close to its Michaelis constant. When the concentration is only a fraction of K_{MS} the apparent K_{MO} will be much lower, e.g., a substrate concentration of 5 mM corresponds to an apparent K_{MO} of only 0.02 mM. This value is much below the solubility of oxygen in water, leaving an insignificant evolutionary pressure to evolve a glucose oxidase with higher oxygen reactivity. Similar arguments can be made for many other oxygen dependent enzymes, although there one way or another always is an evolutionary pressure when applying this argumentation. However, it is not always beneficial for an organism that the catalytic velocity of nonessential enzymes approach the physical boundary, as discussed at length by Bar-Even et al. (2011) [21].

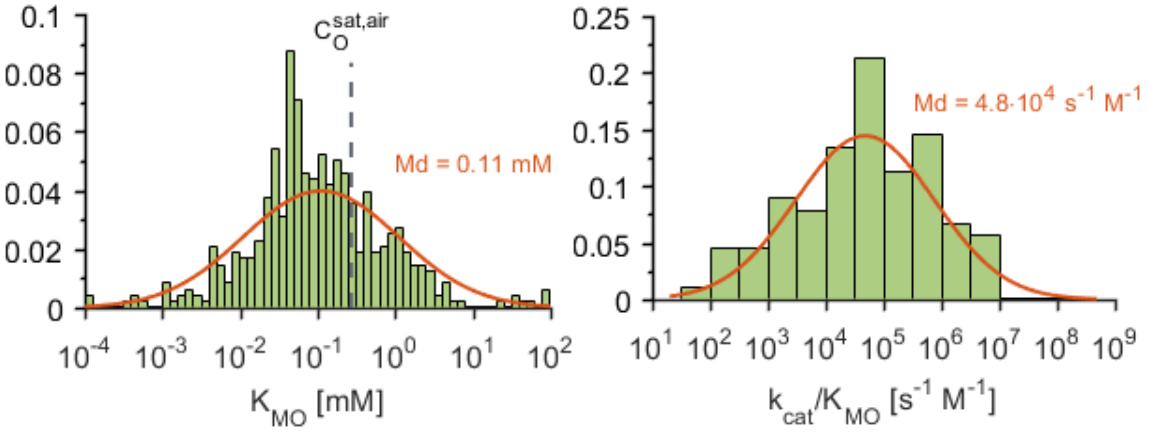

Figure 4.3. Distribution of Michaelis constants for oxygen found in the BRENDA database [18] (489 entries) and the corresponding bimolecular rate constants for the reaction of an enzyme with oxygen (89 entries). Figures show the median (Md) of the fitted distribution.

Although the Michaelis constant for oxygen gives an indication of which half-reaction will be limiting at an oxygen concentration below saturation, the bimolecular rate constant (k_{cat}/K_{MO}) is a direct measure of the reaction rate when the dissolved oxygen concentration approaches zero, i.e. the enzyme being fully oxygen limited. The median of the oxygen bimolecular rate constants found in BRENDA is $4.8 \cdot 10^4$ M^{-1} s^{-1} (Figure 4.3), a value well below what is typical considered the diffusion limit (10^8 – 10^9 M^{-1} s^{-1}) [21,22]. In fact no entries found in BRENDA come close to the diffusion limit, the closest being an aci-reductone dioxygenase from *Klebsiella pneumoniae* with a rate constant of $5.5 \cdot 10^6$ M^{-1} s^{-1} [23]. Interestingly, *K. pneumonia* is a facultative anaerobic soil bacterium and therefore potentially exposed to environments with low oxygen concentration. Nevertheless, the bimolecular rate constant is far from the values seen for cytochrome oxidases in the respiratory pathway, which exhibit bimolecular rate constants close to, or at, the diffusion limit, e.g. quinol oxidase from *E. coli* with a rate constant of $2 \cdot 10^9$ M^{-1} s^{-1} [24]. Furthermore, the respiratory enzymes have extremely low K_{MO} values (<1 µM)[17,25]. This enables these enzymes to always have priority of any oxygen available in the cell, making perfect sense from an evolutionary standpoint. Intracellular oxygen dependent enzymes therefore have to compete with the electron transport chain for the available oxygen, which potentially could result in intracellular enzymes having lower values of K_{MO} than extracellular enzymes, where the competition for oxygen presumable is lower. There are indications that this argument could

be valid. For example the low K_{MO} values of Homogentisate 1,2-dioxygenase and (4-Hydroxyphenyl)pyruvate dioxygenase, both being non-haem iron dependent intracellular enzymes (Table 4.1).

Table 4.1. Collection of kinetics constants for various oxygen dependent enzymes.

Enzyme	Reaction	Mechanism	k_{cat} (s^{-1})	K_{MS} (mM)	K_{MO} (mM)	k_{cat}/K_{MO} ($M^{-1}\,s^{-1}$)	Ref.
Glucose oxidase	Glucose + O_2 → Gluco-δ-lactone + H_2O_2	Ping pong	1150	110	0.48	$2.4\ 10^6$	[19]
Lactose oxidase	Lactose + O_2 → Lactobionic acid + H_2O_2	Ping pong	94	0.066	0.97	$9.7\ 10^4$	[26]
D-Amino acid oxidase	Alanine + O_2 → Pyruvate + NH_3 + H_2O_2	Ping pong	330	2.6	3.0	$1.1\ 10^5$	[27]
Homogentisate 1,2-dioxygenase	Homogentisate +O_2 → maleylacetoacetate + H_2O	Ordered	16.2	0.0010	0.099	$1.6\ 10^5$	[28]
(4-hydroxyphenyl) pyruvate dioxygenase	(4-hydroxyphenyl) pyruvate + O_2 → homogentisate + CO_2	Ordered	6.8	0.0027	0.069	$9.9\ 10^4$	[29]
Polyphenol Oxidase	2 Esculetin + O_2 → 2 o-quinone + 2 H_2O	Ping pong[a]	928	0.63	0.040	$2.3\ 10^7$	[30]
Choline oxidase	Choline + O_2 → betaine aldehyde + H_2O_2	Ordered	61	1.7	0.703	$8.7\ 10^4$	[31]
P450cam	2 $Putidaredoxin_{red}$ + O_2 → 2 $Putidaredoxin_{ox}$ + H_2O	Ping pong[a]	66	0.0038	0.083	$8.05\ 10^5$	[32]
Aci-reductone dioxygenase	1,2-Dihydroxy-3-keto-5-(methylthio)pentene + O_2 → 2-keto-4-(methylthio)butyrate + HCOOH	Ordered	260	0.052	0.047	$5.5{\cdot}10^6$	[23]

[a] uni uni bi uni ping pong

The evolutionary pressure exerted on enzymes and organisms containing them is a thought provoking topic. Searching for enzymes in organisms living in environments of low oxygen concentrations could lead to the identification of oxygen dependent enzymes with a lower Michaelis constant for oxygen, and potentially higher bi molecular rate constant with oxygen. Places to look, could be at high altitudes, in oxygen minimum layers of the oceans, or in soils known for hypoxic environments [33–35]. In such places the evolutionary pressure might have enabled the evolution of oxygen dependent enzymes functioning well under low oxygen conditions, or alternatively there could be enzymes closely related to ancestral enzymes from periods of Earth's history with little atmospheric oxygen (i.e. before the 'Great Oxidation Event' 2.4-2.1 billion years ago [36]).

The oxygen reactivity and affinity varies significantly between oxygen dependent enzymes. Many industrially relevant enzymes, such as sugar and amino acid oxidases, show high values of K_{MO} relative to the solubility of oxygen in water at atmospheric conditions (Table 4.1). This can potentially limit the catalytic rates obtainable in industrial scale reactors.

4.5 Importance of K_{MO} for biocatalytic oxidation processes

The conditions enzymes are exposed to in industrial biocatalytic reactions are far from those experienced in Nature. The largest difference being the high concentration of substrate and the corresponding high concentration of product (>100 mM) required for an efficient down-stream process. Although, problems of substrate and product inhibition can be alleviated using substrate feeding [37], *in situ* product removal [38] and cascade biocatalysis [39], the concentrations inevitable will by significantly higher than the micro-molar concentrations experienced in cellular environments.

Likewise, oxygen dependent enzymes applied in industrial processes will experience high concentrations of their 'primary' substrate, whereas the concentration of oxygen will never reach beyond the solubility limit under the process conditions. In reality, the oxygen concentration will be much lower than the solubility limit due to the requirement to transfer oxygen from the gas-phase used for aeration to the liquid phase where it is consumed. The driving force for oxygen transfer is given by the difference between the oxygen saturation concentration and the bulk oxygen concentration (Eq. 4.7).

$$OTR = k_L a \left(C_{O_2}^{sat} - C_{O_2}\right) \qquad \text{Eq. 4.7}$$

For highly intensified aerobic processes, such as microbial fermentation processes, the cost of aeration (i.e. compression and stirring) is a major contributor to the final production cost [40]. To limit the cost of oxygen transfer, a large driving force is required which results in operation at low oxygen concentrations. Furthermore, the magnitude of the volumetric mass transfer coefficient (k_La) is limited by the power input and aeration rate. This means that an oxygen dependent biocatalytic process is typically limited to a productivity of approximately 100 mmol O_2 L^{-1} h^{-1} obtainable at a k_La of 500 h^{-1} with a driving force corresponding to 80% of saturation, when using air for aeration [41].

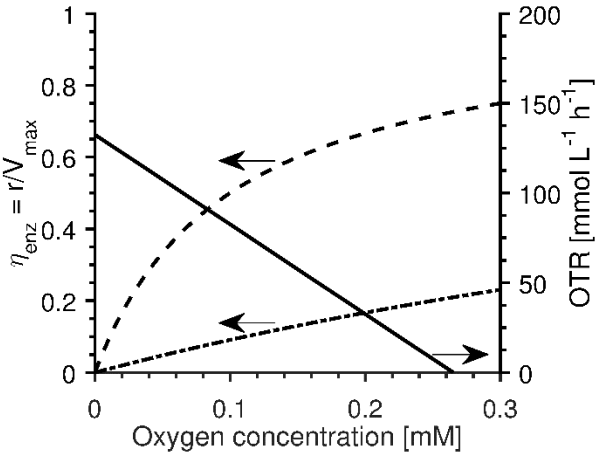

Figure 4.4. Trade-off between on one hand supplying oxygen while on the other ensuring a high enzyme efficiency (η_{enz}), i.e. low enzyme requirement. The plot shows the effect of changing Michaelis constant for oxygen (K_{MO}) from 1 mM (-.) to 0.1 mM (--) for an enzyme fully saturated with 'primary' substrate. The oxygen transfer rate (OTR) is based on a volumetric mass transfer coefficients (k_La) of 500 h^{-1} using air for aeration.

Hence, in an industrial reactor, the oxygen requiring enzyme will be exposed to oxygen concentrations much below the saturation concentration of air at atmospheric conditions. This means, that if the enzyme has a K_{MO} close to or above the solubility of oxygen in water, the availability of oxygen will limit the catalytic rate of the enzyme. In fact, the rate of reaction will be almost linearly dependent on the oxygen concentration in solution, because the enzyme will be far from saturated with oxygen, while being fully saturated with the 'primary' substrate. Being able to transfer oxygen from the air to the reaction media (i.e. having a large driving force) while utilizing an oxygen dependent enzyme efficiently (i.e. being as close to oxygen saturation as possible) represents a very important trade-off for the operation of an oxygen dependent biocatalytic process. Figure 4.4 illustrates this trade-off for an enzyme displaying a K_{MO} above the solubility of oxygen in water at atmospheric conditions. The figure highlights the possibilities to alleviate the oxygen limitation of the enzyme either by decreasing the K_{MO} through protein engineering, here illustrated by 10-fold reduction. The figure shows how the enzyme utilization efficiency change depending on the effective oxygen concentration in solution. The enzyme utilization efficiency being defined as the reaction rate at the operating conditions relatively to the maximum rate if the enzyme was saturated with both substrates. The enzyme utilization efficiency is directly proportional to the amount of enzyme required to reach the required volumetric productivity.

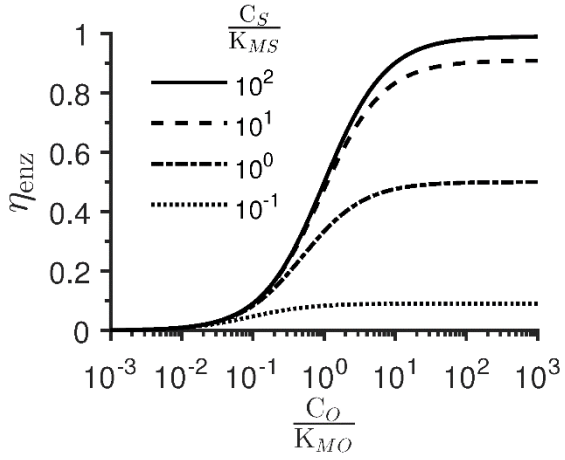

Figure 4.5. Effect of changing the concentration of oxygen in solution (measured as the ratio C_O/ K_{MO}) and the 'primary' substrate concentration (measured as the ratio C_S/ K_{MS}) on the enzyme utilization efficiency ($\eta_{enz} = r/V_{max}$) for an enzyme following ping pong bi bi mechanism.

The importance of the oxygen concentration in solution depends on the K_{MO} of the enzyme. Figure 4.5 shows how the utilization efficiency of a two-substrate enzyme change depending on the ratio of the concentration of oxygen to K_{MO} at different ratios 'primary' substrate concentration to K_{MS}. In industrial operations, the latter ratio is in most cases above 10^0, except if severe substrate inhibition of the enzyme is experienced. From the figure, it is clear that a reactor needs to be operated at an oxygen concentration of at least 10 times K_{MO} to avoid loss of enzyme utilization, and thus greatly increasing the amount of enzyme required to reach a desired volumetric productivity. The extent of enzyme utilization will change along a typical batch process as the 'primary' substrate is consumed and thus decreasing the

dependency of the reaction rate on the oxygen concentration. However, this will typically only happen in the very end of a batch, and thus the oxygen concentration will be dominating the overall reaction rate, especially if substrate is continuously fed to the reactor.

4.5.1 Industrial application of enzymes with high Michaelis constants for oxygen

Ideally, protein engineers should develop enzymes with high reaction rates at low oxygen concentrations (i.e. low K_{MO}) or develop enzymes based on an enzyme template naturally showing a low K_{MO} value. However, depending on the limiting step of the catalytic cycle it is not given that it is possible to obtain low K_{MO} enzyme variants through directed evolution. In cases where an enzyme with high K_{MO} relative to the solubility of oxygen in water has to be applied, process engineers have to consider operating conditions in relation to the previously described trade-off between supplying oxygen and utilizing the applied enzyme efficiently. The best operating conditions is defined both by the cost of supplying oxygen and the cost of the enzyme. By applying a cost correlation for the cost of oxygen transfer as a function of agitation and aeration rate the optimal oxygen concentration in solution was found for different values of K_{MO} and cost of enzyme at an oxygen transfer rate of 100 mmol L^{-1} h^{-1} (Figure 4.6) (based on Chapter 3). At a high price of enzyme, it is cheaper to decrease the driving force while increasing agitation and aeration to increase the volumetric oxygen transfer coefficient (Eq. 7). Thereby, less enzyme is required, while the cost of aeration increases. When applying an enzyme with higher K_{MO} the benefit of increasing the oxygen concentration is larger. However, the oxygen concentration in solution can only be increased up to a certain point, where the agitation and aeration of the reactor is pushed to its limits, i.e. if the concentration was further increased there would not be enough driving force for transferring the required amount of oxygen.

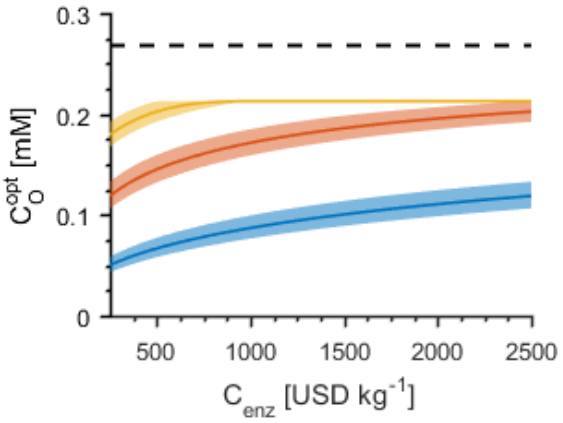

Figure 4.6. Oxygen concentration that result in the lowest total cost (oxygen supply and enzyme cost) for a 12.5 m^3stirred reactor bubbled with air at a headspace pressure of 1 atm. calculated for an enzyme having a K_{MO} of 0.1 mM (blue), 1 mM (red) or 5 mM (yellow). Operating at an oxygen transfer rate of 100 mmol L^{-1} h^{-1}. (--) marks the solubility limit of oxygen in water at atmospheric conditions.

Having enzymatic processes being limited by oxygen has often encouraged scientists to consider alternatives to the traditional air bubbled stirred reactor, such as applying pure oxygen for aeration, pressurization of the reactor, or applying membrane aeration (Chapter 3). Applying pure oxygen aeration or increasing the headspace pressure of the stirred reactor is

especially advantageous when dealing with an enzyme exhibiting a high K_{MO}, because the oxygen concentration in solution can be increased while ensuring a high driving force for oxygen transfer due to the higher partial pressure of oxygen in the gas phase [6,43]. Recently, it was concluded that there were no statistically significant direct economic benefit from applying alternative oxygen supply methods (Chapter 3). Nevertheless, in that study the effect of the enzyme utilization efficiency was not taken into consideration. When doing so there can in fact be a large benefit of applying pure oxygen sparging or reactor pressurization (Figure 4.7). If applying a very cheap enzyme (250 USD kg^{-1}) there is no or little benefit of the alternative oxygen supply methods. However, when applying an enzyme with a cost of 2500 USD kg^{-1}, a price more realistic for a fine/specialty chemical enzyme [44], there can be up to a 40% saving in combined cost of oxygen supply (covering both capital and running costs of the reactor) and enzyme cost. The benefit of using pure oxygen or pressurization depends on the value of K_{MO}. At a high K_{MO}, relatively to the solubility of oxygen, the advantage will be larger than at low K_{MO}, where the increase in specific reaction rate when increasing the dissolved oxygen concentration will be smaller.

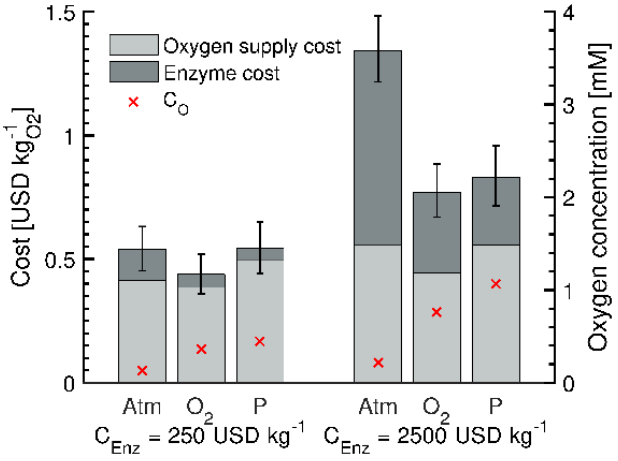

Figure 4.7. Optimization of oxygen concentration in solution (C_{O2}) to minimize oxygen supply cost and enzyme cost depending on price of enzyme (C_{enz}) and oxygen supply conditions (atmospheric headspace pressure using air for sparging (atm), atmospheric headspace pressure using pure oxygen (95%) for sparging (O_2), and 10 bar headspace pressure using air for sparging (P)). The cost is normalized per kg of oxygen supplied to the reactor. The figure is based on an enzyme having a K_{MO} of 1 mM.

Another interesting aspect of an oxygen limited enzymatic process, is that continuous operation of a stirred tank reactor does not result in a loss of productivity compared to a similar reactor in batch operation. For a typical reaction, a substantial loss in productivity is expected when operating a continuous stirred tank reactor at high conversions, because the reaction rate is defined by the substrate concentration leaving the reactor, which will be low. The reaction rate of an oxygen limited enzyme reaction will be almost independent of the 'primary' substrate concentration ($K_{MS}^{app} \ll C_S$). Because oxygen is supplied continuously to the reactor independently of the operational regime, the oxygen concentration and therefore the volumetric productivity will be comparable for the two operational modes, up to high conversions (>95%) where the low substrate concentration could limit the enzymatic rate in

continuous operation dependent on the value of K_{MS}. With the above in mind, continuous oxygen dependent biocatalysis in stirred tank reactors is possible, thereby avoiding alternative reactor configurations displaying 'plug-flow' behavior, which are difficult to operate due to the biphasic flow [45].

4.6 Improving oxygen reactivity using protein engineering

The oxygen reactivity of enzymes has been extensively studied in the scientific literature to understand the enzymatic mechanisms of oxygen activation, how enzymes avoid being oxidized and inactivated by the reactive intermediates, and how oxygen is guided to the active site [15,46–49]. Despite oxygen being a small molecule, distinct channels for oxygen transfer, pockets for oxygen 'storage' and oxygen binding sites have been identified in many oxygen dependent enzymes [50–52]. Interestingly, single amino-acid residues often acts as gatekeepers for oxygen transfer through oxygen channels. For example, by changing one such amino acid, a flavin dependent oxidase can be changed into a dehydrogenase not reacting with oxygen [53,54]. Along similar lines, pockets displaying high oxygen affinity have been identified in D-amino acid oxidase, which serve as oxygen reservoirs and increase the local oxygen concentration close to the active-site above that of the solvent, thus increasing the reactivity of the enzyme with oxygen [55,56]. Despite the already high oxygen reactivity (measured by the k_{cat}/K_{MO} value) of many enzymes (Figure 4.3 and Table 4.1), the observations that the protein structure affects the oxygen reactivity has encouraged research into improving the oxygen reactivity of enzymes using protein engineering. This has mainly involved rational protein engineering of amino acid residues in oxygen channels or close to the active site, which resulted in increases in oxygen reactivity of 1.4-3 fold for enzymes already displaying high reactivity with oxygen ($k_{cat}/K_{MO} > 10^5\ M^{-1}\ s^{-1}$) [50,53,56,57]. Site-directed mutagenesis is suitable when testing hypotheses on well-characterized enzymes. However, when developing enzymes for industrial applications, where detailed structure-function relationships are unknown, directed-evolution approaches are typically more efficient [58,59]. Nevertheless, performing the required high-throughput screening at reduced oxygen concentrations could pose a practical challenge. For instance, one example of applying a directed evolution approach to develop an enzyme variant with higher oxygen reactivity has been reported in the scientific literature [52]. Here error-prone PCR was applied together with an assay performed at reduced oxygen conditions (2.5%) in a glovebox. Two rounds of mutagenesis resulted in a variant of D-amino acid oxidase with five mutations, not in close proximity of the active-site, which displayed a 5-fold lower K_{MO} and a 2-fold higher k_{cat}/K_{MO}.

As for enzymes in general, engineers should be careful when choosing an oxygen dependent enzyme for further development or process implementation solely based on its bimolecular rate constant, as this can lead to suboptimal choices [60,61]. Although, the pitfalls of using k_{cat}/K_{MO} as an indicator for enzyme performance are smaller for oxygen dependent enzymes operating at oxygen concentrations close to or below K_{MO}, enzymes displaying the same bimolecular rate constant but different performance at industrially relevant oxygen concentration can be envisioned. The ideal enzyme would have a k_{cat}/K_{MO} value as close as possible

to the diffusion limit and a K_{MO} of approximately 1/10 of the operating oxygen concentration, i.e. a K_{MO} of 5 μM if operating at 20% of air saturation. Nevertheless, it is important to consider the full kinetics of the enzyme because both the reactivity towards the 'primary' substrate and oxygen has to be taken into account. Full kinetic characterization may therefore become a bottleneck in enzyme development due to the difficulty of varying the oxygen concentration in standard microtiter plate measurements. Recently, we have reported a microfluidic platform capable of performing autonomous and fast characterization of oxygen dependent enzymes, which has the potential to alleviate this constraint if made commercially available [14].

Directed evolution approaches, preferably together with computational studies to predict target residues that potentially could alter oxygen binding and reactivity, combined with high-throughput screening at conditions experienced in an industrial setting, i.e. high 'primary' substrate concentration and low oxygen concentration (<20% of air-saturation) and full kinetic characterization can enable faster development of biocatalysts better suited for industrial applications.

4.7 Concluding remarks and future perspectives

Many oxygen dependent enzymes display a Michaelis constant for oxygen (K_{MO}) in the range of, or above, the solubility of oxygen in water at atmospheric conditions. The high K_{MO} relative to the solubility of oxygen in water means that enzymes at industrial conditions operates at catalytic rates much below their maximum potential. Although, this can to some extent be alleviated by using oxygen supply methods to increase the effective oxygen concentration in solution, such as enriched air sparging, moderate reactor pressurization, or eventually feeding of hydrogen peroxide being degraded by catalase, the benefits in terms of reduced enzyme requirements of developing enzyme variants with oxygen kinetic traits customized to fit the industrial conditions are substantial. The already high oxygen reactivity (k_{cat}/K_{MO}) of most oxygen dependent enzymes makes further improvements difficult, but not impossible if combining directed evolution approaches with appropriate screening conditions, molecular dynamic simulations, and automated kinetic characterization of the enzyme.

4.8 Methods

4.8.1 Mining of the BRENDA database

k_{cat} and K_M values for oxygen were extracted from the BRENDA database using Python (2.7.13, Python Software Foundation, Delaware, USA) and the Simple Object Access Protocol (SOAP) web service. Information for all enzymes reported as having oxygen as a substrate were extracted, including all information on unnatural substrates and mutated versions of natural enzymes. Bi molecular rate constants (k_{cat}/K_{MO}) could not be extracted directly from the database, therefore k_{cat} values and K_{MO} values were paired based on enzyme number, originating organism and comments on the entry, thus allowing the calculation of k_{cat}/K_{MO}.

4.8.2 Optimal oxygen concentration and costing of oxygen supply and enzyme

Costing of reactor, compressor, and agitator including their energy requirements were calculated as reported elsewhere (Chapter 3). The calculations were all performed for a 12.5 m^3 reactor with a liquid filling volume of 80% of the total volume. An average enzyme was used in the calculation, being an enzyme requiring ½ mole of O_2 per mole product (i.e. an oxidase combined with catalase), following ping pong bi bi kinetics, and having a K_{MO} of 1 mM and a k_{cat} of 1000 s^{-1}, and an enzyme size of 50 kDa. The concentration of the 'primary' substrate were assumed to be high enough to fully saturate the enzyme. In all calculations the oxygen requirement was assumed to be 100 mmol L^{-1} h^{-1}, and the total cost of oxygen supply and oxygen dependent enzyme were minimized by changing the oxygen concentration in solution, the agitation power input, and the volumetric air flow rate. The power input and the volumetric air flow rate were constrained to maximum 5 W L^{-1} and 2 volume per volume per minute (vvm). Furthermore, the air flow rate was constrained to avoid flooding of the bottom impeller. The enzyme cost was assumed to be 2500 USD kg^{-1} unless otherwise stated, this is a typical cost of an enzyme for applied for fine or specialty chemical production [44]. The uncertainty of the predictions were estimated based on the uncertainties on the input parameters using Monte Carlo simulations as explained elsewhere (Chapter 3) [62].

4.9 References

[1] Hollmann F, Arends IWCE, Buehler K, Schallmey A, Bühler B, **2011**. Enzyme-mediated oxidations for the chemist, Green Chem. 13(2):226.

[2] Kroutil W, Mang H, Edegger K, Faber K, **2004**. Biocatalytic Oxidation of Primary and Secondary Alcohols, Adv. Synth. Catal. 346(23):125–142.

[3] Holtmann D, Fraaije MW, Arends IWCE, Opperman J, Hollmann F, **2014**. The taming of oxygen : biocatalytic oxyfunctionalisations, Chem. Commun. 50:13180–13200.

[4] Turner NJ, **2011**. Enantioselective oxidation of C-O and C-N bonds using oxidases., Chem. Rev. 111(7):4073–87.

[5] Baldwin CVF, Woodley JM, **2006**. On Oxygen Limitation in a Whole Cell Biocatalytic Baeyer-Villiger Oxidation Process, Biotechnol. Bioeng. 95(3):362–369.

[6] Hua L, Nordkvist M, Nielsen PM, Villadsen J, **2007**. Scale-up of enzymatic production of lactobionic acid using the rotary jet head system, Biotechnol. Bioeng. 97(4):842–849.

[7] Ringborg RH, Woodley JM, **2016**. The Application of Reaction Engineering to Biocatalysis, React. Chem. Eng. 1(1):10–22.

[8] Burton SG, Cowan DA, Woodley JM, **2002**. The search for the ideal biocatalyst, Nat. Biotechnol. 20(1):37–45.

[9] Bommarius AS, Blum JK, Abrahamson MJ, **2011**. Status of protein engineering for biocatalysts: How to design an industrially useful biocatalyst, Curr. Opin. Chem. Biol. 15(2):194–200.

[10] Michaelis L, Menten ML, **1913**. Die Kinetik der Invertinwirkung, Biochem Z. 49(February):333–369.

[11] Johnson KA, Goody RS, **2011**. The original Michaelis constant: Translation of the 1913 Michaelis-Menten Paper, Biochemistry. 50(39):8264–8269.

[12] Segel IH, Enzyme Kinetics: Behavior and Analysis of Rapid Equilibrium and Steady-State Enzyme Systems, **1993**, John Wiley & Sons, Inc., New York.

[13] Valentine JS, Dioxygen Reactions, in: I. Bertini, H.B. Gray, S.J. Lippard, J.S. Valentine (Eds.), Bioinorg. Chem., **1994**, University Science Books, Mill Valley, CA: pp. 313–523.

[14] Ringborg RH, Toftgaard Pedersen A, Woodley JM, **2017**. Automated determination of oxygen-dependent enzyme kinetics in a tube-in-tube flow reactor, Submitted. .

[15] Mattevi A, **2006**. To be or not to be an oxidase: challenging the oxygen reactivity of flavoenzymes, Trends Biochem. Sci. 31(5):276–283.

[16] Baron R, McCammon JA, Mattevi A, **2009**. The oxygen-binding vs. oxygen-consuming paradigm in biocatalysis: structural biology and biomolecular simulation, Curr. Opin. Struct. Biol. 19(6):672–679.

[17] D'Mello R, Hill S, Poole RK, **1995**. The oxygen affinity of cytochrome bo' in

Escherichia coli determined by the deoxygenation of oxyleghemoglobin and oxymyoglobin: K(m) values for oxygen are in the submicromolar range, J. Bacteriol. 177(3):867–870.

[18] Schomburg I, Chang A, Ebeling C, Gremse M, Heldt C, Huhn G, Schomburg D, **2004**. BRENDA, the enzyme database: updates and major new developments, Nucleic Acids Res. 32(90001):431D–433.

[19] Gibson QH, Swoboda BEP, Massey V, **1964**. Kinetics and Mechanism of Action of Glucose Oxidase, J. Biol. Chem. 239(11):3927–3934.

[20] Wong CM, Wong KH, Chen XD, **2008**. Glucose oxidase: Natural occurrence, function, properties and industrial applications, Appl. Microbiol. Biotechnol. 78(6):927–938.

[21] Bar-Even A, Noor E, Savir Y, Liebermeister W, Davidi D, Tawfik DS, Milo R, **2011**. The moderately efficient enzyme: Evolutionary and physicochemical trends shaping enzyme parameters, Biochemistry. 50(21):4402–4410.

[22] Alberty R, Hammes GG, **1958**. Application of the theory of diffusion-controlled reactions to enzyme kinetics, J. Phys. Chem. 62(2):154–159.

[23] Dai Y, Pochapsky TC, Abeles RH, **2001**. Mechanistic studies of two dioxygenases in the methionine salvage pathway of Klebsiella pneumoniae, Biochemistry. 40(21):6379–6387.

[24] Borisov VB, Gennis RB, Hemp J, Verkhovsky MI, **2011**. The cytochrome bd respiratory oxygen reductases, Biochim. Biophys. Acta - Bioenerg. 1807(11):1398–1413.

[25] Longmuir IS, **1954**. Respiration rate of bacteria as a function of oxygen concentration., Biochem. J. 57(1):81–87.

[26] Nordkvist M, Nielsen PM, Villadsen J, **2007**. Oxidation of Lactose to Lactobionic Acid by a Microdochium nivale Carbohydrate Oxidase : Kinetics and Operational Stability, 97(4):694–707.

[27] Pollegioni L, Langkau B, Tischer W, Ghisla S, Pilone MS, **1993**. Kinetic mechanism of D-amino acid oxidases from Rhodotorula gracilis and Trigonopsis variabilis, J. Biol. Chem. 268(19):13850–13857.

[28] Amaya AA, Brzezinski KT, Farrington N, Moran GR, **2004**. Kinetic analysis of human homogentisate 1,2-dioxygenase, Arch. Biochem. Biophys. 421(1):135–142.

[29] Johnson-Winters K, Purpero VM, Kavana M, Nelson T, Moran GR, **2003**. (4-Hydroxyphenyl)pyruvate dioxygenase from Streptomyces avermitilis: The basis for ordered substrate addition, Biochemistry. 42(7):2072–2080.

[30] Munoz-Munoz JL, Garcia-Molina F, Varon R, Rodriguez-Lopez JN, Garcia-Canovas F, Tudela J, **2007**. Kinetic characterization of the oxidation of esculetin by polyphenol oxidase and peroxidase., Biosci. Biotechnol. Biochem. 71(2):390–396.

[31] Ghanem M, Fan F, Francis K, Gadda G, **2003**. Spectroscopic and Kinetic Properties of Recombinant Choline Oxidase from Arthrobacter globiformis, Biochemistry.

42(51):15179–15188.

[32] Purdy MM, Koo LS, Ortiz de Montellano PR, Klinman JP, **2004**. Steady-state kinetic investigation of cytochrome P450cam: interaction with redox partners and reaction with molecular oxygen., Biochemistry. 43(1):271–81.

[33] Wright JJ, Konwar KM, Hallam SJ, **2012**. Microbial ecology of expanding oxygen minimum zones, Nat. Rev. Microbiol. 10(6):381–394.

[34] Seibel BA, **2011**. Critical oxygen levels and metabolic suppression in oceanic oxygen minimum zones, J. Exp. Biol. 214(2):326–336.

[35] Blossfeld S, Gansert D, Thiele B, Kuhn AJ, Lösch R, **2011**. The dynamics of oxygen concentration, pH value, and organic acids in the rhizosphere of Juncus spp., Soil Biol. Biochem. 43(6):1186–1197.

[36] Lyons TW, Reinhard CT, Planavsky NJ, **2014**. The rise of oxygen in Earth's early ocean and atmosphere., Nature. 506(7488):307–15.

[37] Kim PY, Pollard DJ, Woodley JM, **2007**. Substrate supply for effective biocatalysis, Biotechnol. Prog. 23(1):74–82.

[38] Lye GJ, Woodley JM, **1999**. Application of in situ product-removal techniques to biocatalytic processes, Trends Biotechnol. 17(10):395–402.

[39] Xue R, Woodley JM, **2012**. Process technology for multi-enzymatic reaction systems., Bioresour. Technol. 115:183–95.

[40] Grotkjær T, Commercial Development of Fermentation Processes, in: J. Villadsen (Ed.), Fundam. Bioeng., **2016**, Wiley-VCH Verlag GmbH & Co. KGaA, Weinheim: pp. 499–545.

[41] Charles M, **1985**. Fermentation scale-up: Problems and possibilities, Trends Biotechnol. 3(6):134–139.

[42] Toftgaard Pedersen A, Rehn G, Woodley JM, **2017**. A Techno-Economic Comparison of Oxygen Supply Methods in Biocatalysis, Prep. .

[43] Pilone MS, Pollegioni L, **2002**. D-amino acid oxidase as an industrial biocatalyst, Biocatal. Biotransformation. 20(3):145–159.

[44] Tufvesson P, Lima-Ramos J, Nordblad M, Woodley JM, **2011**. Guidelines and cost analysis for catalyst production in biocatalytic processes, Org. Process Res. Dev. 15(1):266–274.

[45] Toftgaard Pedersen A, Carvalho T, Sutherland E, Rehn G, Ashe R, Woodley JM, **2017**. Characterisation of a continous agitated cell reactor for oxygen dependent biocatalysis, Biotechnol. Bioeng. 114(6):1222–1230.

[46] Klinman JP, **2007**. How do enzymes activate oxygen without inactivating themselves?, Acc. Chem. Res. 40(5):325–333.

[47] Gadda G, **2012**. Oxygen activation in flavoprotein oxidases: The importance of being positive, Biochemistry. 51(13):2662–2669.

[48] Solomon EI, Chen P, Metz M, Lee S-K, Palmer AE, **2001**. Oxygen Binding, Activation, and Reduction to Water by Copper Proteins, Angew. Chemie Int. Ed. 40(24):4570–4590.

[49] Chaiyen P, Fraaije MW, Mattevi A, **2012**. The enigmatic reaction of flavins with oxygen, Trends Biochem. Sci. 37(9):373–380.

[50] Baron R, Riley C, Chenprakhon P, Thotsaporn K, Winter RT, Alfieri A, Forneris F, van Berkel WJ, Chaiyen P, Fraaije MW, Mattevi A, McCammon JA, **2009**. Multiple pathways guide oxygen diffusion into flavoenzyme active sites, Proc Natl Acad Sci U S A. 106(26):10603–10608.

[51] Di Russo N V., Condurso HL, Li K, Bruner SD, Roitberg AE, **2015**. Oxygen diffusion pathways in a cofactor-independent dioxygenase, Chem. Sci. 6(11):6341–6348.

[52] Rosini E, Pollegioni L, Ghisla S, Orru R, Molla G, **2009**. Optimization of D-amino acid oxidase for low substrate concentrations - towards a cancer enzyme therapy., FEBS J. 276(17):4921–32.

[53] Piubelli L, Pedotti M, Molla G, Feindler-Boeckh S, Ghisla S, Pilone MS, Pollegioni L, **2008**. On the oxygen reactivity of flavoprotein oxidases: An oxygen access tunnel and gate in Brevibacterium sterolicum cholesterol oxidase, J. Biol. Chem. 283(36):24738–24747.

[54] Leferink NGH, Fraaije MW, Joosten HJ, Schaap PJ, Mattevi A, van Berkel WJH, **2009**. Identification of a gatekeeper residue that prevents dehydrogenases from acting as oxidases, J. Biol. Chem. 284(7):4392–4397.

[55] Saam J, Rosini E, Molla G, Schulten K, Pollegioni L, Ghisla S, **2010**. O2 reactivity of flavoproteins: Dynamic access of dioxygen to the active site and role of a H+ relay system in D-amino acid oxidase, J. Biol. Chem. 285(32):24439–24446.

[56] Rosini E, Molla G, Ghisla S, Pollegioni L, **2011**. On the reaction of D-amino acid oxidase with dioxygen: O2 diffusion pathways and enhancement of reactivity., FEBS J. 278(3):482–92.

[57] Hernández-Ortega A, Lucas F, Ferreira P, Medina M, Guallar V, Martínez AT, **2011**. Modulating O2 reactivity in a fungal flavoenzyme: Involvement of aryl-alcohol oxidase Phe-501 contiguous to catalytic histidine, J. Biol. Chem. 286(47):41105–41114.

[58] Turner NJ, **2003**. Directed evolution of enzymes for applied biocatalysis., Trends Biotechnol. 21(11):474–8.

[59] Kuchner O, Arnold FH, **1997**. Directed evolution of enzyme catalysts, Trends Biotechnol. 15(12):523–530.

[60] Fox RJ, Clay MD, **2009**. Catalytic effectiveness, a measure of enzyme proficiency for industrial applications, Trends Biotechnol. 27(3):137–140.

[61] Eisenthal R, Danson MJ, Hough DW, **2007**. Catalytic efficiency and kcat/KM: a useful comparator?, Trends Biotechnol. 25(6):247–249.

[62] Sin G, Gernaey K V, Lantz AE, **2009**. Good modelling practice (GMoP) for PAT

applications: Propagation of input uncertainty and sensitivity analysis, Biotechnol. Prog. 25:1043–1053.

Chapter 5

Automated determination of oxygen-dependent enzyme kinetics in a tube-in-tube flow reactor

This chapter is based upon an accepted research paper and its supporting information:

Ringborg RH, Toftgaard Pedersen A, Woodley JM. 2017. Automated determination of oxygen-dependent enzyme kinetics in a tube-in-tube flow reactor, ChemCatChem, Accepted, DOI: 10.1002/cctc.201700811

5.1 Abstract

Enzyme-mediated oxidation is of particular interest to synthetic organic chemists. However, the implementation of such systems demands knowledge of enzyme kinetics. Conventional wisdom holds that collecting kinetic data for biocatalytic oxidations is fraught with difficulties such as limited oxygen supply and low oxygen solubility in water. Herein is presented a novel method for the collection of such kinetic data using a pressurized tube-in-tube reactor, operated in the low-dispersed flow regime to generate time-series data, with minimal material consumption. Experimental development and validation of the instrument reveals not only the high accuracy of the kinetic data obtained, but also the necessity of making measurements in this way to enable the accurate evaluation of high K_{MO} enzyme systems. For the first time, this paves the way to integrate kinetic data into the protein engineering cycle (i.e. the cycle of protein mutagenesis followed by mutant screening/characterization).

5.2 Introduction

Selective oxidation is one of the most important transformations in synthetic organic chemistry [1–3]. The importance of achieving high product yields in such transformations makes enzymes particularly interesting as potential catalysts on account of their exquisite selectivity in comparison with their chemo-catalytic counterparts. However, for process application it is often difficult to reach the required reaction intensity (reaction rate and product concentration). In particular, issues such as low enzymatic activity, product/substrate inhibition, cofactor regeneration and unfavorable thermodynamic equilibria need to be solved using biocatalytic reaction and protein engineering. These problems are commonly investigated by studying the kinetic behavior of an enzyme under different conditions. Subsequently, using these data, challenges in reaching the required intensity can be addressed by either protein engineering or alternatively process engineering solutions to circumvent kinetic limitations. However, it would be much better that solutions arise from a combination of both approaches for the most efficient development of biocatalytic processes. Regardless of the approach taken, enzyme improvement naturally starts in the hands of the protein engineer who typically screens for improved enzymes using single point measurements (i.e. at a single substrate concentration) to go through massive quantities of enzyme variants [4]. In this way, protein engineering is frequently able to deliver improved enzymes capable of catalyzing the conversion of non-natural substrates [5]. However, single point measurements only reveal apparent kinetics constants, such as the so-called specificity constant (V_{max}/K_M), which can be misleading as the basis for selecting the optimal enzyme [6–8]. At points in development where selection is from a smaller pool of protein variants, it would be desirable to quantify the kinetics in full in order to have an adequate basis for deciding on the best enzyme for a given reaction, and reactor configuration. Moreover, it is necessary to determine the activity of an enzyme of interest over the full range of potential operating conditions in order to truly assess the possibility of process implementation. On this premise, we suggest that comprehensive kinetic investigations should be integrated into the improvement cycle of an enzyme. In this way, it would be possible to direct screening to focus on evolving improved enzymatic kinetic properties, suitable for process implementation. In order to realize such a scheme, it is beneficial to develop an automated characterization system [9].

Traditionally, kinetic characterization of enzymes has been carried out using spectrophotometric assays or by generating time-series data by analyzing samples from a batch reactor using offline analysis [9]. However, the complexity of these experimental methods is greatly increased when characterizing oxygen dependent enzymes, due to the need for control of the dissolved oxygen concentration. Obtaining control of the dissolved oxygen concentration requires a steady supply of oxygen, typically via bubbling with air or molecular oxygen, and a dissolved oxygen probe to measure the concentration in solution. Measurements of reaction rates of oxygen dependent enzymes are therefore typically done in small (min. 50-100 mL) stirred reactors equipped with oxygen and/or air sparging and a dissolved oxygen probe, determining the reaction rate using offline analysis [10]. Alternatively, measurement can be performed in smaller vials (down to a few milliliter) equilibrated with an oxygen/nitrogen

mixture prior to starting the experiment, following the reaction by measuring the depletion of oxygen [11]. Both methods are labor intensive and especially the latter can be difficult to carry out with a sufficiently precise control of the dissolved oxygen concentration. Furthermore, both methods are limited by the concentration of oxygen in water in equilibrium with pure oxygen at ambient pressure (1.3 mM), since pressurization of standard laboratory equipment is often not a possible. This hampers the precise determination of kinetic constants, especially in cases where the Michaelis constant for oxygen (K_{MO}) is close to or above the oxygen solubility. Hence, neither of the current available methods are suitable for determining kinetics of oxygen dependent enzymes with an effort justifying characterization of multiple enzyme variants, for example when investigating the effect of amino acid substitutions on macro-kinetic constants.

Herein a new microfluidic tool for kinetic characterization of oxygen dependent enzymes is presented, which overcomes the problems of the existing methods. The setup uses a continuous flow reactor to allow full kinetic characterization of an oxygen dependent enzyme within 24 hours of autonomous operation using only a fraction of the material typically required. The setup precisely controls the dissolved oxygen concentration without direct contact between gas and liquid, thereby avoiding destabilization of enzymes sensitive to gas-liquid interfaces, which would otherwise complicate the results.

5.3 Description of apparatus

The developed apparatus combines microfluidic technology with oxygen supply across a gas-permeable membrane. In essence, enzyme is put in contact with an alcohol (or another oxidizable substrate) in a tubular reactor, where the dissolved oxygen concentration is constant and known, after which the extent of reaction can be quantified using a suitable detector (Figure 5.1).

Three syringe pumps supply the liquid reaction media composed of enzyme, substrate and buffer, to the tubular reactor. The flow rate and ratio between each of the components are controlled carefully using computer software. The three liquid streams are mixed using a static mixer prior to entering the reactor, thereby ensuring a homogeneous reaction mixture in the inlet of the reactor. The reactor is a so-called tube-in-tube reactor (TiTR), which is composed of an inner tube constructed of a material exhibiting high permeability to oxygen, and an outer tube practically impermeable to oxygen and nitrogen [12,13]. The liquid reaction mixture is pumped through the inner tube, while a mixture of nitrogen and oxygen is supplied in the space between the two tubes using two high precision mass-flow controllers. The gas is humidified before entering the TiTR to avoid stripping of water from the reaction mixture through the membrane. Both the inner and the outer tube can be pressurized up to 10 bar using pressure regulators on the outlets. A defined volume (100 nL or 5 µL) of the liquid reaction media leaving the reactor is injected into a UV-vis detector measuring the absorbance over the full UV-vis spectrum (190-710 nm), thus allowing quantification of substrate and/or product either by following a single wavelength or by applying chemometric analysis to a range of wavelengths.

The entire setup, meaning pumps, mass flow controllers, injection valve, detector, and pressure regulators are all computer controlled. Thereby, fully automated operation is achieved, where the computer software automatically changes oxygen and substrate concentrations and collects data. This means that 30 min to 1 hour of manual labor is required for stock preparation after which the setup runs for 16-24 hours, depending on the number of data points required, to fully characterize an enzyme.

A significant downside of determining reaction kinetics in tubular reactors, opposed to continuous stirred reactors, is the waiting time required between each steady-state to obtain time-series data required for determining catalytic rates. In the TiTR setup this waiting time is minimized by applying ramping of the liquid flow and analyzing the transient change in the substrate and product concentration [14]. This technique requires careful control of the flow regime inside the inner tube in order to ensure near perfect plug-flow despite the laminar conditions [15].

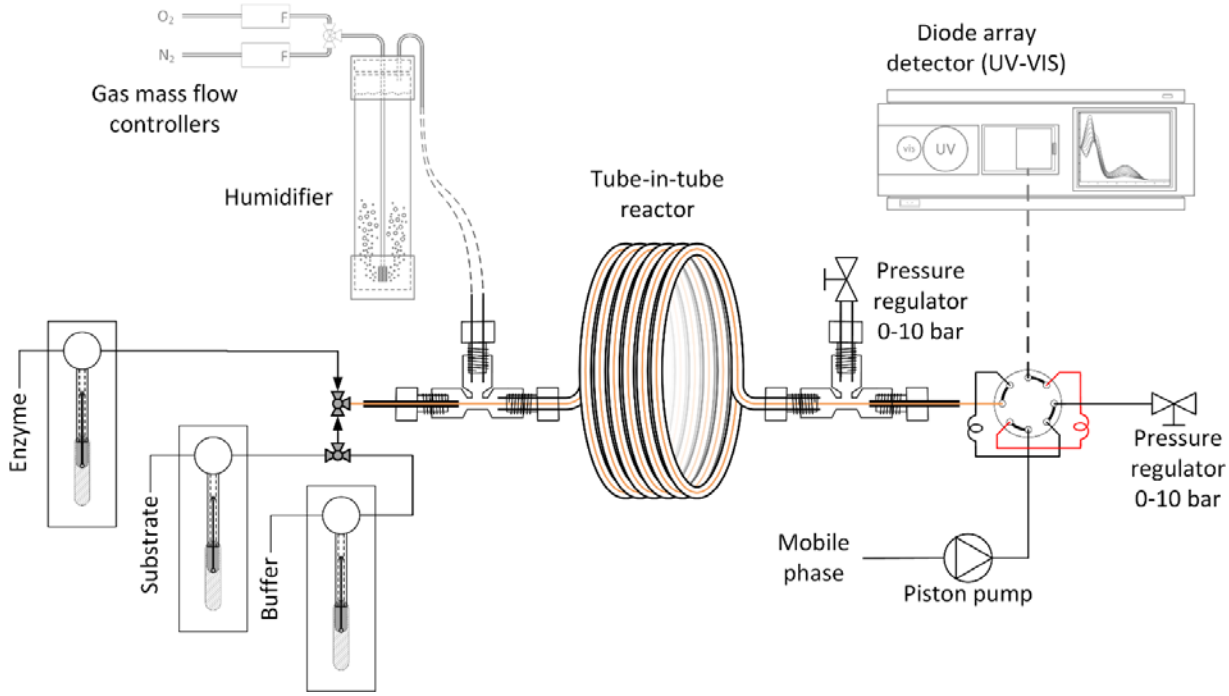

Figure 5.1. Schematic of tube-in-tube reactor setup for automated determination of oxygen dependent enzyme kinetics.

5.3.1 Tube-in-tube reactor

Ley and co-workers first described the tube-in-tube reactor for the flow synthesis of carboxylic acids using carbon dioxide [12]. Later, the applications have been extended to various chemical and also enzymatic reactions using gases such as ammonia, oxygen, hydrogen, and carbon monoxide [16–20]. The TiTR is, as in most applications described in the scientific literature, constructed from an outer tube made of polytetrafluoroethylene (PTFE) that is almost impermeable to oxygen, and an inner tube made of a co-polymer of tetrafluoroethylene and 2,2-bis(triflouromethyl)- 4,5-diflouro-1,3-dioxole (brand name Teflon AF-2400). The Teflon AF-2400 has a very high permeability to oxygen and the same high chemical

resistance known from PTFE. The small diameter of the inner tube results in a very large surface area to volume ratio (10^4 m^2/m^3), which combined with the high oxygen permeability of Teflon AF-2400 results in a very large oxygen transfer capability of the system (Figure 5.2). It is therefore possible to keep the dissolved oxygen concentration in the inner fiber within 99% of the saturation concentration at a given gas phase partial pressure of oxygen, even when running an oxygen consuming enzymatic reaction in the inner tube. Thus, precise control of the dissolved oxygen concentration is achieved by changing the composition and pressure of the gas supplied between the two tubes. It is however essential that the pressure of the inner tube is always higher than the pressure between the two tubes to avoid bubble formation in the liquid reaction media.

The length and tube diameters of the reactor were chosen to enable liquid flow rates resulting in low dispersed flow (see Section 4.2.3) at the relatively low residence times (2-10 min.) required for initial rate determination. A small inner diameter of 0.009" (230 µm) and a total reactor length of 3 m was chosen, resulting in a total inner fiber volume of 125 µL (the precise volume was later determined using residence time distribution measurements).

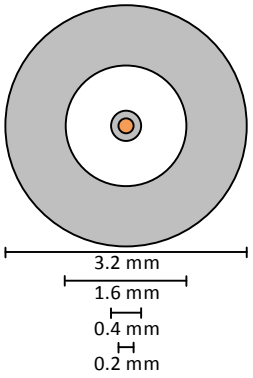

Figure 5.2. Cross section of the tube-in-tube reactor. White section is occupied with gas mixture and orange section with liquid reaction mixture.

The polymer material used for fabricating the inner tube of the TiTR reactor could potentially be chosen from a range of different polymers exhibiting high oxygen transfer rates, such as PDMS and PTMSP. PTMSP in fact has gas permeabilities of up to one order of magnitude higher than those of Teflon AF-2400 (Table 5.1). However, its chemical resistance towards aliphatic and aromatic hydrocarbons limits its practical applications [21,22]. PDMS has a much higher chemical resistance than PTMSP, but there are still significant compatibility issues with some solvents and small hydrophobic compounds, such as a range of amines and aldehydes [23]. The high chemical resistance of Teflon AF-2400 towards practically all chemical compounds (except perfluorinated hydrocarbons) makes it the ideal choice for constructing the inner tube of the TiTR. Furthermore, the low surface roughness of fluoropolymers limits the problem of protein absorption to the membrane [24].

Table 5.1. Oxygen and nitrogen permeability of selected polymers at 25 °C.

Material	Oxygen (Barrer[g])	Nitrogen (Barrer[g])
PTMSP[a,d]	9710	6890
Teflon AF-2400[c]	990	490
PDMS[b,e]	800	400
PTFE[c,f]	4.2	1.4

[a] [25] [b] [26] [c] [27]

[d] poly(1-trimethylsilyl-1-propyne) [e] polydimethylsilxoane [f] polytetrafluoroethylene

[g] 1 Barrer = 10^{-10} $cm^3(STP)\cdot cm/cm^2\cdot s\cdot cm_{Hg}$

5.3.2 Substrate and product quantification

Online analysis of reaction components is a key criteria for fast and automated operation. The suitability of detector technology depends on the reaction media and molecular species one wants to analyze and the speed of analysis required. Typically, chemical reactions are conducted in organic solvents where techniques such as infrared (IR) or near-infrared (NIR) spectroscopy excel [14]. However, for reactions in water IR spectroscopy is difficult to perform due to the broad IR absorption of water. To measure in aqueous solutions techniques such as ultraviolet-visible (UV-vis) absorbance or Raman spectroscopy are much better options. However, Raman spectroscopy is a very expensive technology compared to UV-vis spectroscopy, primarily due to the requirements to fine optics and a high-quality laser [28]. UV-vis spectroscopy was therefore chosen as the analysis method for the TiTR setup, although it limits the application to substrates and products containing chromophores that have a difference in absorbance spectrum. Nevertheless, oxidoreductases often produce a carbonyl-containing product, making it relatively easy to follow the product formation using UV-vis absorption (Figure 5.3). In some cases, as for the oxidation of 5-hydroxymethylfurfural to 2,5-diformylfuran, it is not possible to follow the conversion at a single wavelength due to overlapping substrate and product absorption spectra (Figure 5.3 right). In such cases, the substrate and product concentrations can be elucidated by applying multivariate data analysis, such as partial least squares (PLS) regression.

In principle, the UV-vis detector can be placed directly on outlet of the TiTR in an inline fashion. However, the volume of the flow cell in the detector (14 µL) is relatively large compared to the liquid flow rate through the system (maximum 77.5 µL/min). Therefore, the residence time in the flow cell would be substantial, compared to the residence time in the reactor. This means that the measurements must be corrected for the dilution effect, which is not straightforward due to the presumable imperfect mixing in the flow cell. Thus, inline analysis would introduce additional uncertainty to the measurements. The current setup therefore relies on a multiport injection valve, to collect a defined sample volume, which is injected into the detector using an auxiliary liquid stream. This limits the sampling frequency but increases reliability and precision.

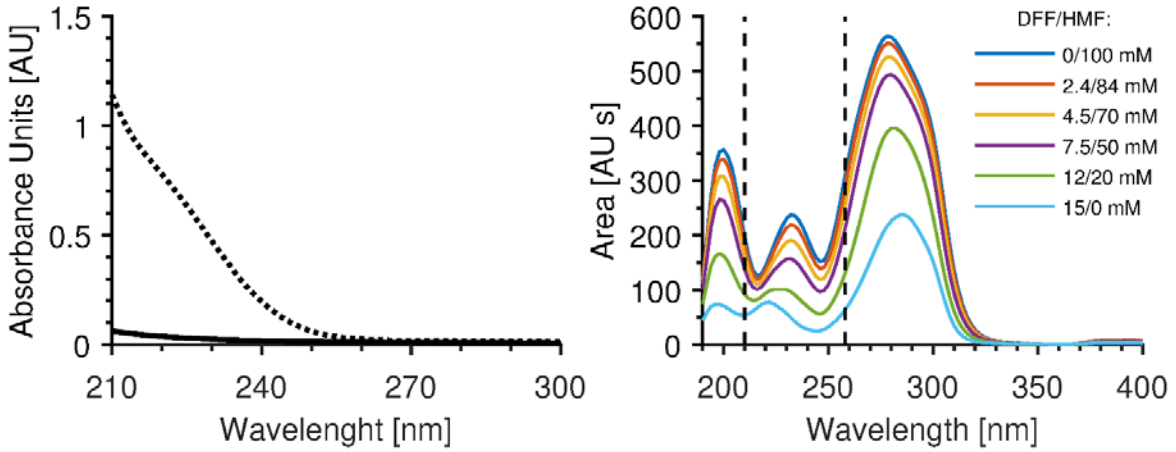

Figure 5.3. Left: Absorbance spectrum of 10 mM glucose (-) and gluconic acid (..). Right: Absorbance spectrum of 5-hydroxymethyl furfural (HMF) and 2,5-diformylfuran (DFF) at various concentrations. The vertical lines represents the range of wavelength on which the calibration is based.

5.3.3 Time-series data from a tubular reactor

Kinetic analysis in tubular flow reactors typically involves long waiting times between steady states of which multiple are required to obtain initial rates. This results in large consumption of materials and in inefficient use of the available apparatus. Recently, Moore and Jensen (2014) published a novel method for obtaining concentration-time data from tubular reactors by continuously monitoring the outlet species concentrations and manipulating the inlet flowrate once an initial steady state was obtained. Initially the inlet flow rate is kept constant and a steady state obtained. Hereafter the inlet flow rate is gradually decreased while keeping the ratio between the pump speeds constant, so the inlet concentrations of substrate and enzyme are not changed. Through careful control of the flow rate in the system, the instantaneous residence time of each fluid element leaving the reactor is known. Each fluid element therefore acts as a small batch reactor, whereby a concentration-time data series can be obtained by analyzing the amount of substrate and product in the reactor effluent during the flow rate ramp. Moore and Jensen (2014) verified the reliability of this approach for chemical reactions, while Ringborg (2016) showed the applicability to enzymatic reactions.

After the initial steady state at a residence time, τ_0, has been reached, a linear ramp in the instantaneous residence time is initiated corresponding to a change in inlet flowrate, q, as described by Eq. 5.1.

$$q(t) = \frac{V_r}{\tau_0 + \alpha t} \qquad \text{Eq. 5.1}$$

Where V_r is the reactor volume, α is the slope of the linear ramp in instantaneous residence time, and t the time measured from initiating the ramp. From this follows that the residence time of a fluid element leaving the reactor at time t, can be described by Eq. 5.2.

$$\tau = (1 - e^{-\alpha})\left(\frac{\tau_0}{\alpha} + t\right) \qquad \text{Eq. 5.2}$$

Eq. 5.2 only holds for fluid elements entering the reactor after initiation of the residence time ramp. For fluid elements entering the reactor before initiating the ramp (i.e. $t_i < 0$, t_i being the time of entrance) and leaving after ramp initiation, the residence time is described by Eq. 5.3.

$$\tau = t - \tau_0 \left(\frac{1}{\alpha} \ln \left(\frac{\tau_0 + \alpha t}{\tau_0} \right) - 1 \right) \qquad \text{Eq. 5.3}$$

Eq. 5.4 gives the entrance time of a fluid element leaving the reactor at time, t.

$$t_i = \tau_0 \left(\frac{1}{\alpha} \ln \left(\frac{\tau_0 + \alpha t}{\tau_0} \right) - 1 \right) \qquad \text{Eq. 5.4}$$

The mathematical prove of the above equations are given in the supplementary information of Moore and Jensen (2014). Figure 5.4 shows the relationship between the residence time and time after initiation of the flow rate ramp for different values of α. A small α corresponds to slow ramping of the instantaneous residence time, which gives longer experiments but on the other hand enabling a larger data density if the analysis method is not instantaneous. This is especially useful when applying online UV-vis spectroscopy using flow injection analysis, which has a limited sampling frequency.

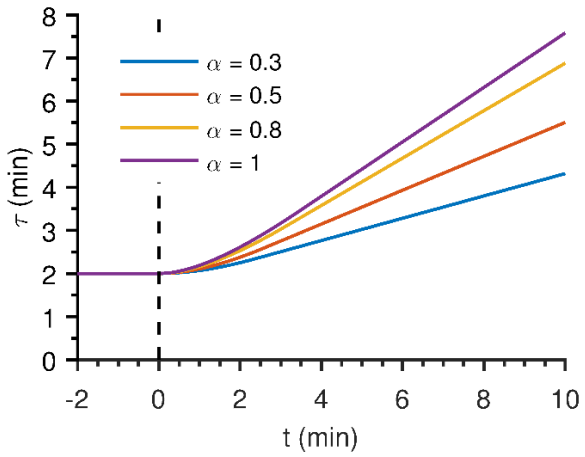

Figure 5.4. Residence time of fluid element leaving the reactor at time t after initiation of flow rate ramp.

Low dispersed flow

The flow rate ramping method assumes plug-flow behavior of the tubular reactor. Typically, plug-flow behavior is only obtained at turbulent flow conditions, something which is nearly impossible to obtain in micro-reactors due their small dimensions. However, at very low linear velocities and small diffusion lengths the rate of radial diffusion becomes much faster than the convective mass transfer in the axial direction. In other words, diffusion evens out the parabolic flow profile, whereby near-perfect plug-flow behavior can be obtained, despite the laminar flow regime [15]. At these conditions, the flow can be considered non-dispersed (Figure 5.5).

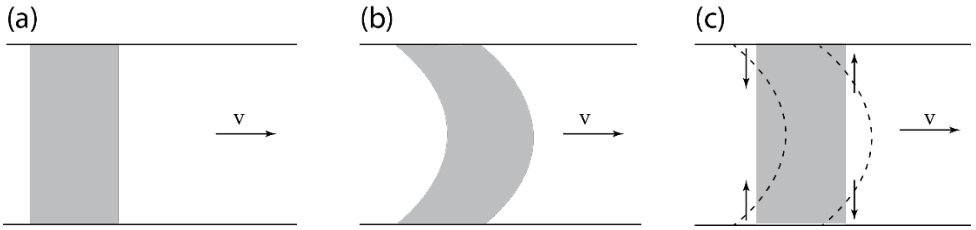

Figure 5.5. a) Ideal plug-flow behaviour desired to simplify reactor modelling. B) Parabolic flow profile obtained when operating in the laminar flow regime c) At non-dispersed flow conditions, small diffusion lengths and low linear velocity, diffusion evens out the parabolic flow profile to obtain plug-flow. Adapted from [29]**.**

The degree of dispersion can be described by the dimensionless Bodenstein number (Bo, Eq. 5.5), which is representing the ratio of convection to dispersion [15].

$$\mathrm{Bo} = \frac{\nu \mathrm{L}}{\boldsymbol{D}} \qquad \text{Eq. 5.5}$$

Where ν is the linear velocity of the liquid stream, L is the length of the reactor, and **D** is the Taylor's dispersion coefficient defined by Eq. 5.6.

$$\mathbf{D} = \mathrm{D} + \frac{\nu^2 d_t^2}{4\beta D} \approx \frac{\nu^2 d_t^2}{4\beta D} \qquad \text{Eq. 5.6}$$

Where D is the diffusion coefficient, d_t is the hydraulic diameter of the tube, and β is a geometry depending parameter, which for circular tubes is 48 [30].

At high Bodenstein numbers (Bo > 1000), the dispersion in a channel is neglectable, meaning that near-perfect plug-flow behavior is experienced. At medium Bodenstein numbers (Bo = 100-1000) smaller deviations from plug-flow is observed, while large deviations occur for small Bodenstein numbers (Bo < 100) [15]. For the TiTR reactor, with an inner diameter of 200 µm, this corresponds to a minimum residence time of 208 and 21 seconds to comply with the plug-flow and small deviations from plug-flow criteria, respectively. Hence, the residence time ramp typically is initiated from a steady state at a residence time of 120 seconds and ramped to a final residence time of 300 seconds.

5.4 Result and discussion

In order to demonstrate the performance of the instrument, the well-known enzyme, glucose oxidase (GOx, E.C. 1.1.3.4), was selected. The GOx enzyme catalyzes the oxidation of glucose to glucono-δ-lactone, with molecular oxygen, which is reduced to hydrogen peroxide. Following the enzymatic reaction, glucono-δ-lactone is spontaneously hydrolyzed to gluconic acid, which formation can be followed spectrophotometrically. The formed hydrogen peroxide is removed by the addition of catalase, which facilitates its instantaneous conversion into water and half the stoichiometric amount of oxygen. The removal of hydrogen peroxide forces the reaction to proceed in a unidirectional manner and also protects GOx from oxidation. GOx has been shown to follow a ping-pong bi bi reaction mechanism (Scheme 1) [31].

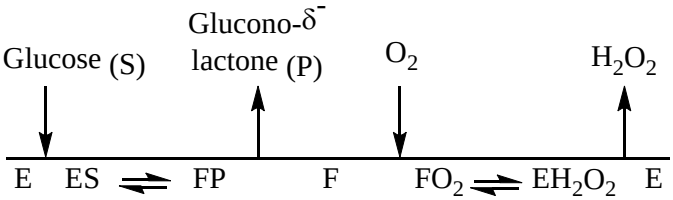

Scheme 1. Cleveland representation of the glucose oxidase ping-pong bi bi mechanism. E denotes the oxidized free form of the enzyme whereas F denotes the reduced form of the free enzyme.

The rate expression can be derived using the classical stead-state assumption and any of the various methods for deriving enzymatic rate expressions, which all lead to the expression shown in Eq. 5.7.

$$\frac{\mathrm{r}}{E_T} = \frac{k_{cat}\, S\, O}{S\, O + \mathrm{K_{MO}}\, S\, + \mathrm{K_{MS}}\, \mathrm{O}} \qquad \text{Eq. 5.7}$$

5.4.1 Reactor volume

The determination of liquid volume of the system is of crucial importance when calculating the residence time at a given flow rate and thereby the accuracy of the determined initial rates. It is possible to calculate the volume based on the inner diameter of the inner tube and the dead volume of the fittings. However, this is rather unprecise because the tolerance of the inner tubing diameter is typically ±25 µm or more, which leads to a variation of volume of ± 28.5 µL for a three meter long reactor. The volume of the inner tube and any dead-volumes present in fittings and connections was determined by introducing a step-change in the inlet concentration of gluconic acid and recording the residence time distribution by following the gluconic acid concentration in the outlet of the reactor (Figure 5.6). By integrating the cumulative residence time distribution, the volume was determined to 155 ± 1.8 µL.

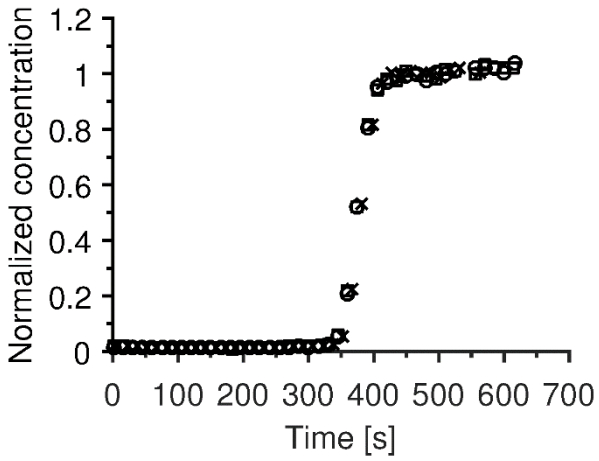

Figure 5.6. Residence time distribution experiments. Three repetitions of a step change response with a flow rate of 25 µL/min.

5.4.2 Calibration

The difference in absorbance between glucose and gluconic acid makes quantification of the gluconic acid concentration straightforward using a single wavelength (Figure 5.3). 210 nm was chosen as the preferred wavelength. The absorbance-time data was integrated to obtain

a peak area, which was correlated with a gluconic acid concentration as seen in Figure 5.7. Glucose (and the enzyme) also absorb light at 210 nm, however, the absorbance is small and the concentration of glucose is almost constant. The contribution of such can therefore be neglected, since only the rate of reaction is of interest and not the absolute gluconic acid concentration.

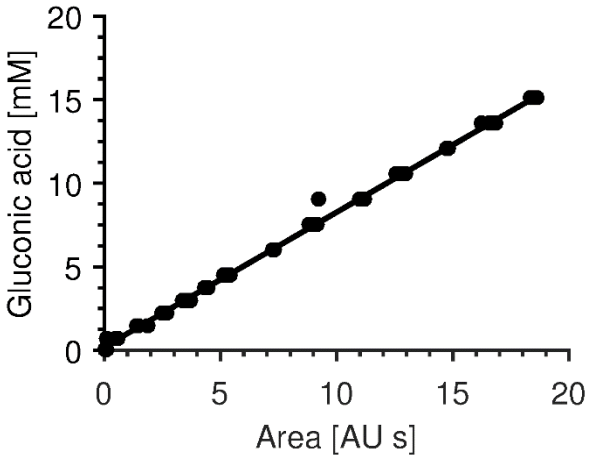

Figure 5.7. Calibration of gluconic acid at a wavelength λ = 210 nm

5.4.3 Validation of flow ramp method

The validity of the flow manipulation method for generating time-series data has been thoroughly validated by Moore and Jensen (2014). However, to verify that the data generated was reliable also for enzyme catalyzed reactions, data generated using the ramp method was compared with steady-state experiments (Figure 5.8). The steady-state data was collected after waiting four residence times. The results show that there is little to no difference between the two sampling methods, indicating that that the low dispersed flow condition was met and the ramping method valid.

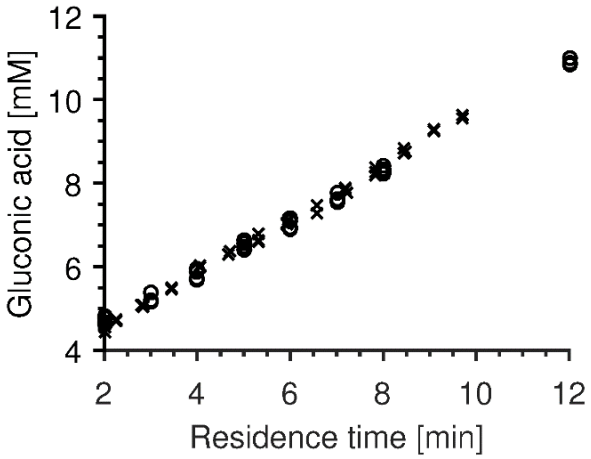

Figure 5.8. Comparison of running the setup in a steady state mode (o) and ramp mode (x), experiments were carried out with 0.1 mg/mL GOx enzyme, 100 mM glucose, 0.52 mM O_2 and with 100 mM potassium phosphate buffer at pH 7.

5.4.4 Mass transfer limitations

The high oxygen permeability of Teflon AF-2400 combined with the very large surface area to volume ratio for the TiTR reactor (17000 m^2/m^3), results in very high oxygen mass transfer rates, corresponding to a volumetric mass transfer coefficient of 16000 h^{-1}. Calculations show, that this enables operation at a dissolved oxygen concentration within 99% of the oxygen solubility at the given conditions, even with a reaction in the liquid phase consuming oxygen at a rate of more than 5 mmol L^{-1} min^{-1}. To confirm that no oxygen limitations was experienced, the enzyme concentration was varied while keeping the oxygen concentration constant at 0.52 mM (Figure 5.9), which is in a range where the reaction rate of glucose oxidase is highly dependent on the oxygen concentration. A linear dependency between enzyme concentration and rate of reaction was observed, as one would expect if mass transfer does not influence the rate of reaction.

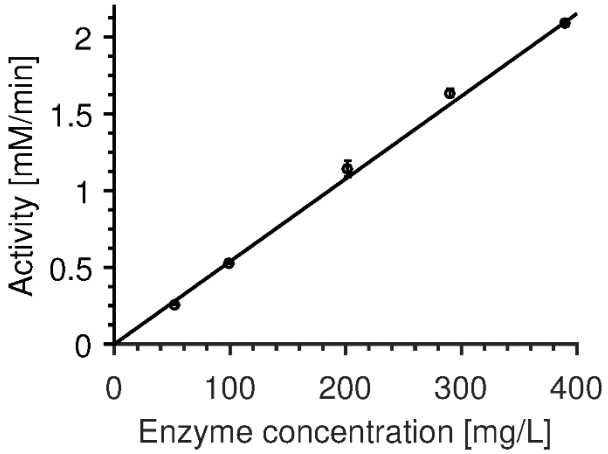

Figure 5.9. Activity as a function of enzyme concentration at an oxygen concentration of 0.52 mM and a glucose concentration of 100 mM.

5.4.5 Glucose oxidase kinetics

Initial enzyme rates obtained in the TiTR setup was validated by comparison with data previously published by Toftgaard Pedersen et al. (2017). In these experiments, initial rates were measured in an aerated stirred tank reactor with adjustable oxygen/nitrogen feed. The comparison reveals an excellent correlation between the two systems and the combined result of the experiments confirms the validity of enzyme kinetics determined in the TiTR setup (Figure 5.10).

The fit of Eq. 5.7 to the data revealed a relatively high Michaelis constant for oxygen of 0.52 mM (Table 5.2), which also is seen from the unsaturated enzyme kinetics observed at high glucose concentrations and atmospheric pressure (Figure 5.10). It is generally accepted, that in order to reliably quantify Michaelis constants it is necessary to measure enzyme kinetics in a sufficiently large range of substrate concentrations, minimum 5-fold and preferably 10-fold higher and lower than the true K_M. In the TiTR setup, this was achieved by increasing the operating pressure of the setup to six bar to increase the solubility of oxygen to 7.13 mM

(using pure O_2 at 25 ˚C). Enzyme saturation was thereby obtained even at the highest concentration of glucose (Figure 5.11), enabling a more reliable prediction of all the kinetic parameters (Table 5.2).

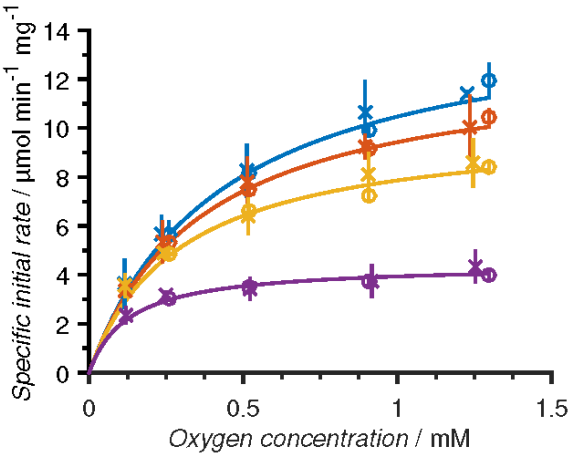

Figure 5.10. Specific initial reaction rate vs oxygen concentration at different levels of glucose in Batch (x) and TiTR (o). Blue – 400 mM glucose, red – 200 mM glucose, yellow – 100 mM glucose and purple – 25 mM glucose, full lines are the model fit to the TiTR results. The experiments were carried out at pH 7, 25 °C and atmospheric pressure. The batch data is scaled by a factor 0.79 to correct for time dependent degradation of the enzyme formulation between the experiments.

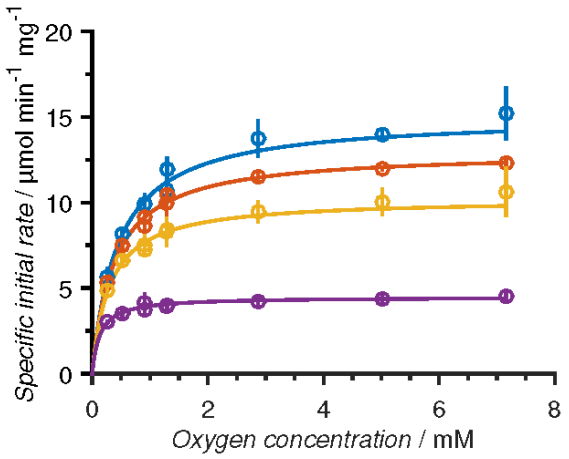

Figure 5.11. Data collected in the TiTR at 1 atm (0.14-1.3 mM O2) and 6 bar (0.9-7.13 mM O2) plotted and fitted together. Blue – 400 mM glucose, red – 200 mM glucose, yellow – 100 mM glucose and purple – 25 mM glucose, o – marks TiTR results, full lines are the model fit. The experiments were carried out at pH 7 and 25 °C.

Table 5.2. Parameter estimations based on different experimental data.

Parameter	**Batch reactor[a] (1 atm)**	**TiTR (1 atm)**	**TiTR (1 atm + 6 bar)**
k_{cat} [µmol min^{-1} mg^{-1}][b]	17.58 ± 0.62[c]	17.78 ± 1.39	17.82 ± 0.47
K_{MO} [mM]	0.45 ± 0.04	0.51 ± 0.09	0.52 ± 0.03
K_{MS} [mM]	73.1 ± 6.87	75.2 ± 9.38	74.57 ± 5.55

[a] From [10] [b] Based on milligrams of liquid formulation [c] The batch data is scaled by a factor 0.79 to correct for time dependent degradation of the enzyme formulation between the experiments

The TiTR setup was fully automated and computer controlled, thereby enabling characterization of an oxygen dependent enzyme within 24 hours with minimal manual labor. While the preparation of solutions is identical for both batch and TiTR, the batch setup requires approximately four working days of manual labor to characterize an enzyme to the extend shown above. Furthermore, the small dimension of the TiTR system makes it possible to collect one initial rate measurement per 1.4 mL of reaction mixture, which is much less, than the 50-150 mL used in the alternative sparged batch setup. Overall, the TiTR system enables faster enzyme characterization, while significantly reducing labor intensity and material consumption.

5.5 Possibilities and future developments

An automated enzyme characterization tool, as described above, opens many possibilities for oxygen dependent biocatalysis, especially if such a tool can be made commercially available to the broader community of enzymologists, protein engineers, and chemical engineers working with the development of biocatalytic processes.

Currently, new enzyme variants are evaluated by measuring the specific reaction rate at a single oxygen concentration (air saturation), which is far from typical operational conditions in an industrial reactor. In an industrial reactor, the oxygen concentration is low to allow a large oxygen transfer rate from the sparging air to the liquid reaction mixture. The oxygen reactivity of the enzyme is therefore in many cases determining the efficiency of enzymatic reaction, i.e. the enzyme loading required to reach a desired productivity (see Chapter 4). Easy determination of the kinetic parameters for both the primary substrate and oxygen will enable protein engineers to evaluate not only the ability of an enzyme to convert a given substrate, but also the ability of the enzyme to catalyze the reaction at low oxygen concentrations. This will eventually allow protein engineers to develop enzymes with improved oxygen reactivity (see Chapter 7) and ensure that enzyme variants chosen for further development are efficient at industrial conditions. The access to precise kinetic data will also allow chemical engineers to design the biocatalytic process at an earlier stage. This enables earlier identification of potential process bottlenecks and more accurate cost calculations, which simplifies target setting for biocatalyst performance metrics required as feedback to the protein engineers developing the biocatalyst.

Table 5.3. Permeability of Teflon AF-2400 for gases interesting for biocatalytic reactions. Adapted from: [27]

Gas	**Permeability (Barrer[a])**
Oxygen	990
Carbon dioxide	2800
Hydrogen	2200
Ethylene	350
Methane	340
Ethane	180

[a] 1 Barrer = 10^{-10} $cm^3(STP)\cdot cm/cm^2\cdot s\cdot cm_{Hg}$

The TiTR setup is capable of characterizing the kinetics of most enzymes requiring oxygen as long as the enzyme uses a substrate or produces a (co-)product that absorbs light in the UV-vis range. The application is however not limited to oxygen dependent enzymes alone, but can in principle be used to study many other enzymes requiring gaseous substrates (Figure 5.12), due to the generally high gas permeability of Teflon AF-2400 (Table 5.3). In general, gases of synthetic potential have low aqueous solubility meaning that reliable kinetic characterization of enzymes employing such gases as substrates will be difficult in current state-of-the-art laboratory equipment. The TiTR setup can therefore significantly reduce the effort required when working with enzymes such as hydrogenases requiring hydrogen, formate dehydrogenases requiring carbon dioxide, ammonia lyases requiring ammonia, and methane monooxygenases requiring methane [32–35]. Additionally, the small volume of the TiTR system makes safe handling of toxic gases very easy.

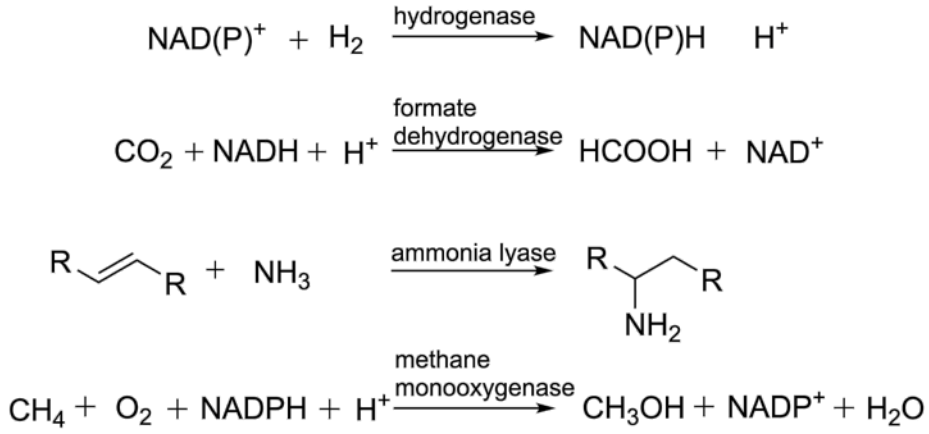

Figure 5.12. Examples of other gas dependent reactions that could be characterized in the tube-in-tube reactor.

5.6 Conclusions

In conclusion, we have developed and validated an automated flow reactor system that rapidly and accurately determines the kinetics of oxygen dependent enzymes. Here the oxygen level is controlled and can achieve high concentrations which are up to 25-fold higher than what is possible using air at atmospheric conditions. It was possible to use the low dispersed flow regime in the reactor to generate time-series data with an enzymatic catalyst despite its low diffusivity and the resulting data were in good agreement with experiments conducted in a batch system. The system is capable of characterizing the kinetics of any enzyme within the oxidoreductase class EC 1, where reactions frequently results in changes to the UV-spectra to enable quantification of conversion. The tool presented here could introduce kinetic characterization of oxidoreductases into the catalyst development cycle, where biocatalytic reaction engineering can be used to guide both process and protein engineering [9,36].

5.7 Experimental section

5.7.1 Materials

Glucose oxidase (EC 1.1.3.4) from *Aspergillus niger* (Novozym® 28166) was kindly supplied by Novozymes A/S (Bagsværd, DK). Catalase (EC 1.11.1.6) from bovine liver with specific activity 3172 U/mg was acquired from Sigma Aldrich (St. Louis, MO, USA). Glucose, gluconic acid, and buffer chemicals were of highest quality available from Sigma Aldrich, VWR (Radnor, PA, USA), or Thermo Fisher Scientific (Waltham, MA, USA).

5.7.2 Experimental setup

Reaction mixture was supplied to the setup using three identical syringe pumps (Cavro XLP 6000, TECAN®, Männedorf, Switzerland) equipped with 100 µL syringes. The outlet of the pumps were mixed in a micro mixer (402-0005B, ASI Corp., Richmond, CA, USA) before entering the reactor. A defined gas mixture of nitrogen and oxygen was supplied using two mass-flow controllers (SmartTrak 50, Sierra Instruments, Monterey, CA, USA). The gas was prehumidified by bubbling it through a water column (constructed in-house) before the gas entered the reactor. This ensured that the gas reached a relative humidity of 100% to avoid stripping of water from the reaction mixture in the reactor. The tube-in-tube reactor (TiTR) was constructed using an outer PTFE tube and an inner tube made of Teflon AF-2400, see below. Teflon AF-2400 is an amorphous fluoropolymer made as a copolymer of 2,2-bistriflouromethyl-4,5-diflouro-1,3-dioxole and tetrafluoroethylene [37].

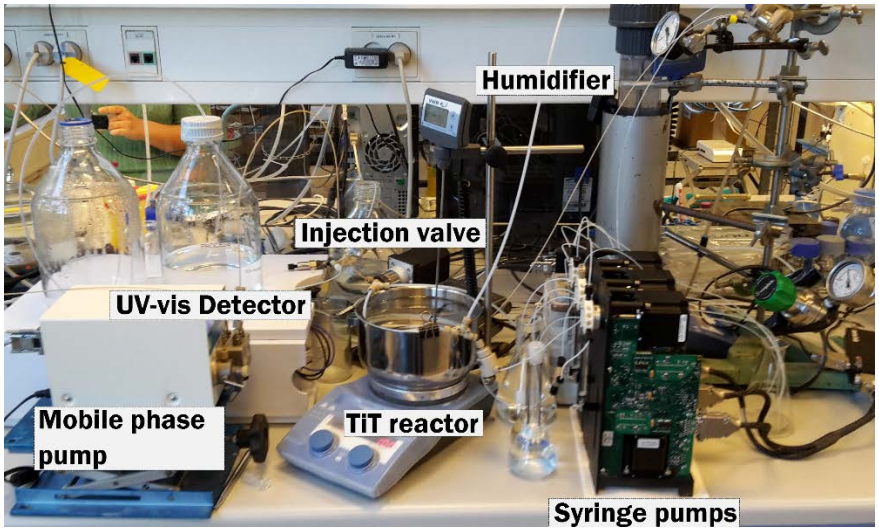

Figure 5.13. Picture of tube-in-tube reactor setup.

The reactor was capable of being pressurized up to 10 bar on both the gas and liquid side using an adjustable gas backpressure regulator (KBP1G0D4A5A2, Swagelok, Solon, OH, USA) and an adjustable liquid backpressure regulator (ZNF1FPK-5, VICI, Houston, TX, USA). The TiTR was submerged in a temperature-controlled water-bath. The reaction progress was followed by analyzing the composition in the liquid outlet using an UV/VIS diode array detector (G1315A, Agilent Technologies, Santa Clara, CA, USA) equipped with a 14 µL flow cell with a 1 cm path length. Samples were injected into the flow cell using an 8-

port actuated injection valve (VICI) equipped with two 5 µL injection loops. Mobile phase (deionized water buffered to pH of reaction mixture) was continuously flushed through the flow cell using an HPLC pump (Smartline 100, 10 mL ceramic pump heads, KNAUER, Berlin, Germany). The detector was not installed in-line because of dilution effects in the flow cell, i.e. the flowrate relative to the volume of the flow cell results in a system with a response time greater than the change induced by the reduction in flow rate.

Control of syringe pumps, oxygen and nitrogen flow rate, injection valve and the detector was automated using LabVIEW (National Instruments, Austin, TX, USA).

Tube-in-tube reactor

The TiTR design, with various dimensions depending on the application, has been described in detail in several scientific publications [12,13,17,20]. The TiTR used in this work was constructed from a small diameter Teflon AF-2400 tubing (I.D. 0.23 mm, O.D. 0.41 mm, Biogeneral Inc., San Diego, CA, USA), to obtain low-dispersed flow even at low residence times. The inner Teflon Af-2400 was encased by PTFE tubing (1.6 mm I.D., O.D. 3.2 mm, BOLA, Grünsfeld, Germany), practically impermeable to oxygen and nitrogen. The two tubes were each three meters long. The inner diameter of the outer tube was selected to provide a relatively large cross sectional area. This ensured that the gas-side pressure drop across the reactor was minimal and enabled the precise control of the gas-side pressure to ensure a uniform dissolved oxygen concentration along the entire length of the reactor. On the other hand, a liquid-side pressure drop of up to one bar could not be avoided. However, as long as the liquid-side pressure is maintained well above the gas-side pressure no gas bubbles are formed in the liquid stream, and the dissolved oxygen concentration can be controlled solely by the gas-side partial pressure of oxygen.

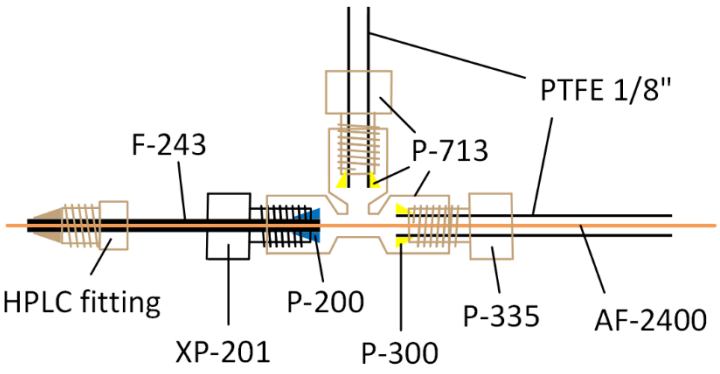

Figure 5.14. Final assembly of either end of the TiTR reactor. Orange line represents the inner Teflon AF-2400 fibre.

The construction of the TiTR is straightforward and possible with of-the-shelf components. The most critical step was to ensure an air and liquid tight inlet and outlet connection. The T-connection merging the gas and liquid lines into the tube-in-tube reactor was constructed with the following fittings (IDEX-HS, Lake Forrest, IL, USA): T-connector for 1/8” tubing

(P-713), which included nuts for 1/8” tubing (P-335) and ferrules for 1/8” tubing (P-300), nuts for 1/16” tubing (XP-201), ferrules for 1/16” tubing (P-200), and tube sleeve (I.D. 0.46 mm, O.D. 1.6 mm, F-243). The final assembly can be seen in Figure 5.14.

5.7.3 Protocol

Pumps were initially primed with the designated substrate, buffer and enzyme solutions, and were thereafter set to run continuously to reach steady state. In parallel, the mass-flow controllers were set to produce a defined mixture of oxygen and nitrogen. To ensure steady state, the system was set to wait a total of three residence times for all set points. After which a sample was injected into the detector, and the ramp method initiated. The method gradually lowers the flow rate, without changing the inlet concentration any component, from the initial steady state value to increase the residence time. By analyzing the output of the reactor, precise time series data can be obtained. The slope of the residence time ramp, α, was set to 0.5 in all experiments reported in this work and the ramp in flow rate was run for 15 min. (real time) generating data from a residence time of 2 min. to 10 min. Samples were collected every minute resulting in 11 samples for each initial rate experiment. The flow rate for each syringe pump and percentage of oxygen in the gas was controlled by LabVIEW, which automatically changed the set-point according to a predefined list of set-points.

Samples were analyzed on the diode array UV/Vis detector. Before a sample was injected, the detector was balanced and zeroed. Once it reported ready, the injection valve was turned to inject a sample using the flow of the mobile phase. Thereafter, spectral data was collected over time with a frequency of 20 Hz whereby 3-dimensional (time-wavelength-absorbance) data was obtained. The absorbance was measured from 210 to 600 nm with a slit width of 4 nm and a step width of 1 nm.

To characterize an enzyme, three stock solutions were made – one containing 0.5 mg/mL glucose oxidase in buffer, one containing buffer, and one containing 500 mM glucose in buffer. All solutions were buffered to pH 7.0 using 100 mM potassium phosphate buffer. The enzyme solution was pumped at a constant ratio of 1/5 of the total flow rate through the reactor, while the ratios of buffer and glucose solutions were varied according to the glucose concentration set-point. The total gas flow was kept constant at 1 NL/min, while the volume fraction of oxygen in the gas was varied from 5-100%. For the experiments reported, the reactor was left to run at atmospheric pressure and in a separate experiment pressurized to 6 bars.

Data handling and parameter estimation was performed in MATLAB (MathWorks, Natick, MA, USA). Initially, the raw data from LabVIEW was converted to concentrations by using a calibration model. A linear model was fitted to the concentration-time data to obtain the initial rate as the slope. The data was discarded if the linear model was not describing the data sufficiently well ($R^2 < 0.9$). The parameters of the enzyme kinetic model (ping pong bi bi) was estimated using non-linear least square regression taken into account the uncertainty of the initial rate data.

5.8 References

[1] Kroutil W, Mang H, Edegger K, Faber K, **2004**. Biocatalytic Oxidation of Primary and Secondary Alcohols, Adv. Synth. Catal. 346(23):125–142.

[2] Hollmann F, Arends IWCE, Buehler K, Schallmey A, Bühler B, **2011**. Enzyme-mediated oxidations for the chemist, Green Chem. 13(2):226.

[3] Punniyamurthy T, Velusamy S, Iqbal J, **2005**. Recent advances in transition metal catalyzed oxidation of organic substrates with molecular oxygen, Chem. Rev. 105(6):2329–63.

[4] Fallah-Araghi A, Baret J-C, Ryckelynck M, Griffiths AD, **2012**. A completely in vitro ultrahigh-throughput droplet-based microfluidic screening system for protein engineering and directed evolution, Lab Chip. 12(5):882–891.

[5] Bornscheuer UT, Huisman GW, Kazlauskas RJ, Lutz S, Moore JC, Robins K, **2012**. Engineering the third wave of biocatalysis, Nature. 485(7397):185–94.

[6] Eisenthal R, Danson MJ, Hough DW, **2007**. Catalytic efficiency and kcat/KM: a useful comparator?, Trends Biotechnol. 25(6):247–249.

[7] Koshland DE, **2002**. The application and usefulness of the ratio k(cat)/K(M)., Bioorg. Chem. 30(3):211–213.

[8] Fox RJ, Clay MD, **2009**. Catalytic effectiveness, a measure of enzyme proficiency for industrial applications, Trends Biotechnol. 27(3):137–140.

[9] Ringborg RH, Woodley JM, **2016**. The Application of Reaction Engineering to Biocatalysis, React. Chem. Eng. 1(1):10–22.

[10] Toftgaard Pedersen A, Carvalho T, Sutherland E, Rehn G, Ashe R, Woodley JM, **2017**. Characterisation of a continous agitated cell reactor for oxygen dependent biocatalysis, Biotechnol. Bioeng. 114(6):1222–1230.

[11] Brugger D, Krondorfer I, Shelswell C, Huber-Dittes B, Haltrich D, Peterbauer CK, **2014**. Engineering Pyranose 2-Oxidase for Modified Oxygen Reactivity, PLoS One. 9(10):e109242.

[12] Polyzos A, Brien MO, Petersen TP, Baxendale IR, Ley S V, **2011**. The Continuous-Flow Synthesis of Carboxylic Acids using CO 2 in a Tube-In-Tube Gas Permeable Membrane Reactor, Angew. Chemie. 50:1190–1193.

[13] O'Brien M, Baxendale IR, Ley S V., **2010**. Flow ozonolysis using a semipermeable Teflon AF-2400 membrane to effect gas - Liquid contact, Org. Lett. 12(7):1596–1598.

[14] Moore JS, Jensen KF, **2014**. Batch kinetics in flow: Online IR analysis and continuous control, Angew. Chemie - Int. Ed. 53(2):470–473.

[15] Nagy KD, Shen B, Jamison TF, Jensen KF, **2012**. Mixing and dispersion in small-scale flow systems, Org. Process Res. Dev. 16(5):976–981.

[16] Brzozowski M, O'Brien M, Ley S V, Polyzos A, **2015**. Flow chemistry: Intelligent processing of gas-liquid transformations using a tube-in-tube reactor, Acc. Chem. Res. 48(2):349–362.

[17] O'Brien M, Taylor N, Polyzos A, Baxendale IR, Ley S V., **2011**. Hydrogenation in flow: Homogeneous and heterogeneous catalysis using Teflon AF-2400 to effect gas–liquid contact at elevated pressure, Chem. Sci. 2(7):1250.

[18] Koos P, Gross U, Polyzos A, O'Brien M, Baxendale I, Ley S V, **2011**. Teflon AF-2400 mediated gas-liquid contact in continuous flow methoxycarbonylations and in-line FTIR measurement of CO concentration., Org. Biomol. Chem. 9(20):6903–8.

[19] Cranwell PB, O'Brien M, Browne DL, Koos P, Polyzos A, Peña-López M, Ley S V, **2012**. Flow synthesis using gaseous ammonia in a Teflon AF-2400 tube-in-tube reactor: Paal–Knorr pyrrole formation and gas concentration measurement by inline flow titration, Org. Biomol. Chem. 10(30):902–911.

[20] Tomaszewski B, Schmid A, Buehler K, **2014**. Biocatalytic production of catechols using a high pressure tube-in-tube segmented flow microreactor, Org. Process Res. Dev. 18(11):1516–1526.

[21] Pinnau I, He Z, **2004**. Pure- and mixed-gas permeation properties of polydimethylsiloxane for hydrocarbon/methane and hydrocarbon/hydrogen separation, J. Memb. Sci. 244(1–2):227–233.

[22] Nagai K, Masuda T, Nakagawa T, Freeman BD, Pinnau I, **2001**. Poly[1-(trimethylsilyl)-1-propyne] and related polymers: synthesis, properties and functions, Prog. Polym. Sci. 26(5):721–798.

[23] Lee JN, Park C, Whitesides GM, **2003**. Solvent Compatibility of Poly(dimethylsiloxane)-Based Microfluidic Devices, Anal. Chem. 75(23):6544–6554.

[24] Drummond CJ, Georgaklis G, Chan DYC, **1996**. Fluorocarbons: Surface Free Energies and van der Waals Interaction, Langmuir. 12(11):2617–2621.

[25] Robeson L., **1999**. Polymer membranes for gas separation, Curr. Opin. Solid State Mater. Sci. 4(1999):549–552.

[26] Merkel TC, Bondar VI, Nagai K, Freeman BD, Pinnau I, **2000**. Gas sorption, diffusion, and permeation in poly(dimethylsiloxane), J. Polym. Sci. Part B Polym. Phys. 38(3):415–434.

[27] Nemser SM, Roman IC, **1991**, Perfluorodioxole Membranes, US 5051114.

[28] Jestel NL, Raman Spectroscopy, in: K.A. Bakeev (Ed.), Process Anal. Technol. Spectrosc. Tools Implement. Strateg. Chem. Pharm. Ind., **2010**, John Wiley & Sons, Ltd., Chichester: pp. 195–243.

[29] Ringborg RH, Application of a microfluidic tool for the determination of enzyme kinetics, Technical University of Denmark, **2016**.

[30] Datta S, Ghosal S, **2009**. Characterizing dispersion in microfluidic channels, Lab Chip. 9(17):2537–2550.

[31] Gibson QH, Swoboda BEP, Massey V, **1964**. Kinetics of Action of Glucose, J. Biol. Chem. 239(11):3927–3934.

[32] Chan SI, Lu YJ, Nagababu P, Maji S, Hung MC, Lee MM, Hsu IJ, Minh PD, Lai JCH, Ng KY, Ramalingam S, Yu SSF, Chan MK, **2013**. Efficient oxidation of methane to methanol by dioxygen mediated by tricopper clusters, Angew. Chemie - Int. Ed. 52(13):3731–3735.

[33] Lauterbach L, Lenz O, Vincent KA, **2013**. H2-driven cofactor regeneration with NAD(P)+-reducing hydrogenases, FEBS J. 280(13):3058–3068.

[34] Shi J, Jiang Y, Jiang Z, Wang X, Wang X, Zhang S, Han P, Yang C, **2015**. Enzymatic conversion of carbon dioxide, Chem. Soc. Rev. Chem. Soc. Rev. 44(44):5981–6000.

[35] Turner NJ, **2011**. Ammonia lyases and aminomutases as biocatalysts for the synthesis of a-amino and b-amino acids, Curr. Opin. Chem. Biol. 15(2):234–240.

[36] Woodley JM, **2013**. Protein engineering of enzymes for process applications, Curr. Opin. Chem. Biol. 17(2):310–316.

[37] Resnick PR, Buck WH, Teflon AF Amorphous-Fluoropolymers, in: Mod. Fluoropolymers, **1997**, John Wiley & Sons, Ltd., Chichester: pp. 397–419.

Chapter 6

Process requirements of galactose oxidase catalyzed oxidation of alcohols

This chapter is based upon a published research paper and its supporting information:

Toftgaard Pedersen A, Birmingham WR, Rehn G, Charnock SJ, Turner NJ, Woodley JM. 2015. Process requirements of galactose oxidase catalyzed oxidation of alcohols, Organic Process Research and Development 19(11):1580-1589

6.1 Abstract

Biocatalytic oxidation reactions have the potential to substitute many chemically catalyzed oxidations in the pharmaceutical and fine chemical industry due to their superior regio- and stereo-selectivity and low environmental impact. Galactose oxidase (GOase) has been shown to be a promising biocatalyst for the oxidation of primary and secondary alcohols to their corresponding aldehydes and ketones respectively. However, GOase requires a number of additives to sustain its catalytic function, such as the enzyme catalase for degradation of the by-product hydrogen peroxide as well as single electron oxidants to reactivate the enzyme upon loss of the amino acid radical in its active site. In this work the addition of catalase, single electron oxidants, and copper ions was investigated systematically in order to find the minimum concentrations required to obtain a fully active GOase. Furthermore, it was found that the concentration and type of buffer is essential for the activity of GOase, which was significantly more active in sodium phosphate buffer than in other buffers investigated. Enzyme stability and oxygen requirements are of crucial importance for the implementation of oxidase based processes. GOase was shown to be completely stable for 120 h in buffer with stirring at 25 °C, and the activity even increased 30% if the enzyme solution was also aerated in a similar experiment. The high K_M for oxygen of GOase (>5 mM) relative to the solubility of oxygen in water reveals a trade-off between supplying oxygen at a sufficiently high rate and ensuring a high degree of enzyme utilization, i.e. ensuring the highest possible specific rate of reaction. Nevertheless, the good stability and high activity of GOase bode well for its future application as an industrial biocatalyst.

6.2 Introduction

Oxidation reactions are one of the most important types of reactions in industrial chemistry. Bulk industrial scale oxidations are frequently conducted using noble metal catalysts and readily available oxidants such as molecular oxygen or hydrogen peroxide [1]. In contrast, the pharmaceutical and fine chemical industry mainly employs stoichiometric amounts of inorganic oxidants to supply the required redox equivalents. However, these reactions typically have poor selectivity and a large environmental impact due to extensive waste generation, the use of solvents with a poor environmental profile and the requirements for additional synthetic steps for protection and deprotection of labile functional groups [2,3]. Biocatalysis may help to overcome many of the limitations experienced in the fine chemical industry, as a result of the regio- and stereo-selective nature of enzymatic reactions and their environmentally benign operating conditions [4,5]. In nature, redox reactions are catalyzed by oxidoreductases (EC 1), such as dehydrogenases, oxygenases, oxidases, and peroxidases, and include several reaction types of high industrial importance.

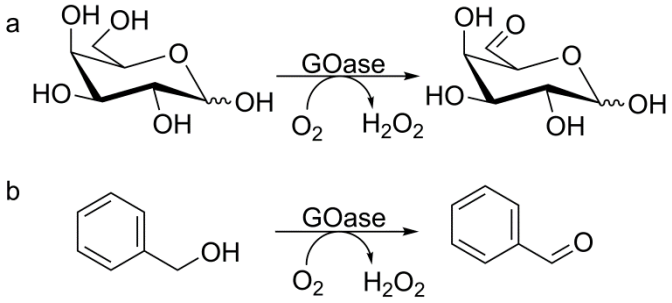

Figure 6.1. Examples of oxidations catalyzed by galactose oxidase (GOase) a) Oxidation of galactose. b) Oxidation of benzyl alcohol.

The copper dependent enzyme galactose oxidase (GOase, EC 1.1.3.9) is an example of an industrially relevant oxidase that naturally catalyzes the oxidation of the C6 hydroxyl group of D-galactose to the corresponding aldehyde, while simultaneously reducing molecular oxygen to hydrogen peroxide (Figure 6.1a) [6–8]. GOase and mutants thereof, catalyze oxidations of a wide range of substrates with potential industrial application [9,10]. Firstly, GOase can be used to modify naturally occurring polysaccharides with terminal galactose moieties (or other saccharides through GOase mutants) by oxidizing the C6 hydroxyl groups and enabling further chemical or enzymatic modifications of the aldehyde such as amination [11–14]. Secondly, GOase can be applied in the synthesis of a range of industrially relevant compounds containing ketones and aldehydes, such as diformylfuran obtained by selective oxidation of 5-hydroxymethylfurfural [15,16]. Finally, GOase mutants able to enantioselectively oxidize secondary alcohols enable the use of the enzyme for kinetic resolution of racemic mixtures of secondary alcohols [17].

The substrate specificity of wild-type GOase is rather restricted, accepting galactose containing polysaccharides and also some primary alcohols such as dihydroxyacetone and benzyl alcohol [10,18]. A great effort has therefore been put into modifying galactose oxidase via mutagenesis to broaden its substrate specificity [17,19,20]. A variety of altered substrate specificities for GOase variants have been reported in the scientific literature, such as increased galactose activity [20], novel glucose 6-OH activity [21], increased fructose 6-OH activity [19], increased activity on mannose and N-acetylglucose [22] and activity towards a range of secondary alcohols [17,21]. A particularly interesting GOase mutant is the M_{3-5} variant described by Escalettes and Turner [17], which is able to selectively oxidize the *(R)*-enantiomer of secondary benzylic alcohols to the corresponding ketones. M_{3-5} GOase is capable of accepting a range of primary and secondary alcohols, and compared to the wild-type enzyme, the activity towards non-polar substrates is significantly increased.

The GOase used in this study was produced intra-cellularly in *E. coli* and is therefore not loaded with copper during the fermentation and expression, due to the toxicity of copper towards E. *coli* at the concentrations required to ensure full saturation of GOase. After cell disruption and centrifugation, copper can be loaded into the apoenzyme through dialysis against copper containing buffer or more simply by adding copper(I/II) salts to the reaction mixture [23,24]. The two electron oxidation catalyzed by GOase is accomplished by an active site comprised of a tyrosine radical coordinated to a copper(II) ion, which during oxidation of the substrate is reduced to a non-radical tyrosine copper(I) complex (Figure 6.2) [7,8]. Subsequently, copper is reoxidized and the radical reformed by reduction of molecular oxygen to hydrogen peroxide. The tyrosine radical readily undergoes single electron reduction to form an inactive non-radical copper(II) complex. The inactive form of GOase can be reactivated by further reduction to form the active copper(I) complex, or reformation of the radical by single electron oxidation [7]. In practice, only reoxidation, and not further reduction, of the inactive state is performed to ensure a fully active enzyme, typically using mild chemical oxidants such as potassium ferricyanide ($K_3[Fe(CN)_6]$). However, it has also been shown that protein based single electron oxidants such as peroxidases can regenerate the active radical center [25,26]. Hydrogen peroxide formed during catalysis has been shown to inhibit and inactivate GOase [27,28], thus removal of hydrogen peroxide is a necessity for enzymatic function. This is most effectively done using catalase, which breaks down one mole of hydrogen peroxide to one mole of water and half a mole of oxygen. This reduce the stoichiometric oxygen requirements of the overall reaction by half and hence the oxygen requirements of the process.

As more chemical and biological additives are required to ensure an effective biocatalytic process, process development and implementation becomes more complicated. Despite the complexity of the reaction system a systematic investigation into the requirements of additives for GOase is lacking in the scientific literature. Therefore the present study has investigated the role of additives required for a successful biooxidation reaction based on GOase, and the implications these have on process development and implementation. To do this, the oxidation of benzyl alcohol to benzaldehyde was used as a model system (Figure 6.1b),

since it displays many of the challenges associated with other more industrially relevant reactions, such as low solubility of substrates/products, volatile reaction components, unnatural substrates for the enzyme, and requirements for sufficient oxygen transfer. The investigation focused on two different enzyme purity levels: one being highly purified enzyme as it normally is used in early stage protein characterization, and the second being a crude cell-free extract, which is a type of preparation more relevant for industrial scale application.

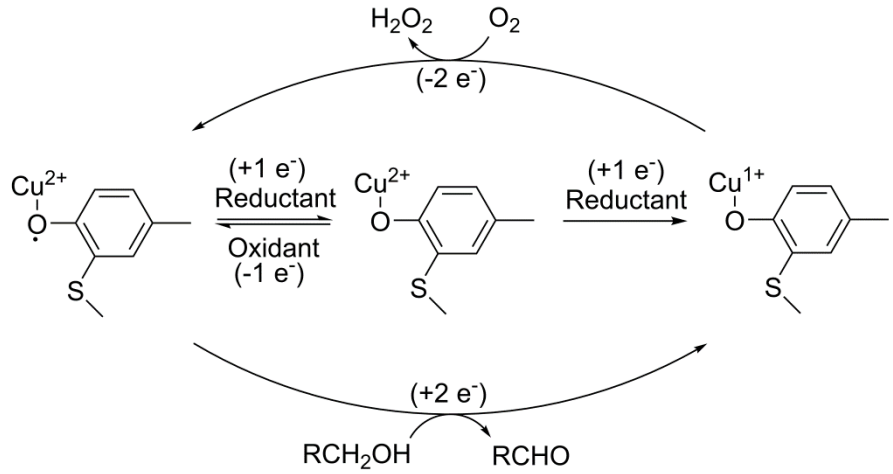

Figure 6.2. Catalytic cycle of GOase including the reduction to the semi-oxidized inactive form. The active site is simplified to only shown the copper-Tyr272 coordination. Adapted with permission from reference 8. Copyright (2003) American Chemical Society.

Oxygen supply is essential for oxygen dependent enzyme catalysis and can become a limiting factor upon scale-up of biocatalytic oxidation reactions [29]. Additionally, the supply of oxygen through bubbling with air may significantly increase the deactivation rate of some enzymes [30–32]. Analysis of the enzyme stability in the presence of a gas-liquid interface and the influence of the oxygen concentration in solution on the reaction rate is therefore essential when evaluating the potential of a biooxidation process. In the present work, this analysis has been performed for GOase based on experimental data for the model system studied.

6.3 Results and Discussion

6.3.1 Purified Enzyme

pH Optimum

The optimum pH for GOase $M_{3\text{-}5}$ was determined in a standard liquid phase horseradish peroxidase (HRP) /ABTS coupled assay, varying only the reaction pH from 6.0 to 8.0 in sodium phosphate buffer (NaPi). The highest activity was observed at pH 7.0-8.0 for oxidation of benzyl alcohol (Figure 6.3a). Given this activity range, all subsequent experiments with both purified GOase and GOase in crude lysate were performed at pH 7.4.

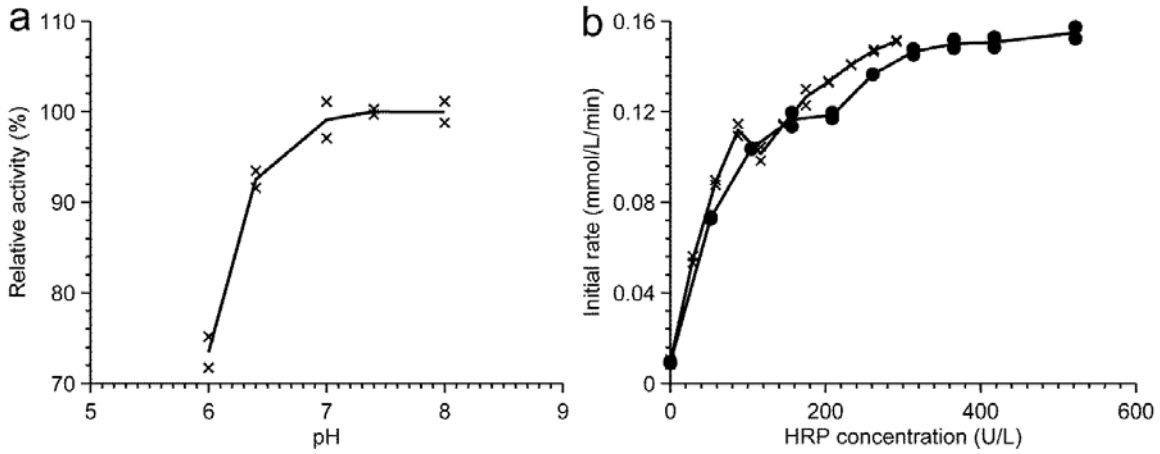

Figure 6.3. a) Effect of pH on the activity of purified GOase in 50 mM NaPi. b) Effect of two different isoenzymes of horseradish peroxidase (HRP) on the activity of purified GOase. Type I (x), Type IV (●).

Activation by horseradish peroxidase

HRP has long been known to activate GOase [26,33]. Although the mechanism of the phenomenon is not fully understood, it can nonetheless be exploited as a means of increasing GOase activity to shorten conversion time in a biocatalytic reaction. Because a high requirement of HRP could potentially be cost prohibitive for a scaled process, it is of financial interest to identify the minimal amount of HRP required to fully activate GOase. Type IV HRP is a common form of HRP used in coupled assays with a chromogenic substrate to monitor the formation of H_2O_2. Type I HRP, an isoenzyme form of HRP, was used as a comparison for activation of the purified enzyme. Because of the low and varied amount of HRP used in the activation experiments, a typical HRP/ABTS assay could not be used to measure GOase activity. Instead, titration of GOase activation by HRP was performed in a cuvette-based assay measuring the formation of NADPH through oxidation of the benzaldehyde product to benzoic acid by an aldehyde dehydrogenase. Activation of 0.0078 mg/mL GOase $M_{3\text{-}5}$ reached maximum of initial rate of 0.15 mmol/L/min in the presence of 365 U/L type IV HRP, while 291 U/L of type I HRP was needed to reach the same level of activity (Figure 6.3b). This is compared to an initial rate of 0.0094 mmol/L/min in the absence of HRP. In addition to demonstrating the ability of different types of HRP to activate GOase, the 16-fold increase in specific activity over the samples with no HRP present shows that activation is essential for a high rate of catalysis.

Effect of H_2O_2 and protection by catalase

Previous studies have demonstrated that the wild type GOase is irreversibly inactivated by H_2O_2, accumulating as a by-product of alcohol oxidation, although inactivation only occurs during catalysis and the enzyme is actually stable when exposed to H_2O_2 under resting conditions [28]. To confirm that these observations similarly apply to the GOase $M_{3\text{-}5}$ construct containing a series of mutations, where of particular concern is the addition of an oxidizable active site methionine residue, the enzyme was incubated in the presence of various concentrations of H_2O_2 and then assayed either with H_2O_2 present or after removal by catalase. Specific activity measurements clearly indicate a loss in GOase activity in a concentration

dependent manner only when H_2O_2 remains in the reaction during catalysis (Figure 6.4a). The samples that were treated with catalase showed increasing activity with increasing concentration of H_2O_2 that initially suggested another form of activation event within this system. However, this activity increase was the result of higher concentrations of dissolved oxygen in the buffer after H_2O_2 was eliminated by catalase (Figure 6.4a). The effect of catalase in the biocatalytic reaction was demonstrated to be two-fold, first providing protection against activity loss by removing H_2O_2, and second through regeneration of dissolved oxygen to continue alcohol oxidation.

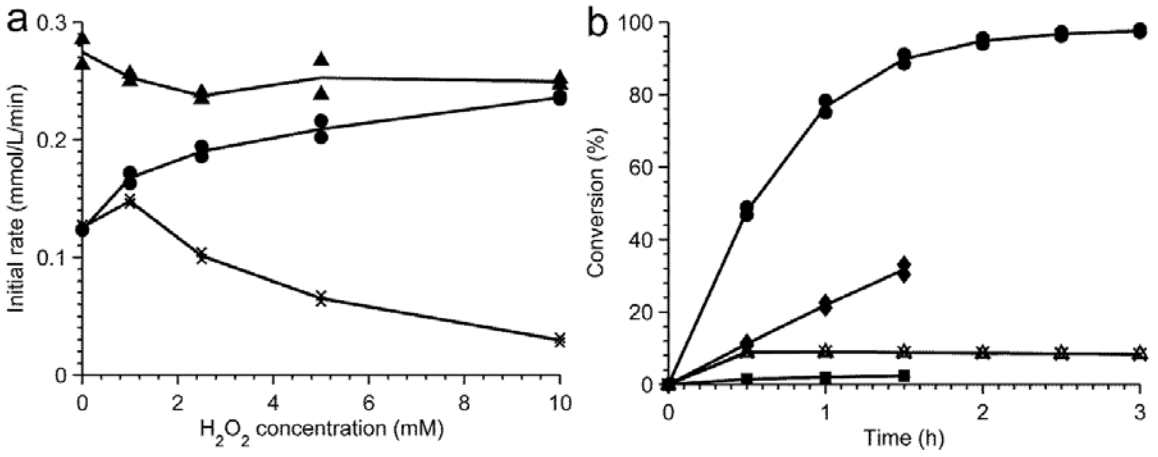

Figure 6.4. a) Effect of hydrogen peroxide on the activity of purified GOase. GOase was incubated with indicated concentrations of H2O2 for 10 min, after which the reaction was started by addition of substrate (x), catalase (to break down all H2O2) and then substrate (●), catalase and additional H2O2 to bring the total addition up to 10 mM, and then substrate (▲). b) Effect of catalase and horseradish peroxidase (HRP) on conversion of 25 mM benzyl alcohol. (●) HRP and catalase added, (♦) catalase but not HRP added, (■) no catalase or HRP added, (∆) HRP but no catalase added, (x) HRP added, catalase added after 1.5 h.

Analytical scale biocatalytic reaction

As a first step toward translating the above parameters to a production setting, the effect on conversion rate of several of these variables was examined in analytical scale biocatalytic reaction with purified enzyme. Oxidation of benzyl alcohol to benzaldehyde was monitored over time in small scale reactions with, and without, HRP present to activate GOase, as well as with, and without, catalase present to remove H_2O_2 and regenerate oxygen (Figure 6.4b). Excluding HRP resulted in a significant loss in initial conversion rate (11% of 25 mM benzyl alcohol at 30 min point) compared to the optimized reaction with both HRP and catalase present (48% conversion at 30 min). In the absence of catalase, GOase lost all activity within 30 min, and only minimal (≈2%) conversion was observed in the samples that contained neither HRP nor catalase. Under optimized conditions (with HRP and with catalase) 95% conversion to benzaldehyde was achieved after 2 h. The conversions over time for each set of experiments verified the results observed in the initial rate experiments, proving that GOase activation and inactivation processes are extremely important considerations for continued productive oxidation of alcohols by this biocatalyst.

While the above experiment conclusively shows that H_2O_2 has an effect on GOase activity, it does not clearly indicate if the effect is due to GOase inhibition or deactivation. To distinguish between these two potential modes of action, samples were prepared initially without catalase so that H_2O_2 could accumulate, then catalase was added after 1.5 h of reaction to remove the detrimental compound. If H_2O_2 acts to inhibit GOase, removal by catalase would have been expected to recover benzaldehyde production. Instead, we found that no activity returned after removal, confirming that H_2O_2 directly deactivates GOase.

6.3.2 Cell-free extract

CFE characterization

The activity of cell free extract was found to be 3.8 U/mg under standard assay conditions, corresponding to 4.9% of the activity obtained when using purified GOase (77.5 U/mg). This correlates well with a protein yield of 4-5% by weight from STREP-tag purification and estimations of protein content from bicinchoninic acid assay (BCA) quantification of total protein (0.45 mg/mg CFE) and SDS gel band density (data not shown). The CFE did not contain peroxidase activity when measured using ABTS and H_2O_2. However, the CFE showed some catalase activity in a simple qualitative measurement through observing bubble formation upon H_2O_2 addition. The CFE was lyophilized from NaPi buffer, pH 7.4, at a concentration corresponding to 0.17 mM at 100 mg CFE/L.

Requirements for copper and single electron oxidants

GOase in CFE formulation was loaded with copper by adding $CuSO_4$ directly to the reaction mixture. Figure 6.5 shows the dependence of the initial rate of reaction on the amount of added $CuSO_4$. Initially the reaction rate increased almost linearly with the concentration of Cu^{2+} until an apparent optimum was reached at 15 μM (for 100 mg CFE/L), after which the initial rate dropped to reach a constant plateau at approximately 80% of the maximum rate. One would expect the profile to follow the normal binding curve, due to the equilibrium between copper in the active site and copper in solution. The observed results may be caused by interactions between other constituents of the system, such as inhibition of HRP by Cu^{2+} that previously has been reported in the scientific literature [34].

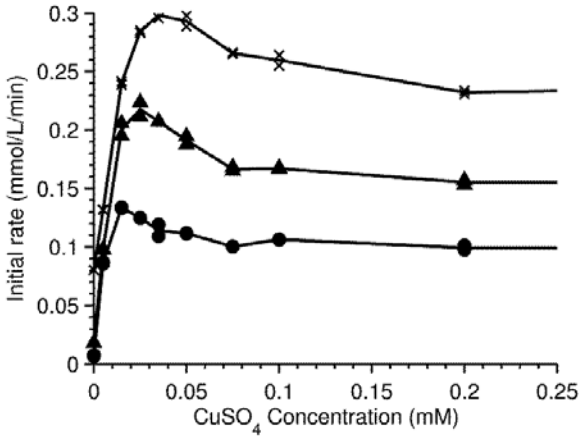

Figure 6.5. Effect of copper sulfate on reaction rate in 4 mL vials at 100 mg/L (●), 200 mg/L (▲), and 500 mg/L (x) of CFE GOase

The apparent optimum Cu^{2+} concentration increased with increasing concentration of CFE and was found to be 15, 25, and 35 μM for 100, 200 and 500 mg CFE/L, respectively. The low concentration of GOase (≈0.35 μM enzyme at 500 mg CFE/L) will not significantly reduce the concentration of Cu^{2+} in solution by binding in the active site, and hence not the concentration at which the enzyme is fully loaded. Sequestering of Cu^{2+} by cell debris and other proteins in the CFE is therefore a more likely explanation for the increase in the optimal $CuSO_4$ concentration with increasing concentration of CFE. An additional note is that the initial rates do not scale with enzyme concentration. This is likely due to the high K_M for oxygen (>3 mM) [27] relative to the solubility of oxygen (0.268 mM, air at 1 atm, 25 ˚C) [35], implying that even a small change in oxygen concentration will have a large effect on the reaction rate. Conversely, an increase in enzyme concentration will therefore not result in a proportional increase in reaction rate, due to oxygen transfer limitations resulting in a lower concentration of oxygen in the vial.

As shown previously, single electron oxidants such as HRP are crucial for ensuring a fully activated GOase. Inorganic oxidants such as potassium ferricyanide are an alternative to protein based oxidants. HRP reactivates the enzyme presumably by utilizing the hydrogen peroxide formed in the oxidation reaction, and is therefore only required in catalytic amounts. On the other hand, potassium ferricyanide is required in stoichiometric amounts, and a minimum concentration is necessary to reach the redox potential required to ensure that all the GOase is fully activated. Figure 6.6 shows the effect of different amounts of horseradish peroxidase (HRP) or potassium ferricyanide at different CFE concentrations. By adding only small amounts of HRP the initial rate increased several fold, until an apparent optimum was reached at a HRP concentration of 40 U/L, independent of the GOase concentration. Surprisingly, the smooth increase in activity seen when using purified GOase (Figure 6.3b) was not observed when CFE was applied. Additionally, the CFE requires much less HRP than the purified enzyme to reach full activation (40 U/L vs. 291 U/L). This suggests that the optimum is caused by interactions between HRP and components present in the CFE, and that these interactions enhance the ability of HRP to activate GOase, however this process remains unclear. In the case of potassium ferricyanide the activity of GOase increased with increasing ferricyanide concentration until the enzyme was fully activated in the presence of 10 mM ferricyanide. The fully activated enzyme using potassium ferricyanide displayed an initial rate of 0.17 mmol/L/min (100 mg CFE/L), which is identical to the rate observed when using the optimum HRP concentration. This indicates that the optimal value seen when using HRP for activation does in fact correspond to a fully active enzyme.

If CFE is subjected to the same HRP titration assay used to measure the activity of purified protein, no dependence on HRP concentration can be observed, i.e. the enzyme appears fully activated without addition of HRP. However, after incubating CFE with $CuSO_4$ for 15 min before initiating the reaction, the initial activation effect disappears and the reaction rate drops to zero in the absence of HRP. This is also seen in the longer assays used for CFE characterization, where linear initial rates (5-15 min) are not seen for HRP or ferricyanide

concentrations below 10 U/L and 0.02 mM, respectively. These results confirm that the tyrosyl-radical is formed immediately upon copper loading to successfully generate the active enzyme [24], and, since this happens just prior to reaction, there is no time for the radical to decay as in the case for the copper loaded purified enzyme. However, the radical is not indefinitely stable even under conditions where substrate is available to oxidize, so the presence of an oxidant is still required to reactivate GOase to maintain activity for the full duration of the biocatalytic reaction.

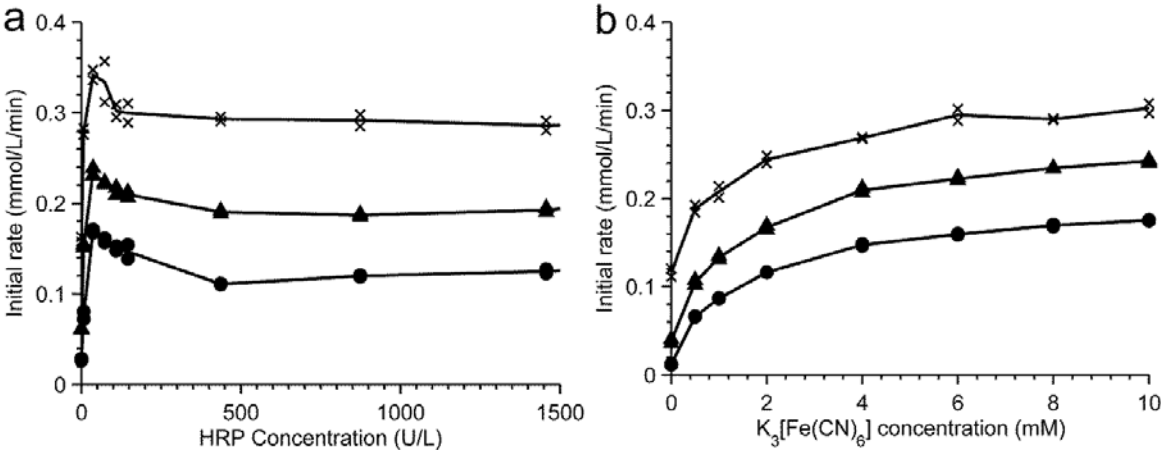

Figure 6.6. Effect of single electron oxidation on the activity of GOase. a) Effect of horseradish peroxidase (HRP) at a GOase concentration of 100 mg/L (●), 200 mg/L (▲), and 500 mg/L (x). b) Effect of potassium ferricyanide ($K_3[Fe(CN)_6]$) at a GOase concentration of 100 mg/L (●), 200 mg/L (▲), and 500 mg/L (x).

Buffer system

Influence of ions and ionic strength on enzyme activity and stability is a well-established phenomenon [36]. Different salts affect the enzyme stability and activity through the interaction with charged groups on the protein and the essential water molecules surrounding the protein molecule [37]. The interaction between ions and GOase has primarily been limited to studies investigating the inhibitory effect of ions that bind to the active site, such as cyanide and azide [18,38]. In general, few observations regarding the effect of ionic strength, buffer concentration or buffer type have been published, most likely because most ions do not affect the enzyme function of wild-type GOase. Interestingly, Saysell and co-workers [39] studied the interaction between a Trp290His GOase mutant with six different buffers. Here it was shown that buffers containing free OH groups (such as phosphate) interact with the inactive semi-reduced form of the Trp290His mutant, whereas no interaction was seen for the wild-type. The interaction can be ascribed to a shielding effect of the active site by Trp290, which is significantly reduced when the tryptophan is exchanged for histidine, thereby leaving the active site accessible to solvents that can interact with the copper center [39]. Despite identifying the interaction, the positive or negative effects on enzyme activity of these interacting buffers was not investigated. In an analogous way to the histidine mutant, the Trp290Phe mutation in GOase $M_{3\text{-}5}$ may be expected to show a similar effect from buffer interactions. However, analysis of crystal structures suggest that the shielding of the active site is just as effective for the Trp290Phe mutant as for the wild type [40]. Despite this, a

significant impact of the buffer identity and concentration on the activity of M_{3-5} GOase was identified in the present study (Figure 6.7). Ionic strength appears to be crucial for the activity of GOase, and for all investigated buffer types the activity initially increased with increasing buffer strength. For diglycine (GlyGly)/NaOH buffer, 3-(N-morpholino)propanesulfonic acid (MOPS)/NaOH, and NaPi a stable plateau was reached, while the activity when using N-ethylmorpholine (NEM)/HCl decreased at higher buffer concentrations. Interestingly, the activity in NaPi increased much more than in other buffer systems, the reason for this could be the free OH group of phosphate interacting with copper in the active site as suggested by Saysell and co-workers for the Trp290His mutant. Attempts to reach the same activation effect seen by NaPi using other inorganic salts (such as NaCl) only had a limited effect (data not shown). A buffer system using the conjugated NEM acid/base pair and using MOPS to adjust the ratio follows the same behavior as the NEM/HCl system (data not shown), which suggest that it is primarily NEM and not chloride ions that inhibits GOase. The reason for the decrease in activity could be complexation between amines and Cu^{2+}, however, according to the scientific literature tertiary amines with substituents consisting of two or more carbon atoms are too sterically hindered to chelate [41].

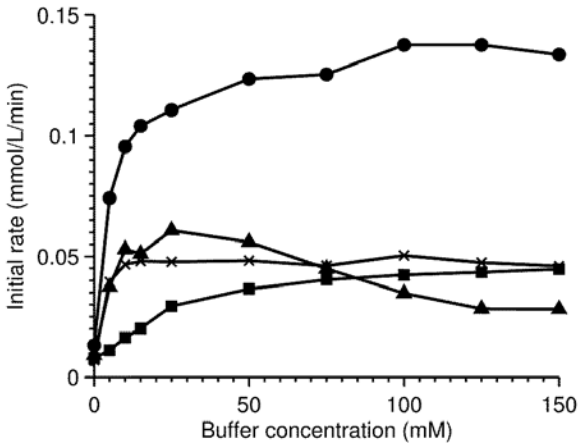

Figure 6.7. Effect of buffer type on initial activity of GOase at pH 7.4. Sodium phosphate (●), diglycine (GlyGly)+NaOH (x), 3-(N-morpholino)propanesulfonic acid (MOPS) +NaOH (□), N-ethylmorpholine (NEM)+HCl (▲).

Enzyme kinetics and stability

The catalytic mechanism of GOase can be described by the ping-pong bi bi mechanism, where the alcohol substrate is oxidized in one catalytic half-reaction followed by reoxidation of the enzyme by reduction of oxygen to hydrogen peroxide in a second half-reaction (Figure 2) [42–45]. There are only a few studies in the literature that report all kinetic constants for galactose oxidase – these being k_{cat}, K_{MS}, and K_{MO}. In studies where only the alcohol substrate is varied the reported k_{cat} and K_M values will only be apparent values making it difficult to compare results obtained in different studies since the oxygen concentration is not necessarily identical. Kwiatkowski an co-workers [27] investigated the oxidation of galactose at 20 °C and reported a k_{cat} of 1180 s^{-1}, a K_M for galactose of 175 mM and a K_{MO} of 3 mM, the last value reported as uncertain since full saturation of the enzyme could not be achieved under the experimental conditions. Furthermore, the values are derived based on the ordered

bi bi mechanism, an assumption that later has been refuted [43,44]. A more precise measurement of K_{MO} was achieved by Humphreys and co-workers [45] by performing the reaction at 10 °C, hereby decreasing the reaction rate and the concentration of oxygen at which enzyme saturation was observed. At this temperature the K_{MO} was determined to be 0.44 mM, while the k_{cat} and K_M for 1-o-methyl-α-D-galactopyranoside was 1165 s^{-1} and 144 mM, respectively. For the oxidation of benzyl alcohol using GOase M_{3-5} cell lysate, our initial investigation suggests a K_{MO} >5 mM, a K_M for benzyl alcohol of ≈150 mM and a k_{cat} of ≈50 U/mg CFE.

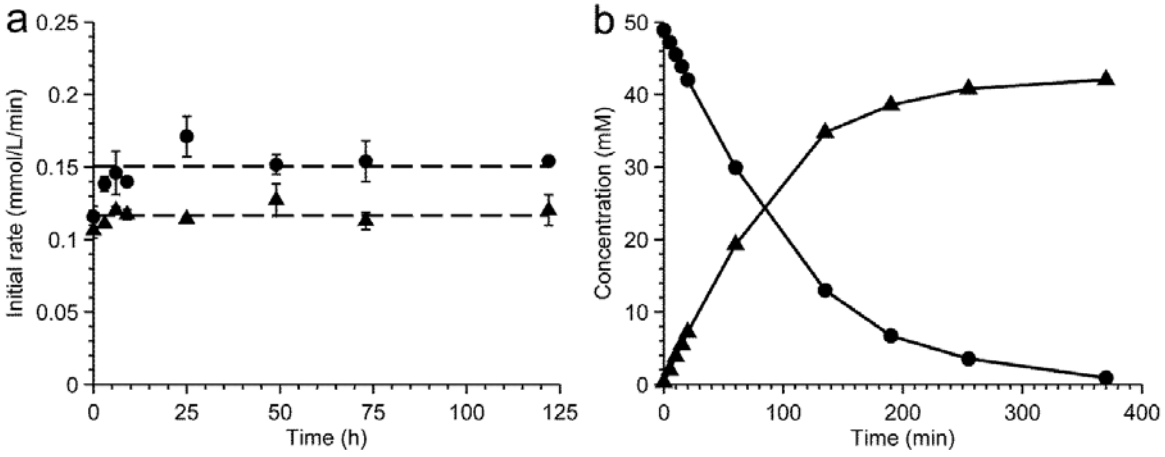

Figure 6.8. a) Stability of GOase in 50 mM NaPi pH 7.4 exposed to stirring (250 rpm, two Rushton turbines) with aeration (air; 0.5 vvm) at 25 °C (●) and stirring without aeration at 25 °C (▲). (--) The average value in the interval 3-122 h. b) Bioconversion of 50 mM benzyl alcohol (●) to benzaldehyde (▲) in a sparged bioreactor (250 rpm stirring, aeration using air at 1 vvm) using 500 mg CFE/L, 800 U HRP/L, 50 µM $CuSO_4$, and 100 mM NaPi pH 7.4.

The stability of GOase has not attracted much attention in the scientific literature, even though it is of great importance for the implementation of GOase in industrial processes. Sun and co-workers [20] describe a GOase mutant that shows increased thermostability and long term stability over the wild-type. The mutant retained 80% of the initial activity after 8 days of storage at room temperature in the presence of catalase and $CuSO_4$, as opposed to the wild-type that lost 50% after 8 days under identical conditions. Figure 6.8a shows the stability of GOase M_{3-5} CFE during five days of stirring at 25 °C in 50 mM NaPi, pH 7.4. The stability of GOase was investigated both with and without bubbling with air, since gas-liquid interfaces previously have been shown to deactivate certain enzymes [31,32,46]. GOase did not lose activity during the period investigated, even when exposed to aeration rate of 0.5 vvm (volume/volume/min), a typical value employed at industrial scale. In fact, the bubbling apparently activated GOase during the first 6-9 h, after which a stable plateau was reached with an apparent activity that was 30% higher than the activity of the enzyme not exposed to bubbling. The oxygen concentration was approximately the same in the two systems and the evaporation of water was negligible (<2%/day). The increased activity can therefore not be explained by a higher initial oxygen concentration in the assay or increased enzyme concentration due to evaporation of solvent.

Figure 6.8b shows a typical biocatalytic oxidation of 50 mM benzyl alcohol in a sparged bioreactor using a GOase concentration of 500 mg CFE/L. Full conversion was reached after 6 h of reaction. Due to sparging with air, the produced benzaldehyde was stripped into the gas phase and lost with the off-gas, despite the condenser attached to the bioreactor. This explains why only a concentration of 42 mM benzaldehyde was measured despite the fact that almost all of the 50 mM benzyl alcohol was converted.

6.4 Process implications

6.4.1 Requirements for additives

As shown in the previous sections, oxidation of alcohols using GOase requires not only the enzyme itself, but also several additives to enable efficient use of the enzyme. The requirement for copper in the active site of GOase is inevitable. Copper can either be loaded prior to the reaction by applying dialysis or copper salts can be added directly to the reaction mixture. Direct addition of copper to the reaction mixture has been shown to effectively load copper into the active site (Figure 6.5), and is therefore preferred in order to avoid the additional cost and processing effort involved in applying dialysis at large scale.

A single electron oxidant required to restore the radical in the active site is also critical to obtain a fully active enzyme, since without an oxidant the enzyme loses its activity within 15 min of reaction when GOase is applied in the form of CFE. Both inorganic oxidants and proteins capable of single electron oxidation can be used as demonstrated in Figure 6.3a and Figure 6.6 for ferricyanide and HRP. A minimum of 40 U/L of HRP is required to fully activate GOase independent of the concentration of GOase when added as a CFE. At a GOase concentration of 500 mg CFE/L this corresponds to a molecular ratio between the two enzymes of 59:1 (GOase:HRP), assuming a Type I HRP with a specific activity of 146 U/mg and that the formulation from Sigma Aldrich contains only protein. However, for purified protein approximately 300 U/L of HRP was needed to reach full activity, which corresponds to an enzyme ratio of 8:1 when transferring the result directly to a system with an enzyme concentration of 500 mg CFE/L. The difference between purified protein and CFE might be an artefact seen due to the complexity of the system, and therefore the safest choice is to design the reaction system based on the HRP level dictated by the purified protein experiments. In this case, the requirements to HRP will be a significant cost addition to the process, since the production cost per gram protein of HRP and GOase most likely will be comparable at industrial scale. However, if a ratio of only 59:1 is required to ensure a fully active enzyme for an entire Biocatalytic reaction, the cost contribution from HRP will be almost negligible. The ratio of GOase to HRP will of course depend on the specific activity of HRP and will increase with increasing concentration of GOase, but a high enzyme concentration implies high oxygen consumption that eventually will become a bottleneck.

The alternative to HRP is an inorganic oxidant such as ferricyanide. Ferricyanides, and the reduced form, ferrocyanide, are widely applied in the production of pigments, in wine refining, as anticaking agent, and historically as a bleaching agent in photography [47]. These large scale applications imply a relatively low cost for potassium ferricyanide, combining

this with the limited concentration needed to obtain a fully activated enzyme (10 mM corresponding to 3.3 g/L of potassium ferricyanide) means that ferricyanide activation most likely will be significantly cheaper than HRP activation (especially if a GOase-HRP ratio of 8:1 is required), assuming that the activation is persistent throughout the biotransformation. Ferricyanides are also applied in organic chemistry for many oxidation reactions, such as oxidation of tertiary amines [48], oxidative coupling of phenols [49], and oxidative hydroxylation of pyridinium salts [50]. The reactions typically require strongly alkaline pH, however most reactions also proceed at a pH close to neutral, but at a much lower rate [48]. GOase substrates of industrial relevance could potentially be larger molecules with several labile functional groups, where the increased specificity compared to chemical alternatives will be the main driver for the implementation of an enzymatic process. A potential problem might therefore be by-product formation via reactions between ferricyanide and functional groups present in the molecule, such as substituted aromatics rings. The extent of by-product formation via ferricyanide reactions will be highly dependent on the functional groups present in the substrate molecule, and potential by-product formation will have to be evaluated on a case-by-case basis. In the case of benzyl alcohol oxidation, no by-product formation due to side-reactions with ferricyanide was observed.

Interestingly, we discovered that the GOase activity depends heavily not only on the ionic strength of the reaction mixture, but also on the type of buffer applied. A sodium phosphate buffer turned out to result in significantly higher reaction rates than any other buffer or salt investigated. This discovery is very important to keep in mind when designing a process, since too low a buffer concentration will result in significant activity reduction. Furthermore, the cost contribution from the buffer requirements will be significant, unless an efficient recycling of the reaction medium can be established.

6.4.2 Oxygen requirements

Oxidases require oxygen, which in biotechnology traditionally is supplied by bubbling air through the reactor. The transfer of oxygen from the gas phase to the liquid phase is notoriously slow due to the low solubility of oxygen in water under normal operating conditions (0.268 mM, 25 °C, 1 atm air) and hence a low driving force for mass transfer. The supply of oxygen to the reactor therefore sets an upper limit to the reaction rates that can be obtained. The maximum oxygen transfer rate in an industrial scale bioreactor is typically around 100 mmol/L/h (corresponding to a volumetric mass transfer coefficient, k_La, of approximately 500 h^{-1}) when the concentration of oxygen in solution is close to zero (i.e. maximum driving force) and air is applied for aeration [51]. Stoichiometric amounts of oxygen are required in a GOase catalyzed oxidation. However, by recycling oxygen via catalase mediated degradation of the hydrogen peroxide by-product the requirements for oxygen can be halved. The typical industrial scale oxygen transfer rate therefore limits the maximum volumetric productivity to 200 mmol/L/h, corresponding to 21 g/L/h in the case of benzaldehyde, a value which is in range with typical requirements for industrial implementation [52]. However, since oxygen is a substrate for the enzyme the reaction rate depends on the concentration of oxygen in solution. The Michaelis constant for oxygen, K_{MO}, is ≈5 mM for GOase,

which is significantly above the solubility of oxygen at normal operating conditions. This means that the reaction rate will be almost directly proportional to the dissolved oxygen concentration, when operating at, or close to, atmospheric pressure and assuming saturation of the enzyme with the alcohol substrate. This reveals a trade-off between an efficient use of the enzyme, i.e. the biocatalyst yield (g product/g enzyme), and a sufficient oxygen transfer rate to sustain the desired volumetric productivity (g product/L/h). At low oxygen concentrations relative to saturation, the oxygen transfer rate will be high whereas the specific reaction rate will be low, and vice versa at an oxygen concentration close to saturation. This is exemplified in Figure 6.9, where the rate of oxygen transfer to the reactor and oxygen consumption by an enzymatic reaction is depicted as a function of the concentration of oxygen in solution. The figure shows the oxygen consumptions for two different values of K_{MO}, and the oxygen transfer rate when bubbling with air or pure oxygen at two different volumetric mass transfer coefficients. The operating points for the given examples will be the intersection of the lines. For GOase with a K_{MO} of 5 mM the operating point, when using air and a typical industrial scale k_La value of 500 h^{-1}, will be at an oxygen concentration of 0.21 mM (79% air saturation) corresponding to an oxygen consumption rate of 30 mmol/L/h and therefore a volumetric productivity of 60 mmol/L/h (or 6.4 g/L/h in the case of benzaldehyde). At this operating point the enzyme functions at a rate corresponding to only 7% of V_{max} at the applied benzyl alcohol concentration. Hence, the enzyme is severely oxygen limited, or in other words, the efficiency is significantly lower than that which could have been at a higher oxygen concentration. The effect will be most severe in the beginning of the reaction, since the apparent K_{MO} will decrease as the reaction progresses and the substrate concentration approach zero.

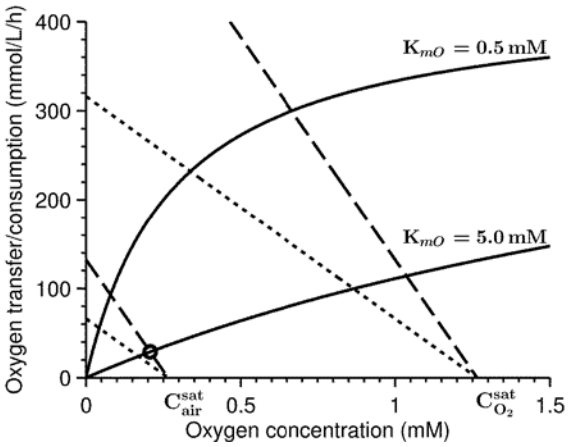

Figure 6.9. Rate of oxygen transfer to the reactor using air ($C_{air}^{sat} = 0.267$ mM) or pure oxygen ($C_{air}^{sat} = 1.27$ mM) at two different volumetric mass transfer coefficients (--) k_La = 250 h^{-1} (– –) k_La = 500 h^{-1}, and the enzymatic rate of oxygen consumption at two different K_{MO} as a function of oxygen concentration. The plot is based on a K_M for benzyl alcohol of 150 mM, a k_{cat} of 50 U/mg CFE, an enzyme concentration of 500 mg CFE/L and a substrate concentration of 200 mM. The operating points of the given examples will be the intersections between the lines, such as the point illustrated by a circle.

The above analysis illustrates the importance of K_{MO} to the performance of oxygen dependent enzymes at industrial scale, a fact that is often overlooked when developing new biocatalysts. The key objective from a process engineering point of view is therefore not only to supply enough oxygen to sustain a desired productivity, but supplying it at the right oxygen concentration, which for many oxidases is the highest concentration possible due to the relatively high K_{MO}. The optimal oxygen level will depend on the cost of the biocatalyst relative to the operating and capital costs of the process.

The oxygen transfer rate can be increased by applying enriched air, i.e. air with higher oxygen content and/or increased reactor pressure, thereby increasing the driving force for oxygen transfer by increasing the oxygen saturation concentration. The incentive to implement solutions to increase oxygen transfer is two-fold, since both higher oxygen transfer rate and dissolved oxygen concentration can be obtained thereby potentially increasing both the volumetric productivity and biocatalyst yield. This benefit has to be weighed against the added cost from purifying air, increasing reactor strength and increased safety precautions when dealing with a higher oxygen partial pressure in combination with volatile organic compounds.

6.4.3 Biocatalyst stability

The stability of enzymes may be significantly reduced when exposed to gas-liquid interfaces, due to the tendency of protein to unfold when in contact with the hydrophobic air [30–32]. Thus, supply of oxygen by bubbling with air can pose a problem for oxidase catalyzed reactions. However, in the case of GOase deactivation at the gas-liquid interface is not an issue (Figure 6.8) in fact the enzyme appears to be activated during the first 9 h of bubbling. The stability trials were designed to mimic the reaction conditions, but since they were conducted in the absence of substrate the observed stability may be different from the actual stability during catalysis, i.e. the operational stability. The importance of determining the stability during catalysis can also be seen from the experiment with different levels of hydrogen peroxide (Figure 6.4a), where it is shown that GOase is not deactivated by H_2O_2 in the absence of catalytic action. However, during catalysis GOase is deactivated within minutes in the presence of small amounts of H_2O_2. This indicates that it is the reduced form of the enzyme that is susceptible to deactivation by H_2O_2 and not the oxidized form predominantly present in the absence of an alcohol substrate. Similarly, other deactivation mechanisms such as oxidation of amino acids side-chains in the active site by dissolved oxygen may only take place at certain stages of the catalytic cycle.

6.5 Conclusion

Benzyl alcohol oxidation catalyzed by galactose oxidase (GOase) was used as a model system for the investigation of reaction additive requirements to obtain an efficient biotransformation:

- Catalase was necessary to keep the concentration of hydrogen peroxide, formed as a by-product, at a minimum in order to avoid enzyme deactivation. Interestingly,

GOase was completely stable in the presence of H_2O_2 up to 10 mM, when not actively catalyzing an oxidation.

- Addition of a single electron oxidant such as horseradish peroxidase (HRP) or potassium ferricyanide was required to regenerate the active site radical upon decay. 40 U/L of HRP was required to fully activate GOase added as cell-free extract (CFE), while approximately 300 U/L was needed to fully activate purified GOase. Potassium ferricyanide was also capable of activating GOase in this case 10 mM was required for full activation.
- Copper, required in the active site, was loaded into the enzyme by adding $CuSO_4$ to the reaction mixture containing crude GOase. The optimal concentration was found to be 15, 25, and 35 μM of $CuSO_4$ for 100, 200 and 500 mg CFE/L, respectively.
- Buffer type and concentration was found to be essential for GOase activity, minimum 100 mM of preferably sodium phosphate buffer pH 7-8 resulted in the highest activity.

The process aspects of GOase catalyzed oxidation reactions were discussed in light of the determined requirements for additives, the stability of GOase, and the trade-off between sufficient oxygen transfer and full utilization of the enzyme due to the high K_M for oxygen relative to the solubility of oxygen at normal process conditions. The resulting reaction parameters are critical for implementation of GOase in an industrial scale biocatalytic oxidation process.

6.6 Experimental section

6.6.1 Materials

All reagents used were of the highest grade available from Sigma Aldrich (St. Louis, Missouri, USA). Catalase with an activity of 3172 U/mg (one unit (U) corresponds to the amount of enzyme which decomposes 1 µmol H_2O_2 per min at pH 7.0 and 25 °C) and horseradish peroxidase (HRP) with an activity of 145.7 U/mg (Type I) or 261 U/mg (Type IV) (1 U corresponds to the amount of enzyme that forms 1 mg purpurogallin from pyrogalin in 20 sec. at pH 6.0 and 20 °C) was acquired from Sigma Aldrich. Galactose oxidase mutant M_{3-5} from *Fusarium* NRLL 2903[17] as a cell-free extract (CFE), $NADP^+$ and aldehyde dehydrogenase (ALDH(003)) was acquired from Prozomix (Haltwhistle, UK). GOase M_{3-5} was purified as previously described.[14] Solutions were made using deionized water and fresh enzyme solutions were made every day.

6.6.2 Purified enzyme

Liquid phase determination of pH optimum

The pH optimum for purified GOase M_{3-5} was determined in a liquid phase HRP/ABTS coupled assay at 420 nm as previously described.[17,22] Activity was measured on a 96-well plate in triplicate at 30 °C with 10 µL GOase M_{3-5} dilution in 90 µL reaction mix (containing 0.23 mg/mL HRP and 0.4 mg/mL ABTS in 100 mM sodium phosphate buffer (NaPi) at the indicated pH levels) and initiated by addition of 100 µL 50 mM benzyl alcohol in water. Initial rates were normalized by protein concentration to calculate specific activities for each assay condition. 1U corresponds to the amount of enzyme which converts 1 µmol of substrate per min at pH 7.4 and 30 °C.

Activation of GOase M_{3-5} by HRP

Purified GOase M_{3-5} specific activity for benzyl alcohol was measured in a cuvette at 340 nm by following the production of NADPH from subsequent oxidation of benzaldehyde to benzoic acid by aldehyde dehydrogenase (ALDH(003), Prozomix). The 1 mL reaction contained 2.5 mg/mL $NADP^+$, 25 mM benzyl alcohol, 0.5 mg/mL ALDH(003), 0.0078 mg/mL GOase M_{3-5} and between 0-522 U/L HRP in 50 mM NaPi, pH 7.4. The reaction was initiated by addition of GOase (10 µL of 0.78 mg/mL stock) before measuring at 340 nm. Reactions were performed in duplicate.

Deactivation of GOase M_{3-5} by H_2O_2 and protection by catalase

The effect of H_2O_2 on the specific activity of purified GOase M_{3-5} for benzyl alcohol oxidation was measured similar to the activation by HRP. GOase was incubated at room temperature in 50 mM NaPi, pH 7.4 in the presence of H_2O_2 for 10 min in a cuvette. H_2O_2 was either degraded prior to assay by addition of catalase, or allowed to remain in the sample during the assay. In a third sample series, catalase was added to remove H_2O_2, and then additional H_2O_2 was added to bring the final assay concentration to 10 mM H_2O_2. This experiment was performed to equally oxygenate the reaction mix prior to the assay. The remaining reaction components were added to give a 1 mL reaction containing 2.5 mg/mL $NADP^+$, 25 mM benzyl alcohol, 0.5 mg/mL ALDH(003), 0.0039 mg/mL GOase M_{3-5}, 522

U/L HRP (Type IV), 0 or 220 U/mL catalase and 0-10 mM H_2O_2. The reaction was initiated by addition of benzyl alcohol before measuring at 340 nm. Reactions were performed in duplicate.

Biocatalytic reactions comparing GOase deactivation versus inhibition by H_2O_2
The effect of H_2O_2 on GOase conversion of benzyl alcohol was measured over time. Duplicate reactions were performed in 50 mM NaPi, pH 7.4 with 0.01 mg/mL purified GOase M_{3-5}, 25 mM benzyl alcohol, 10% dimethyl sulfoxide, with or without 330 U/L HRP (Type IV), and with or without 440 U/mL catalase. After 1.5 h, catalase (to 440 U/mL) was added to two samples that contained no catalase initially. Aliquots of 25 µL were removed from each sample in 30 min intervals and extracted into 500 µL dichloromethane by vortexing. The samples were centrifuged, and the organic layer was dried over magnesium sulfate. Filtered samples were analyzed on an Agilent (Santa Clara, California, USA) 6850 gas chromatograph system equipped with an FID. Analytes were separated on an HP-1MS column (Agilent) using a temperature gradient held initially at 50 °C for 4 min, and then ramped up by 25 °C/min to 225 °C. The retention times for benzyl alcohol and benzaldehyde were 7.46 min and 6.67 min, respectively.

6.6.3 Cell-free extract

Characterization
GOase content in the cell free extract powder was approximated in several experiments. Protein content in the CFE powder was determined using the Pierce BCA Protein Assay Kit (Life Technologies) following the manufacturer's protocol. Band density corresponding to GOase M_{3-5} on SDS-PAGE was estimated to be 10% of the soluble protein fraction. Purification of GOase M_{3-5} from 5 g of CFE using previously published methods[14] yielded 200 mg of isolated enzyme. Specific activity of the cell free extract was measured in the liquid phase HRP/ABTS assay described above, and normalized to the concentration of CFE powder. Peroxidase activity in the CFE was also tested with this assay by addition of 1, 2.5 or 5 mM H_2O_2 and ABTS to the lysate solution (0.25 mg/mL final), however, no activity was observed. The presence of catalase activity was confirmed in the CFE by the appearance of bubbles after addition of H_2O_2 (5 mM final) to a solution of 0.05 mg/mL CFE.

Investigation of reaction conditions
Experiments with systematic variation in the concentration of copper sulfate, horseradish peroxidase, potassium ferricyanide, and buffers were carried out in 4 mL vials that were heated to 25 °C and mixing at 800 min^{-1} in a HLC BioTech thermoshaker (Bovenden, Germany). The standard reaction conditions were 50 mM NaPi buffer at pH 7.4, 0.05 mM $CuSO_4$, 875 U/L HRP, 20000 U/L catalase, 100 mg/L CFE GOase, and 25 mM benzyl alcohol, unless otherwise stated. The working volume was in all experiments 3 mL, thereby leaving 1 mL headspace to enable oxygen transfer to the liquid phase. Samples were taken after 5, 10 and 15 min of reaction by removing the cap, thereby allowing air to enter the headspace and hence avoiding complete oxygen depletion. The experiments were performed in duplicate.

Biocatalytic reaction in an aerated reactor

A complete biooxidation reaction was conducted in a 250 mL reactor (MiniBio® with my-Control®) from Applikon Biotechnology (Delft, Netherlands). The reactor was equipped with a sintered metal sparger to ensure efficient oxygen supply and two Rushton turbines for mixing. The reaction conditions were as follows: 100 mM NaPi buffer at pH 7.4, 50 mM benzyl alcohol, 800 U/L HRP, 50 µM $CuSO_4$, 20000 U/L catalase, 500 mg/L CFE GOase, 25 °C, 250 min^{-1} stirring, and 1 vvm air sparging. At regular time intervals samples were withdrawn for analysis.

Stability experiments

Stability experiments were carried out in the 250 mL reactors described above with a working volume of 150 mL. 300 mg/L CFE were solubilized in 50 mM NaPi buffer at pH 7.4 and stirred at 250 rpm with or without aeration, 0.5 vvm air. Samples were withdrawn from the reactor at regular time intervals and the residual activity was determined in 4 mL vials as described above. The residual activity was determined as the average of three assays.

Analysis

The reaction was stopped by addition of 800 µL 1 M HCl to 200 µL reaction aliquot. Samples were analyzed on a Thermo Fisher Scientific (Waltham, Massachusetts, USA) Dionex Ultimate 3000 HPLC equipped with a Diode Array Detector. Analytes were separated at 30 °C on a Phenomex (Torrance, California, USA) Kinetex C18 column (5 µm, 100 Å, 250 x 4.6 mm) using 30% acetonitrile in water with 0.1% trifluoroacetic acid as mobile phase. Benzyl alcohol, benzaldehyde and benzoic acid were analyzed at 254 nm, and the retention times were 2.8 min, 5.4 min and 3.6 min, respectively.

6.7 References

[1] Punniyamurthy T, Velusamy S, Iqbal J, **2005**. Recent advances in transition metal catalyzed oxidation of organic substrates with molecular oxygen, Chem. Rev. 105(6):2329–63.

[2] Sheldon RA, Arends IWCE, Ten Brink G-J, Dijksman A, **2002**. Green, catalytic oxidations of alcohols, Acc. Chem. Res. 35(9):774–81.

[3] Sheldon RA, **2007**. The E Factor: fifteen years on, Green Chem. 9(12):1273.

[4] Turner NJ, **2011**. Enantioselective oxidation of C-O and C-N bonds using oxidases., Chem. Rev. 111(7):4073–87.

[5] Hollmann F, Arends IWCE, Buehler K, Schallmey A, Bühler B, **2011**. Enzyme-mediated oxidations for the chemist, Green Chem. 13(2):226.

[6] Avigad G, Amaral D, Asensio C, Horecker BL, **1962**. The D-galactose oxidase of Polyporus circinatus, J. Biol. Chem. 237(9):2736–2743.

[7] Whittaker JW, **2005**. The radical chemistry of galactose oxidase, Arch. Biochem. Biophys. 433(1):227–39.

[8] Whittaker JW, **2003**. Free radical catalysis by galactose oxidase, Chem. Rev. 103(6):2347–63.

[9] Pickl M, Fuchs M, Glueck SM, Faber K, **2015**. The substrate tolerance of alcohol oxidases, Appl. Microbiol. Biotechnol. 99:6617–6642.

[10] Siebum A, van Wijk A, Schoevaart R, Kieboom T, **2006**. Galactose oxidase and alcohol oxidase: Scope and limitations for the enzymatic synthesis of aldehydes, J. Mol. Catal. B Enzym. 41(3–4):141–145.

[11] Parikka K, Tenkanen M, **2009**. Oxidation of methyl alpha-D-galactopyranoside by galactose oxidase: products formed and optimization of reaction conditions for production of aldehyde, Carbohydr. Res. 344(1):14–20.

[12] Yalpani M, Hall L, **1982**. Some chemical and analytical aspects of polysaccharide modifications. II. A high-yielding, specific method for the chemical derivatization of galactose-containing polysaccharides: Oxidation with galactose oxidase followed by reductive amination, J. Polym. Sci. 20:3399–3420.

[13] Schoevaart R, Kieboom T, **2004**. Application of Galactose Oxidase in Chemo-Enzymatic One-Pot Cascade Reactions Without Intermediate Recovery Steps., Top. Catal. 27(1–4):3–9.

[14] Bechi B, Herter S, Mckenna S, Riley C, Leimkühler S, Turner NJ, Carnell AJ, **2014**. Catalytic bio-chemo and bio-bio tandem oxidation reactions for amide and carboxylic acid synthesis, Green Chem. 16:4524–4529.

[15] McKenna S, Leimkühler S, Herter S, Turner NJ, Carnell A, **2015**. Enzyme Cascade Reactions: Synthesis of Furandicarboxylic Acid (FDCA) and Carboxylic Acids using Oxidases in Tandem, Green Chem. 17:3271–3275.

[16] Qin Y-Z, Li Y-M, Zong M-H, Wu H, Li N, **2015**. Enzyme-catalyzed selective

oxidation of 5-hydroxymethylfurfural (HMF) and separation of HMF and 2,5-diformylfuran using deep eutectic solvents, Green Chem. 17(7):3718–3722.

[17] Escalettes F, Turner NJ, **2008**. Directed evolution of galactose oxidase: generation of enantioselective secondary alcohol oxidases, ChemBioChem. 9(6):857–60.

[18] Mendonça MH, Zancan GT, **1987**. Purification and characterization of intracellular galactose oxidase from Dactylium dendroides, Arch. Biochem. Biophys. 252(2):507–514.

[19] Deacon SE, Mahmoud K, Spooner RK, Firbank SJ, Knowles PF, Phillips SE V, McPherson MJ, **2004**. Enhanced fructose oxidase activity in a galactose oxidase variant, ChemBioChem. 5(7):972–979.

[20] Sun L, Petrounia IP, Yagasaki M, Bandara G, Arnold FH, **2001**. Expression and stabilization of galactose oxidase in Escherichia coli by directed evolution, Protein Eng. 14(9):699–704.

[21] Sun L, Bulter T, Alcalde M, Petrounia IP, Arnold FH, **2002**. Modification of galactose oxidase to introduce glucose 6-oxidase activity, ChemBioChem. 3(8):781–783.

[22] Rannes JB, Ioannou A, Willies SC, Grogan G, Behrens C, Flitsch SL, Turner NJ, **2011**. Glycoprotein Labeling Using Engineered Variants of Galactose Oxidase Obtained by Directed Evolution., J. Am. Chem. Soc. 133(22):8436–8439.

[23] Whittaker MM, Whittaker JW, **2003**. Cu(I)-dependent biogenesis of the galactose oxidase redox cofactor, J. Biol. Chem. 278(24):22090–22101.

[24] Rogers MS, Hurtado-Guerrero R, Firbank SJ, Halcrow MA, Dooley DM, Phillips SE V, Knowles PF, McPherson MJ, **2008**. Cross-Link Formation of the Cysteine 228-Tyrosine 272 Catalytic Cofactor of Galactose Oxidase Does Not Require Dioxygen., Biochemistry. 47(39):10428–10439.

[25] Kersten PJ, **1990**. Glyoxal oxidase of Phanerochaete chrysosporium: its characterization and activation by lignin peroxidase, Proc. Natl. Acad. Sci. U. S. A. 87(8):2936–2940.

[26] Kwiatkowski LD, Kosman DJ, **1973**. On the role of superoxide radical in the mechanism of action of galactose oxidase, Biochem. Biophys. Res. Commun. 53(3):715–721.

[27] Kwiatkowski LD, Adelman M, Pennelly R, Kosman DJ, **1981**. Kinetic Mechanism of the Cu (II) Enzyme Galactose Oxidase, J. Inorg. Biochem. 14(3):209–222.

[28] Hamilton GA, Adolf PK, De Jersey J, DuBois GC, Dyrkacz GR, Libby RD, **1978**. Trivalent copper, superoxide, and galactose oxidase, J. Am. Chem. Soc. 100(6):1899–1912.

[29] Law HEM, Baldwin CVF, Chen BH, Woodley JM, **2006**. Process limitations in a whole-cell catalysed oxidation: Sensitivity analysis, Chem. Eng. Sci. 61(20):6646–6652.

[30] Van Hecke W, Ludwig R, Dewulf J, Auly M, Messiaen T, Haltrich D, Van Langenhove H, **2009**. Bubble-free oxygenation of a bi-enzymatic system: effect on

biocatalyst stability, Biotechnol. Bioeng. 102(1):122–31.

[31] Bommarius AS, Karau A, **2005**. Deactivation of Formate Dehydrogenase (FDH) in solution and at gas-liquid interfaces, Biotechnol. Prog. 21(6):1663–1672.

[32] Thomas CR, Geer D, **2011**. Effects of shear on proteins in solution, Biotechnol. Lett. 33(3):443–56.

[33] Cleveland L, Coffman RE, Coon P, Davis L, **1975**. An investigation of the role of the copper in galactose oxidase., Biochemistry. 14(6):1108–1115.

[34] Guilbault GG, Brignac Jr P, Zimmer M, **1968**. Homovanillic Acid as a Fluorometric Substrate for Oxidative Enzymes, Anal. Chem. 40(1):190–196.

[35] Wilhelm E, Battino R, Wilcock RJ, **1977**. Low-pressure solubility of gases in liquid water, Chem. Rev. 77(2):219–262.

[36] Zhao H, **2005**. Effect of ions and other compatible solutes on enzyme activity, and its implication for biocatalysis using ionic liquids, J. Mol. Catal. B Enzym. 37(1–6):16–25.

[37] Zhang Y, Cremer PS, **2006**. Interactions between macromolecules and ions: the Hofmeister series, Curr. Opin. Chem. Biol. 10(6):658–663.

[38] Paukner R, Staudigl P, Choosri W, Haltrich D, Leitner C, **2015**. Expression, purification, and characterization of galactose oxidase of Fusarium sambucinum in E. coli, Protein Expr. Purif. 108:73–79.

[39] Saysell CG, Barna T, Borman CD, Baron AJ, McPherson MJ, Sykes AG, **1997**. Properties of the Trp290His variant of Fusarium NRRL 2903 galactose oxidase: Interactions of the GOase(semi) state with different buffers, its redox activity and ability to bind azide, J. Biol. Inorg. Chem. 2(6):702–709.

[40] Rogers MS, Tyler EM, Akyumani N, Kurtis CR, Spooner RK, Deacon SE, Tamber S, Firbank SJ, Mahmoud K, Knowles PF, Phillips SE V, McPherson MJ, Dooley DM, **2007**. The stacking tryptophan of galactose oxidase: A second-coordination sphere residue that has profound effects on tyrosyl radical behavior and enzyme catalysis, Biochemistry. 46(15):4606–4618.

[41] Kandegedara A, Rorabacher DB, **1999**. Noncomplexing tertiary amines as “better” buffers covering the range of pH 3-11. Temperature dependence of their acid dissociation constants, Anal. Chem. 71(15):3140–3144.

[42] Whittaker MM, Whittaker JW, **2001**. Catalytic reaction profile for alcohol oxidation by galactose oxidase, Biochemistry. 40(24):7140–7148.

[43] Whittaker MM, Ballou DP, Whittaker JW, **1998**. Kinetic isotope effects as probes of the mechanism of galactose oxidase, Biochemistry. 37(23):8426–8436.

[44] Borman CD, Saysell CG, Sykes AG, **1997**. Kinetic studies on the reactions of Fusarium galactose oxidase with five different substrates in the presence of dioxygen, J. Biol. Inorg. Chem. 2:480–487.

[45] Humphreys KJ, Mirica LM, Wang Y, Klinman JP, **2009**. Galactose oxidase as a

model for reactivity at a copper superoxide center, J. Am. Chem. Soc. 131(13):4657–4663.

[46] Ganesh K, Joshi JB, Sawant SB, **2000**. Cellulase deactivation in a stirred reactor, Biochem. Eng. J. 4(2):137–141.

[47] Gail E, Gos S, Kulzer R, Lorösch J, Rubo A, Sauer M, Kellens R, Reddy J, Steier N, Hasenpusch W, Cyano Compounds, Inorganic, in: Ullmanns Encycl. Ind. Chem., **2012**, Wiley-VCH Verlag GmbH & Co. KGaA, Weinheim: pp. 673–710.

[48] Hull LA, Davis GT, Rosenblatt DH, **1969**. Oxidations of Amines. IX. Correlation of Rate Constants for Reversible One-Electron Transfer in Amine Oxidation with Reactant Potentials, J. Am. Chem. Soc. 91(23):6247–6250.

[49] Küenburg B, Czollner L, Fröhlich J, Jordis U, **1999**. Development of a Pilot Scale Process for the Anti-Alzheimer Drug (-) -Galanthamine Using Large-Scale Phenolic Oxidative Coupling and Crystallisation-Induced Chiral Conversion Abstract :, Org. Process Res. Dev. 3(6):425–431.

[50] Gnecco D, Marazano C, Enriquez RG, Teran JL, Del Rayo Sanchez M, Galindo SA, **1998**. Oxidation of chiral non-racemic pyridinium salts to enantiopure 2- pyridone and 3-alkyl-2-pyridones, Tetrahedron: Asymetry. 9(12):2027–2029.

[51] Charles M, **1985**. Fermentation scale-up: Problems and possibilities, Trends Biotechnol. 3(6):134–139.

[52] Straathof A, Panke S, Schmid A, **2002**. The production of fine chemicals by biotransformations, Curr. Opin. Biotechnol. :548–556.

Chapter 7

Kinetic characterization of galactose oxidase variants

The following chapter consists of unpublished results from a study performed in close collaboration with William R. Birmingham and Prof. Nicholas J. Turner at the University of Manchester (U.K.), who have performed all protein engineering work to develop the characterized enzyme variants.

7.1 Introduction

Kinetic characterization of enzymes is important not only during enzyme engineering in order to choose the best variant(s) for further development, but also during process development since detailed kinetic data allows engineers to design reactors and product removal strategies. The development of the TiTR (Chapter 5) has enabled fast and autonomous characterization of oxygen dependent enzymes. This allows the characterization of many variants of an enzyme to identify the phenotypic results of changes to the proteins' amino acid sequence.

Galactose oxidase (GOase) catalyzes the industrially interesting oxidation of 5-hydroxymethylfurfural (HMF) to 2,5-diformylfuran (DFF) (Figure 7.1) [1,2]. HMF is a potential sugar-derived platform molecule for the biobased chemical industry, from which a multitude of products can be synthesized [3]. DFF and derivatives thereof, are interesting products for the production of specialty polymers [4]. However, the chemical oxidation is difficult to conduct at high yields due to over-oxidation of DFF to the mono- and diacid. Over-oxidation to 5-formylfuran-2-carboxylic acid (FFCA) is also possible in the biocatalytic reaction, but typically only to a low extend. Thus, the GOase catalyzed reaction could be a route to DFF.

In the following, we characterize the kinetics of a number of GOase variants to illustrate the importance of knowing the kinetics when developing enzymes as industrial catalysts. The variants have been developed for various substrates and purposes. A particular important aspect of the study was to develop and screen for GOase variants displaying a higher activity

at low oxygen concentration, because it earlier has been found that the Michaelis constant for oxygen of GOase is above the solubility of oxygen in water [5,6]. Development or identification of enzymes displaying higher activity at low oxygen concentrations (i.e. higher k_{cat}/K_{MO} or lower K_{MO}) by screening at a reduced oxygen concentration has only been reported once in the scientific literature, where D-amino acid oxidase was engineered to display a five-fold lower K_{MO} and a two-fold higher k_{cat}/K_{MO} [7]. Although there also are examples of site-directed mutagenesis studies leadings to increased bi molecular rate constants with oxygen [8–11]. Engineering of GOase to display increased activity at low oxygen concentration has never been reported

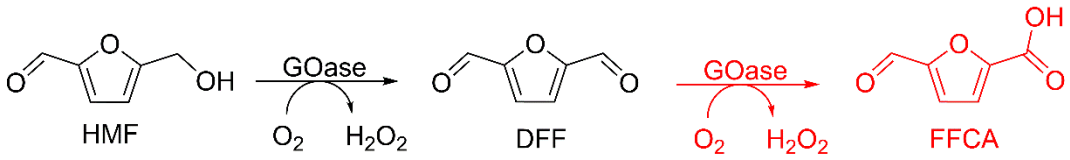

Figure 7.1. Oxidation of 5-hydroxymethylfurfural (HMF) to 2,5-diformylfuran (DFF) by galactose oxidase (GOase) and the potential over-oxidation to the 5-formylfuran-2-carboxylic acid (FFCA).

7.2 Results and discussion

7.2.1 Enzyme variants investigated

The development of the GOase applied in this study (Figure 7.2) dates back to two papers by Arnold and co-workers describing, first, a GOase variant expressible in *E. coli* with improved activity towards galactose and increased stability [12], and second, a GOase variant with activity towards oxidation of glucose [13]. Based on the latter variant (M_3), Escallettes and Turner (2008) engineered GOase to stereoselectively accept secondary aryl alcohols [14]. Since then, the variant ($M_{3\text{-}5}$) has been further evolved at the University of Manchester to increase the activity towards oxidation of HMF to DFF. Initially, the variant G_2 was identified as being more active in the oxidation of HMF. As the importance of Michaelis constant for oxygen was realized, existing mutant libraries was screened under a very low oxygen atmosphere (0.2% O_2) in a glove box. The screen at low oxygen conditions revealed several hits not obtained when screening at atmospheric conditions, where the most active was the variant C_4, with phenylalanine at position 290 changed to tryptophan. Interestingly, the double mutant CLS showed high activity when removed from the low oxygen atmosphere, so this was included in the following work together with the F194W mutant of G_2 and CLS and the G_2 F194W F290W (i.e. C_4 and the F194W alteration). The F194W variants were included because it is a modification often reported in the scientific literature. All amino acid substitutions from M_1 onwards are close to the active site and presumably taking part in substrate binding.

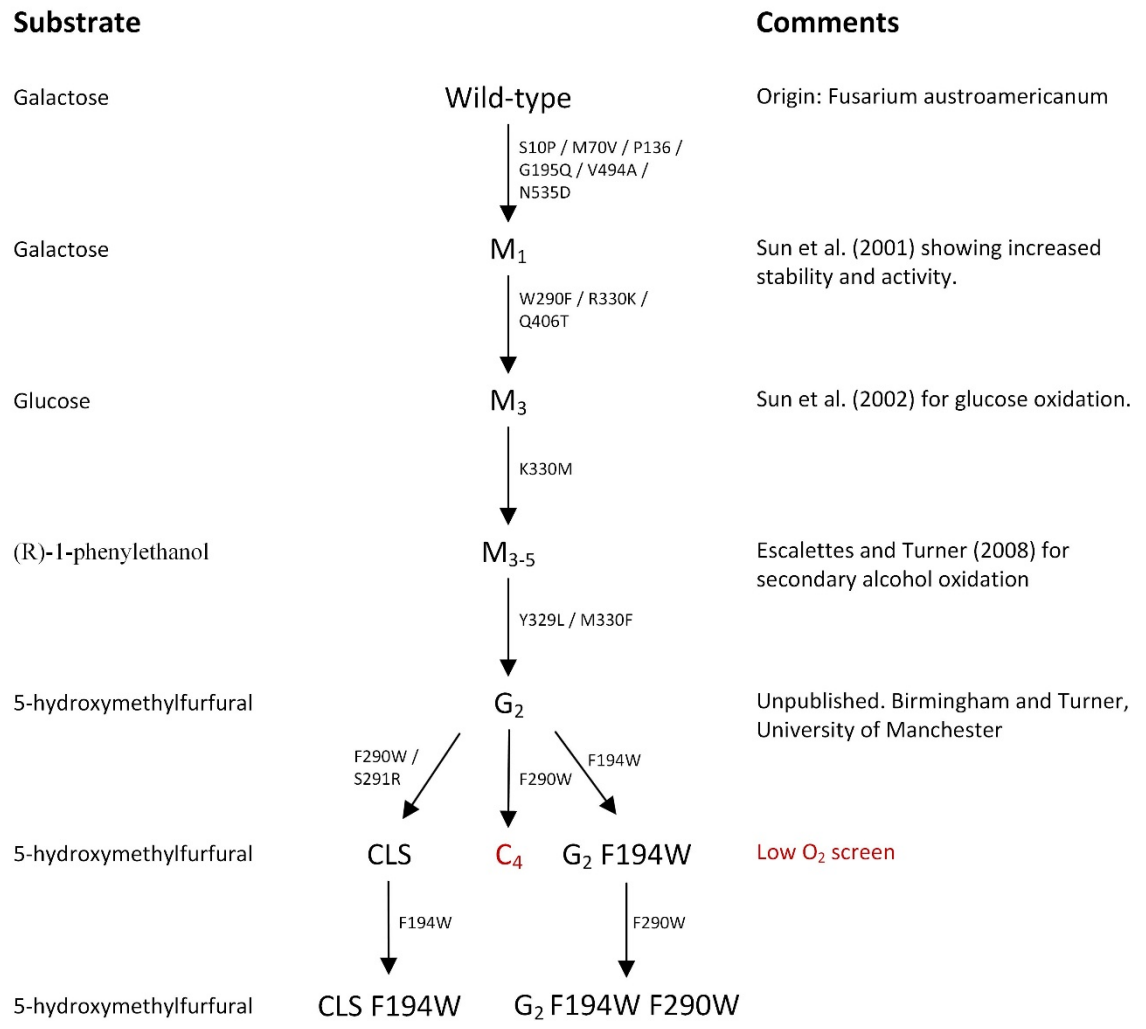

Figure 7.2. Galactose oxidase variants and their relationship. The protein engineering work to develop the variants was carried out by William R. Birmingham at the University of Manchester (U.K.) in the group of Prof. Nicholas J. Turner.

7.2.2 Stability of galactose oxidase

During the adaptation of the TiTR to accommodate measurements of kinetics for the HMF to DFF reaction catalyzed by GOase, we experienced problems with instability of GOase in the enzyme stock solution during the experiment. Therefore, the storage stability of GOase in the presence of different system components was investigated using the TiTR (Figure 7.3). Surprisingly, GOase was significantly less stable when stored in the presence of HRP, while other system components did not affect the stability. It is important to note that it is the stability of the apo-enzyme being studied here, because GOase is not loaded with copper until the first catalytic cycle.

The action of HRP is to form the tyrosine radical upon copper loading into the apo-enzyme. The radical is required for the enzyme to perform the two-electron oxidation, but the radical may also react with compounds not otherwise a substrate for the enzyme whereby the radical is reduced and the enzyme left in an inactive state. HRP is therefore also required during the

reaction to ensure that any inactive enzyme is reoxidized to its active state. Formation of a stable radical in the apo-GOase has also been reported [15], and one can therefore speculate that it is the radical in the active site causing the observed deactivation. This could possibly be via radical reactions with amino acids in the active site. However, at this point it is pure speculation.

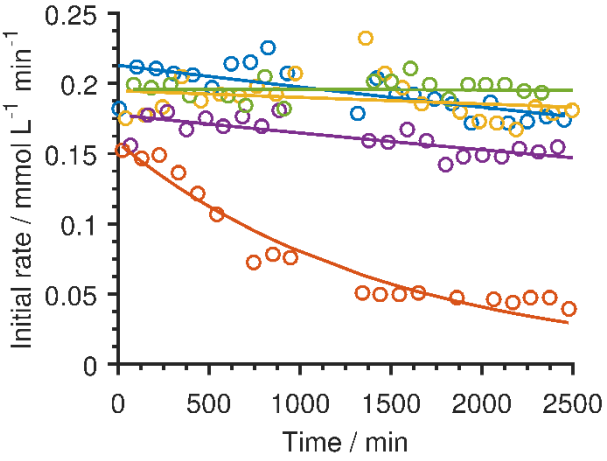

Figure 7.3. Galactose oxidase stability in presence of reaction components. Initial rate of reaction over time for GOase $M_{3\text{-}5}$ incubated at 25 ˚C in buffer (blue), with 1000 U/L horseradish peroxidase in buffer (red), with 20000 U/L catalase in buffer (yellow), with 0.1 mM $CuSO_4$ in buffer (purple), and incubated on 0 ˚C (on ice) with buffer (green). 100 mM sodium phosphate buffer, pH 7.4. GOase was supplied as CFE.

The problem of GOase instability during the kinetic analysis could not simple be solved by mixing the HRP in both substrate and buffer solution, because the stability of HRP is decreased in presence of HMF (data not shown) and therefore would not be constant during the experiment. Instead, we installed a fourth syringe pump to supply a stock solution of HRP. Nevertheless, the issue of GOase (and HRP) stability indicated above needs to be investigated in more detail to see if a similar deactivation takes place during the reaction and if it can be circumvented.

7.2.3 Kinetic parameters for galactose oxidase variants

The kinetic parameters of the investigated GOase variants are presented in Table 7.1. Unfortunately, it was not possible to determine the parameters for the CLS variants. This was due to significantly longer lag-time (>10 min) for these enzyme variants, making it impossible to determine the correct initial rate (i.e. the ‘steady-state’ rate) in the TiTR because the full reaction rate was not reached within the maximum residence time in the reactor. The reason for this increased lag-time is unknown, but it could be due a slower binding of copper caused by the S291R mutation.

Table 7.1. Kinetic parameters of galactose oxidase variants determined in the tube-in-tube reactor using HMF as substrate at 25°C. The kinetic parameters are obtained by fitting the ping pong bi bi Michaelis-Menten equation to initial rate data.

Variant	K_{MO} (mM)	K_{MS} (mM)	k_{cat} (s^{-1})	k_{cat}/K_{MO} ($M^{-1}s^{-1}$)	k_{cat}/K_{MS} ($M^{-1}s^{-1}$)
M_1 [a]	0.16±0.11	53±18	23.5±4.7	(1.5± 1.1)·10^5	(0.04± 0.02)·10^4
M_{3-5}	1.39±0.46	14.9±4.5	651±132	(4.7± 1.8)·10^5	(4.4± 1.6)·10^4
G_2	0.367±0.07	1.83±0.3	120±6	(3.3± 0.6)·10^5	(6.6± 1.1)·10^4
C_4 [a]	0.152±0.02	6.19±0.41	166±4	(10.9± 1.5)·10^5	(2.7± 0.2)·10^4
G_2 F194W [b]	2.00±0.36	3.00±0.6	427±35	(2.1± 0.4)·10^5	(14.2± 3.1)·10^4
G_2 F194W F290W [b]	3.52±1.4	50.8±21	1560±509	(4.4± 2.3)·10^5	(3.1± 1.6)·10^4
CLS	N.D. [c]				
CLS F194W	N.D. [c]				

[a] determined using purified enzyme, others using cell-free extract

[b] highly uncertain estimation of GOase content in cell-free extract

[c] not determined (N.D.) due to very long lag-phase

Of the successfully characterized GOase variants, the low K_{MO} of C_4 stands out, although M_1 also has a low K_{MO} but catalyze the oxidation of HMF very inefficiently (considering the high K_{MS} and relatively low k_{cat}). Similarly, the bimolecular rate constant with oxygen (k_{cat}/K_{MO}, referred to as the oxygen reactivity) is more than two fold higher than the variant displaying the second highest oxygen reactivity, M_{3-5}. The high oxygen reactivity of C_4 is not surprising, as the variant was identified in the low oxygen screen. This confirms that it is feasible to run assays under low oxygen conditions to identify enzymes with a higher oxygen reactivity. Furthermore, the result shows that it is possible to modify the oxygen reactivity of GOase.

Interestingly, the bimolecular rate constant with the 'primary' substrate, HMF, appears to be almost inversely related to the bimolecular rate constant for oxygen, if disregarding M_1 displaying the lowest reactivity with both substrates (Figure 7.4). This could be related to the difference in hydrophobicity of oxygen and HMF, oxygen being rather hydrophobic while HMF is hydrophilic. However, this does not correlate with the hydrophobicity of the amino acids being substituted, e.g. G_2 to C_4 (F290W) exchange a highly hydrophobic amino acid

to a less hydrophobic. The inverse correlation suggests that there could be a 'golden' optimum in 'primary' substrate and oxygen reactivity, not necessarily maximizing either of them.

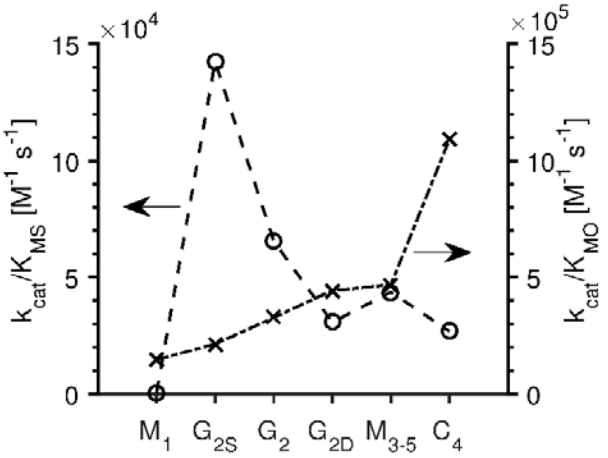

Figure 7.4. Bimolecular rate constants (k_{cat}/K_M) values for HMF and oxygen for he investigated galactose oxidase variants.

The kinetic data confirms that G_2, the variant chosen due to its apparent higher activity with HMF, is a better enzyme for catalyzing the oxidation of HMF than the parent $M_{3\text{-}5}$, when considering the bimolecular rate constant with HMF used as the evaluation criteria (the bimolecular rate constant is not dependent on the oxygen concentration as shown in Chapter 4). However, the oxygen reactivity of G_2 is lower than $M_{3\text{-}5}$, the following section will illustrate the importance of this.

7.2.4 Best variant under industrial conditions

High correlation between the parameters of the Michaelis-Menten equation makes direct comparison of e.g. K_{MO} values problematic. Furthermore, it is difficult to determine which of the variants is the better catalyst just based on the kinetic parameters. Therefore, it is better to compare the variants by considering the activity at a given oxygen and HMF concentration relevant to an industrial biocatalytic reaction. Figure 7.5 compares the reaction rate of the enzyme variants at two oxygen concentrations, 100% and 20% air saturation, and an HMF concentration of 200 mM. As discussed previously, 20% air saturation is a realistic oxygen level in an aerated industrial reactor due to the requirement of an oxygen transfer driving force, whereas 100% air saturation corresponds to the oxygen concentration in standard laboratory assays without control of the dissolved oxygen. The conditions in an industrial reactor will change as the reaction proceeds (unless it is operated continuously), in the beginning the reaction will be fast and slow down as substrate is consumed leading to an increase in oxygen concentration towards the end of the batch to balance supply and consumption of oxygen. However, for GOase with HMF as substrate the K_{MS} value are low compared to the typical initial substrate concentration, this means that the enzyme with be saturated with substrate until the very end of the reaction. Therefore, the conditions (including the oxygen

concentration) will be constant throughout the majority of the reaction time. Thus, the activity at single set of oxygen and HMF concentrations can represent the efficiency of a variant throughout a batch reaction (disregarding deactivation or product inhibition of the enzyme).

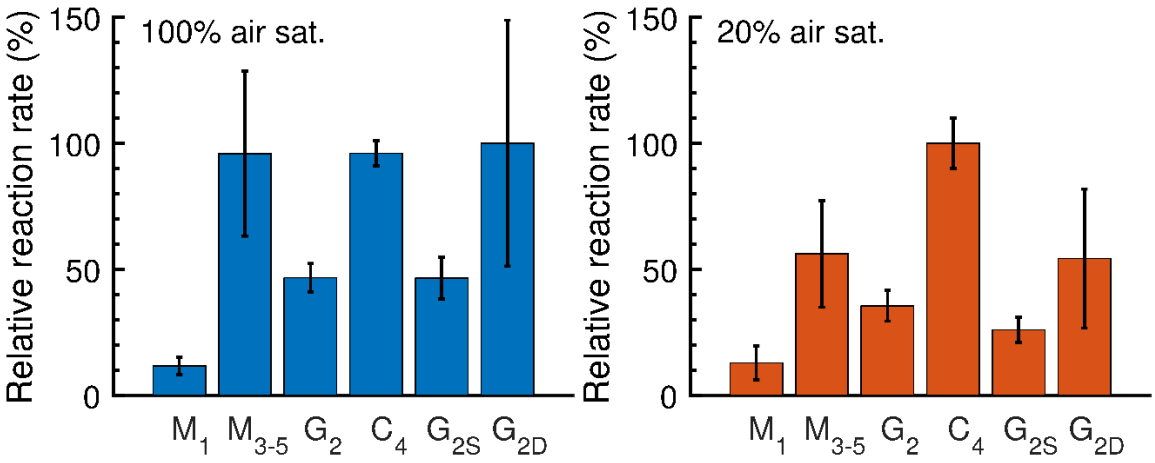

Figure 7.5. Comparison of relative reaction rates calculated from the kinetic parameters of the investigated galactose oxidase variants at an HMF concentration of 200 mM and at two oxygen concentrations – 100% air saturation (0.267 mM) and 20% air saturation (0.053 mM). G_{2S} = G_2 F194W, G_{2D} = G_2 F194W F290W.

The comparison of reaction rates clearly illustrates the importance of the oxygen reactivity as enzymes are taken from the test-tube to stirred reactors (i.e. the difference in oxygen concentration). The C_4 variant displays two-fold the activity over the second best candidate at the industrially relevant oxygen concentration, which directly translates into a two-fold decrease in enzyme requirements. Furthermore, the comparison illustrates the importance of fully characterizing the kinetics of enzyme variants before choosing a candidate for further rounds of mutagenesis or process development. If the best variant was chosen solely on its activity in a colorimetric assay at air saturation, a suboptimal choice of M_{3-5} or G_2 F194W F290W could have been made, as these variants would show similar activity to C_4.

7.3 Conclusion and future perspectives

The work described illustrates the importance of carefully characterizing the kinetics of oxygen dependent enzyme before choosing the variant for further development of the biocatalyst and eventually the bioprocess. Furthermore, it shows that it is possible to change the oxygen reactivity of GOase by substituting single amino acids. This bodes well for further protein engineering efforts as the screening was performed on an enzyme library limited to few amino acid positions, not chosen based on their potential involvement in oxygen binding. Thus, generation of focused enzyme libraries using molecular dynamics simulations stands a good chance to further enhance the oxygen reactivity [11]. Ideally, the inhibitory kinetics of the variants should be included in the comparison. Inhibition studies can easily be performed using the TiTR. However, it would require additional initial rates and thus increase the material consumption and length of experiments. Furthermore, enzyme stability needs to be included as a selection criterion, although the stability often can be improved in subsequent rounds of protein engineering without significantly affecting the activity [16,17].

7.4 Experimental section

7.4.1 Materials

All reagents used were of the highest grade available from Sigma-Aldrich (St. Louis, Missouri, U.S.A.). Catalase with an activity of 3172 U/mg (one unit (U) corresponds to the amount of enzyme which decomposes 1 μmol H_2O_2 per min at pH 7.0 and 25 °C) and horseradish peroxidase (HRP) with an activity of 145.7 U/mg (Type I) (1 U corresponds to the amount of enzyme that forms 1 mg purpurogallin from pyrogalin in 20 s. at pH 6.0 and 20 °C) were acquired from Sigma-Aldrich. Galactose oxidase variants were engineering at the University of Manchester (Manchester, U.K.) and produced as a cell-free extract (CFE) by Prozomix (Haltwhistle, U.K.). Purified variants were produced and purified by the University of Manchester.

7.4.2 Tube-in-tube reactor

The TiTR was used to characterize the GOase variants. The setup was described in detail in Chapter 5, although minor modifications were required. First, an additional syringe pump was added to feed HRP separately, and secondly, the injection valve was change to a 4-port actuated valve with a 100 nL internal injection loop (VICI, Houston, TX, USA). The latter was required due to the high UV absorbance of HMF and DFF.

The UV absorbance spectra of HMF and DFF overlap, and thus multivariate data analysis was required to elucidate the substrate and product concentration. The chemometric model was built and calibrated using the PLS_Toolbox (Eigenvector Research, Manson, WA, USA) for MATLAB (MathWorks, Natick, MA, USA). Figure 7.6 shows the calibration curves for HMF and DFF.

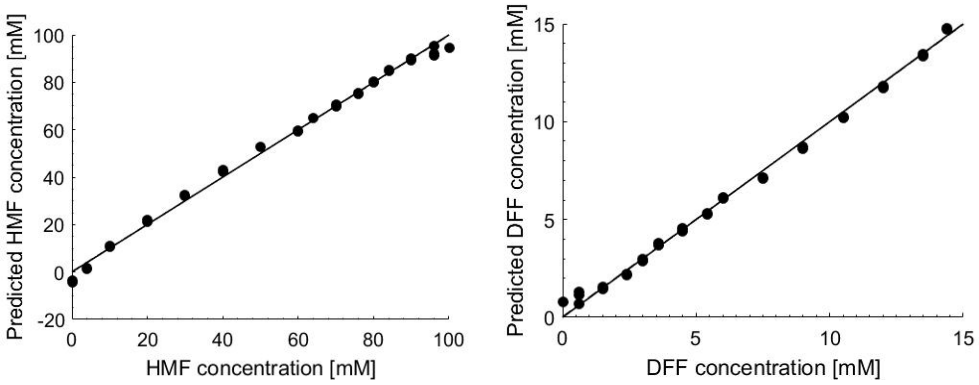

Figure 7.6. Calibration curves for 5-hydroxymethylfurfural (HMF) and 2,5-diformylfuran (DFF).

7.4.3 Kinetic characterization

Four stock solutions containing 1) buffer, catalase, $CuSO_4$ 2) buffer, catalase, CuSO4, HMF 3) buffer, GOase 4) buffer, HRP were fed to the TiTR using syringe pumps as described previously. 100 mM sodium phosphate buffer, pH 7.4 was used in all solutions. The amount of catalase and HRP corresponded to an activity in the reactor of 20000 U L^{-1} and 1000 U L^{-}

[1], respectively. The concentration of $CuSO_4$ in stock solutions corresponded to a concentration in the reactor of 100 μM. The GOase concentration was varying dependent on the activity of the enzyme to obtain an initial rate in the range 0.2-0.5 mmol L^{-1} min^{-1}.

Determination of the amount of GOase in the cell-free extract is required in order to calculate the value of k_{cat}. For M_{3-5} and G_2, the amount has been determined with good precisions to 5% (w/w) of the formulation. However, for G_2 F194W and G_2 F194W F290W the amount had to be estimated by comparing band intensities on an SDS-gel. The expression level of G_2 F194W and G_2 F194W F290W was estimated to ¼ of that of M_{3-5} and G_2. Ideally, all measurements should have be done using purified enzyme.

7.4.4 Galactose oxidase stability

Stability of GOase was investigated using the TiTR. The five conditions were tested simultaneously with samples being withdrawn for analysis at regular time intervals. The conditions in the assay were 12.5 mM HMF, 2.6 mM oxygen, and 100 mM sodium phosphate buffer pH 7.4.

7.5 References

[1] McKenna S, Leimkühler S, Herter S, Turner NJ, Carnell A, **2015**. Enzyme Cascade Reactions: Synthesis of Furandicarboxylic Acid (FDCA) and Carboxylic Acids using Oxidases in Tandem, Green Chem. 17:3271–3275.

[2] Qin Y-Z, Li Y-M, Zong M-H, Wu H, Li N, **2015**. Enzyme-catalyzed selective oxidation of 5-hydroxymethylfurfural (HMF) and separation of HMF and 2,5-diformylfuran using deep eutectic solvents, Green Chem. 17(7):3718–3722.

[3] van Putten R-J, van der Waal JC, Jong de E, Rasrendra CB, Heeres HJ, Vries JG de, **2013**. Hydroxymethylfurfural, A Versatile Platform Chemical Made from Renewable Resources, Chem. Rev. 113(3):1499–1597.

[4] Tong X, Ma Y, Li Y, **2010**. Biomass into chemicals: Conversion of sugars to furan derivatives by catalytic processes, Appl. Catal. A Gen. 385(1–2):1–13.

[5] Toftgaard Pedersen A, Birmingham WR, Rehn G, Charnock SJ, Turner NJ, Woodley JM, **2015**. Process Requirements of Galactose Oxidase Catalyzed Oxidation of Alcohols, Org. Process Res. Dev. 19(11):1580–1589.

[6] Humphreys KJ, Mirica LM, Wang Y, Klinman JP, **2009**. Galactose oxidase as a model for reactivity at a copper superoxide center, J. Am. Chem. Soc. 131(13):4657–4663.

[7] Rosini E, Pollegioni L, Ghisla S, Orru R, Molla G, **2009**. Optimization of D-amino acid oxidase for low substrate concentrations - towards a cancer enzyme therapy., FEBS J. 276(17):4921–32.

[8] Rosini E, Molla G, Ghisla S, Pollegioni L, **2011**. On the reaction of D-amino acid oxidase with dioxygen: O2 diffusion pathways and enhancement of reactivity., FEBS J. 278(3):482–92.

[9] Piubelli L, Pedotti M, Molla G, Feindler-Boeckh S, Ghisla S, Pilone MS, Pollegioni L, **2008**. On the oxygen reactivity of flavoprotein oxidases: An oxygen access tunnel and gate in Brevibacterium sterolicum cholesterol oxidase, J. Biol. Chem. 283(36):24738–24747.

[10] Hernández-Ortega A, Lucas F, Ferreira P, Medina M, Guallar V, Martínez AT, **2011**. Modulating O2 reactivity in a fungal flavoenzyme: Involvement of aryl-alcohol oxidase Phe-501 contiguous to catalytic histidine, J. Biol. Chem. 286(47):41105–41114.

[11] Baron R, Riley C, Chenprakhon P, Thotsaporn K, Winter RT, Alfieri A, Forneris F, van Berkel WJ, Chaiyen P, Fraaije MW, Mattevi A, McCammon JA, **2009**. Multiple pathways guide oxygen diffusion into flavoenzyme active sites, Proc Natl Acad Sci U S A. 106(26):10603–10608.

[12] Sun L, Petrounia IP, Yagasaki M, Bandara G, Arnold FH, **2001**. Expression and stabilization of galactose oxidase in Escherichia coli by directed evolution, Protein Eng. 14(9):699–704.

[13] Sun L, Bulter T, Alcalde M, Petrounia IP, Arnold FH, **2002**. Modification of galactose oxidase to introduce glucose 6-oxidase activity, ChemBioChem. 3(8):781–783.

[14] Escalettes F, Turner NJ, **2008**. Directed evolution of galactose oxidase: generation of enantioselective secondary alcohol oxidases, ChemBioChem. 9(6):857–60.

[15] Whittaker JW, **2003**. Free radical catalysis by galactose oxidase, Chem. Rev. 103(6):2347–63.

[16] Arnold FH, Wintrode PL, Miyazaki K, Gershenson A, **2001**. How enzymes adapt: Lessons from directed evolution, Trends Biochem. Sci. 26(2):100–106.

[17] Bommarius AS, Blum JK, Abrahamson MJ, **2011**. Status of protein engineering for biocatalysts: How to design an industrially useful biocatalyst, Curr. Opin. Chem. Biol. 15(2):194–200.

Chapter 8

General discussion

Throughout the thesis, different process development aspects for biocatalytic oxidations have been addressed. In the following chapter, the findings and developments will be summarized and discussed in a broader context of process development for oxygen dependent enzyme processes. Additionally, the interesting possibilities to improve the activity of enzymes at low oxygen concentrations are discussed. Finally, the perspectives for galactose oxidase as an industrial biocatalyst are elucidated.

8.1 Development of oxygen dependent enzyme processes

The time and effort required for developing a biocatalytic process varies with the starting point. If an active and stable biocatalyst is at hand, the development can be fast, whereas if the activity and stability has to be developed from a low starting point the time and effort required will be substantial, and the risk that the required biocatalyst metrics are not met will be significant.

The development of an oxygen dependent biocatalytic process starts with the identification of an enzyme with decent activity towards the target substrate, or alternative by applying protein engineering (e.g. directed evolution) to develop such from an enzyme showing some activity. Thereafter, we suggest a thorough characterization of the enzyme kinetics (oxygen reactivity, inhibition, etc.) and stability (influence of gas-liquid interfaces, substrate/product, and oxygen). Based on this, an early-stage economic assessment is made to identify potential bottlenecks and the key parameters to target for further enzyme improvements through protein engineering. Through close collaboration between protein and reaction engineers the enzyme is further developed to fit the process conditions, and process decisions are made in terms of oxygen supply method, eventual substrate supply and product removal. In this period of development, it is important to assess whether the challenges experienced are most efficiently overcome using protein or reaction engineering. Finally, an economic evaluation is required to evaluate if process meets the requirements to allow detailed process engineering and larger scale demonstration to commence.

Thus, the development of oxygen dependent enzyme processes can be simplified to four main areas of focus (Figure 8.1), namely characterization of the enzyme(s) in terms of stability and kinetics and the process engineering aspects of supplying substrate and removing product, and the supply of oxygen. The enzyme characteristics directly influences the process decisions in terms of how, and if, to supply substrate or remove product, and the choice of oxygen supply methods to limit enzyme deactivation, ensure a sufficient oxygen concentration in solution and minimize stripping of volatile compounds, etc.

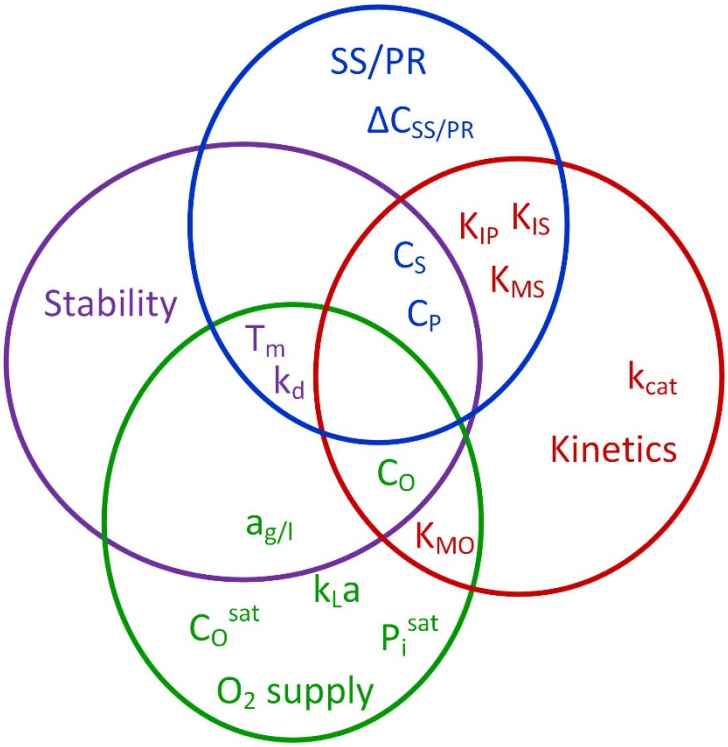

Figure 8.1. The four aspects of process development for oxygen dependent enzyme processes and their interrelation. SS/PR: substrate supply/product removal. $\Delta C_{SS/PR}$: driving force required for SS/PR, C_S: substrate concentration, C_P: product concentration, CO: oxygen concentration, C_O^{sat}: oxygen saturation concentration, k_La: volumetric mass transfer coefficient, $a_{g/l}$: gas-liquid interfacial area, P_i^{sat}: partial pressure of volatile compound (could also be solvent for PR), T_m: enzyme melting temperature (thermodynamic stability), k_d: enzyme deactivation rate constant (kinetic stability), K_I: inhibition constants, K_M: Michaelis constants, k_{cat}: rate constant.

In the following subsections, each of the areas are discussed in more detail in relation to the insights gained from the work presented in the previous chapters.

8.1.1 Enzyme stability

Enzyme stability is best characterized by determining a deactivation rate constant preferable as a function of the operating conditions [1]. When doing so, it is important to distinguish between the stability of enzyme carrying out catalysis and enzyme being inactive, as the apparent stability can vary accordingly. For two-substrate enzymes that exist in two distinct forms, such as oxygen dependent enzymes following the ping pong bi bi mechanism, there can even be stability differences between the enzyme forms. As an example, the radical in the active site of galactose oxidase (GOase) is only present in the oxidized form of the en-

zyme. As radicals are notoriously reactive, this form of the enzyme could very well be deactivated faster than the reduced enzyme form, although this is pure speculation as it has not been experimentally investigated.

Determining the enzyme stability during a reaction is not straight forward, as one needs to determine the activity at a standard set of conditions at each time point (i.e. constant concentration of 'primary' substrate, oxygen and product, and at constant temperature). Normally, the best option is to take out a sample and determine the stability in an appropriate assay. Alternatively, if a full kinetic model is available (also covering product inhibition) the rate of reaction at a given time point can be compared with the rate predicted by the kinetic model. This approach requires that the kinetic model can be trusted for predicting full time courses, something that is difficult to validate if the enzyme is unstable under typical operating conditions. In any case, it is important to investigate the possible mechanisms of deactivation, which for oxygen dependent enzymes typically are gas-liquid interface instability, aldehyde deactivation and oxidative damage by reactive oxygen species, as discussed in Chapter 2.

For GOase, studied in this thesis, the operational stability of the enzyme has not been investigated in detail. Nevertheless, results of exposing an enzyme, not carrying out a reaction, to aeration indicates that the enzyme is not destabilized by gas-liquid interfaces. However, preliminary results suggests that the enzyme is severely inhibited and deactivated at high concentrations (>50 mM) of benzaldehyde (data not shown). Aldehyde deactivation of enzyme is an increasing important topic, that on one hand possibly can be solved by implementation of *in situ* product removal, while one the other hand also is a topic for protein engineering to tackle, as there are indications that it can be solved through substitution of amino acids. However, a general and proven method for significantly increasing the stability in presence of aldehydes using protein engineering is still lacking in the scientific literature.

8.1.2 Kinetic characterization of oxygen dependent enzymes

Kinetic characterization of enzymes are important not only during development of the biocatalyst to identify the optimal candidate(s) for further development, but also in process development. The access to trustworthy kinetic models enables sizing of reactors, design of reactor concepts such as substrate feeding and product removal, and optimization of reaction conditions, as is known from traditional chemical engineering [2]. For oxygen dependent enzymes, trustworthy kinetic models, also covering the reaction with oxygen, are even more important because of the generally high Michaelis constant for oxygen relatively to the solubility of oxygen in water. In fact, the reaction rate between the reduced enzyme and oxygen will be rate limited for most enzymes, as discussed in Chapter 4. Precisely knowing the enzyme kinetics will therefore allow reaction engineers to optimize the process conditions and the oxygen supply to maximum the enzyme utilization efficiency and thus minimize the enzyme consumption.

Currently, the kinetics of enzyme reactions are studied in spectrophotometric assays (typically in 96 well-plates) or in stopped-flow apparatuses [2]. However, for oxygen dependent

enzymes this is not a possibility because of the inability to control the dissolved oxygen concentration. The only alternative is therefore to conduct experiments in batch reactors with agitation and sparging of air/oxygen to control the oxygen concentration combined with off-line analysis of product formation rate. Therefore, it was quickly realized that a tool for fast and efficient kinetic characterization of oxygen dependent enzymes could significantly improve not only the process development, but also the biocatalyst development, i.e. the protein engineering and screening efforts. This lead to the development of the tube-in-tube reactor (TiTR) presented in Chapter 5, which enables autonomous characterization of enzymes with minimal material consumption.

We believe, that if the TiTR and the software required to operate the setup and analyze the results would be further improved primarily in terms of material consumption and user-friendliness, the setup could be commercialized and thus be made available for the general enzyme development community. This would enable protein engineers to implement detailed kinetic characterization earlier in the development cycle (i.e. in between rounds of protein engineering to improve enzyme performance) and thus enable the selection of enzyme variants with the greatest potential for industrial implementation, as exemplified by GOase variants in Chapter 7. Furthermore, it would give process engineers access to high quality kinetic data when developing biocatalytic oxidation processes.

The TiTR also enables the determination of inhibition parameters for the studied enzyme, which is important when deciding whether or not to implement substrate feeding or product removal strategies. Another potential limitation for oxygen dependent enzymes is the inhibition of auxiliary enzymes, such as catalase, that are required to maintain the activity of the oxygen dependent enzyme. As an example, the horseradish peroxidase required for the activity of GOase has in preliminary studies shown to be deactivated and inhibited by benzaldehyde (data not shown). High activity of auxiliary enzymes throughout the time course a batch is of course necessary for obtaining a successful process, and something that should be studied in detail.

8.1.3 Oxygen supply

As discussed throughout this thesis, the supply of oxygen is of great importance because oxygen typically limits the reaction rate, the air-liquid interface potentially deactivates enzymes, the aeration gas may strip volatile compounds from the reactor and the cost of aeration may add substantially to the final product cost of lower value products.

It was shown in Chapter 3 that bubble aeration in stirred reactors (or bubble columns at very large scale) is the cheapest oxygen supply method when only considering the cost of agitation and aeration, and not the cost savings obtained from other process improvements such as decreased evaporation of volatile compounds or decreased enzyme deactivation. Pressurization of the reactor headspace or aeration using pure oxygen did increase the maximum specific oxygen transfer rate. However, neither increased headspace pressure nor pure oxygen sparging resulted in statistically significant reduction of aeration costs. Membrane aeration could, in the best case scenario, obtain specific aeration costs close to those obtained

in a bubbled stirred tank reactor. However, this required pressurization of both the reactor and the membrane module to at least 25 bars in order to reduce the required membrane area, something that has not been demonstrated experimentally for a membrane aeration system. The last option considered was hydrogen peroxide feeding followed by decomposition by catalase. In general, the analysis showed that the method was not competitive from an economic standpoint due to the high cost of hydrogen peroxide (relative to the cost of supplying oxygen from air) nor from a technological standpoint, because avoiding locally high concentrations of hydrogen peroxide could be difficult at large scale.

The potential economic benefits of other process improvement, such as decreased enzyme deactivation, by applying a given oxygen supply method is more difficult to access in a general manner, because the values will change from case to case. Nevertheless, an analysis in Chapter 4 showed the clear economic benefit from applying an oxygen supply method capable of increasing the dissolved oxygen concentration when utilizing an enzyme with a Michaelis constant for oxygen above the solubility limit. Here in was shown that by increasing the headspace pressure to 10 bars, or preferably bubbling with pure oxygen instead of air, the dissolved oxygen concentration in solution could be increased without decreasing the oxygen transfer rate. Thereby, the enzyme being limited by oxygen would operate closer to its maximum velocity, and thus reduce the overall cost by decreasing the enzyme requirement while maintaining the desired productivity. This example highlights the importance of carefully characterizing an enzyme before choosing a suitable oxygen supply method. A similar analysis can be made for other process improvement, e.g. decreased stripping of a volatile compound or decreased deactivation of a gas-liquid interface sensitive enzyme.

8.2 Improving the oxygen reactivity of enzymes through protein engineering

The analysis presented in Chapter 4 clearly showed that at a point in the development of an enzyme towards a certain reaction, it would no longer be the binding and reaction of the 'primary' substrate that determines the overall rate of reaction at industrial scale, but rather the binding and reaction of oxygen with the reduced enzyme. This is primarily due to the low solubility of oxygen in water and the requirement to a driving force to transfer oxygen from a gas-phase, combined with the high K_{MO} values of many oxygen dependent enzymes relative to the solubility of oxygen.

The oxygen reactivity (measured by the bimolecular rate constant, i.e. the ratio of k_{cat}/K_{MO}) of most oxygen dependent enzymes are excellent (i.e. $>10^5$ s^{-1} M^{-1}) although not at the diffusion limit (10^8-10^9 s^{-1} M^{-1}). At this point, it is not clear if and how much the bimolecular rate constant of a typical oxygen dependent enzyme can be improved, because of the already high oxygen reactivity of most enzymes and the particularly unfavorable initial electron transfer to molecular oxygen. Chapter 7 illustrated that by screening a GOase mutant library at reduced oxygen conditions it was possible to identify a variant different from those typically identified when screening at atmospheric conditions. The identified variant showed a significantly improved bimolecular rate constant with oxygen and lower K_{MO} value when

characterized in the TiTR, thus confirming the increased reactivity at low oxygen conditions. Interestingly, the bimolecular rate constant with the 'primary' substrate, HMF, had decreased, but when considering the catalytic rate obtainable at typical 'primary' substrate and oxygen concentrations at industrial scale, the newly identified variant was performing significantly better.

This preliminary study shows the importance of including the effect of oxygen in the screening efforts when developing novel enzymes, especially in the later stages of protein engineering, and that it is possible to change the oxygen reactivity of GOase through modification of single amino acid residues. Combining molecular dynamics simulations of oxygen diffusion through the protein to predict hotspots for amino acid substitution with a directed evolution effort dedicated to improving oxygen reactivity could potentially lead to even further improvements [3,4]. Nevertheless, it is impossible to know how close to the diffusion limit it is possible to get, even with a significant protein engineering effort. In any case, even small improvements in the reaction rate at low oxygen concentrations are directly translated into reduced enzyme requirements and thus potentially significant cost savings.

8.3 The application of galactose oxidase as an industrial biocatalyst

GOase efficiently catalyzes oxidations of a range of primary alcohols to aldehydes. Protein engineering has proven that it is possible to extend the substrate scope significantly beyond the natural substrates and even as far as secondary alcohols. However, GOase requires a range of additives thus making it a complex system. The radical in the active site is very reactive, and may react with the solvent or trace molecules that can donate a single electron. The radical is protected from solvent interactions by the shells of amino acids surrounding it, and 'wrong' mutations to the shells can result in an enzyme that readily loses its radical and renders it inactive [5]. The partially reduced, inactive form of GOase can be reactivated by supplying a single electron oxidant, which typically is horseradish peroxidase (HRP). Additionally, GOase, in the form applied in this project, requires copper in the reaction mixture to ensure that the enzyme is fully loaded at all times, and catalase to decompose the hydrogen peroxide generated in the reaction. Thus, the reaction system is composed of three enzymes that all are required to be stable throughout the reaction and preferably not inhibited to a significant extend by reaction components.

Neither the stability nor the inhibition profile of horseradish peroxidase or catalase has been the subject of a detailed investigation in this work. Nevertheless, a preliminary investigation showed that HRP was significantly inhibited by benzaldehyde and that the normally stable enzyme was significant deactivated in the presence of benzyl alcohol and benzaldehyde (data not shown). Furthermore, a recent study has questioned the stability of catalase from bovine liver (the most widely applied catalase in biocatalytic studies) whereas catalase from *Aspergillus Niger* appeared significantly more stable [6]. The stability and inhibition of the auxiliary enzymes should be a topic for further investigation before applying GOase in an industrial process. To overcome potential stability problems of HRP, it can be considered to exchange the peroxidase to soybean peroxidase that has been reported to be more stable in presence of organic compounds [7].

As mentioned above, other preliminary data suggests that GOase has significant problems of both deactivation and inhibition by benzaldehyde, which results in problems of obtaining high conversions at high substrate loadings. The deactivation and inhibition need to be further characterized, and methods to alleviate the problem should be pursued. This could be protein engineering strategies to improve the enzyme tolerance to high concentrations of aldehydes or *in situ* product removal strategies could be implemented, such as a secondary organic phase. In case of a two-phase system, the solvent should preferably be high boiling to avoid evaporation and have a high affinity for benzaldehyde while a low affinity for benzyl alcohol. This could be p-xylene or undecane.

Overall, GOase has the potential to become a widely industrially applicable biocatalyst for oxidizing primary and secondary alcohols, especially if the problems of aldehyde deactivation and inhibition are solved.

8.4 References

[1] Bommarius AS, Paye MF, **2013**. Stabilizing biocatalysts, Chem. Soc. Rev. 42(15):6534–65.

[2] Ringborg RH, Woodley JM, **2016**. The Application of Reaction Engineering to Biocatalysis, React. Chem. Eng. 1(1):10–22.

[3] Baron R, Riley C, Chenprakhon P, Thotsaporn K, Winter RT, Alfieri A, Forneris F, van Berkel WJ, Chaiyen P, Fraaije MW, Mattevi A, McCammon JA, **2009**. Multiple pathways guide oxygen diffusion into flavoenzyme active sites, Proc Natl Acad Sci U S A. 106(26):10603–10608.

[4] Saam J, Ivanov I, Walther M, Holzhütter H-G, Kuhn H, **2007**. Molecular dioxygen enters the active site of 12/15-lipoxygenase via dynamic oxygen access channels., Proc. Natl. Acad. Sci. U. S. A. 104(33):13319–24.

[5] Saysell CG, Barna T, Borman CD, Baron AJ, McPherson MJ, Sykes AG, **1997**. Properties of the Trp290His variant of Fusarium NRRL 2903 galactose oxidase: Interactions of the GOase(semi) state with different buffers, its redox activity and ability to bind azide, J. Biol. Inorg. Chem. 2(6):702–709.

[6] Morthensen ST, Meyer AS, Jørgensen H, Pinelo M, **2017**. Significance of membrane bioreactor design on the biocatalytic performance of glucose oxidase and catalase: Free vs. immobilized enzyme systems, Biochem. Eng. J. 117:41–47.

[7] Kamal JKA, Behere D V., **2008**. Kinetic stabilities of soybean and horseradish peroxidases, Biochem. Eng. J. 38(1):110–114.

Chapter 9

Conclusions

Oxidation reactions catalyzed by oxygen dependent enzymes are a promising alternative and complement to chemical oxidations especially in the fine- and specialty-chemical industry. However, to date the industrial implementation of biocatalytic oxidations is still limited. In this thesis, work aiming at bridging the gap between interesting enzymes under development and industrial implementation has been reported to facilitate the broader adaption and implementation of oxygen dependent enzymes in the chemical industry. The main conclusions drawn from the investigation are summarized below:

- Bubble aeration in stirred tanks was found to be the most effective way of supplying oxygen to a biocatalytic reaction when only considering the cost of aeration and agitation and excluding derived cost reductions, such as increased enzyme stability by avoiding gas-liquid interfaces. Increasing the headspace pressure or bubbling with pure oxygen could increase the maximum oxygen transfer rate, but does not increase the cost of supplying oxygen.
- Alternative oxygen supply methods, such as membrane aeration and hydrogen peroxide decomposition, were found to be significantly more expensive to employ. Nevertheless, when considering derived effects, such as a greater enzyme utilization efficiency if operating at a higher oxygen concentration, alternative oxygen supply methods may turn out to be cost effective if developed further.
- The oxygen reactivity of enzymes are often not considered when developing an oxygen dependent enzyme. Nevertheless, many industrially relevant enzymes display Michaelis constants for oxygen (K_{MO}) close to or above the solubility of oxygen in water. Thus, the catalytic rate will in practice be limited by the availability of oxygen. Recognizing this is important when deciding upon protein engineering objectives and designing oxygen supply methods.
- Automated kinetic characterization of oxygen dependent enzymes was achieved by the development of the tube-in-tube reactor (TiTR). The TiTR employs membrane aeration, pressurization, and pure oxygen to control the oxygen concentration in solution up to a concentration 50-times the saturation concentration at ambient conditions. By carefully controlling the flow regime in the reactor, time-series data could

be generated by ramping the flow and continuously analyzing the product formation using UV-vis spectroscopy.

- The TiTR enabled the characterization of six galactose oxidase (GOase) variants for their ability to catalyze the oxidation of 5-hydroxymethylfurfural (HMF). The kinetic characterization confirmed that a variant identified in a high-throughput screen at low oxygen conditions was indeed more active in a reaction at low oxygen concentrations. It was show that the variant had a 10-fold lower K_{MO} and a 2-fold higher k_{cat}/K_{MO} than the second best characterized variant, making it a significantly better biocatalyst at industrially relevant oxygen concentrations. The study confirmed that it is possible to improve the oxygen reactivity of GOase using protein engineering.
- GOase was investigated as a potential industrial biocatalyst for the oxidation of alcohols to aldehydes and ketones. It was found to be a complex enzyme system because not only was catalase required for the degradation of hydrogen peroxide, but also copper and a single electron oxidant in the form of a peroxidase were required to ensure the full activity of the enzyme. Furthermore, the buffer type and concentration had a significant impact on the activity. Nevertheless, the high activity of GOase and the broad range of possible substrates it can covert makes it suitable as a target for further development.

Chapter 10

Future perspectives

In the following chapter, a range of recommendations for future research topics will be suggested and discussed.

10.1 Protein engineering challenges

Three specific challenges for protein engineering that would significantly improve the industrial viability of oxygen dependent processes are listed below.

Lowering the Michaelis constant for oxygen, K_{MO}, while maintaining or improving the oxygen reactivity, k_{cat}/K_{MO}, could significantly reduce the enzyme requirements for many industrially relevant enzymes as discussed in lengths throughout the thesis.

A general methodology for improving the gas-liquid interface stability of enzymes and generation of examples upon which it is feasible, could encourage development of enzymes otherwise discarded due to poor gas-liquid interface stability. To enable this, a better understanding of the phenomenon of unfolding at the gas-liquid interface and subsequent deactivation or aggregation is required.

The aldehyde tolerance of enzymes is a general problem experienced when aldehydes are either a substrate or a product of an oxidation reaction. So far, there are still only limited examples of successful protein engineering strategies to improve an enzyme that otherwise shows limited aldehyde tolerance. The deactivation effect will vary depending on the reactivity of the aldehyde, and it is probably not possible in all cases to increase the tolerance to an extent that allows industrial implementation without a form of *in situ* product removal (ISPR). Nevertheless, some aldehyde tolerance is important to uphold a driving force for ISPR.

10.2 Oxygen supply methods

During this thesis, it has been established that the alternatives to aerated stirred tank reactors would not be economically advantageous if just considering the cost of agitation and aeration, and only headspace pressurization or pure oxygen aeration of a stirred tank would result in a similar cost of transferring oxygen. The construction of bioreactors for handling above

ambient pressures are standard procedure if not in the biotechnological industry then in the chemical.

Although membrane aeration adds to the cost of oxygen supply, it offers the advantage of improving the stability of enzyme sensitive to gas-liquid interfaces. Instability to gas-liquid interfaces can potentially put a stop to industrial implementation of many enzymes, if the stability cannot easily be improved through protein engineering. Membrane aeration can therefore be of significant importance for oxygen dependent enzyme processes (or other gas dependent enzymatic processes for that matter) in the future. Membrane aeration has been demonstrated at pilot scale and a few examples of industrial scale wastewater treatment plant trials exist. However, as demonstrated in this thesis, moderate pressurization of the membrane module and the reactor is necessary in order to bring down the cost of oxygen supply. Pressurization of membrane modules in general is standard procedure. Nevertheless, laboratory and pilot scale demonstration of pressurized membrane aeration will be paramount to validate the cost of oxygen supply and the advantages when applied in oxygen dependent biocatalysis.

10.3 Application of a tube-in-tube reactor for industrial scale synthesis

The tube-in-tube reactor (TiTR), applied for the analysis of oxygen dependent enzyme kinetics, offers the possibility to conduct biocatalytic oxidation reactions in flow at high oxygen concentrations and at high oxygen transfer rates. The TiTR was originally developed for preparative scale organic synthesis [1], and later also applied for biocatalytic oxidation reactions on a gram-scale [2,3]. For biocatalytic oxidations, high volumetric productivities (>10 g L^{-1} h^{-1}) were obtained in the TiTR due to the high oxygen concentration and transfer rate [2,3]. The small tube dimensions applied for the kinetic characterization corresponds to a specific surface area of 17000 m^2/m^3. Together with the high oxygen permeability of the inner membrane, this results in a volumetric mass transfer coefficient in the range of ≈20000 h^{-1}, two orders of magnitude above the k_La typically found in stirred reactors. The construction of the TiTR from polymer tubes allows moderate pressurization to be straightforward, as long as both the inner and outer tube is pressurized to avoid significant cross-membrane pressures. The above ambient pressure of oxygen (up to 10 bars in the current setup) combined with the high k_La value results in oxygen transfer rates up to three orders of magnitude above what can be expected in bubbled stirred reactors. The large oxygen transfer potential can be used to transfer oxygen (i.e. having a large driving force) or to increase the oxygen concentration in solution thus using the applied enzyme more efficiently, or a combination of these. Additionally, the membrane-assisted aeration in the TiTR enables the application of enzymes sensitive to gas-liquid interfaces.

These obvious advantages makes the TiTR an interesting option for larger scale synthesis if constructed as a fiber-bundle reactor with the reaction mixture inside the membrane fibers and pressurized oxygen in the casing around the bundle. Although such a reactor would enable much higher productivities and more efficient use of high K_{MO} enzymes, there are also a range of potential drawbacks of the technology. First, the membrane material, Teflon

AF-2400, is very expensive (the resin price is ≈25000 USD kg^{-1}). The material requirement for each membrane fiber is limited, but the total requirement will be substantial. Second, the small dimensions of the fibers currently used will result in large pressure drops (for the 3 m TiTR the pressure drop is as high as 1 bar even at the very low flow rates applied) that will only increase with the increasing length to obtain the volume and residence time required to reach close to full conversion. Therefore, fibers with larger diameters are required, which will increase the diffusion lengths and reduce the specific surface area, thus decrease the oxygen transfer capabilities. Larger inner diameters could lead to substantial radial oxygen gradients as showed by Yang and Jensen (2013), although this was for a fast chemical reaction [4].

Nevertheless, a fiber-bundle reactor constructed from a chemical resistant material with high gas permeability could potentially be a future reactor for conducting biocatalytic reactions requiring a gaseous substrate. It will require more research to develop a functional system, demonstrate the applicability, and ensure the economic viability. Furthermore, the cost of membrane material has to decrease, either through a reduced cost of Teflon AF-2400 or through the development of a cheaper alternative.

10.4 Oxygen dependent biocatalysis in alternative media

Enzyme catalysis in neat (or nearly anhydrous) organic solvents has been extensively studied due to the clear industrial advantages such as increased solubility of non-polar substrates, reversal of hydrolysis reactions, alteration of specificity, and the ability to use enzymes in chemical processes without performing a solvent swap [5]. For oxygen dependent biocatalysis, the foremost advantage would be the increased solubility of oxygen in hydrophobic solvents compared to that in water [6,7]. As examples, the molar solubility of oxygen in toluene, acetone, and hexane is 7, 9, and 13 times that of oxygen in water at 25 °C and 1 bar gas pressure, respectively. However, the solubility in molar fractions are 42, 38, and 98 times that of oxygen in water, respectively, due to the larger molar volume of the organic solvents. It is difficult to predict the direct effect of an increased molar fraction of oxygen on the enzyme activity with oxygen. The reaction rate will be dependent on the thermodynamic activity of the reactants (converging towards the concentration in dilute aqueous systems), which will change with the solvent, and of course the ability of the enzyme to function in the organic solvent. Nevertheless, a larger molar fraction of oxygen will correspond to an increased tendency of enzyme-oxygen collisions and thus presumable an increased reaction rate. Similarly, the higher solubility of oxygen in organic solvents will translate into a higher driving force for oxygen transfer, thus increasing the maximum oxygen transfer rate. On the other hand, the use of potentially volatile organic solvents will require very careful control of the reactor (pressure and oxygen content in aeration gas) to avoid the formation of explosive atmospheres, and from a safety perspective, preferable higher boiling solvents should be applied. Alternatively, membrane aeration could be developed as a safer alternative to bubble aeration. Finally, organic solvents need to be recycled, which especially for high boiling solvents can be a difficult and energy consuming process.

Examples of the use of oxygen dependent enzymes in organic solvents (although only mixtures of water miscible solvents and water) do exist, such as the application of monolignol oxidase and cholesterol oxidase in mixtures of water and water miscible solvents [8,9]. However, the examples are still limited and the area requires significant research to enable the application of oxygen dependent enzymes in anhydrous organic solvents.

Ionic liquids are an alternative to organic solvents, which are the topic of much research including for biocatalytic applications, due to their ability to dissolve almost anything [10]. For oxygen dependent biocatalysis, ionic liquids could serve as a solvent due the immediate advantages of zero partial pressure (i.e. no evaporation) and high oxygen solubility (at best, 100 times higher than for water on a mole fraction basis) [11]. However, as for most ionic liquid applications, it will require efficient strategies for removing the product from the ionic liquid, and regeneration and recycling of the often expensive ionic liquids.

Another interesting development is the application of enzymes for gas-phase catalysis, such as the recent example of hydroxylation of methane to methanol by methane monooxygenase (MMO) embedded in a hydrogel [12]. By carefully designing the hydrogel structures, the specific surface area could be maximized to reduce mass transfer limitations. Further developments in this area could enable gas-phase biocatalytic reaction at industrial scale thus avoiding the slow transfer of gaseous compounds to an aqueous phase. One could even imagine a process where co-factors, such as NADH required by the MMO, are regenerated using hydrogenases supplied with hydrogen also from the gas-phase.

10.5 References

[1] Polyzos A, Brien MO, Petersen TP, Baxendale IR, Ley S V, **2011**. The Continuous-Flow Synthesis of Carboxylic Acids using CO 2 in a Tube-In-Tube Gas Permeable Membrane Reactor, Angew. Chemie. 50:1190–1193.

[2] Tomaszewski B, Lloyd RC, Warr AJ, Buehler K, Schmid A, **2014**. Regioselective biocatalytic aromatic hydroxylation in a gas-liquid multiphase tube-in-tube reactor, ChemCatChem. 6(9):2567–2576.

[3] Tomaszewski B, Schmid A, Buehler K, **2014**. Biocatalytic production of catechols using a high pressure tube-in-tube segmented flow microreactor, Org. Process Res. Dev. 18(11):1516–1526.

[4] Yang L, Jensen KF, **2013**. Mass Transport and Reactions in the Tube-in-Tube Reactor, Org. Process Res. Dev. 17:927–933.

[5] Doukyu N, Ogino H, **2010**. Organic solvent-tolerant enzymes, Biochem. Eng. J. 48(3):270–282.

[6] Battino R, Rettich TR, Tominaga T, **1983**. The Solubility of Oxygen and Ozone in Liquids, J. Phys. Chem. Ref. Data. 12(2):163–178.

[7] Sato T, Hamada Y, Sumikawa M, Araki S, Yamamoto H, **2014**. Solubility of oxygen in organic solvents and calculation of the Hansen solubility parameters of oxygen, Ind. Eng. Chem. Res. 53(49):19331–19337.

[8] Pils S, Schnabl K, Wallner S, Kljajic M, Kupresanin N, Breinbauer R, Fuchs M, Rocha R, Schrittwieser JH, Kroutil W, Daniel B, Macheroux P, **2016**. Characterization of the monolignol oxidoreductase AtBBE-like protein 15 L182V for biocatalytic applications, J. Mol. Catal. B Enzym. 10.1016/j.molcatb.2016.10.018.

[9] Doukyu N, Shibata K, Ogino H, Sagermann M, **2008**. Purification and characterization of Chromobacterium sp. DS-1 cholesterol oxidase with thermal, organic solvent, and detergent tolerance, Appl. Microbiol. Biotechnol. 80(1):59–70.

[10] van Rantwijk F, Sheldon RA, **2007**. Biocatalysis in ionic liquids, Chem. Rev. 107(6):2757–2785.

[11] Anderson JL, Dixon JK, Brennecke JF, **2002**. Solubility of CO2, CH4, C2H6, C2H4, O2, and N2 in 1-hexyl-3-methylpyridinium Bis(trisflouromethylsulfonyl)imide: Comparison to other Ionic Liquids, Acc. Chem. Res. 40(11):1208–1216.

[12] Blanchette CD, Knipe JM, Stolaroff JK, DeOtte JR, Oakdale JS, Maiti A, Lenhardt JM, Sirajuddin S, Rosenzweig AC, Baker SE, **2016**. Printable enzyme-embedded materials for methane to methanol conversion, Nat. Commun. 7:11900.

Appendix A

Supporting information for Chapter 3

A.1 Nomenclature

Parameter	Description	Unit
a	Area available for mass transfer	m^2
A_{mf}	Membrane module footprint	m^2
AF	Annuity factor	y^{-1}
c	concentration	mol m^{-3}
C_C	Cost of capital	USD
C_{SC}	Specific cost of capital	USD h^{-1}
C_I	Pressure vessel correlation factor	USD kg^{-1}
CI	Chemical engineering plant cost index	-
D	Vessel diameter	m
D_f	Membrane fiber diameter	m
D_{bf}	Distance between membrane fibers, fraction of fiber diameter	-
D_T	Vessel diameter	m
E_j	Welding joint efficiency	-
f	Vessel filling fraction	-
F	Fraction of oxygen in gas transferred to liquid	-
F_{fe}	Fraction of tank height used to expose membrane fibers	-
F_g	Molar flow of gas	mol s^{-1}
F_{sat}	Degree of liquid saturation in membrane outlet	-
Fl_G	Gas flow number	-
Fr	Froude number	-
g	Gravitational acceleration	m s^{-2}
H	Vessel height	m
IR	Interest rate	y^{-1}
k_{cat}	Enzyme rate constant	s^{-1}

k_La	Volumetric mass transfer coefficient	s^{-1}
k_H	Henry's constant	bar m^3 mol^{-1}
K_L	Membrane mass transfer coefficient	mol h^{-1} bar^{-1} m^{-2}
K_M	Michaelis constant	mol m^{-3}
L_f	Membrane fiber length	m
m_v	Pressure vessel weight	kg
m_s	Pressure vessel shell weight	kg
m_h	Pressure vessel head weight	kg
m_{H2O2}^{feed}	Mass fraction of H_2O_2 in feed	-
M	Molar mass	kg mol^{-1}
N	Stirrer speed	s^{-1}
N_f	Number of membrane fibers	-
p	Pressure	Pa
P	Power input	kW
P_O	Impeller power number	-
P_g/P	Ungassed to gassed power draw ratio	-
P/V	Power input per unit volume	kW m^{-3}
Q_l	Liquid flow rate	m^3 s^{-1}
Q_g	Gas flow rate	m^3 s^{-1}
r	Reaction rate	mol m^{-3} s^{-1}
R	Ideal gas constant	Pa m^3 K^{-1} mol^{-1}
S	Equipment scaling parameter	-
S_S	Maximum allowable working stress	Pa
SF	Equipment scaling exponent	-
t_B	Batch time	h
t_C	Corrosion allowance	m
t_D	Depreciation time	y
t_P	Plant running time	h y^{-1}
t_s	Pressure vessel shell wall thickness	m
t_h	Pressure vessel head wall thickness	m
T	Temperature	K
v_s	Superficial gas velocity	m s^{-1}
V	Volume	m^3
W	Work	kW
Greek letters		
ρ_L	Density of liquid	kg m^{-3}
ρ_m	Density of metal	kg m^{-3}
κ	Compression factor	-
φ	Packing density, membrane module	-
η	Efficiency	-

A.2 Detailed description of technologies and assumptions

A.2.1 Reactor dimensions

Bioreactors are typically not filled to their maximum capacity due to the volume increase upon aeration and the risk of foam formation. Therefore, a filling level of 80% of the total reactor volume is assumed for all supply methods, although it can be argued that a reduced head-space can be tolerated for methods not employing direct bubbling of the reaction medium. The reactor is assumed to have an aspects ratio (H/T, height to tank diameter) of 3. The 100 m^3 reactor is stirred by three Rushton turbines (D/T = 0.3, impeller diameter to tank diameter) when mixing is required, while the 10 m^3 reactor is stirred by two Rushton turbines. Rushton turbines might not be the ideal choice for oxygen transfer, but the characteristics in terms of expected mass transfer coefficient and flooding characteristics are well known [1], and for this analysis, the improvement of choosing another impeller would be minimal compared to the uncertainties assumed.

A.2.2 Stirred tank reactor

Oxygen mass transfer in a stirred tank reactor (STR) is typically predicted using empirical correlations relating the volumetric mass transfer coefficient (k_La) to the power input per unit volume (P/V), the superficial gas velocity (v_S), and the viscosity of the medium [2]. A correlation developed by Van't Riet (1979) for fermentation volumes up to 2.6 m^3 was applied in the simulations. The power input was taken as the combined power input from aeration and mechanical agitation, since power input from aeration is significant at large scale [3]. The superficial gas velocity was taken in the top and bottom of the reactor to calculate the k_La at the given conditions based on which an overall k_La for the reactor was calculated by calculating the logarithmic mean. This was done to allow for the change in gas volume through the reactor as oxygen is consumed and the remaining gas expands. The driving force for oxygen transfer was calculated as the logarithmic mean of the driving force in the inlet and outlet.

In general, there are two degrees of freedom when operating a STR – the stirring speed and the aeration rate. The conditions resulting in the lowest total cost of oxygen transfer were found by a nonlinear constrained optimization routine, minimizing the total cost of oxygen transfer by changing the total power input and the aeration rate. The minimization was constrained to a total power input of 0-5 kW m^{-3} and an aeration rate of 0-2 vvm. Furthermore, the minimization was constrained by the flooding-loading conditions for a Rushton turbine to avoid flooding of the bottom impeller to ensure the validity of the k_La correlation [1]. By applying these constrains, the maximum k_La for the large reactor (100 m^3) was 1203 h^{-1} at 5 kW m^{-3} and 0.91 vvm, while the maximum for the small reactor (10 m^3) was 1138 h^{-1} at 5 kW m^{-3} and 2 vvm.

The cost of the reactor vessel is calculated based on the total weight of the reactor constructed in stainless steel [4]. Thereby the effect of increased pressure on the cost can be incorporated. For enriched air applications, the cost of pure oxygen will be a major cost contributor. The cost of pure oxygen is determined by the volume required, the purity of the oxygen, and the

cost of electricity. For simplicity the cost of oxygen is assumed to be 80 USD MT^{-1} delivered on-site with a purity of 95%, which is in line with the typical cost of oxygen [5,6]. No additional capital costs for handling and storing pure oxygen were taken into account in the analysis.

A.2.3 Membrane aeration

Submerged and external membrane aeration were considered in the analysis. Both systems rely on hollow fiber modules, since these are well suited for membrane contacting due to the limited pressure drop and high specific surface area. The membranes can be made of porous or dense materials such as polypropylene, polyethylene or polymethylsiloxane. The membrane introduces an additional barrier for oxygen transfer, which together with the liquid film layer resistance makes up the overall resistance to oxygen transfer. The overall resistance (i.e. the inverse of the mass transfer coefficient) can be estimated by combining the liquid film resistance, calculated from empirical correlations of the Sherwood number at given hydraulic diameter and linear velocity, and the membrane resistance. The linear velocity in a hollow fiber bundle submerged in a stirred reactor will change dependent on location in the reactor and it is difficult to estimate without the use of computational fluid dynamics [7]. For the external membrane module configuration the linear velocity can be freely chosen through the design of the module, in practice the optimal velocity will depend on the increase in pressure drop across the module and reduction in mass transfer coefficient upon further increase in velocity. Therefore, the overall mass transfer coefficient was assumed to be 0.2 mol h^{-1} bar^{-1} m^{-2}, independently of the stirring rate of the reactor (in the case of a submerged module) and the membrane module configuration (in the case of an external module). This value is similar to mass transfer coefficients reported for both porous and dense membranes [8,9].

Membrane fouling is an often encountered problem for membrane separations, which greatly reduces the mass transfer coefficient across the membrane. However, for membrane aeration fouling is not considered a problem, primarily because no solute is transferred from the liquid stream and therefore no concentration polarization happens [10]. Voss et al. (1999) showed that membrane aeration could function in a wastewater treatment plant for several hundred days without cleaning and without significant performance decrease. In case cleaning is needed when applying membrane aeration in a bioreactor, it is assumed the costs are low compared to other costs and can be covered by the general maintenance expenses.

Another important parameter for membrane aeration is the cross membrane pressure at which bubbles start to form on the liquid side of the membrane due to saturation of liquid at the membrane surface. The formation of bubbles cause a decrease in oxygen transfer rate and for gas-liquid interface sensitive enzymes, they might increase deactivation rate. Bubble formation depends on the type of membrane and the resistance across it, typically the bubble point for porous membranes are below one bar, while it for dense non-porous membranes can be up to four bars, and for composite membranes is as high as seven bars [11,12]. Hence, a maximum cross-membrane pressure of four bars was assumed for the analysis.

For the submerged membrane configuration, the packing density of the hollow fibers in the reactor determine the limit for the oxygen transfer rate. An outer fiber diameter of 1 mm and distance between fibers of 1.5 mm was assumed. This corresponds to a module packing density of 0.29. Additionally, it was assumed that the membrane module cannot occupy more than 25% of reactor volume and that 75% of the reactor height can be used for exposing membrane fibers. Overall, this corresponds to a maximum specific membrane area in the reactor of 272 m^2/m^3.

For the external membrane configuration, the oxygen transfer rate will be directly proportional to the circulation rate of reaction media through the membrane module. The cost of pumping the liquid is determined by the pressure drop in the circulation loop. The pressure drop across the membrane module itself was found to be insignificant due to the limited linear velocity and length of module required to saturate the liquid to the desired degree. However, because of the high recirculation rates required a significant pressure drop can be assumed due to friction in pipes and fluid distributors. A pressure drop of three bars was assumed in the analysis.

The fraction of oxygen transferred from the gas to the liquid and membrane pressure are design parameter which are important for the cost of oxygen transfer. Additionally for the external configuration, the dissolved oxygen concentration leaving the module can be varied to minimize the cost. The set of design parameters resulting in the lowest total oxygen transfer cost were found using a non-linear minimization routine constrained by the physical boundaries and the maximum four bar cross-membrane pressure. Furthermore, external membrane aeration was constrained by a maximum recirculation rate of 10 reactor volumes per hour. For both membrane configurations, the technology were evaluated at increased reactor pressures and when applying enriched air to increase the driving force across the membrane.

A.2.4 Hydrogen peroxide degradation

in situ generation of oxygen via hydrogen peroxide degradation using catalase reduce the capital costs, since air compression and intensive stirring is avoided. However, an additional operating expense is introduced due to the need for hydrogen peroxide and catalase. As for other chemicals, the cost of hydrogen peroxide is highly dependent on the amount required and the location of delivery. Ciriminna et al. (2016) recently reported the cost of hydrogen peroxide to 700-1200 USD MT^{-1} on a 100% (w/w) basis, a base-case cost of 950 USD MT^{-1} was assumed for the analysis. Catalase is an enzyme produced in bulk-quantities for which the cost typically lies in the range of 250-1000 USD MT^{-1} crude protein [13], a base-case cost of 625 USD MT^{-1} was assumed.

A potential short coming of the technology is the oxidizing nature of hydrogen peroxide, that may damage catalase and the oxygen requiring biocatalyst(s) present in the reaction medium [14,15]. It is therefore highly important to keep the concentration of hydrogen peroxide below a critical limit at which enzyme deactivation can be avoided. The critical limit together with the kinetics of the enzyme determines the concentration of catalase required.

Furthermore, mixing becomes important as scale increase to mix the concentrated hydrogen peroxide feed into the bulk liquid to avoid regions of the reactor with high hydrogen peroxide concentrations. For the analysis, it was assumed that a power input of 0.5 kW m^{-3} was sufficient to ensure efficient mixing.

Hydrogen peroxide is potentially explosive at high concentrations. Safe handling of hydrogen peroxide solutions up to 70 % (w/w) is possible, as solutions below 70% (w/w) do not contain enough energy to vaporize water and therefore cause a steam explosion. The cost of hydrogen peroxide storage and safe handling was not included in the cost analysis. The water added with the hydrogen peroxide takes up capacity in the reactor in the analysis this was compensated for by increasing the reactor size appropriately.

A.2.5 Other assumptions

A number of values essential for scaling and costing of the oxygen supply methods, and not taken into account in the Monte Carlo simulations, were assumed values obtained in literature or by expert knowledge. The most important of these have been mentioned in the sections above. All parameter values not included in the Monte Carlo simulations are listed in Table A.1.

Table A.1. Parameters required for calculations but not varied in Monte Carlo simulations.

Parameter	Value	Units	Reference
General parameters			
Reactor fill	80%	-	*Estimation*
Liquid density, ρ_L	1000	kg m^{-3}	
Henry's constant, oxygen	1.3	mol m^{-3} bar^{-1}	NIST
Oxygen content, pure oxygen	95%	-	[6]
Capital cost estimation			
Depreciation time, t_d	15	Y	[13]
Batch time, t_b	16	H	*Estimation*
Plant running time, t_p	5840	h/y	
Interest rate, IR	7%	-	[13]
Lang factor	5	-	[4]
Maintenance	5% of FCC		[4]
Fixed OPEX	15% of FCC		[4]
Labor cost	32	USD/h	[16]
Labor requirement ($10m^3/100m^3$)	0.5/1	Workers/reactor	*Estimation*
Pressure vessel			

Joint efficiency, E_j	0.85	-	[4]
Maximum allowable working stress, S_S	79300	kPa	[4]
Corrosion allowance, t_c	3.8	Mm	[4]
Density, SS316	7833	kg m^{-3}	[4]
Aerated stirred tank reactor			
Impeller to tank diameter ratio, D/T	0.3	-	[17]
Number of impellers	3		*Estimated*
Impeller power number, P_o	5.6	-	[1]
Gassed to ungassed power number, P_g/P_o	0.5	-	[18]
Membrane aeration			
Fiber diameter, D_f	10^{-3}	M	[19]
Fiber distance, fraction of D_f, D_{bf}	1.5	-	*Estimation*
Fiber length, fraction of reactor length, F_{fe}	0.75	-	*Estimation*
Hydrogen peroxide degradation			
H_2O_2 concentration, feed	70	% (w/w)	[20]
Catalase k_{cat}	$7 \cdot 10^5$	s^{-1}	[21]
Catalase K_M	43.6	mol m^{-3}	[21]
Catalase M_w	230	kg mol^{-1}	[21]

A.3 Cost estimation and scaling of equipment

The cost of individual equipment parts were estimated using generally accepted methods [4,22]. The cost of individual equipment was calculated from values reported in the scientific literature (Table A.2), which was scaled according to equipment size and updated to current price levels using the Chemical Engineering Plant Cost Index (Eq. S1, Table 4). The only exceptions being the fermenter, which was scaled using the methods described in section S3.1.1, and membrane cost which was scaled linearly.

$$C = C_0 \left(\frac{S}{S_0}\right)^{SF} \left(\frac{CI_{cur}}{CI_{ref}}\right) \quad \text{Eq. S1}$$

In general, prices were obtained in U.S. dollars, but whenever conversion from Euro was required a conversion factor of 0.94 EUR/USD was used.

Table A.2. Equipment base cost, base size, cost year and scaling factor.

Equipment	Size	Base cost (USD)	Cost year	Scaling exp.	Reference
Fermenter, Large	303 m^3	400500	2009	-	[23]
Fermenter, Small	30.3 m^3	95400	2009	-	[23]
Agitator, Large	600 kW	580000	2009	0.7	[23]
Agitator, Small	60 kW	63000	2009	0.7	[23]
Compressor	100 kW	69000	2002	0.67	[4]
Pump, Large	$2 \cdot 10^4$ gpm · psi	1500	1968	0.64	[22]
Pump, Small	$2 \cdot 10^3$ gpm · psi	650	1968	0.36	[22]

Table A.3 lists the Chemical Engineering Plant Cost Indices used in the costing of equipment.

Table A.3. Chemical Engineering Plant Cost Index for years used in cost estimation.

Year	CI
1968	115
2002	395.6
2009	521.9
2015	556.8

The capital cost are converted into an hourly cost using an annuity factor (AF, Eq. S2) and the plant running time per year, t_p, as shown in Eq. S3 [13].

$$AF = \frac{IR}{(1-(1+IR)^{-t_D}} \quad \text{Eq. S2}$$

$$C_{SC} = \frac{C_C AF}{t_p} \quad \text{Eq. S3}$$

A.3.1 Equipment scaling

Reactor vessel

Good cost correlations for pressurized fermentation vessels are not available in the scientific literature. The cost of the fermenter was therefore calculated from weight based cost correlation as described in Peters et al. (2003) for pressure vessel and applied by [24] (Eq. S4).

$$C = C_I \, m_v^{-0.34} \qquad \text{Eq. S4}$$

Where C is a unit cost in dollars per kg, m_v is the total mass of the pressure vessel, and C_I is a parameter calculated from existing data. For the current case, C_I is calculated from the bioreactor costs given in Table 3, with the weight of these calculated using the design procedure described below. For the 125 m^3 (100 m^3 liquid volume) bioreactor, CI was calculated to 311 USD kg^{-1}, while it for the 12.5 m3 bioreactor was calculated to 287 USD kg^{-1}.

The minimum wall thickness, t, for the cylindrical shell and torispherical heads is calculated from Eq. S5-S6 using a maximum allowable working stress, S_s, for Stainless Steel 316 of 79,300 kPa, a joint efficiency, E_j, of 0.85, and corrosion allowance, t_c, of 3.8 mm [4]. The design pressure of the vessel is taken as the sum of the hydrostatic pressure in the bottom of the fermenter, the headspace pressure and 2.5 bar safety margin. Based on the wall thickness, the weight of the vessel can be calculated using Eq. S7-S8 and the density of stainless steel 316 of 7833 kg/m^3.

$$t_s = \frac{p \, \frac{1}{2} D_T}{S_s \, E_j - 0.6 \, p} + t_c \qquad \text{Eq. S5}$$

$$t_h = \frac{0.885 \, p \, \frac{1}{2} D_T}{S_s \, E_j - 0.1 \, p} + t_c \qquad \text{Eq. S6}$$

$$m_s = \rho_m \, \pi \, OD \, H \, t_s \qquad \text{Eq. S7}$$

$$m_h = \rho_m \frac{\pi \left(D_T + \frac{D_T}{24} + 2t_h \right)^2 t_h}{4} \qquad \text{Eq. S8}$$

Agitation and aeration for bubble aeration in stirred tanks

The oxygen transfer rate in stirred tanks is typically modelled assuming that all resistance towards gas transfer lies in the liquid film layer. In other words, the oxygen transfer rate is a function of the mass transfer coefficient, k_L, the interfacial area available for mass transfer, a, and the difference between the oxygen concentration at the gas-liquid interface (i.e. the saturation concentration at the given conditions), C_{O2}^{sat}, and the dissolved oxygen concentration in the bulk liquid, C_{O2}. The interfacial area is difficult to determine for gas-liquid mixing, therefore the mass transfer coefficient and the interfacial area is taken as one, the volumetric mass transfer coefficient, k_La.

$$OTR = k_L a \, (c_{O2}^{sat} - c_{O2}) \qquad \text{Eq. S9}$$

Typically, k_La is predicted from empirical correlations of the power input per unit volume, P/V, the superficial gas velocity, v_s, and the viscosity of the medium [2]. Since most biocatalytic oxidations are conducted in media with a viscosity close to that water, a correlation developed by Van't Riet (1979) for non-viscous media was applied to predict k_La at both scales investigated. Although one should be careful when applying such correlations in reactor geometries different from where it is developed. The applied correlation are originally developed for a 2.6 m^3 reactor.

$$k_La = 2.6 \cdot 10^{-2}(P/V)^{0.4}v_s^{0.5}\ [s^{-1}] \qquad \text{Eq. S10}$$

The superficial gas velocity was calculated from the cross-sectional area of the bioreactor and the volumetric gas flow rate. Hence, the superficial gas velocity will vary with hydrostatic pressure up through the water column. Furthermore, oxygen is consumed by the biocatalytic reaction, whereby the total molar flow decreases through the reactor, assuming that the gas phase is not well mixed. This is especially important for pure oxygen sparging, where the consumption of oxygen results in a proportional reduction in gas volume, since no or very little nitrogen is diluting the gas. To accommodate for this phenomena, k_La was calculated at the bottom and the top of the reactor, and an overall k_La was calculated as the logarithmic mean of the two values. Similarly, a logarithmic mean was used to accommodate the changing driving force as oxygen is consumed.

The optimization to find the minimum cost at a given oxygen transfer rate is constrained to avoid flooding of the bottom impeller, as this greatly reduces the power draw and the validity of the k_La correlation [1]. Flooding of turbines occurs when the gas flow number, Fl_G, of the turbine (which is proportional to the ratio of the air flow rate from the sparger to the pumping capacity of the agitator) is greater than a critical value, $(Fl_G)_F$. For a Rushton turbine the critical value is given by Eq. S11 [1].

$$(Fl_G)_F = 30(D/T)^{3.5}(Fr)_F \qquad \text{Eq. S11}$$

The Froude number, Fr, describes the ratio of inertial to buoyancy forces, and is given by Eq. S12. The gas flow number is given by Eq. S13 [1].

$$Fr = \frac{N^2D}{g} \qquad \text{Eq. S12}$$

$$Fl_G = \frac{Q_g}{ND^3} \qquad \text{Eq. S13}$$

For a given impeller diameter, D, these equations can be used to calculate a minimum stirring speed, N, to avoid flooding at a gas flow rate, Q_g. The stirring speed relates to the power drawn by the agitator via Eq. S14.

$$P = \rho_L N^3 D^5 P_O\left(P_g/P\right) \qquad \text{Eq. S14}$$

The power number, P_O, for a Rushton turbine in turbulent conditions can safely be assumed to be 5.6 [1]. An impeller pumping a gas-liquid dispersion draws less power than an impeller pumping only liquid. This phenomenon is described by the ungassed to gassed power draw ratio, P_g/P, which changes with the rate of aeration. However, for typical aeration rates the

ratio is approximately 0.5 [18]. It is furthermore assumed that the 2-3 Rushton turbines is fully independent of each other.

Aeration in membrane systems

In many aspects membrane aeration is similar to bubble aeration in stirred tanks, with the difference that the gas-liquid interface is created by a membrane instead of by mechanical mixing of gas and liquid. The calculation of oxygen transfer rate is therefore also analogues to the method described above for stirred tank aeration. The following analysis is adapted from the well explained analysis of membrane aeration by Côté et al. (1988).

The oxygen transfer rate from the gas phase, through the membrane, to the liquid phase is described by Eq S15. Where the main difference from the stirred tank reactor is that the area available for oxygen transfer is known and that the mass transfer coefficient, K_L, describes not only the liquid film resistance to oxygen transfer but also the resistance in the membrane.

$$OTR = K_L\, a\, \Delta p_{O2} \qquad \text{Eq. S15}$$

The driving force for oxygen transfer is the difference in partial pressure of oxygen, Δp_{O2}, which changes along the membrane module. For the submerged membrane module the partial pressure in the bulk liquid is constant along the module, while the partial pressure in the membrane fibers change from the entrance to the exit (Eq. S16).

$$(\Delta p_{O2})_{SM} = \frac{p_{O2}^{in} - p_{O2}^{out}}{\ln\left(\frac{p_{O2}^{in} - p_{O2}^{bulk}}{p_{O2}^{out} - p_{O2}^{bulk}}\right)} = \frac{p_{O2}^{in} - (1-F)\, p_{O2}^{in}}{\ln\left(\frac{p_{O2}^{in} - k_H\, c_{O2}^{bulk}}{(1-F)\, p_{O2}^{in} - k_H\, c_{O2}^{bulk}}\right)} \qquad \text{Eq. S16}$$

$$(\Delta p_{O2})_{EM} = \frac{(p_{O2}^{in} - p_{O2}^{in,l}) - (p_{O2}^{out} - p_{O2}^{out,l})}{\ln\left(\frac{p_{O2}^{in} - p_{O2}^{in,l}}{p_{O2}^{out} - p_{O2}^{out,l}}\right)} \qquad \text{Eq. S17}$$

$$= \frac{(p_{O2}^{in} - k_H\, c_{O2}^{bulk}) - ((1-F)p_{O2}^{in} - F_{sat} y_{O2} P_m)}{\ln\left(\frac{p_{O2}^{in} - F_{sat} y_{O2} P_m}{(1-F)p_{O2}^{in} - k_H\, c_{O2}^{bulk}}\right)}$$

From the above equations, it is clear that two degrees of freedom exist for a submerged membrane reactor, namely the fraction of oxygen transferred from the gas, F, and the membrane pressure, P_m. For the external membrane configuration, an additional degree of freedom is available, namely the degree of saturation in the liquid outlet from the membrane module, F_{sat}, which determines the circulation rate required to supply a given amount of oxygen.

The submerged membrane configuration is limited by the membrane area that physically can fit into the reactor. In this case, the limit was set based on a maximum fraction of the reactor footprint that can be taken up by membrane module. The membrane module being a bundle of hollow fibers, with each fiber having a diameter, D_f, and a distance to all neighboring fibers of, $D_{bf} \cdot D_f$. The packing density of the membrane module, φ, is given by Eq. S18.

$$\phi = \frac{\pi}{\sqrt{3}\left(1 + D_{bf}\right)^2} \quad \text{Eq. S18}$$

The required fiber length, L_f, is calculated from the fiber diameter and the required membrane area calculated from Eq. S15-S17. The total number of fibers, N_f, required is calculated from the tank height, H, and the fraction of the tank height that can be used to expose fibers, F_{fe}.

$$N_f = \frac{L_f}{H\, F_{fe}} \quad \text{Eq. S19}$$

The membrane module footprint can then be calculated using Eq. S20.

$$A_{mf} = \frac{\pi N_f D_f^2}{4\phi} \quad \text{Eq. S20}$$

Hydrogen peroxide degradation

Scheme 2 shows the degradation reaction of hydrogen peroxide.

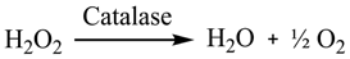

Scheme 2. Degradation of hydrogen peroxide by catalase

The kinetics of the hydrogen peroxide degradation typically follows Michaelis-Menten enzyme kinetics [21]. Therefore, Eq. S21 gives the rate of hydrogen peroxide degradation, and therefrom the rate of oxygen production. The concentration of hydrogen peroxide used, is the maximum concentration tolerated by the biocatalyst, $c_{H_2O_2}^{max}$.

$$r_{H_2O_2} = 2r_{O_2} = \frac{k_{cat} c_{cat} c_{H_2O_2}^{max}}{K_M + c_{H_2O_2}^{max}} \quad \text{Eq. S21}$$

Pure hydrogen peroxide cannot be handled safely at industrial scale. Therefore, an aqueous solution is fed to the reactor. The water fed with the hydrogen peroxide takes up space and therefore a larger reactor is required. The increase in liquid volume is calculated from Eq. S22.

$$\Delta V = \left(1 - m_{H2O2}^{feed}\right) \frac{r_{H_2O_2} M_{H_2O_2}}{m_{H2O2}^{feed}\, \rho_L\, t_b} \quad \text{Eq. S22}$$

Agitator

The agitation power is calculated as the difference between the total power required to meet a given oxygen transfer rate and the power input from aeration. The aeration gas dissipates power to the liquid media as the compressed gas expands as it travels up through the water column. The power input from aeration is therefore highly dependent on the scale of operation, at small scale the power input from aeration is insignificant while at large scales it cannot be ignored as it is a significant portion of the total power input [3]. Eq. S23 and S24 determines the power input from aeration.

$$\left(\frac{P}{V}\right)_g = F_g\ R\ T \log\left(1 + \frac{p_{hy}}{p_{hs}}\right) \quad \text{Eq. S23}$$

$$p_{hy} = \rho_l\ g\ H\ f \quad \text{Eq. S24}$$

The power consumption of the motor used for agitation is given from the energy efficiency of the gear and motor, η_{agi}.

$$W_{agi} = \frac{\left(\frac{P}{V}\right)_{agi}}{\eta_{agi}} \quad \text{Eq. S25}$$

Compressor

The compressor power requirement is calculated based on the increase in pressure and air flow rate using the equation for adiabatic compression (Eq. S26) and an adiabatic efficiency, η_{comp}.

$$W_{comp} = \frac{R\ T_1 F_g}{\eta_{comp}} \frac{\kappa_{air}}{\kappa_{air} - 1}\left(\left(\frac{p_2}{p_1}\right)^{\frac{\kappa_{air}-1}{\kappa_{air}}} - 1\right) \quad \text{Eq. S26}$$

Where the compressibility factor for air, κ_{air}, is 1.4 [4], and the inlet pressure, p_1, is 1 atm.

Pump

The power required to pump liquid is calculated based on the pressure increase required (or the pump lifting height) and the volume of liquid being pumped (Eq. S27).

$$W_{pump} = \frac{\Delta p\ Q_l}{\eta_{pump}} \quad \text{Eq. S27}$$

A.4 Capital and operational cost distribution

This section compares the distribution of costs for the investigated oxygen supply methods using the base case parameter values. The distribution will change with the desired oxygen transfer rate, i.e. at high rates the influence of capital costs are lower than at low rates. The technologies are therefore compared at constant oxygen supply rate of 50 mol m^{-3} h^{-1}, which all technologies can deliver. The technologies are compared at the 100 m^3 scale, for 10 m^3 the distribution of cost are comparable although the capital costs are more important due to economy of scale.

A.4.1 Stirred tank reactor

Figure A.1-A.3 shows the cost distribution for the a bubble aeration stirred tank applying air at atmospheric headspace pressure, applying pure oxygen at atmospheric headspace pressure, and applying air at a headspace pressure of 10 bar, respectively. In each case, the optimization routine used throughout the paper has been used to optimize the power input and aeration rate to obtain the lowest total cost of oxygen transfer at the given conditions.

In general, the largest part of the cost can be associated with the cost of the bioreactor and the cost of labor. When pure oxygen is applied for aeration the capital costs decrease since air compression is obviated, because the pure oxygen is assumed to be delivered on-site already pressurized. On the other hand, the cost of pure oxygen adds to the operating costs. For pressurized operation, the reactor costs increase due to the increased material use to be able to withstand the increased pressure. Furthermore, both operating and capital costs for compression increase because the air needs to be compressed to the higher pressure of the bioreactor. Agitation requirements decrease due to the higher driving force for oxygen transfer, which means that a smaller volumetric oxygen transfer coefficient is necessary to obtain the desired oxygen transfer rate. This translates into a lower power input and/or superficial gas velocity.

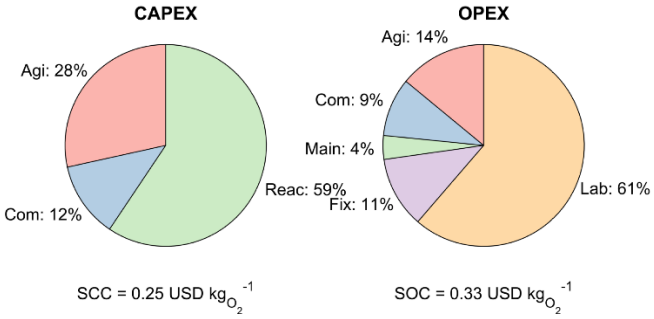

Figure A.1. Cost distribution for stirred tank aeration at an oxygen transfer rate of 50 mol m^{-3} h^{-1}.

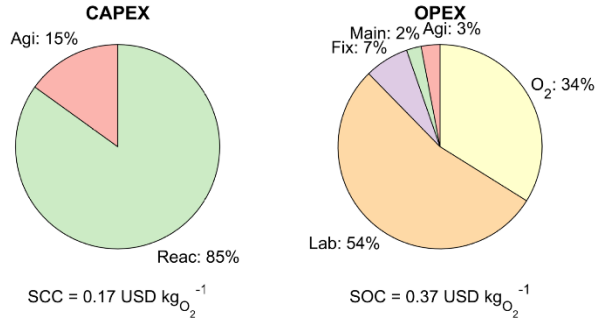

Figure A.2. Cost distribution for stirred tank aeration using pure oxygen at an oxygen transfer rate of 50 mol m^{-3} h^{-1}.

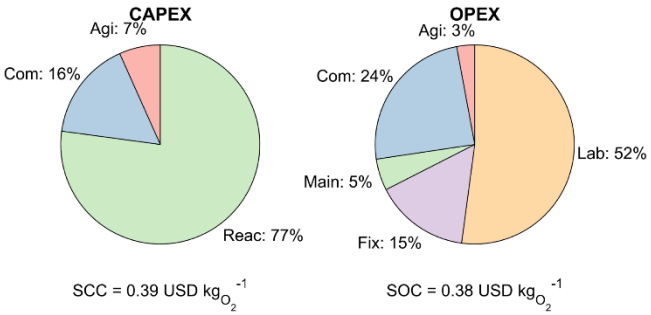

Figure A.3. Cost distribution for stirred tank aeration pressurized to 10 bar at an oxygen transfer rate of 50 mol m^{-3} h^{-1}.

A.4.2 Submerged membrane reactor

Figure A.4-A.6 shows the cost distribution for a submerged membrane reactor operated at atmospheric reactor headspace pressure applying air, at atmospheric headspace pressure applying pure oxygen, and at 25 bar headspace pressure applying pure oxygen, respectively. In each case, the optimization routine is used to minimize the total cost of oxygen supply by changing the cross-membrane pressure and the fraction of oxygen being transferred from the gas coming into the membrane module.

The biggest cost for submerged membrane aeration is the cost of membrane. The required membrane area can be reduced by applying pure oxygen for aeration. However, only by applying headspace reactor pressure the membrane cost can be brought down to levels where other costs such as reactor cost and cost of oxygen starts to be influential.

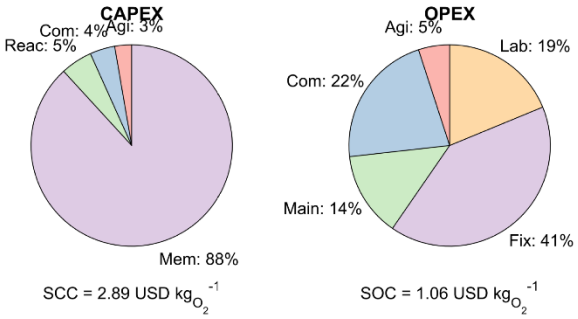

Figure A.4. Cost distribution for submerged membrane aeration at an oxygen transfer rate of 50 mol m^{-3} h^{-1}.

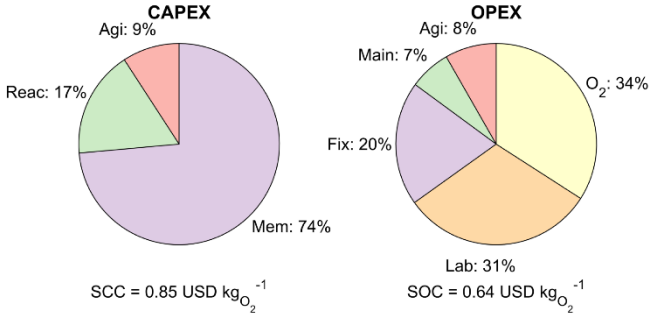

Figure A.5. Cost distribution for submerged membrane aeration using pure oxygen at an oxygen transfer rate of 50 mol m^{-3} h^{-1}.

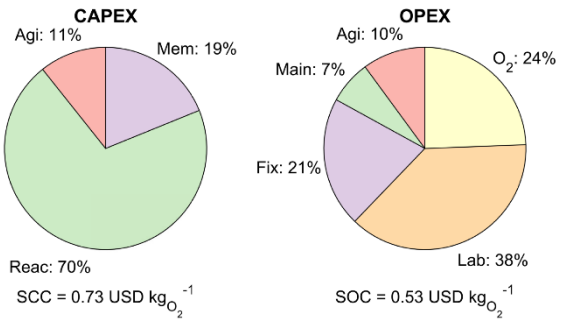

Figure A.6. Cost distribution for submerged membrane aeration with reactor pressurized to 25 bar and using pure oxygen at an oxygen transfer rate of 50 mol m^{-3} h^{-1}.

A.4.3 External membrane reactor

Figure A.7-A.9 shows the cost distribution for an external membrane reactor operated at atmospheric reactor headspace pressure applying air, at atmospheric headspace pressure applying pure oxygen, and at 25 bar headspace pressure applying pure oxygen, respectively. In each case, the optimization routine is used to minimize the total cost of oxygen supply by changing the cross-membrane pressure, the fraction of oxygen being transferred from the gas coming into the membrane module, and the saturation level of the reaction media leaving the membrane module.

As for submerged membrane aeration, the membrane is contributing the most to the overall cost of an unpressurized reactor system using air for aeration, although the cost of pumping the liquid through the external membrane module also adds significantly to the overall cost. When pure oxygen is applied to increase the driving force for oxygen transfer across the membrane, the overall cost is reduced, although the cost of membrane and electricity cost for circulation still is the two major costs. When the headspace pressure is increased to 25 bar, both the cost of membrane and the cost of pumping is reduced dramatically. The required membrane area is decreased due to the increased driving force, and the pumping rate is reduced because the media can contain more oxygen due to the increased pressure. At this operating condition, the pressurized bioreactor is the most important cost contributor.

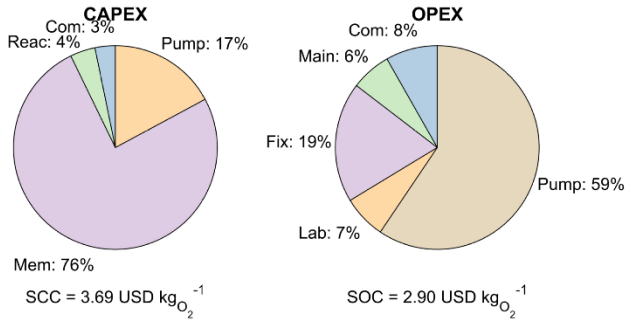

Figure A.7. Cost distribution for external membrane aeration at an oxygen transfer rate of 50 mol m^{-3} h^{-1}.

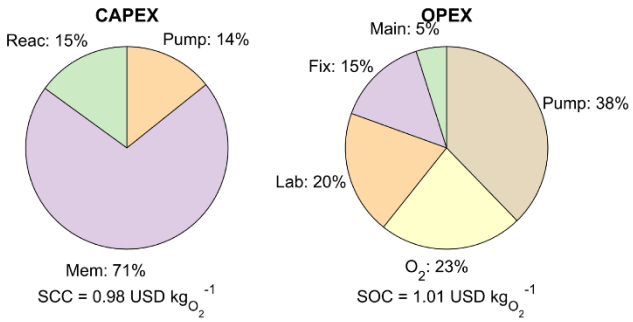

Figure A.8. Cost distribution for external membrane aeration using pure oxygen at an oxygen transfer rate of 50 mol m^{-3} h^{-1}.

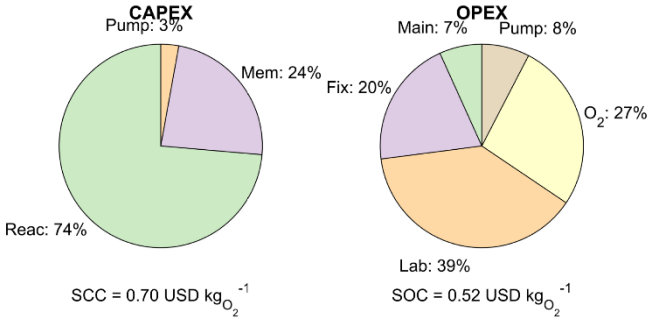

Figure A.9. Cost distribution for external membrane aeration with reactor pressurized to 25 bar using pure oxygen at an oxygen transfer rate of 50 mol m^{-3} h^{-1}.

A.4.4 Hydrogen peroxide decomposition by catalase

The cost of oxygen supply via hydrogen peroxide decomposition by catalase is driven solely by the cost of hydrogen peroxide, which accounts for 74% of the total cost of oxygen supply (Figure A.10). The capital cost constitutes only a minor part of the total cost, since the reactor is unpressurized and only modest agitation is required. The cost of catalase required to break down the added hydrogen peroxide accounts for 6% of the total cost for supply oxygen.

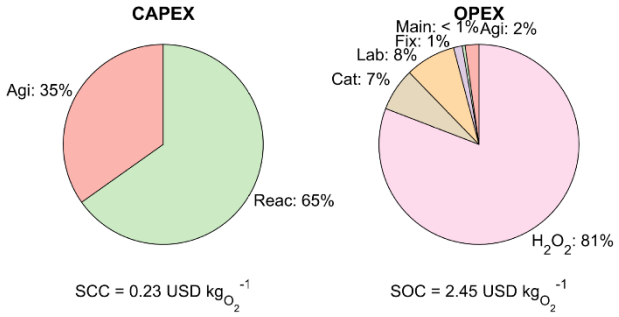

Figure A.10. Cost distribution for *in situ* oxygen generation via hydrogen peroxide degradation at an oxygen transfer rate of 50 mol m^{-3} h^{-1}.

A.5 Cost of oxygen supply and operating condition

This section gives an overview of the total cost of oxygen supply for the investigated technologies as a function of oxygen supply rate and operating conditions. Additionally, the cost is broken down into capital and operating costs. The costs are only presented for the 100 m^3 reactor, although the optimization of pressure is shown for both the 10 m^3 and 100 m^3 scale.

The costs presented are a result of the optimization routine given the input parameters from the Monte Carlo simulation.

A.5.1 Stirred tank reactor

The effects of pressure and mole fraction of oxygen in the sparging air on the cost of oxygen transfer was investigated at three different oxygen transfer rates (Figure A.11-A.15).

Effect of pressure

In general, the effect of applying head-space pressure on the cost of oxygen transfer is small. At large oxygen transfer rates a slight overpressure result in a marginally smaller cost of

oxygen transfer, while it at low oxygen transfer rates results in a higher cost. This is also seen from Figure A.13, which shows the optimal pressure as a function of oxygen transfer rate at 10 m^3 and 100 m^3 scale.

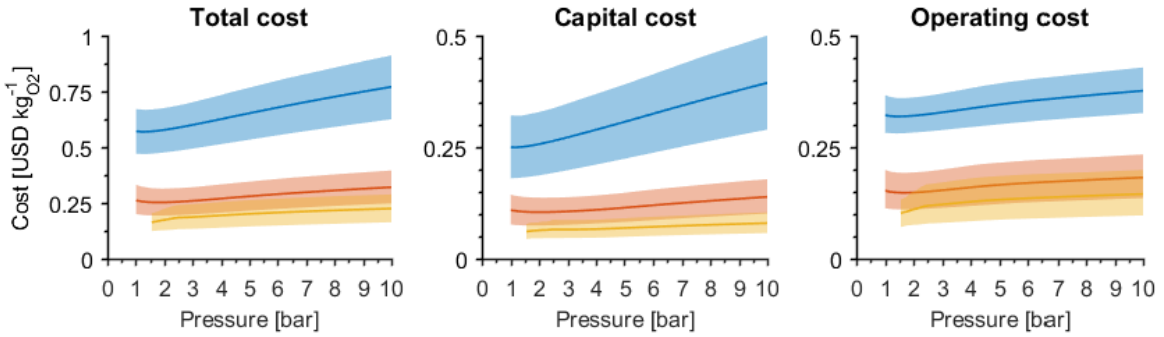

Figure A.11. Effect of pressure on the cost of oxygen transfer for stirred tank aeration at an oxygen transfer rate of 50 mol m^{-3} h^{-1} (blue), 200 mol m^{-3} h^{-1} (red) and 500 mol m^{-3} h^{-1} (yellow) in 100 m^3 reactor. The dashed area represents 95% confidence intervals.

Figure A.12 shows the effect of pressure on the required power input and aeration rate. As expected, both decrease at increasing headspace pressure due to the larger driving force for oxygen transfer.

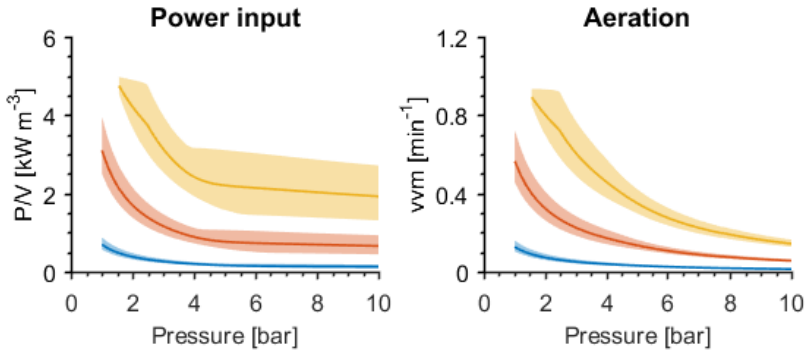

Figure A.12. Optimized operational parameters for stirred tank aeration as a function of reactor headspace pressure at an oxygen transfer rate of 50 mol m^{-3} h^{-1} (blue), 200 mol m^{-3} h^{-1} (red) and 500 mol m^{-3} h^{-1} (yellow) in 100 m^3 reactor. The dashed area represents 95% confidence intervals.

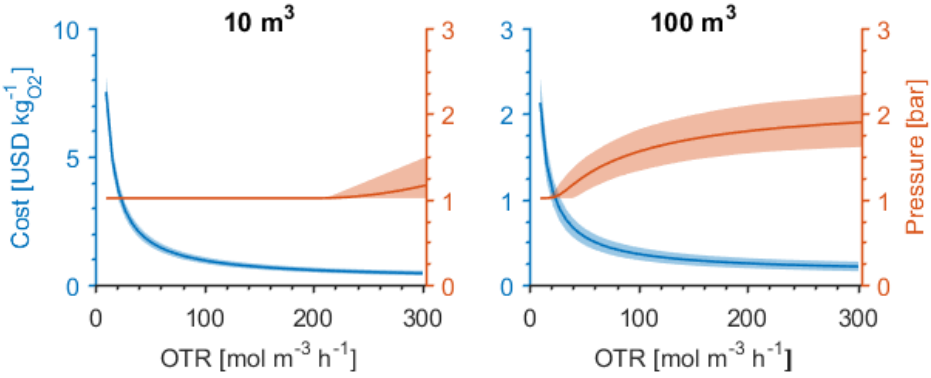

Figure A.13. Optimal pressure and corresponding cost of oxygen transfer at both 10 m^3 and 100 m^3 scale.

Effect of enriched air

Enriched air aeration in general do not affect the cost of oxygen transfer (Figure A.14). As the amount of oxygen in the inlet air increase, the capital cost decrease becuase a lower power input and aeration rate is required (Figure A.15). Overall, there is no real economic benefit of using enriched air, although there possible can be a slight advantage if using pure oxygen, especially if this can be sourced at a price in the lower end of the range assumed in this study.

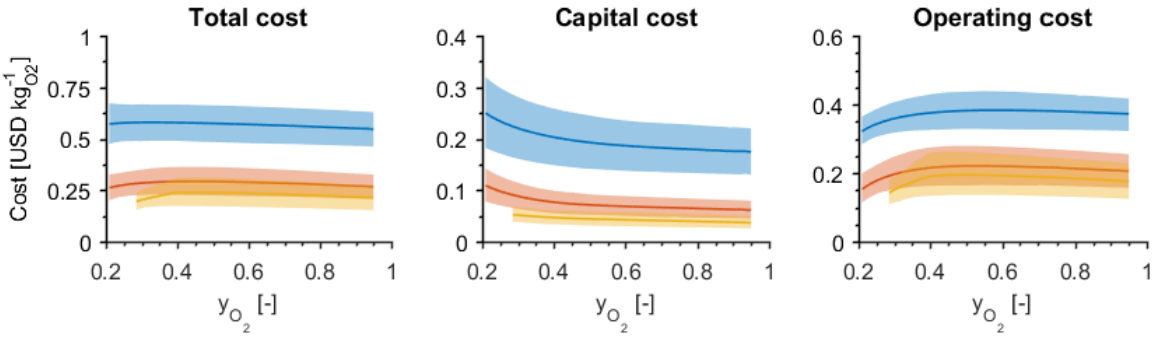

Figure A.14. Effect of oxygen content in gas on the cost of oxygen transfer for stirred tank aeration at an oxygen transfer rate of 50 mol m^{-3} h^{-1} (blue), 200 mol m^{-3} h^{-1} (red) and 500 mol m^{-3} h^{-1} (yellow) in 100 m^3 reactor. The dashed area represents 95% confidence intervals.

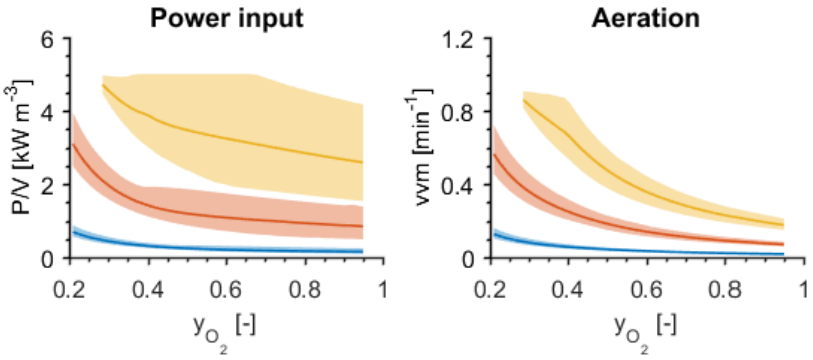

Figure A.15. Optimized operational parameters for stirred tank aeration as a function of oxygen content in sparging gas at an oxygen transfer rate of 50 mol m^{-3} h^{-1} (blue), 200 mol m^{-3} h^{-1} (red) and 500 mol m^{-3} h^{-1} (yellow).

A.5.2 Submerged membrane reactor

Figure S70-S18 shows the effect of pressure on the price of oxygen transfer when using submerged membrane aeration and pure oxygen. The effect of enriched air was not studied in detail, because it was found that it was an absolute necessity to bring the cost of oxygen transfer down, and that there was no benefit of operating with partially enriched air.

In general, there are large benefits from increasing the reactor pressure, as this decrease the membrane area required. The optimum pressure increases with increasing oxygen transfer rate (Figure A.16). This is also seen in Figure A.18 where the pressure resulting in the lowest cost of oxygen supply is found. At small scale a lower pressure optimal pressure is found, primarily because the equipment costs are more important at this scale and the relative increase in compressor and reactor cost are greater.

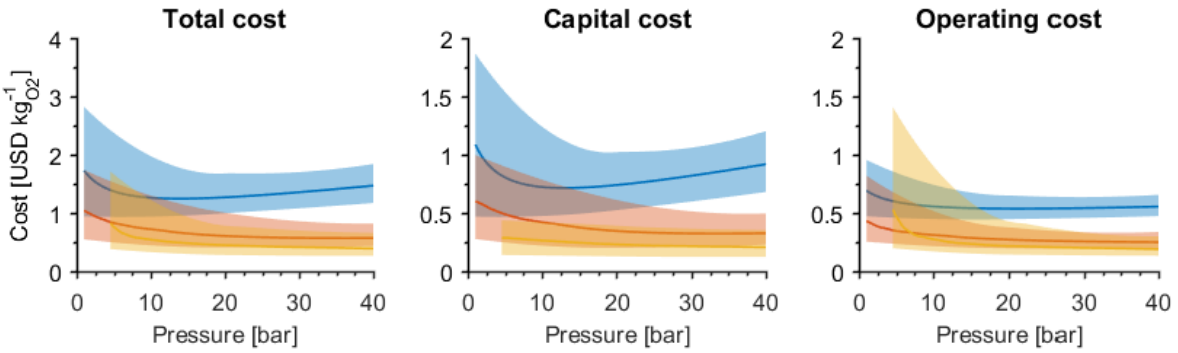

Figure A.16. Effect of reactor pressure on the cost of oxygen transfer for submerged membrane aeration using pure oxygen at an oxygen transfer rate of 50 mol m^{-3} h^{-1} (blue), 200 mol m^{-3} h^{-1} (red) and 500 mol m^{-3} h^{-1} (yellow) in 100 m^3 reactor. The dashed area represents 95% confidence intervals.

Figure A.17 shows how the variables changed in the minimization routine vary with pressure and oxygen supply rate. It is clearly seen, that there never is a benefit of operating below the maximum cross-membrane pressure of 4 bar. In other words, the increased compressor cost is fully covered by the decrease in membrane cost. It is also seen, that as the reactor pressure increase it is beneficial to transfer a larger amount of the oxygen initially present in the inlet gas. This is because the membrane requirement decrease with increasing pressure, and it is therefore not critical to keep a very high driving force across the entire membrane. The reason why all oxygen is not transferred is that it is assume that the 'pure' oxygen contain 5% impurities. If a completely pure stream of oxygen were applied the optimal configuration would be a dead-end filtration, however, then other problems such as build-up of water in the membrane fibers have to be considered.

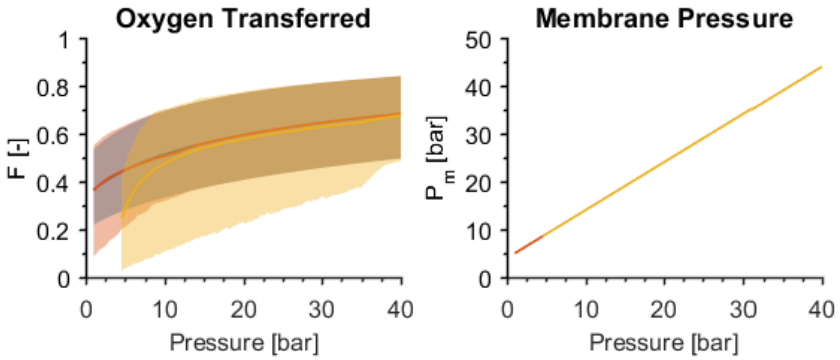

Figure A.17. Optimized operational parameters for submerged membrane aeration using pure oxygen as a function of reactor head-space pressure at an oxygen transfer rate of 50 mol m^{-3} h^{-1} (blue), 200 mol m^{-3} h^{-1} (red) and 500 mol m^{-3} h^{-1} (yellow). Shaded area represents 95% confidence intervals.

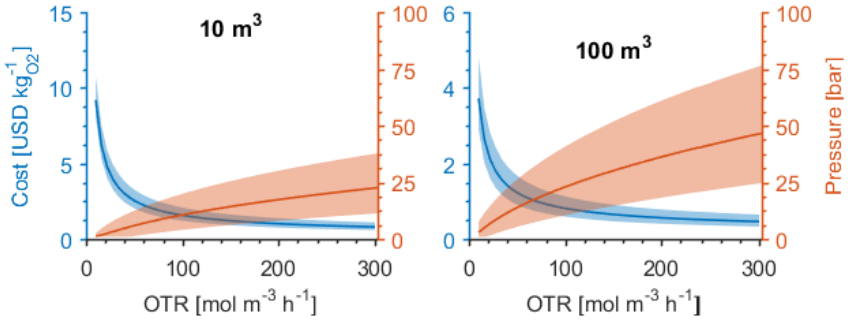

Figure A.18. Optimal reactor pressure and corresponding cost of oxygen transfer as a function of oxygen transfer rate (OTR) for submerged membrane aeration of a 10 m^3 and a 100 m^3 reactor. Shaded area represents 95% confidence intervals.

A.5.3 External membrane reactor

Figure A.19-A.21 shows the effect of pressure on the cost of oxygen transfer for external membrane aeration. As for submerged membrane aeration, the cost of oxygen transfer drops dramatically as the pressure is increased. The optimal pressure is also highly dependent on the oxygen transfer rate (Figure A.21), and as for the submerged membrane aeration, the optimal pressure at small scale is lower than the optimal pressure in large scale. Overall, it can be seen that despite the recirculation of reaction medium the cost of oxygen transfer is similar when the reactor pressure is increased beyond a few bars.

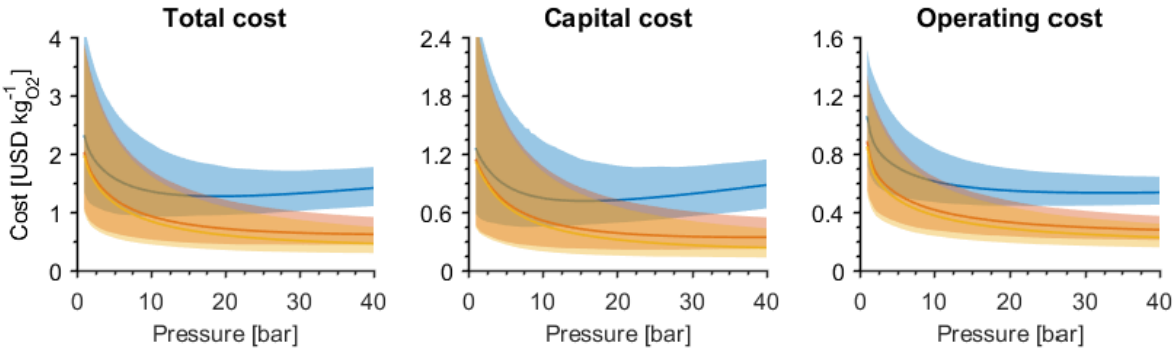

Figure A.19. Effect of reactor pressure on the cost of oxygen transfer for external membrane aeration using pure oxygen at an oxygen transfer rate of 50 mol m^{-3} h^{-1} (blue), 200 mol m^{-3} h^{-1} (red) and 500 mol m^{-3} h^{-1} (yellow) in 100 m^3 reactor. The dashed area represents 95% confidence intervals.

Figure A.20 shows how the three degrees of freedom change depending on the reactor head-space pressure. As for the submerged membrane aeration, the cross-membrane pressure is always at the maximum allowable (4 bar). Furthermore, the same trend in fraction of oxygen transferred from the incoming gas is seen. The degree of saturation of the liquid leaving the membrane module decrease with increasing pressure, because the liquid can contain more oxygen and therefore it becomes cheaper to decrease the liquid saturation leaving the reactor and thereby increasing the driving force available for mass transfer.

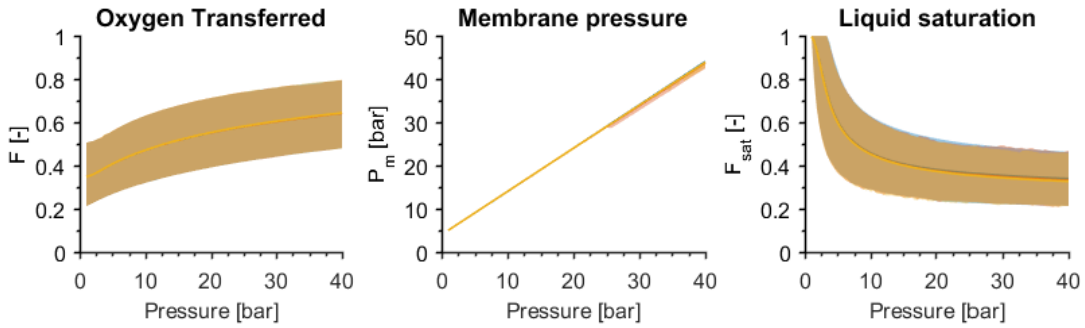

Figure A.20. Optimized operational parameters for external membrane aeration using pure oxygen as a function of reactor head-space pressure at an oxygen transfer rate of 50 mol m^{-3} h^{-1} (blue), 200 mol m^{-3} h^{-1} (red) and 500 mol m^{-3} h^{-1} (yellow). Shaded area represents 95% confidence intervals.

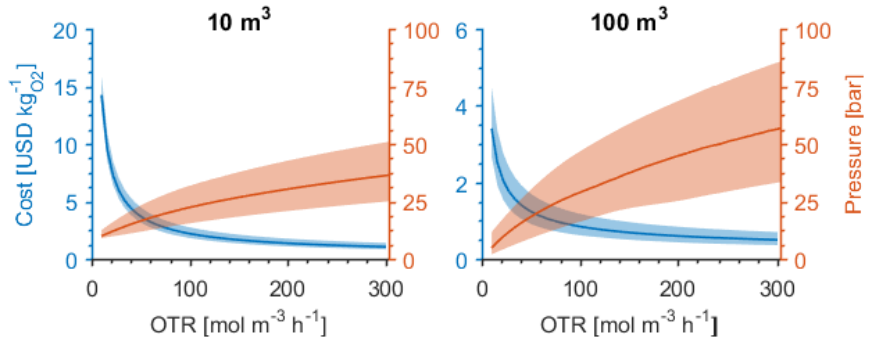

Figure A.21. Optimal pressure and corresponding cost of oxygen transfer as a function of oxygen transfer rate (OTR) for external membrane aeration of a 10 m^3 and a 100 m^3 reactor. Shaded area represents 95% confidence intervals.

A.5.4 Hydrogen peroxide degradation by catalase

Figure A.22 shows the operational, capital and total costs of supplying oxygen via hydrogen peroxide degradation. At low oxygen supply rates the contribution from capital costs are substantial, but this is diminished at high oxygen transfer rates. Here the cost of oxygen transfer is solely driven by the operational costs, which primarily constitutes the cost of hydrogen peroxide.

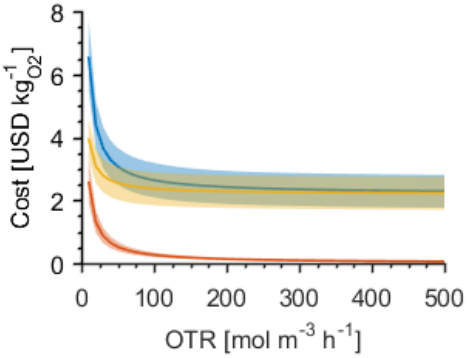

Figure A.22. Total cost (blue), capital cost (red) and operating cost (yellow) when supplying oxygen via degradation of hydrogen peroxide by catalase as a function of oxygen transfer rate (OTR) in 100 m^3 reactor. Shaded area represents 95% confidence intervals.

A.6 Sensitivity analysis

Figure A.23-A.25 shows the results of the sensitivity analysis for the investigated technologies. For bubble aeration of a stirred reactor (Figure A.23), the uncertainty on the capital cost explains the largest part of the variance seen in the total cost of oxygen transfer. When applying pure oxygen, also the cost of oxygen becomes important to the overall uncertainty. In general, the uncertainty on oxygen transfer rate, electricity, agitator efficiency and compressor efficiency only explains a small part of the overall variance in the cost of oxygen transfer.

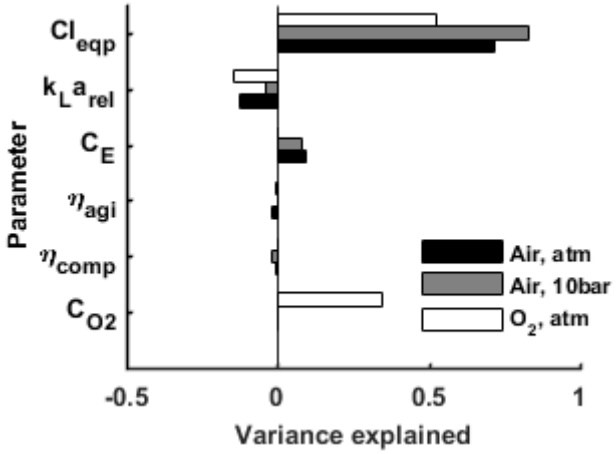

Figure A.23. Sensitivity analysis for bubble aeration in stirred tank at an oxygen transfer rate of 50 mol m^{-3} h^{-1} at 100 m^3 scale. The sign of the explained variance shows the relation with cost of oxygen transfer. A negative sign show that a positive change in the parameter induce a reduction in cost of oxygen transfer, and vice versa.

For membrane aeration (Figure A.24) the by far most important parameters are the cost of membrane and mass transfer coefficient across the membrane. It is only when high pressures are applied that the uncertainty in the capital cost (excluding membrane material) becomes important for the overall uncertainty, since a higher pressure increase the compressor and reactor cost, while reduce the membrane area required.

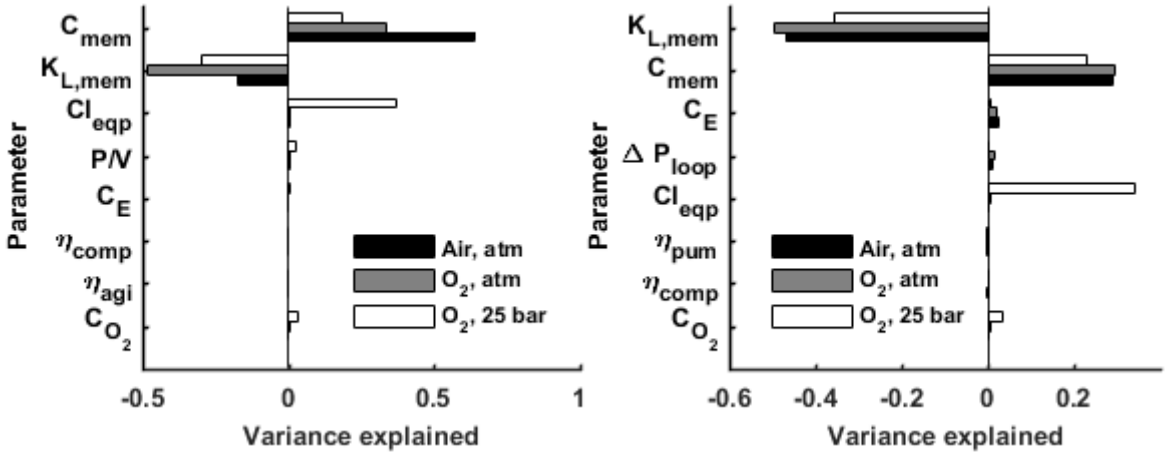

Figure A.24. Sensitivity analysis for submerged membrane aeration (left) and external membrane aeration (right) at an oxygen transfer rate of 50 mol m^{-3} h^{-1} at 100 m^3 scale. The sign of the explained variance shows the relation with cost of oxygen transfer. A negative sign show that a positive change in the parameter induce a reduction in cost of oxygen transfer, and vice versa.

The uncertainty on the cost of hydrogen peroxide is explaining the largest part of the variance seen in the cost of oxygen supply using hydrogen peroxide decomposition (Figure S79). The maximum allowable hydrogen peroxide concentration in the reactor is also important, while other parameters such as the power input, equipment cost, and cost of electricity have little to no importance to the total cost of oxygen supply.

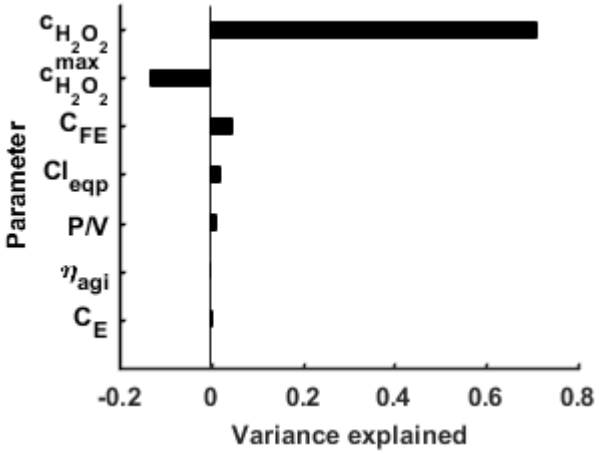

Figure A.25. Sensitivity analysis for hydrogen peroxide decomposition using catalase at an oxygen transfer rate of 50 mol m^{-3} h^{-1} at 100 m^3 scale. The sign of the explained variance shows the relation with cost of oxygen transfer. A negative sign show that a positive change in the parameter induce a reduction in cost of oxygen transfer, and vice versa.

Figure A.26-A.29 shows the correlation between the most important parameters (excluding uncertainty on the equipment cost estimations) on the cost of oxygen transfer. These plots give an overview of the potential reduction in cost of oxygen transfer if an uncertain parameter is changed, e.g. if hydrogen peroxide can be sources at a price in the lower end of the uncertainty interval.

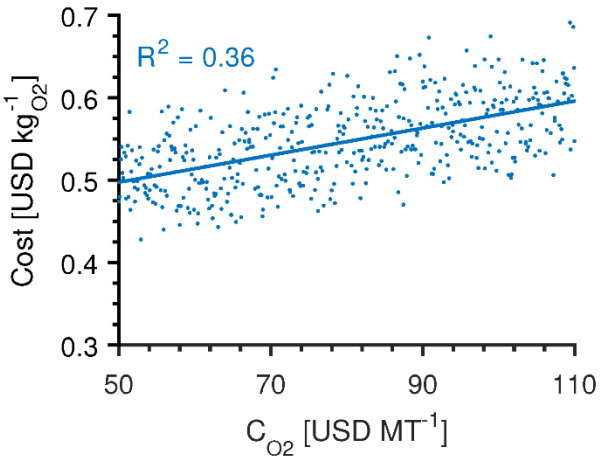

Figure A.26. Correlation between cost of pure oxygen and total cost of oxygen supply for bubble aeration in stirred tank at an oxygen transfer rate of 50 mol m^{-3} h^{-1} at 100 m^3 scale.

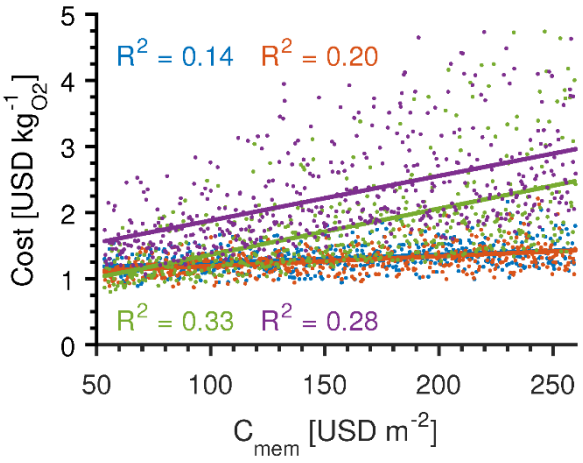

Figure A.27. Correlation between cost of membrane and total cost of oxygen supply for submerged membrane aeration employing pure oxygen at atmospheric pressure (green), submerged membrane aeration employing pure oxygen at 25 bar (blue), external membrane aeration employing pure oxygen at atmospheric pressure (purple), and external membrane aeration employing pure oxygen at 25 bar (red). The data is obtained at an oxygen transfer rate of 50 mol m^{-3} h^{-1} at 100 m^3 scale.

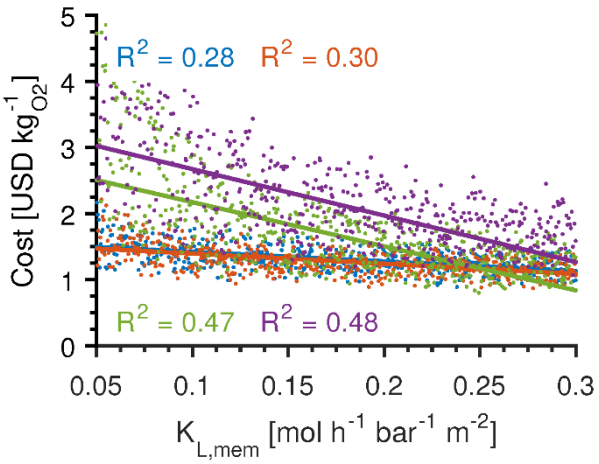

Figure A.28. Correlation between membrane mass transfer coefficient and total cost of oxygen supply for submerged membrane aeration employing pure oxygen at atmospheric pressure (green), submerged membrane aeration employing pure oxygen at 25 bar (blue), external membrane aeration employing pure oxygen at atmospheric pressure (purple), and external membrane aeration employing pure oxygen at 25 bar (red). The data is obtained at an oxygen transfer rate of 50 mol m^{-3} h^{-1} at 100 m^3 scale.

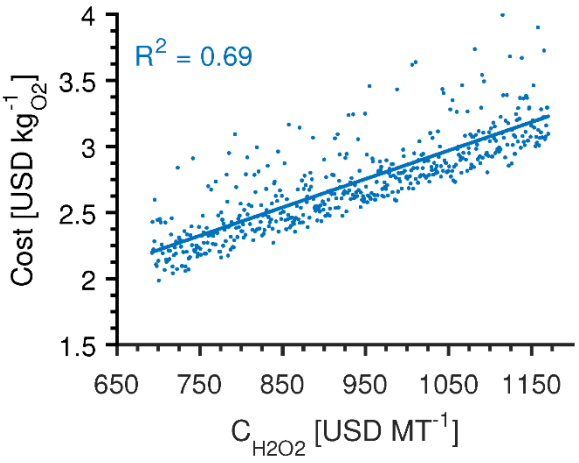

Figure A.29. Correlation between cost of hydrogen peroxide and total cost of oxygen supply using hydrogen peroxide decomposition using catalase at an oxygen transfer rate of 50 mol m^{-3} h^{-1} at 100 m^3 scale.

A.7 References

[1] Nienow AW, **1998**. Hydrodynamics of stirred bioreactors, Appl. Mech. Rev. 51(1):4–32.

[2] Garcia-Ochoa F, Gomez E, **2009**. Bioreactor scale-up and oxygen transfer rate in microbial processes: an overview., Biotechnol. Adv. 27(2):153–76.

[3] Noorman H, Scale-Up and Scale-Down, in: J. Villadsen (Ed.), Fundam. Bioeng., **2016**, Wiley-VCH Verlag GmbH & Co. KGaA, Weinheim: pp. 463–498.

[4] Peters MS, Timmerhaus KD, West RE, Plant Design and Economics for Chemical Engineers, 5th ed., **2003**, McGraw-Hill Education, New York.

[5] Häusler EBG, van der Wielen LAM, Straathof AJJ, **2016**. Evaluation of gas supply configurations for microbial product formation involving multiple gaseous substrates, Bioresour. Bioprocess. 3(1):18.

[6] Kirschner MJ, Oxygen, in: Ullmann's Encycl. Ind. Chem., **2000**, Wiley-VCH Verlag GmbH & Co. KGaA, Weinheim: pp. 317–635.

[7] Kavousi F, Syron E, Semmens M, Casey E, **2016**. Hydrodynamics and gas transfer performance of confined hollow fibre membrane modules with the aid of computational fluid dynamics, J. Memb. Sci. 513:117–128.

[8] Li J, Zhu L-P, Xu Y-Y, Zhu B-K, **2010**. Oxygen transfer characteristics of hydrophilic treated polypropylene hollow fiber membranes for bubbleless aeration, J. Memb. Sci. 362(1–2):47–57.

[9] Côté P, Bersillon J, Huyard A, Faup G, **1988**. Bubble-Free Aeration Using Membranes : Process Analysis, J. Water Pollut. Control Fed. 60(11):1986–1992.

[10] Voss MA, Ahmed T, Semmens MJ, **1999**. Long-Term Performance of Parallel-Flow, Bubbleless, Hollow-Fiber-Membrane Aerators, Water Environ. Res. 71(1):23–30.

[11] Côté P, Bersillon J-L, Huyard A, **1989**. Bubble-free aeration: Mass transfer analysis, 47:91–106.

[12] Casey E, Glennon B, Hamer G, **1999**. Review of membrane aerated biofilm reactors, Resour. Conserv. Recycl. 27(1–2):203–215.

[13] Tufvesson P, Lima-Ramos J, Nordblad M, Woodley JM, **2011**. Guidelines and cost analysis for catalyst production in biocatalytic processes, Org. Process Res. Dev. 15(1):266–274.

[14] Morthensen ST, Meyer AS, Jørgensen H, Pinelo M, **2017**. Significance of membrane bioreactor design on the biocatalytic performance of glucose oxidase and catalase: Free vs. immobilized enzyme systems, Biochem. Eng. J. 117:41–47.

[15] Hernandez K, Berenguer-Murcia A, C. Rodrigues R, Fernandez-Lafuente R, **2012**. Hydrogen Peroxide in Biocatalysis. A Dangerous Liaison, Curr. Org. Chem. 16(22):2652–2672.

[16] Eurostat, Eurostat**2015**. http://ec.europa.eu/eurostat (accessed March 14, 2017).

[17] Villadsen J, Nielsen J, Lidén G, Bioreaction Engineering Principles, 3rd ed., **2011**,

Springer Science+Business Media, New York.

[18] Albaek MO, Gernaey K V., Stocks SM, **2008**. Gassed and ungassed power draw in a pilot scale 550 litre fermentor retrofitted with up-pumping hydrofoil B2 impellers in media of different viscosity and with very high power draw, Chem. Eng. Sci. 63(24):5813–5820.

[19] Baker RW, Membrane Technology and Applications, 3rd ed., **2012**, John Wiley & Sons, Ltd., Chichester.

[20] Ciriminna R, Albanese L, Meneguzzo F, Pagliaro M, **2016**. Hydrogen Peroxide: A Key Chemical for Tomorrow's Sustainable Development, ChemSusChem. 9:3374–3381.

[21] Wang W, Sun M, Liu W, Zhang B, **2008**. Purification and characterization of a psychrophilic catalase from Antarctic Bacillus, Can. J. Microbiol. 54(10):823–828.

[22] Biegler LT, Grossmann IE, Westerberg AW, Systematic Methods of Chemical Process Design, **1999**, Prentice Hall PTR, Upper Saddle River, N.J.

[23] Humbird D, Davis R, Tao L, Kinchin C, Hsu D, Aden A, Process Design and Economics for Biochemical Conversion of Lignocellulosic Biomass to Ethanol, **2011**, Golden, CO.

[24] Albaek MO, Evaluation of the efficiency of alternative enzyme production technologies, Technical University of Denmark, **2012**.

Appendix B

Included publications

Paper I: Ringborg RH*, **Toftgaard Pedersen A***, Woodley JM. 2017. Automated determination of oxygen-dependent enzyme kinetics in a tube-in-tube flow reactor, ChemCatChem, Accepted, DOI: 10.1002/cctc.201700811

*These authors contributed equally to this work

Paper II: **Toftgaard Pedersen A**, de Carvalho TM, Sutherland E, Rehn G, Ashe R, Woodley JM. 2017. Characterization of a Continuous Agitated Cell Reactor for Oxygen Dependent Biocatalysis, Biotechnology and Bioengineering 114(6):1222-1230

Paper III: **Toftgaard Pedersen A**, Birmingham WR, Rehn G, Charnock SJ, Turner NJ, Woodley JM. 2015. Process Requirements of Galactose Oxidase Catalyzed Oxidation of Alcohols, Organic Process Research and Development 19(11):1580-1589

Heterogeneous & Homogeneous & Bio- & Nano-
CHEMCATCHEM
CATALYSIS

Accepted Article

Title: Automated determination of oxygen dependent enzyme kinetics in a tube-in-tube microreactor

Authors: Rolf Hoffmeyer Ringborg, Asbjørn Toftgaard Pedersen, and John M. Woodley

To be cited as: *ChemCatChem* 10.1002/cctc.201700811

Link to VoR: http://dx.doi.org/10.1002/cctc.201700811

A Journal of
ChemPubSoc Europe

WILEY-VCH

www.chemcatchem.org

10.1002/cctc.201700811

Automated determination of oxygen-dependent enzyme kinetics in a tube-in-tube flow reactor

Rolf H. Ringborg*†‡, Asbjørn Toftgaard Pedersen*† and John M. Woodley†

†Department of Chemical and Biochemical Engineering, Technical University of Denmark, DK-2800 Kgs. Lyngby, Denmark. ‡Current address: EchoSkye, DK-2300 Copenhagen S, Denmark.

*These authors contributed equally to this work.

Enzyme-mediated oxidation is of particular interest to synthetic organic chemists. However, the implementation of such systems demands knowledge of enzyme kinetics. Conventionally collecting kinetic data for biocatalytic oxidations is fraught with difficulties such as low oxygen solubility in water and limited oxygen supply. Here, we present a novel method for the collection of such kinetic data using a pressurized tube-in-tube reactor, operated in the low-dispersed flow regime to generate time-series data, with minimal material consumption. Experimental development and validation of the instrument revealed not only the high degree of accuracy of the kinetic data obtained, but also the necessity of making measurements in this way to enable the accurate evaluation of high K_{MO} enzyme systems. For the first time, this paves the way to integrate kinetic data into the protein engineering cycle.

Selective oxidation is one of the most important transformations in synthetic organic chemistry.[1–3] The necessity of achieving high reaction yield in such transformations makes enzymes particularly interesting as potential catalysts, on account of their exquisite selectivity in comparison with their chemo-catalytic counterparts. However, for process application it is often difficult to reach the required reaction intensity (reaction rate and product concentration). In particular, issues such as low enzymatic activity, product/substrate inhibition, co-factor regeneration and unfavorable thermodynamic equilibria need to be solved using biocatalytic reaction engineering. These problems are commonly investigated by studying the kinetic behavior of an enzyme under different conditions. Subsequently, using these data, the challenges in reaching the required productivity can be addressed either by protein engineering or alternatively process engineering to circumvent kinetic limitations. However, it would be much more effective if solutions arose from a combination of both approaches. Regardless of the approach taken, enzyme improvement naturally starts in the hands of the protein engineer who typically screens for improved enzymes using single point measurements (i.e. at a single substrate concentration) to go through many enzyme variants.[4] In this way, protein engineering is able to deliver improved enzymes, also catalyzing the conversion of non-natural substrates.[5] However, single point measurements can only reveal apparent kinetics constants, such as the so-called specificity constant (V_{max}/K_M), which can be misleading as the basis for selecting the optimal enzyme.[6–8] At points in development where selection is from a smaller pool of protein variants, it would be highly desirable to comprehensively quantify the kinetics, in order to have an adequate basis for deciding on the best enzyme for a given reaction, and reactor configuration. Likewise, it is necessary to determine the activity of an enzyme of interest over the full range of potential operating conditions in order to truly assess the possibilities for process implementation. On this premise, we suggest that comprehensive kinetic investigations should be integrated into the improvement cycle of an enzyme for application. In this way it would be possible to direct screening to focus on evolving improved enzymatic kinetic properties, which are ideal for process implementation. In order to realize such a scheme, it is necessary to develop an automated characterization system.[9] Herein, we present one such system focused on collecting kinetic data for oxygen-dependent enzymes.

While studying enzyme kinetics it is important to measure initial rates at substrate concentrations well above, as well as below, the true Michaelis constant(s) in order to determine these kinetic parameters with

sufficient accuracy. In the study of oxygen-dependent enzymes, such investigations are notoriously difficult due to the limited solubility of oxygen in water, and to some extent the concomitant limited supply rate of oxygen. The challenge of controlling the oxygen concentration leads in many cases to experiments being conducted at a single oxygen concentration (usually that in water, in equilibrium with air, at 276 µM). Air saturation is however insufficient to achieve enzyme saturation for several industrially interesting oxidases[10–12] and in any case it introduces uncertainty into parameter estimations. Indeed, conventional experiments can only reveal apparent Michaelis constants which are confined to the tested parameter space and should therefore be compared with great care. Likewise, oxygen supply is often carried out by bubbling air through the reaction solution. However, in doing so, it is necessary to consider the stripping of any volatile substrate(s) and product(s), as well as potential enzyme deactivation at the gas-liquid interface.[13] The constraint on the limited dissolved oxygen concentration in water can be alleviated by pressurizing the reactor or by using enriched air (to increase the partial pressure), whereas the interfacial effect can only be alleviated by introducing a physical barrier between the gas and the liquid.

Recently, the Teflon AF-2400 flouro-polymer[14], which is characterized by high gas permeability, has been used a membrane in the lastest development of the so-called Tube-in-Tube Reactor (TiTR) design[15] which has previously proven useful for the supply of gaseous substrates to liquid reaction media while retaining the chemical resistance of traditional flouro polymers[16,17]. The TiTR is made of an inner Teflon AF-2400 tube encased within an outer PTFE tube with low oxygen permeability. A mixture of oxygen and nitrogen is supplied in the space between the two tubes, whereby the oxygen can be transferred to the liquid reaction mixture in the inner tube through the membrane. We reasoned this would make the TiTR ideal for studying the kinetics of oxygen dependent biocatalytic reactions, since the challenges of conventional systems can be avoided by creating a bubble-free aeration system. The small dimensions of the inner tube (I.D/O.D. 230/410 µm) maximize the surface-to-volume ratio, which combined with the high oxygen permeability of Teflon AF-2400, enables very high oxygen supply rates. The allows operation at dissolved concentrations of oxygen very close to the equilibrium value between the gas phase and the reaction medium, despite a low driving force (i.e. the reactor will operate at a dissolved oxygen concentration within 99% of saturation). Additionally, by pressurizing both the inner and outer tube, the oxygen solubility in the reaction mixture can be increased proportionally. The setup therefore allows control over oxygen as a substrate in oxygen-dependent enzyme reactions. Furthermore, the TiTR satisfies the requirement for negligible change in substrate concentration for measurement of initial rates, since oxygen can be supplied along the reactor as it is consumed. Based on this concept, a system suitable for kinetic characterization of oxygen dependent enzymes was developed by combining the TiTR with precise liquid and gas supply systems and connecting the outlet of the inner tube to a UV-vis detector. By means of a switch valve, samples were carried from the injection loop into the detector, where the solution was subjected to flow injection analysis.

Although such a reactor is very useful for carrying out oxygen-dependent enzyme reactions (under pressure), we realized that a further development was still necessary for the meaningful collection of kinetic data. Laboratory flow reactors typically operate in the laminar flow regime with large axial dispersion, which necessitates steady-state experiments. Such experiments often consume more material, over a longer time period and with a lower sampling frequency than those carried out in equivalent batch apparatus.[18] Recently, a review of Taylor's work surrounding mixing and dispersion[19] has led to the application of low dispersed flow in microreactors.[20] This is a unique regime of laminar flow that occurs only at a microfluidic scale.[20] In this flow regime, the radial mixing from the center of the tube to the edges is governed solely by diffusion. At the micro-scale, the diffusion lengths are by definition very small and this will in turn give very short radial mixing times. Low dispersed flow will therefore flatten the well-known "tongue" profile of laminar flow, and solute concentrations will thereby only change along the length of the reactor. These dynamics mean that the reactor can be described by plug-flow behavior, and this was used in a method recently reported by Moore and Jensen.[21] In this method, at low residence time, steady-state is obtained and the flowrate is subsequently ramped down. By following the conversion during the ramp,

initial rate measurements (i.e. concentration-time profiles) are possible without the need to obtain multiple steady-states. Nevertheless, the reported Moore and Jensen method requires modification for biocatalysis. Low dispersed flow is very dependent on the diffusivity of the solutes, and the large size of enzyme catalysts translates into a two order-of-magnitude lower diffusivity compared to small molecules (10^{-11} cf. 10^{-9} m^2/s)[22,23]. The axial dispersion of enzymes will therefore be much more pronounced, meaning that they are more dispersed along the length of the channel compared to the small molecule reactants and the resulting products. It was therefore necessary to make sure that the enzyme concentration in the entire reactor volume remained constant. This was ensured by achieving steady-state with respect to the enzyme concentration and thereafter keeping the enzyme feed concentration constant, independent of the liquid flowrate. In this way, it was assumed that the degree of dispersion would be dependent upon the diffusion coefficients of the substrate(s) and product(s) alone. The integrated combination of each of the afore-mentioned developments has led to the establishment of the current instrument, which now gives a novel and automated way of kinetically characterizing oxygen-dependent enzymes, see Figure 1. The specific details of the setup are described in the Supporting Information (SI).

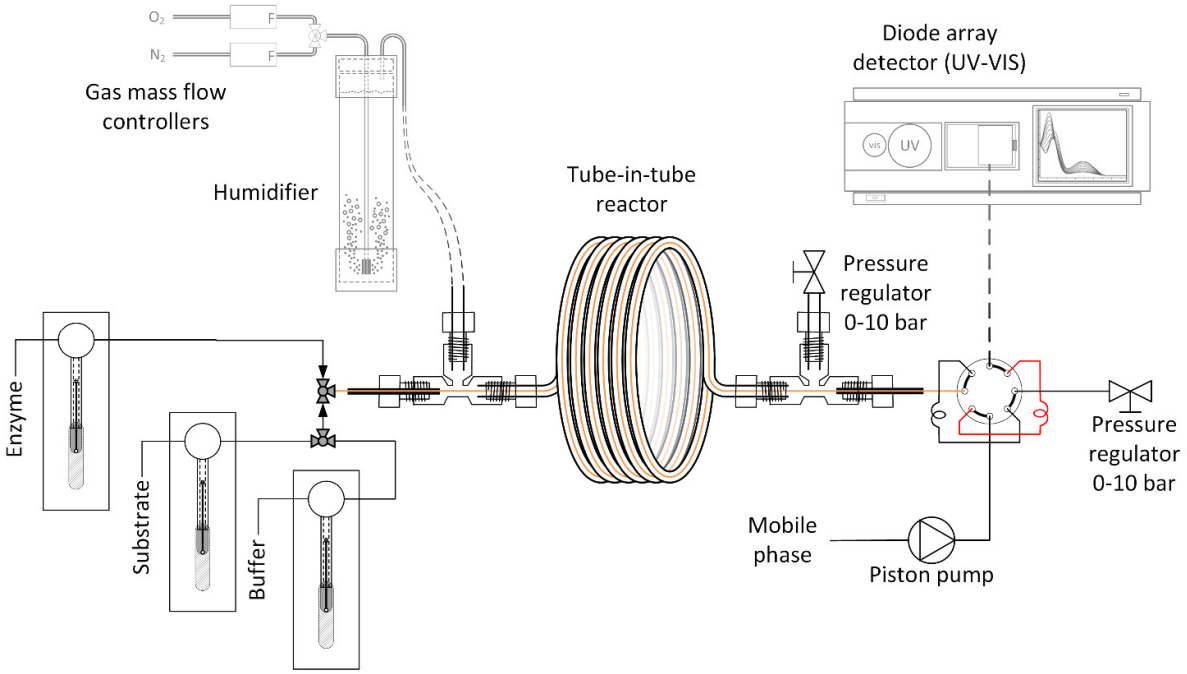

Figure 1 - Experimental setup of the Tube-in-Tube Reactor. The three syringe pumps on the left deliver a liquid solution to the inner membrane tube, illustrated by the orange line. Two mass flow controllers are used to vary the gas composition in the range 5-100 % O_2, supplied to the outer tube. The gas is wetted and heated before entering the reactor to avoid the stripping of water from the inner tube. The gas was fed via an outer tube, made of PTFE. A pressure regulator and a manometer were located at both ends of the two tubes to control the pressure, as well as to ensure an equal or higher pressure on the liquid side of the membrane.

In order to demonstrate the performance of the instrument, the well-known enzyme, glucose oxidase (GOx, E.C. 1.1.3.4), was selected. The GOx enzyme catalyzes the oxidation of glucose to glucono-δ-lactone, using molecular oxygen (which is itself reduced to hydrogen peroxide). Following the enzymatic reaction, Glucono-δ-lactone is spontaneously hydrolysed to gluconic acid, whose formation can be followed spectrophotometrically, see SI. The hydrogen peroxide formed is removed instantaneously by the addition of catalase, which enables its conversion into water and half the stoichiometric amount of oxygen. The removal of hydrogen peroxide forces the reaction to proceed in a unidirectional manner and also protects GOx from oxidation. GOx has been shown to follow a ping-pong bi-bi reaction mechanism (Scheme 1)[24] for which a rate expression can be derived, see Eqn. 1.

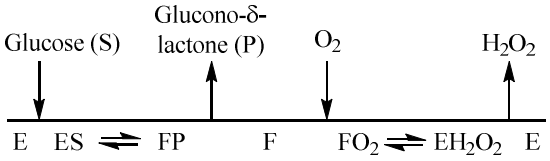

Scheme 1. Cleveland representation of the glucose oxidase ping-pong bi bi mechanism. E denotes the oxidized free form of the enzyme whereas F denotes the reduced form of the free enzyme.

$$\frac{\mathrm{r}}{[E]} = \frac{k_{cat} S\, O}{S\, O + \mathrm{K_{MO}}\, S\, + \mathrm{K_{MS}}\, \mathrm{O}} \qquad \text{(Eqn. 1)}$$

The flow manipulation method applied to produce the equivalent batch data from the setup, requires an accurate determination of the reactor volume. Hence initially residence time distribution experiments were carried out to determine the volume of the reactor (155 ± 1.8 µL, see SI). Next, the results of the flow method were compared with steady-state operation, where it was shown that the setup indeed produces time-series data even with the addition of a slow diffusing (bio)catalyst, see SI. Finally, in order to validate the enzyme kinetics measured in the TiTR, equivalent experiments to those carried out in batch by Toftgaard Pedersen and co-workers[25] were carried out. In the batch experiments the setup used an aerated stirred tank reactor with adjustable oxygen/nitrogen feed. The comparison revealed an excellent correlation between the two systems and the combined results of the validation experiments confirmed that confidence can be placed on the kinetics determined in the TiTR setup (Figure 2).

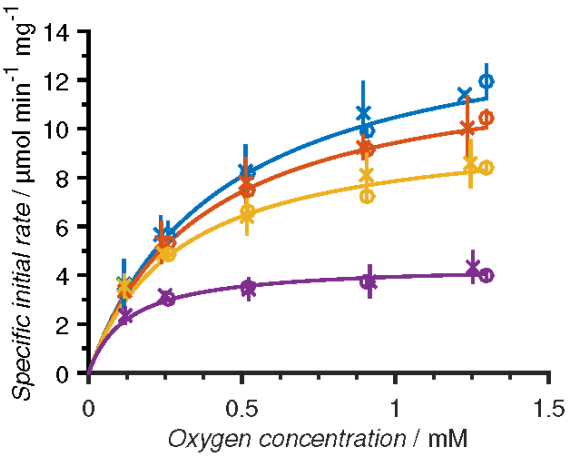

Figure 2. Specific initial reaction rate vs oxygen concentration in Batch (x) and TiTR (o) at a glucose concentration of 400 mM (blue), 200 mM (red), 100 mM (yellow), and 25 mM (purple). Full lines represent the model fit to the TiTR results. The experiments were carried out at pH 7, 25 °C and atmospheric pressure. The batch data was scaled by a factor 0.79 to correct for time dependent degradation of the enzyme formulation between the experiments, see SI.

The fit of Eq. 1. to these data revealed a relatively high Michaelis constant for oxygen of 0.52 mM (Table 1), which is also seen from the unsaturated enzyme kinetics observed at high glucose concentrations and atmospheric pressure (Figure 2). It is generally accepted, that in order to reliably quantify Michaelis constants it is necessary to measure enzyme kinetics in a sufficiently large range of substrate concentrations, using values of a minimum of 5-fold (and preferably 10-fold) higher and lower than the true K_M. In the TiTR setup, this was achieved by increasing the operating pressure of the setup to 6 bar to increase the maximum dissolved oxygen concentration to 7.13 mM (using pure O_2 at 25 ˚C). Enzyme saturation was thereby obtained even at the highest concentration of glucose (Figure 3), enabling a more reliable prediction of all the kinetic parameters (Table 1).

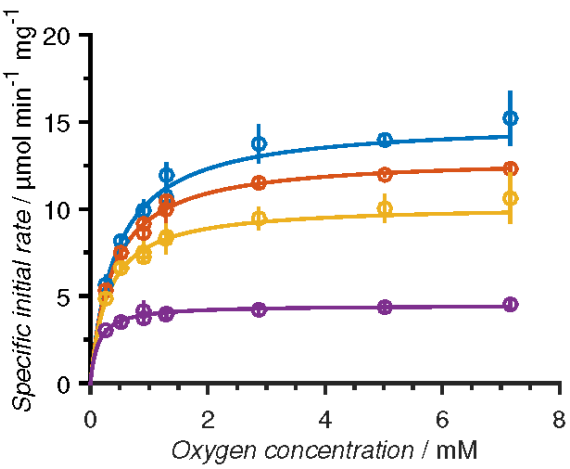

Figure 3. Data collected in the TiTR at 1 atm. (0.14-1.3 mM O_2) and 6 bar (0.9-7.13 mM O_2) at a glucose concentration 400 mM (blue), 200 mM (red), 100 mM (yellow), and 25 mM (purple). Full lines represent the model fit. Experiments were carried out at pH 7 and 25 °C.

Table 1. Parameter estimations based on different experimental data. Pressure is given as absolute pressure. [a] Based on milligrams of liquid formulation [b] The batch data is scaled by a factor 0.79 to correct for time dependent degradation of the enzyme formulation between the experiments, see SI.

Parameter	Batch reactor (1 atm)	TiTR (1 atm)	TiTR (1 atm + 6 bar)
k_{cat} [µmol min^{-1} mg^{-1}][a]	17.58 ± 0.62[b]	17.78 ± 1.39	17.82 ± 0.47
K_{MO} [mM]	0.45 ± 0.04	0.51 ± 0.09	0.52 ± 0.03
K_{MS} [mM]	73.1 ± 6.87	75.2 ± 9.38	74.57 ± 5.55

The TiTR setup was fully automated and computer controlled, thereby enabling characterization of an oxygen-dependent enzyme within 24 hours with minimal manual labor. While the preparation of solutions is identical for both batch and TiTR, the batch setup requires four full days of labor. Furthermore, the small dimensions of the system make it possible to collect one initial rate measurement per 1.4 mL of reaction mixture, which is considerably less than the 150 mL required in the alternative sparged batch setup.

In summary, we have developed and validated an automated flow reactor system that rapidly and accurately determines the kinetics of oxygen-dependent enzymes. The tool allows perfect control of the oxygen concentration in solution, which by pressurizing the system can enable values up to 25-fold higher than that achievable using merely air under atmospheric conditions. Operation in the low dispersed flow regime allowed the generation of time-series data with an enzymatic catalyst, despite its low diffusivity and the resulting data were in good agreement with experiments conducted in a batch system. The system is capable of characterizing the kinetics of any enzyme within the oxidoreductase class (EC 1), where reactions frequently result in changes to the UV-spectra to enable facile quantification of conversion. The application is however not limited to oxygen-dependent enzymes alone, but can in principle be used to study many other enzymes using gaseous substrates, such as hydrogenases (using H_2)[26], formate dehydrogenases (using CO_2)[27] or methane monooxygenases (using CH_4).[28] The tool presented here could introduce kinetic characterization of oxidoreductases into the catalyst development cycle, where biocatalytic reaction engineering can be used to guide both process and protein engineering.[9,29] The need to further improve this development cycle is particularly important in order to facilitate the wider and more effective implementation of biocatalytic reactions, especially in the pharmaceutical industry. [30]

Acknowledgements:

The research leading to these results has received funding from the European Union's Seventh Framework Programme for research, technological development and demonstration under grant agreement n° 613849 supporting the project BIOOX (A.T.P.). The authors acknowledge Novozymes A/S (Bagsværd, DK) for kindly supplying the enzyme used for this research.

Keywords: kinetics • enzymes • tube-in-tube • oxidation • automated

References:

[1] W. Kroutil, H. Mang, K. Edegger, K. Faber, *Adv. Synth. Catal.* **2004**, *346*, 125–142.

[2] F. Hollmann, I. W. C. E. Arends, K. Buehler, A. Schallmey, B. Bühler, *Green Chem.* **2011**, *13*, 226.

[3] T. Punniyamurthy, S. Velusamy, J. Iqbal, *Chem. Rev.* **2005**, *105*, 2329–63.

[4] A. Fallah-Araghi, J.-C. Baret, M. Ryckelynck, A. D. Griffiths, *Lab Chip* **2012**, *12*, 882–891.

[5] U. T. Bornscheuer, G. W. Huisman, R. J. Kazlauskas, S. Lutz, J. C. Moore, K. Robins, *Nature* **2012**, *485*, 185–94.

[6] R. Eisenthal, M. J. Danson, D. W. Hough, *Trends Biotechnol.* **2007**, *25*, 247–249.

[7] D. E. Koshland, *Bioorg. Chem.* **2002**, *30*, 211–213.

[8] R. J. Fox, M. D. Clay, *Trends Biotechnol.* **2009**, *27*, 137–140.

[9] R. H. Ringborg, J. M. Woodley, *React. Chem. Eng.* **2016**, *1*, 10–22.

[10] M. Nordkvist, P. M. Nielsen, J. Villadsen, **2007**, *97*, 694–707.

[11] M. Ghanem, F. Fan, K. Francis, G. Gadda, *Biochemistry* **2003**, *42*, 15179–15188.

[12] L. Pollegioni, B. Langkau, W. Tischer, S. Ghisla, M. S. Pilone, *J. Biol. Chem.* **1993**, *268*, 13850–13857.

[13] A. S. Bommarius, A. Karau, *Biotechnol. Prog.* **2005**, *21*, 1663–1672.

[14] P. R. Resnick, W. H. Buck, in *Mod. Fluoropolymers*, John Wiley & Sons, Ltd., Chichester, **1997**, pp. 397–419.

[15] A. Polyzos, M. O. Brien, T. P. Petersen, I. R. Baxendale, S. V Ley, *Angew. Chemie* **2011**, *50*, 1190–1193.

[16] M. O'Brien, N. Taylor, A. Polyzos, I. R. Baxendale, S. V. Ley, *Chem. Sci.* **2011**, *2*, 1250.

[17] B. Tomaszewski, A. Schmid, K. Buehler, *Org. Process Res. Dev.* **2014**, *18*, 1516–1526.

[18] F. E. Valera, M. Quaranta, A. Moran, J. Blacker, A. Armstrong, J. T. Cabral, D. G. Blackmond, *Angew. Chem. Int. Ed. Engl.* **2010**, *49*, 2478–2485.

[19] G. Taylor, *Proc. R. Soc. London. Ser. A* **1953**, *219*, 186–203.

[20] K. D. Nagy, B. Shen, T. F. Jamison, K. F. Jensen, *Org. Process Res. Dev.* **2012**, *16*, 976–981.

[21] J. S. Moore, K. F. Jensen, *Angew. Chem. Int. Ed. Engl.* **2014**, *53*, 470–473.

[22] E. L. Cussler, *Diffusion: Mass Transfer in Fluid Systems*, Cambridge University Press, **2009**.

[23] M. E. Young, P. A. Carroad, R. L. Bell, *Biotechnol. Bioeng.* **1980**, *22*, 947–955.

[24] Q. H. Gibson, B. E. P. Swoboda, V. Massey, *J. Biol. Chem.* **1964**, *239*, 3927–3934.

[25] A. Toftgaard Pedersen, T. Carvalho, E. Sutherland, G. Rehn, R. Ashe, J. M. Woodley, *Biotechnol. Bioeng.* **2017**, *114*, 1222–1230.

[26] L. Lauterbach, O. Lenz, K. A. Vincent, *FEBS J.* **2013**, *280*, 3058–3068.

[27] J. Shi, Y. Jiang, Z. Jiang, X. Wang, X. Wang, S. Zhang, P. Han, C. Yang, *Chem. Soc. Rev.* **2015**, *44*, 5981–6000.

[28] S. I. Chan, Y. J. Lu, P. Nagababu, S. Maji, M. C. Hung, M. M. Lee, I. J. Hsu, P. D. Minh, J. C. H. Lai, K. Y. Ng, et al., *Angew. Chemie. Int. Ed.* **2013**, *52*, 3731–3735.

[29] J. M. Woodley, *Curr. Opin. Chem. Biol.* **2013**, *17*, 310–316.

[30] M.D. Truppo, *ACS Med. Chem. Lett.* **2017**, DOI: 10.1021/acsmedchemlett.7b00114.

10.1002/cctc.201700811

Keywords: kinetics, enzymes, tube-in-tube, oxidation, automated.

ARTICLE

BIOTECHNOLOGY and BIOENGINEERING

Characterization of a Continuous Agitated Cell Reactor for Oxygen Dependent Biocatalysis

Asbjørn Toftgaard Pedersen,[1] Teresa Melo de Carvalho,[1] Euan Sutherland,[2] Gustav Rehn,[1] Robert Ashe,[2] John M. Woodley[1]

[1]Department of Chemical and Biochemical Engineering, Technical University of Denmark, Søltofts Plads 229, DK-2800 Kgs. Lyngby, Denmark; telephone: +45 45252885; fax: +45 45932906; e-mail: jw@kt.dtu.dk

[2]AM Technology, Manor Park, Runcorn, Cheshire, United Kingdom

ABSTRACT: Biocatalytic oxidation reactions employing molecular oxygen as the electron acceptor are difficult to conduct in a continuous flow reactor because of the requirement for high oxygen transfer rates. In this paper, the oxidation of glucose to glucono-1,5-lactone by glucose oxidase was used as a model reaction to study a novel continuous agitated cell reactor (ACR). The ACR consists of ten cells interconnected by small channels. An agitator is placed in each cell, which mixes the content of the cell when the reactor body is shaken by lateral movement. Based on tracer experiments, a hydrodynamic model for the ACR was developed. The model consisted of ten tanks-in-series with back-mixing occurring within and between each cell. The back-mixing was a necessary addition to the model in order to explain the observed phenomenon that the ACR behaved as two continuous stirred tank reactors (CSTRs) at low flow rates, while it at high flow rates behaved as the expected ten CSTRs in series. The performance of the ACR was evaluated by comparing the steady state conversion at varying residence times with the conversion observed in a stirred batch reactor of comparable size. It was found that the ACR could more than double the overall reaction rate, which was solely due to an increased oxygen transfer rate in the ACR caused by the intense mixing as a result of the spring agitators. The volumetric oxygen transfer coefficient, k_La, was estimated to be 344 h^{-1} in the 100 mL ACR, opposed to only 104 h^{-1} in a batch reactor of comparable working volume. Interestingly, the large deviation from plug flow behavior seen in the tracer experiments was found to have little influence on the conversion in the ACR, since both a plug flow reactor (PFR) model and the backflow cell model described the data sufficiently well.

Biotechnol. Bioeng. 2017;114: 1222–1230.

KEYWORDS: continuous biocatalysis; gas-liquid mixing; glucose oxidase; hydrodynamics; oxygen transfer rate

Introduction

In the recent years, biocatalytic oxidation reactions catalyzed by enzymes or microbes have gained significant scientific interest due to their potential to replace chemically catalyzed reactions suffering from poor selectivity and large environmental impact due to extensive waste generation (Kroutil et al., 2004; Pickl et al., 2015). Biocatalytic oxidations typically use oxygen as the electron acceptor, which is cheap and readily available. However, the transfer of oxygen from air to an aqueous media is notoriously slow, due to the very low aqueous solubility of oxygen, even compared to typical reaction rates of biocatalytic reactions. This often results in biocatalytic oxidations being oxygen limited. Hence, in most cases the biggest challenge for process engineers is to maximize the oxygen transfer capabilities of the available equipment in order to meet the demands to effective enzyme use and volumetric productivity.

Traditionally, batch processes have dominated the fine chemical and pharmaceutical industry, primarily due to their multi-functionality, which provides great flexibility for manufacturing. However, in recent years the move towards continuous processing have gained momentum in an effort to reduce costs, increase quality, improve process control, and reduce waste (Baxendale et al., 2014; Gutmann et al., 2015; Roberge et al., 2008; Wiles and Watts, 2012). Biocatalytic reaction steps implemented in a fine chemical manufacturing process would, therefore, preferably also operate in continuous mode in order to avoid storage of chemical intermediates and enable upstream and downstream integration. While continuous operation of typical single-phase biocatalytic reactions is relatively straightforward, multi-phase flow reactions can be more challenging. Continuous reactors for biocatalytic oxidation reactions are particularly challenging due to the necessity for efficient oxygen transfer, which usually requires mechanical stirring or other means of creating large gas-liquid interfacial areas. The options for continuous reactor types are, therefore, typically limited to continuous stirred tank reactors (CSTRs) and similar reactor types, such as bubble columns, on the macro scale, while falling film reactors and tube-in-tube reactors exists as novel reactor options for continuous processing on the

Conflict of interest: AM Technology owns the rights to and markets the Coflore® technology, including the agitated cell reactor investigated in this publication.

Correspondence to: J.M. Woodley

Contract grant sponsor: European Union's Seventh Framework Programme
Contract grant number: 613849
Received 5 December 2016; Revision received 25 January 2017; Accepted 5 February 2017
Accepted manuscript online 10 February 2017;
Article first published online 23 February 2017 in Wiley Online Library (http://onlinelibrary.wiley.com/doi/10.1002/bit.26267/abstract).
DOI 10.1002/bit.26267

micro-scale (Tomaszewski et al., 2014; Wohlgemuth et al., 2015). Despite the potential of micro-reactors, the chemical industry is, and will be, dominated by macro-scale reactors. Therefore, continuous macro-scale reactors are required as processing alternatives. Nevertheless, CSTRs can often be a poor reactor choice for continuous manufacturing due to their lower volumetric productivity resulting from lower averaged substrate concentrations compared to batch or plug-flow reactors (Tufvesson et al., 2010). One solution is to use multiple CSTRs in series, although this is an option rarely applied in industrial processing due to high capital costs and low flexibility. Hence, alternative reactor technologies have to be considered if the benefits of plug-flow hydrodynamics and continuous manufacturing are to be combined with effective oxygen supply.

The agitated cell reactor (ACR) is one such reactor that enables multiphase mixing in a macro-scale flow reactor (Fig. 1). The reactor consists of a reactor block with ten equally sized cells interconnected by small channels. Each cell is covered by a borosilicate window, to allow visual inspection of the reaction medium, or alternatively by a front entrance port to take-out, or introduce, a liquid or gas stream. Mechanical mixing is induced by freely moving agitators (e.g., spring or cylindrical agitators) placed in each cell of the reactor. The agitator is not moved using a shaft, as for most mechanically stirred reactors, but by lateral shaking of the reactor body (Browne et al., 2011). Theoretically, the intense mixing allows each of the ten cells to perform as a CSTR, whereby the flow profile through the reactor should approach plug-flow behavior.

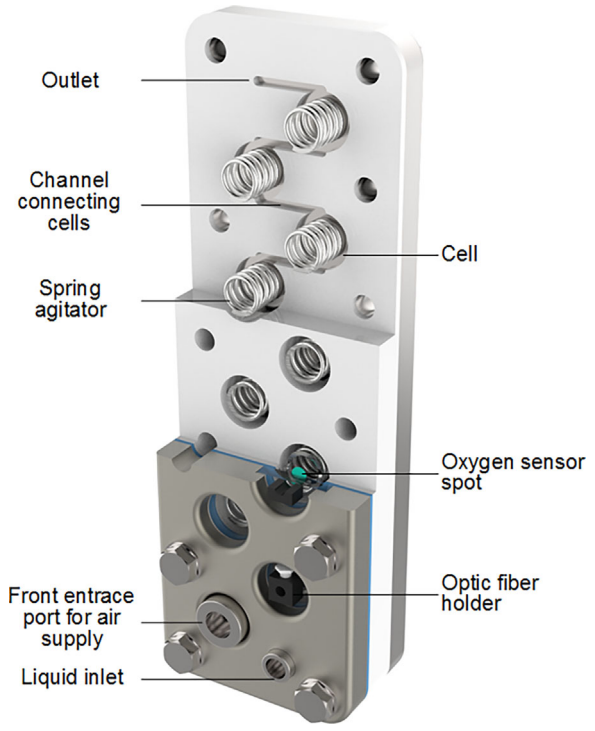

Figure 1. Agitated cell reactor with high shear spring agitators and oxygen sensor spots.

Previously, the versatility of the ACR has been demonstrated for a range of applications, such as continuous processing of slurries (Browne et al., 2011), hydrodechlorination of organic waste (Gómez-Quero et al., 2011), and functionalization of carbon nanotubes (Salice et al., 2012). A few examples also demonstrate the potential of the ACR for carrying out biocatalytic oxidation reactions (Gasparini et al., 2012; Jones et al., 2012). While demonstrating the broad potential of the reactor technology and apparent advantages compared to stirred tank reactors, the previous reports lack a detailed engineering analysis to enable benchmarking of the reactor concept against traditional processing methods. In particular, determination and evaluation of oxygen transfer rates are of key importance. Therefore, this paper reports the first characterization of the oxygen transfer in an ACR. Furthermore, reactor and kinetic models are applied to identify potential shortcomings of the reactor and enable comparison with alternative reactor technologies for performing biocatalytic oxidation reactions.

The oxidation of D-glucose to D-glucono-1,5-lactone, which spontaneously hydrolyses to D-gluconic acid under neutral and alkaline pH, catalyzed by glucose oxidase (EC 1.1.3.4, GOx) is used as a model reaction (Fig. 2). GOx is a relatively fast enzyme and, therefore, only at low enzyme concentrations is required to reach reaction rates where oxygen limitations can be observed. This makes the enzyme ideal when comparing the ACR with other reactor types such as a stirred tank reactor, since an understanding of the oxygen transfer capabilities is essential for running biocatalytic oxidations efficiently.

Materials and Methods

Reagents

Antifoam 204, sodium sulfite, potassium dihydrogen phosphate, dipotassium hydrogen phosphate, sodium hydroxide, D-glucose, and sodium D-gluconate were of the highest grade available from Sigma-Aldrich (St. Louis, MO). Catalase with an activity of 3308 U/mg (one unit (U) corresponds to the amount of enzyme that decomposes 1 μmol H_2O_2 per min at pH 7.0, 25 °C, 10.3 mM H_2O_2) was purchased from Sigma–Aldrich. Liquid formulated glucose oxidase from Aspergillus niger with an activity of 9670 GODU/g (glucose oxidase units; one unit corresponds to the amount of enzyme that produce 1 μmol H_2O_2 per minute at pH 5.6, 30 °C, 0.1 M acetate buffer, 90 mM glucose, measured by the ABTS/peroxidase reaction) was kindly supplied by Novozymes A/S (Bagsværd, Denmark).

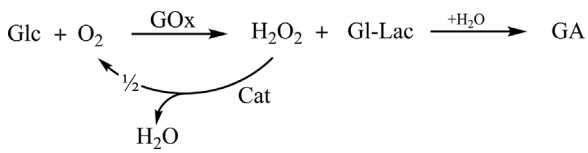

Figure 2. Oxidation of glucose (Glc) to glucono-1,5-lactone (Gl-Lac), which spontaneously hydrolyzes to gluconic acid (GA). The reaction is catalyzed by glucose oxidase (GOx) and the generated hydrogen peroxide is decomposed by catalase (Cat).

Analysis

The reaction was stopped by addition of sodium hydroxide to a final concentration of 0.5 M, the high pH ensured that the equilibrium between gluconic acid and glucono-1,5-lactone was completely shifted towards gluconic acid (Zhang et al., 2007). Samples were analyzed on a Thermo Fisher Scientific (Waltham, MA) Dionex Ultimate 3000 HPLC equipped with a Refractive Index (RI) detector. Glucose and gluconic acid were separated on a Phenomenex (Torrance, CA) Luna NH_2 column (5 μm, 100Å, 250 × 3.0 mm) using 20 mM H_3PO_4 as mobile phase (1 mL/min). The retention time of glucose and gluconic acid was 1.4 and 2.1 min, respectively.

Glucose Oxidase Kinetics

The kinetics for GOx catalyzed oxidation of glucose was investigated by recording the initial rate of reaction (5–25 min) at varying concentrations of glucose and oxygen. The experiments were conducted in a 250 mL stirred tank reactor (MiniBio with my-Control) from Applikon Biotechnology (Delft, The Netherlands). The reactor was equipped with a sintered metal sparger and two Rushton turbines (agitator diameter (D)/vessel diameter (T) ratio of 0.39) for mixing. Two mass-flow controllers were used to set the content of oxygen in the gas used for sparging to vary the dissolved oxygen concentration. The exact dissolved oxygen concentration was measured using a Solvent-Resistant Oxygen Probe (PyroScience Gmbh, Aachen, Germany). All initial rate experiments were conducted at 25 °C and pH 7.0, which was maintained using a 100 mM potassium phosphate buffer. GOx was applied in a concentration of 12.5 mg/L (121 U/L) and catalase was added in a concentration of 5 mg/L (16540 U/L) to ensure close to complete H_2O_2 degradation.

Batch Reactions

Complete oxidation of 100 mM glucose was conducted in the 250 mL reactors described above with a working volume of 150 mL. The reaction conditions were as follows: 400 mM potassium phosphate buffer, pH 7.0, 25 °C, 2 g/L GOx, 0.1 g/L catalase, 0.125 g/L Antifoam 204, 1000 rpm stirring, and sparging with 1 air volume per reactor volume per minute (vvm). The volumetric oxygen transfer coefficient, k_La, for the reactor was determined using the dynamic method (Garcia-Ochoa and Gomez, 2009).

Agitated Cell Reactor

Experiments were conducted in a 100 mL co-current Coflore® Agitated Cell Reactor (ACR, AM Technology, Manor Park, Runcorn, Cheshire, U.K.) equipped with high shear spring agitators. The total reactor volume, subtracting the volume of the spring agitators, was 92 mL. In all experiments, the lateral shaking speed was kept constant at 9 Hz (maximum shaking frequency) and the reactor block was heated to 25 °C using a recirculating heated water unit (Julabo, Seelbach, Germany). Solutions were fed to the first cell (bottom) of the ACR using an Ismatec Reglo ICC multi-channel peristaltic pump (Cole-Parmer GmbH, Wertheim, Germany). Air was also supplied to the first cell through a front entrance port at a constant flow rate of 100 mL/min (25 °C, 1 atm).

Residence time distribution (RTD) experiments were performed to study the hydrodynamics of the ACR. Initially the ACR was filled with a solution of 2 g/L GOx, 0.1 g/L catalase, and 0.125 g/L Antifoam 204 using the peristaltic pump, with an air supply rate of 100 mL/min (25 °C, 1 atm). At time zero the feed was changed to a solution consisting of 100 mM gluconic acid, 2 g/L GOx, 0.1 g/L catalase, and 0.125 g/L Antifoam 204. The cumulative RTD was recorded by analyzing samples from the outlet of the ACR taken at regular time intervals. The air flow rate was kept constant in all experiments.

Steady state experiments were performed with the following reaction conditions: 400 mM potassium phosphate buffer, pH 7.0, 25 °C, 2 g/L GOx, 0.1 g/L catalase, 0.125 g/l Antifoam 204, 100 mL/min (25 °C, 1 atm) air. A solution of glucose in buffer and an enzyme solution in buffer were pumped using the peristaltic pump and mixed immediately before entering the ACR to start the reaction. The concentration of oxygen was measured using Oxygen Sensor Spots (PyroScience Gmbh) that allow contactless measurement of oxygen through a transparent window. The sensor spots were glued to the inside of the compartment window while optical fibers were attached on the outside. In this way the fragile fibers were not in direct contact with the agitators, and the oxygen concentration could be measured over several weeks of experiments without signs of degradation of the sensor spots. Oxygen sensor spots were installed in cell numbers 2, 4, 7, and 10 of the ACR. The sensor spots were calibrated routinely by passing a 1% (w/w) sodium sulfite solution through the reactor to calibrate 0% air-saturation, and by passing buffer through the reactor with aeration to calibrate 100% air-saturation.

Samples from the outlet of the ACR for HPLC analysis were taken when steady state was achieved. Steady state defined as being achieved when the flow to the ACR had been maintained for minimum five residence times and the oxygen measurements in each cell were constant.

Reactor Modeling

The GOx catalyzed oxidation of glucose to gluconic acid can be described by ping-pong bi bi enzyme kinetics (Gibson et al., 1964). The rate of reaction as derived by the Kings-Altman method is given by Equation 1,

$$r = \frac{k_{cat} C_E C_G C_O}{C_G C_O + K_{MO} C_G + K_{MG} C_O} \quad (1)$$

where k_{cat} is the rate constant, K_{MG} and K_{MO} the Michaelis constant for glucose and oxygen, respectively, C_E, C_G, and C_O the concentration of enzyme, glucose, and oxygen, respectively.

When the oxidation is conducted in a batch reactor, the changing glucose concentration can be described by the mass balance for a batch reactor, as seen in Equation 2 combined with the Equation 3, describing the supply and consumption of oxygen including the oxygen regenerated using catalase,

$$\frac{dC_G}{dt} = -r \tag{2}$$

$$\frac{dC_O}{dt} = k_L a\left(C_O^{sat} - C_O\right) - \frac{r}{2} \tag{3}$$

where $k_L a$ is the volumetric mass transfer coefficient and C_O^{sat} is the concentration of oxygen at saturation with air.

The ACR is modelled using two different approaches: (i) using a tanks-in-series with back-mixing model, the so called backflow cell model (Roemer and Durbin, 1967), (Equations 4–7); and (ii) using a plug-flow reactor model (Equation 8–10). Figure 3 shows a schematic representation of the backflow cell model, where a constant backflow rate induces backmixing between cells. This enables the model to describe a system with hydrodynamic behavior changing with the liquid flow rate through the system. In the backflow cell model each of the ten cells of the ACR are assumed to be well mixed, that is no spatial variation in the liquid and gas phase concentrations.

$$\frac{dC_G^i}{dt} = \frac{v_L}{V_L}\left(C_G^{i-1} - C_G^i\right) + \frac{v_B}{V_L}\left(C_G^{i+1} + C_G^{i-1} - 2C_G^i\right) - r_i \tag{4}$$

$$\frac{dC_O^i}{dt} = \frac{v_L}{V_L}\left(C_O^{i-1} - C_O^i\right) + \frac{v_B}{V_L}\left(C_O^{i+1} + C_O^{i-1} - 2C_O^i\right) - \frac{r_i}{2} + k_L a\left(Hp_O^i - C_O^i\right) \tag{5}$$

$$\frac{dp_O^i}{dt} = \frac{v_g}{V_g}\left(p_O^{i-1} - p_O^i\right) - k_L a\left(Hp_O^i - C_O^i\right)\frac{V_L}{V_g}RT \tag{6}$$

$$V_L = \alpha \cdot v_L + \beta \tag{7}$$

where C_G^i,C_O^i, and p_O^i are the concentration of glucose, the concentration of dissolved oxygen, and the gas phase partial pressure of oxygen in cell "i", respectively. v_L is the liquid flow rate into the reactor, v_B is the constant backflow rate between cells, v_g is the gas flow rate into the reactor, V_L is the liquid volume in each cell, V_g is the gas volume in each cell, H is Henry's constant for oxygen, R is the ideal gas constant, and T is the temperature. Equation (7) describes the changing liquid volume in the ACR, which is modelled as a linear function of the liquid flow rate, where α is the slope and β is the intersection with the y-axis. The liquid volume is dependent only on the liquid flow rate, since the flow rate of gas (v_g) and the lateral shaking frequency were kept constant throughout the investigation.

A traditional plug-flow reactor (PFR) model was used for comparison, where both the gas and the liquid were assumed to flow as plugs through the reactor (i.e., without any axial mixing of fluid). The depletion of oxygen from the gas phase is modeled by taking the logarithmic mean of the oxygen partial pressure across the reactor (Equation 10). This method requires iterations when solving the equations, because the partial pressure of oxygen in the gas leaving the reactor is dependent on the consumption rate in the liquid phase, and vice versa.

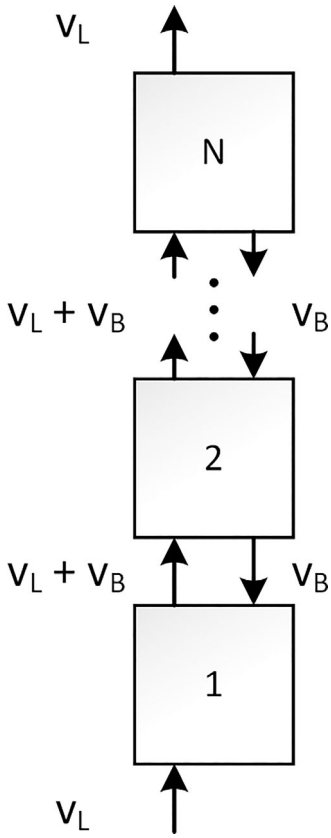

Figure 3. Schematic of the backflow cell model used to model the agitated cell reactor.

$$\frac{dC_G}{d\tau} = -r \tag{8}$$

$$\frac{dC_O}{d\tau} = k_L a\left(C_O^{sat} - C_O\right) - \frac{r}{2} \tag{9}$$

$$C_O^{sat} = H\frac{p_O^{in} - p_O^{out}}{\ln\left(p_O^{in}/p_O^{out}\right)} \tag{10}$$

Results and Discussion

Kinetic Model for Glucose Oxidase Catalyzed Oxidation of Glucose

Figure 4 shows the experimentally obtained initial rates of glucose oxidation using glucose oxidase at various glucose and oxygen concentrations. The ping-pong bi bi two substrate kinetic model was fitted to the data using non-linear regression. It is clear from the fit, that

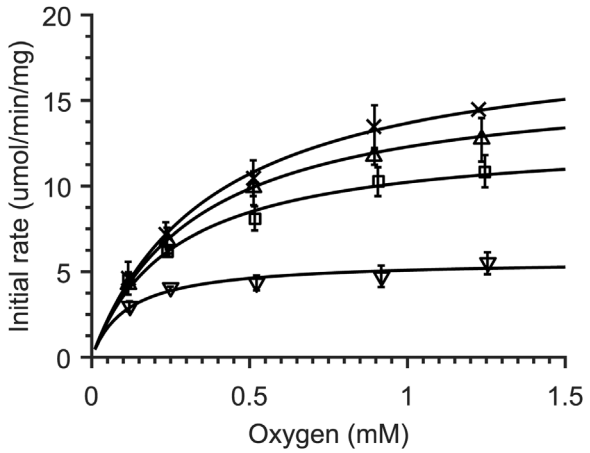

Figure 4. Initial rate of glucose oxidation by glucose oxidase at varying oxygen concentrations and constant glucose concentration of 25 mM (▽), 100 mM (Δ), 200 mM (□), and 400 mM (x) in a 250 mL stirred batch reactor sparged with 1 vvm oxygen/nitrogen mixture. The estimated kinetic parameters (k_{cat}, K_{MG}, K_{MO}) including 95% confidence intervals were 22.4 ± 2.1 μmol/min/mg, 73.8 ± 14.9 and 0.45 ± 0.09 mM, respectively.

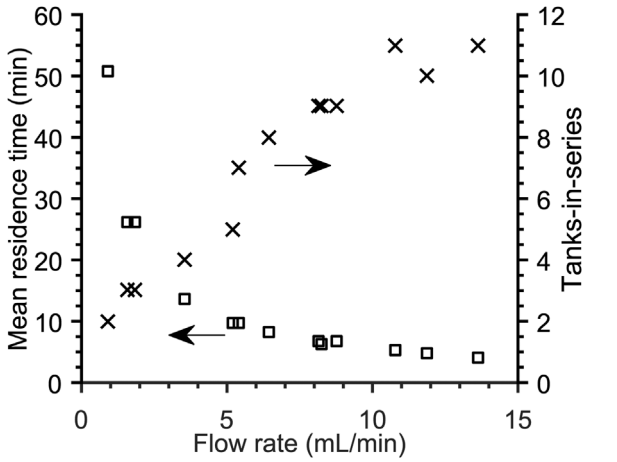

Figure 5. Calculated mean residence times (□) for varying liquid flow rates and number of tanks in series required to describe the residence time distribution (x). All experiments were performed with a constant air flow rate of 100 mL/min.

the model describes the data satisfactorily. The parameters in the kinetic model: rate constant, k_{cat}; the Michaelis constant for glucose, K_{MG}; and the Michaelis constant for oxygen, K_{MO} and their 95% confidence intervals were estimated to 22.4 ± 2.1 μmol/min/mg, 73.8 ± 14.9 and 0.45 ± 0.09 mM, respectively.

Reactor Model

The hydrodynamics in a series of CSTRs will approach that of PFR as the number of tanks-in-series increase. The ACR consists of ten intensively mixed compartments connected in series, and the flow profile would, therefore, be expected to resemble that of a PFR. Classical tracer experiments were performed in order to investigate if the standard PFR model could in fact be used to describe the hydrodynamics of the ACR when having a two-phase flow through the reactor. The concentration of tracer (gluconic acid) in the outlet of the ACR was measured after an introduction of a step change in inlet concentration. The obtained cumulative residence time distribution (RTD) was differentiated to obtain the exit age distribution, from which the mean residence time was calculated. Furthermore, the obtained distribution was compared with the theoretical distribution for n CSTRs in series in order to determine the number of tanks-in-series required to describe the hydrodynamics of the ACR. Interestingly and rather unexpectedly, the number of tanks-in-series required to describe the distributions varied significantly with the liquid flow rate (Fig. 5). At high liquid flow rates (9–14 mL/min) approximately ten tanks-in-series was required to describe the RTD, as one would expect based on the ACR design. However, as the liquid flow rate was lowered the required number of tanks in series decreased, and at the lowest liquid flow rate investigated (0.88 mL/min) only two tanks in series were necessary to describe the obtained RTD. In other words, the results show that the extent of back-mixing in the system increases with decreasing liquid flow rate. We reasoned that such a phenomenon could be explained by gas facilitated liquid transport from lower cells. At high liquid flow rates, the carry-over is insignificant due to the relatively high liquid flow rate through the reactor. Although, at low liquid flow rates the carry-over is higher than the liquid flow rate going into the system resulting in a significant reverse-flow from higher positioned cells to fulfill the mass-balance. This phenomenon is also seen in other gas-liquid reactors, such as bubble columns (Shah et al., 1978).

The lack of axial mixing between tanks is an often encountered shortcoming of the classical tanks-in-series model. The backflow cell model has therefore been proposed as an alternative to the typically applied dispersion model (Roemer and Durbin, 1967). Based on the observation from the RTD experiments, the backflow cell model appears to be able to describe the phenomenon of pronounced backmixing at low liquid flow rates observed in the ACR. Figure 3 shows a schematic of the model, where the increased upwards flow due to gas facilitated liquid transport is denoted ν_B. Additional liquid carried to upper compartments returns to lower positioned cells, thereby, inducing back-mixing. Since the gas facilitated liquid transport is assumed independent of the liquid flow rate going into the reactor, the extent of back-mixing will be high at low liquid flow rates while low at high liquid flow rates.

Based on the RTD, the mean residence time can be calculated and, by knowing the liquid flow rate, the liquid volume in the ACR can also be calculated. It was also seen that the liquid volume increased with increasing liquid flow rate (Fig. 6A), which was expected, since the constant flow rate of air resulted in a decrease in the air/liquid ratio entering the reactor. In order to incorporate the varying liquid volume in the backflow cell model, a linear correlation between liquid volume and liquid flow rate was assumed. By varying the slope (α) and intersection with the y-axis (β) of the linear correlation, together with the additional liquid flow rate between compartments (ν_B), the backflow cell model (consisting of 10 tanks-in-series) was successfully fitted to the experimentally obtained RTDs (Fig. 6B). The solid line in Figure 6A represents the linear

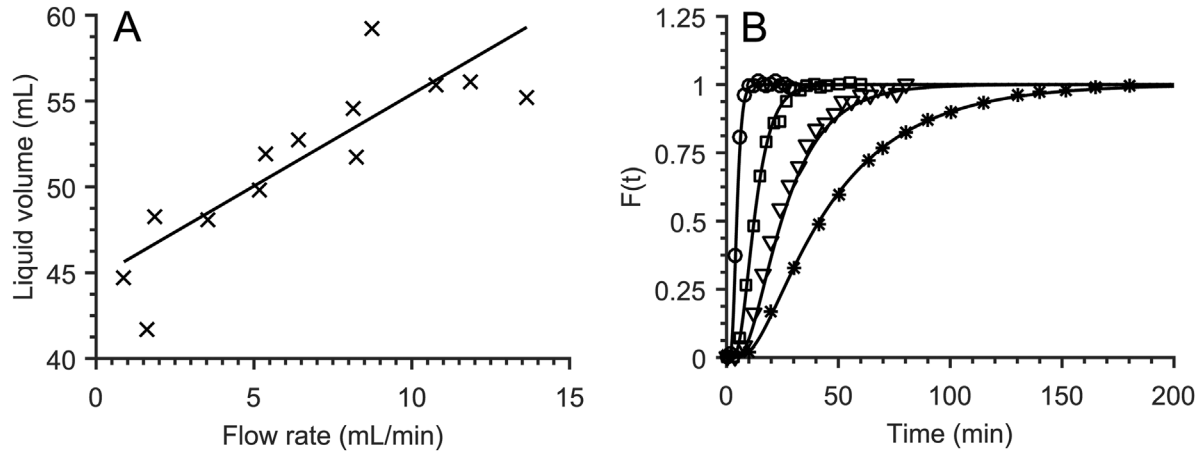

Figure 6. **A**. Calculated liquid volume of the ACR as a function of liquid flow rate. Solid line represents the varying volume in the backflow cell model. **B**. Fit of the backflow cell model with ten compartments to the experimentally obtained cumulative residence time distributions at different liquid flow rates: 0.88 mL/min (○), 1.6 mL/min (□), 3.5 mL/min (▽), 11.9 mL/min (*). The estimated model parameters (see Equations 4–7) including 95% confidence intervals was a v_B of 3.22±0.27 mL/min, an α of 1.07 ± 0.12 min, and a β of 44.7 ± 0.79 mL.

correlation between liquid volume and liquid flow rate resulting in the best fit to the experimental RTDs.

Oxygen Transfer Model

The volumetric mass transfer coefficient for oxygen (k_La) in a batch reactor was determined to be 104 h^{-1} at a stirring speed of 1000 rpm and an aeration rate of 1 vvm based on the direct method. Determination of the value of k_La in the ACR is more challenging, since the oxygen concentration, and therefore the oxygen consumption, changes through the reactor under different operating conditions. However, at an inlet concentration of 100 mM glucose, four steady-state measurements were obtained at different residence times, where the inline oxygen measurements showed insignificant spatial variation through the reactor (see Fig. 8). By taking the average of the oxygen measurements as the oxygen concentration throughout the reactor (e.g., 32.9 ± 7.8 μM for $\tau = 5.8$ min), it was possible to obtain an overall oxygen mass balance across the reactor. Based on the mass balance an average k_La for the ACR of 344 ± 44 h^{-1} was calculated based on the four steady-state values at residence times of 5.8, 10.4, 18.5, and 27.6 min, where the oxygen measurements varied less than 19.2 μM (7% air-saturation) through the reactor. It is assumed that the determined k_La is valid for all the investigated liquid flow rates, despite the changing liquid volume, which could change the interfacial area available for oxygen transfer. However, since the gas hold-up is large for all flow rates, it is not expected that the changes in liquid volume will affect the k_La to a great extent.

Experimental Validation of the Combined Model

The glucose oxidation reaction is strictly irreversible due to the instantaneous decomposition of glucono-1,5-lactone to gluconic acid and the decomposition of the hydrogen peroxide byproduct to water and oxygen. The kinetic model should therefore be valid for the full conversion range despite being developed based only on initial rates, Figure 7.

The enzyme needs to retain most of its activity during the course of the reaction for the kinetic model to be valid. Typically, GOx is a relatively stable enzyme (half-life of 10 h at 60 °C (Ye et al., 1988)). However, operational enzyme stability is often different from storage stability, especially when supplying oxygen using bubble aeration, where the gas-liquid interface in combination with shear effects deactivates some enzymes while others are not affected (Bommarius and Karau, 2005; Toftgaard Pedersen et al., 2015). In the case of GOx, one study reports a significantly increased rate of deactivation in the presence of an air-liquid interface (Betancor et al., 2005). However, more than 97% of the GOx activity could be recovered after one pass through the ACR at a residence time of

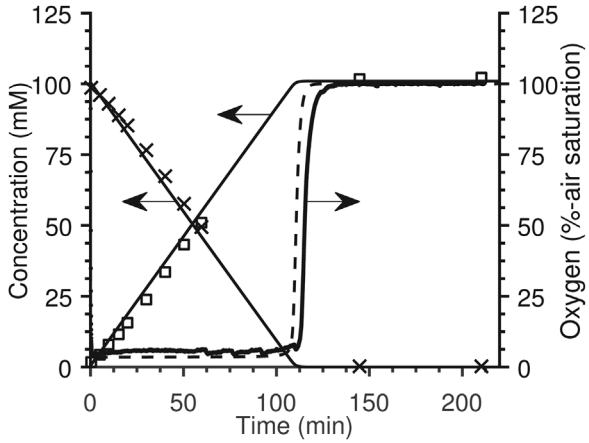

Figure 7. Oxidation of glucose in a 150 mL batch reactor. Concentration of glucose (x), gluconic acid (□), and oxygen (.). Solid lines represents model prediction of glucose and gluconic acid, dashed line represents model prediction of oxygen concentration. 100 mM glucose, 1000 rpm, 1 vvm aeration using air.

47 min, the longest residence time investigated (data not shown), although the high shear experienced in the ACR could increase the deactivation rate beyond what is normally experienced. Furthermore, the good fit of the kinetic model to the batch reaction data indicates that little deactivation of GOx occurred during the reaction.

By combining the kinetic model, the reactor model, and the model for oxygen transfer, a system of equations describing the time course for the glucose oxidation in the ACR can be obtained (see Reactor Modeling Section). The validity of the combined ACR model was tested against a series of steady-state measurements at different residence times as seen in Figures 8 and 9 at an inlet concentration of 100 and 25 mM glucose, respectively. Additionally, the experimental data was compared with the prediction of a PFR model in order to investigate if the non-ideal and changing hydrodynamics observed in the tracer experiments would have an effect on the predicted conversion in the ACR. Surprisingly, both reactor models were capable of describing the glucose and gluconic acid concentration profiles, despite the clear non plug-flow hydrodynamics observed in the RTD experiments. It would be expected that the two models act very similarly at high flow rates (low residence times) since the backflow cell model here would approach ten CSTRs in series and therefore almost an ideal PFR. However, at low flow rates (high residence times) the backflow cell model behaves as two CSTRs in series and hence large deviations from the PFR model would have been expected. Interestingly, the reason for the small differences between the backflow cell model and the PFR model is found in the kinetics of the enzymatic reaction. GOx has a relatively high Michaelis constant for oxygen (0.45 mM) compared to the solubility of oxygen in water (0.27 mM, 1 atm., 25 °C). At the operating conditions for the ACR, the oxygen concentration is approximately 0.03 mM when the majority of the reaction occurs. This means that the enzyme is far from saturated with oxygen, which results in the oxidative part of the catalytic cycle being rate limiting. In other words, the apparent Michaelis constant for glucose is reduced significantly, at an oxygen concentration of 0.03 mM this corresponds to a reduction from 73.8 to 4.96 mM. The oxidation reaction is, therefore, practically zero order with respect to glucose until almost all glucose has been converted, while the reaction is first order in the concentration of oxygen. Since the dissolved oxygen concentration profile in the two models will be almost identical, since oxygen is transferred in the entire reactor and the oxygen consumption rate is constant due to the zero order dependency of the reaction rate on the glucose concentration, the reaction will proceed at an almost equal rate whether the liquid phase hydrodynamics of the reactor is plug-flow or well mixed. It is not until the glucose concentration drops to a level where the enzyme is no longer saturated with glucose, that the differences in hydrodynamics are visible in the concentration-time profile for glucose and gluconic acid.

Figures 8 and 9 also show the steady-state oxygen concentrations measured in cell number 2, 4, 7, and 10 in the ACR. In the predicted oxygen concentration, the difference between the backflow cell model and the PFR model are evident. The backflow cell model is capable of predicting the oxygen concentration and the general trends slightly better than the PFR model, even though the differences between the two models are small.

The differences between the PFR model and the proposed backflow cell model are small when using GOx at the applied conditions. The largest difference observed was 2.3 mM (corresponding to 2.4% difference in the predicted product concentration) at a residence time of 37 min and an inlet glucose concentration of 100 mM. An in silico analysis was conducted using the two models to further investigate if the difference between the backflow cell model and the PFR model would be significant at reaction conditions not investigated experimentally. The largest

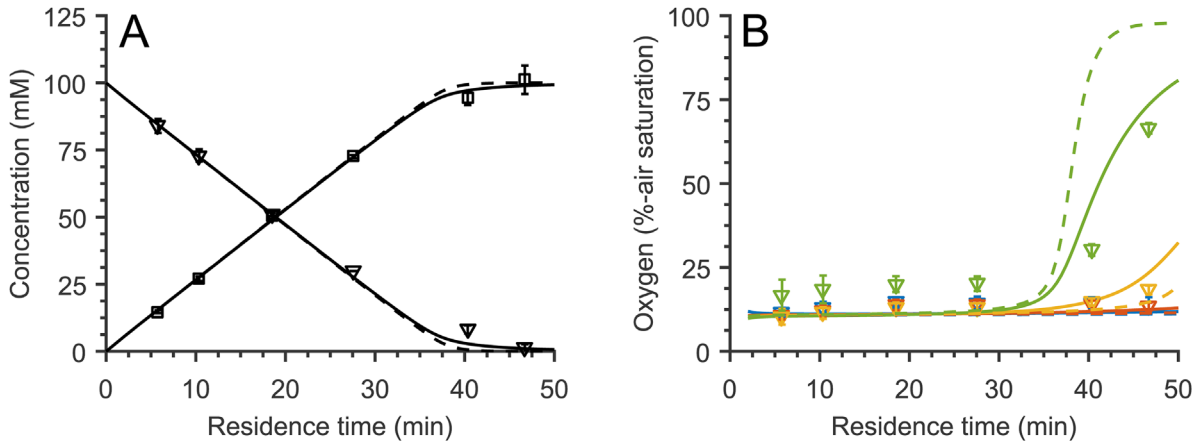

Figure 8. Oxidation of 100 mM glucose in the agitated cell reactor. **A**. Steady-state concentrations of glucose (▽) and gluconic acid (□) in the outlet of the agitated cell reactor at different residence times. Each data point is an average of three samples taken with 5 min intervals. Error bars indicate ±2 S.D. **B**. Steady-state oxygen concentrations in cell number 2 (blue), 4 (red), 7 (yellow), and 10 (green) at different residence times. Each data point is an average over 15 min. Error bars indicate ±2 S.D. Solid lines represent backflow cell model prediction while dashed lines represent the plug-flow model prediction.

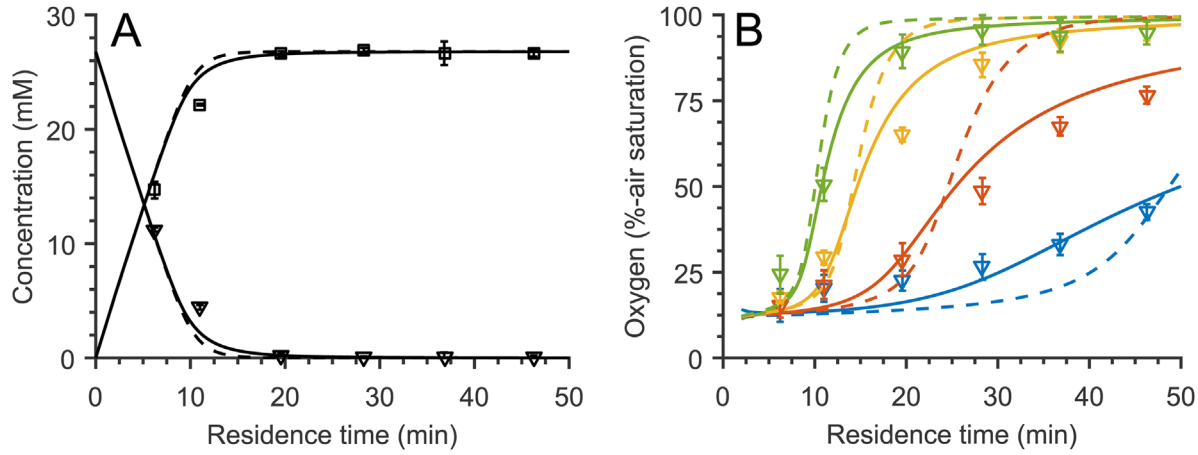

Figure 9. Oxidation of 25 mM glucose in the agitated cell reactor. **A**. Steady-state concentrations of glucose (▽) and gluconic acid (□) in the outlet of the agitated cell reactor at different residence times. Each data point is an average of three samples taken with 5 min intervals. Error bars indicate ±2 S.D. **B**. Steady-state oxygen concentrations in cell number 2 (blue), 4 (red), 7 (yellow), and 10 (green) at different residence times. Each data point is an average over 15 min. Error bars indicate ±2 S.D. Solid lines represent backflow cell model prediction while dashed lines represent the plug-flow model prediction.

hydrodynamic difference was observed at the lowest liquid flow rate through the reactor, that is 1 mL/min to ensure the validity of the proposed model, where the backflow cell model will approach the hydrodynamic of two CSTRs in series. Figure 10 shows the maximum difference between the two models at a given set of kinetic constants. The amount of enzyme, or k_{cat}, yielding the largest difference varies depending of the kinetic constants and the inlet concentration of substrate. The maximal difference between the two models is observed at low values of K_{MO} and high values of K_{MG}, where the enzyme kinetics is first order in glucose and zero order in oxygen. Here a deviation as high as 13.5% is possible, clearly showing the error introduced if the validity of the PFR model is assumed. Nevertheless, for reactions operated at low K_{MG}/c_0 ratios, as many industrial processes are, the error introduced by using the PFR model is limited, as long as the change in reactor volume occupied by liquid with liquid flow rate is taken into account.

Comparison of Batch Reactor and Agitated Cell Reactor

A residence time in the ACR of 47 min was required to reach full conversion of 100 mM glucose, compared to a total time of reaction of 110 min in the batch reactor. The faster reaction rate in the ACR can solely be ascribed to the improved oxygen transfer, caused by the intensively mixed reactor cells, corresponding to a k_La of 344 h^{-1} in the ACR, compared to 104 per h in the batch reactor. However, the relatively high oxygen transfer coefficient in the ACR comes at a cost of significant power consumption through the use of compressed air for moving the reactor block. The ACR is specified to use 0.09 m^3/min of air compressed at 3 bar, which translates into an isothermal decompression energy of 0.5 kW. If all energy was transferred to the reaction fluid, this would correspond to an energy input of 5 kW/L. However, in reality only a fraction of the energy will be dissipated into the reaction liquid, since significant energy losses are expected in the mixing. Without knowing the actual power input to the reaction liquid, it is difficult to compare the efficiency of mixing (i.e., the k_La relative to the power input) of the ACR to the batch reactor operating with a power input of approximately 1.1 W/L. Nevertheless, the large power consumptions of the ACR will become a significant problem upon scale-up, unless a more efficient mixing method is considered.

Counterintuitively, the volumetric oxygen transfer coefficient, k_La, in stirred tank reactors increases with scale for non-viscous reaction media, when keeping geometry, aeration rate (in vvm), and power input constant (Garcia-Ochoa and Gomez, 2009; Stocks, 2013). This is predominantly caused by an increased superficial gas velocity that results in a larger gas hold-up, whereby the specific interfacial area

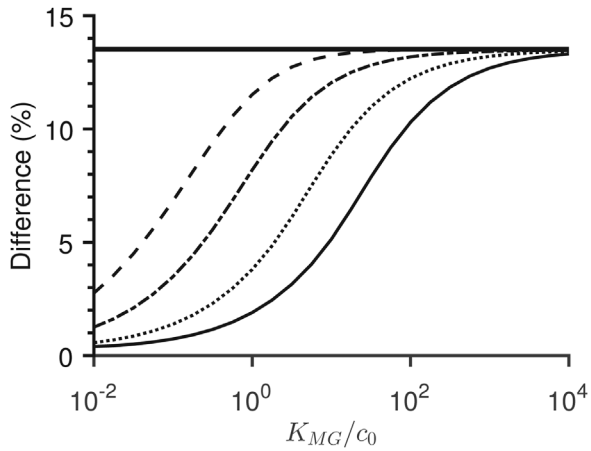

Figure 10. Maximum deviation in predicted product concentration between backflow cell model and the PFR model at a liquid flow rate of 1 mL/min (lower validity boundary of model) and varying values of K_{MO}: 10^{-9} mM (–), 0.1 mM (-.), 1 mM (..), 5 mM (—). Top line is deviation for a reaction being first order in glucose and zero order in oxygen.

available for mass transfer increases (Nienow et al., 1994). Typically, the limitation to k_La is set by the amount of power physically possible to supply to a large scale stirred tank. For industrial scale aerobic bioreactors ($\approx 100\,m^3$) a k_La value of approximately $500\,h^{-1}$ can be expected for low viscosity reaction media (Charles, 1985). For the ACR, a similar increase in k_La upon scale-up cannot be expected, primarily because the gas hold-up in the small scale already is high (35–50% at the conditions investigated) and therefore a small additional increase has limited influence on the gas-liquid interfacial area. Hence, it is not expected that the advantage of increased mass transfer seen for the ACR, compared to a laboratory batch reactor, can be translated into a similar advantage at a larger scale.

Although the ACR may not be the prime candidate for scale up to kilo-ton production of chemicals, the technology offers potential as a production platform for the production of lower volume compounds based on oxygen dependent biocatalysis. The above analysis shows that the oxygen transfer capabilities of the technology are greater than, or in the same order of magnitude upon scale up, as for stirred tank reactors. With a k_La of $344\,h^{-1}$ the ACR would be able to sustain a maximum volumetric productivity of 18.5 g/L/h for an oxidase reaction (assuming a product M_w of 100 g/mol and maximum driving force using air). The ACR, or scaled up versions of it, can therefore be an alternative to traditional reactors when continuous operation is desired. Additionally, the reactor could be used as a high k_La laboratory platform for evaluation of new enzymatic reactions with large oxygen requirements.

Conclusion

The agitated cell reactor (ACR) was successfully used to perform the biocatalytic oxidation of glucose to glucono-1,5-lactone catalyzed by glucose oxidase. A significant improved oxygen transfer rate was observed in the 100 mL ACR compared to a batch reactor of similar volume, resulting in shorter processing times and more efficient use of the biocatalyst. Although the hydrodynamics of the ACR proved to be highly non-ideal when processing a gas-liquid mixture, it was shown that this had little effect on the overall concentration-time profile, due to the high Michaelis constant for oxygen (K_{MO}) relative to the saturation concentration of oxygen. Nevertheless, the importance of the non-ideal hydrodynamics was illustrated when using enzymes with low K_{MO}, especially if operating at a high ratio of Michaelis constant for the primary substrate (K_{MG}) to initial substrate concentration.

The research leading to these results has received funding from the European Union's Seventh Framework Programme for research, technological development and demonstration under grant agreement n° 613849 supporting the project BIOOX.

References

Baxendale IR, Braatz RD, Hodnett BK, Jensen KF, Johnson MD, Sharratt P, Sherlock JP, Florence AJ. 2014. Achieving continuous manufacturing: Technologies and approaches for synthesis, workup, and isolation of drug substance. J Pharm Sci 104:781–791.

Betancor L, Fuentes M, Dellamora-Ortiz G, López-Gallego F, Hidalgo A, Alonso-Morales N, Mateo C, Guisán JM, Fernández-Lafuente R. 2005. Dextran aldehyde coating of glucose oxidase immobilized on magnetic nanoparticles prevents its inactivation by gas bubbles. J Mol Catal B Enzym 32:97–101.

Bommarius AS, Karau A. 2005. Deactivation of Formate Dehydrogenase (FDH) in solution and at gas-liquid interfaces. Biotechnol Prog 21: 1663–1672.

Browne DL, Deadman BJ, Ashe R, Baxendale IR, Ley SV. 2011. Continuous flow processing of slurries: Evaluation of an agitated cell reactor. Org Process Res Dev 15:693–697.

Charles M. 1985. Fermentation scale-up: Problems and possibilities. Trends Biotechnol 3:134–139

Garcia-Ochoa F, Gomez E. 2009. Bioreactor scale-up and oxygen transfer rate in microbial processes: An overview. Biotechnol Adv 27:153–176

Gasparini G, Archer I, Jones E, Ashe R. 2012. Scaling up biocatalysis reactions in flow reactors. Org Process Res Dev 16:1013–1016.

Gibson QH, Swoboda BEP, Massey V. 1964. Kinetics and mechanism of action of glucose oxidase. J Biol Chem 239:3927–3934.

Gómez-Quero S, Cárdenas-Lizana F, Keane M a. 2011. Liquid phase catalytic hydrodechlorination of 2,4-dichlorophenol over Pd/Al2O3: Batch vs. continuous operation. Chem Eng J 166:1044–1051.

Gutmann B, Cantillo D, Kappe CO. 2015. Continuous-flow technology—A tool for the safe manufacturing of active pharmaceutical ingredients. Angew Chemie — Int Ed 54:6688–6728.

Jones E, McClean K, Housden S, Gasparini G, Archer I. 2012. Biocatalytic oxidase: Batch to continuous. Chem Eng Res Des 90:726–731.

Kroutil W, Mang H, Edegger K, Faber K. 2004. Biocatalytic oxidation of primary and secondary alcohols. Adv Synth Catal 346:125–142.

Nienow AW, Hunt G, Buckland BC. 1994. A fluid dynamic study of the retrofitting of large agitated bioreactors: Turbulent flow. Biotechnol Bioeng 44: 1177–1185.

Pickl M, Fuchs M, Glueck SM, Faber K. 2015. The substrate tolerance of alcohol oxidases. Appl Microbiol Biotechnol 99:6617–6642.

Roberge DM, Zimmermann B, Rainone F, Gottsponer M, Eyholzer M, Kockmann N. 2008. Microreactor technology and continuous processes in the fine chemical and pharmaceutical industry: Is the revolution underway? Org Process Res Dev 12:905–910.

Roemer MH, Durbin LD. 1967. Transient response and moments analysis of backflow cell model for flow systems with longitudinal mixing. Ind Eng Chem Fundam 6:120–129.

Salice P, Fenaroli D, de Filippo CC, Menna E, Gasparini G, Maggini M. 2012. Efficient functionalization of carbon nanotubes: An opportunity enabled by flow chemistry. Chem Oggi 30:37–39.

Shah YT, Stiegel GJ, Sharma MM. 1978. Backmixing in gas-liquid reactors. AIChE J 24:369–400.

Stocks SM. 2013. Industrial enzyme production for the food and beverage industries: Process scale up and scale down. In: Microb. Prod. Food Ingredients, Enzym. Nutraceuticals. Cambridge, UK: Woodhead Publishing Limited. p 144–172.

Toftgaard Pedersen A, Birmingham WR, Rehn G, Charnock SJ, Turner NJ, Woodley JM. 2015. Process requirements of galactose oxidase catalyzed oxidation of alcohols. Org Process Res Dev 19:1580–1589.

Tomaszewski B, Schmid A, Buehler K. 2014. Biocatalytic production of catechols using a high pressure tube-in-tube segmented flow microreactor. Org Process Res Dev 18:1516–1526.

Tufvesson P, Fu W, Jensen JS, Woodley JM. 2010. Process considerations for the scale-up and implementation of biocatalysis. Food Bioprod Process 88:3–11.

Wiles C, Watts P. 2012. Continuous flow reactors: A perspective. Green Chem 14:38–54.

Wohlgemuth R, Plazl I, Žnidaršič-Plazl P, Gernaey KV, Woodley JM. 2015. Microscale technology and biocatalytic processes: Opportunities and challenges for synthesis. Trends Biotechnol 33:302–314.

Ye WN, Combes D, Monsan P. 1988. Influence of additives on the thermostability of glucose oxidase. Enzyme Microb Technol 10:498–502.

Zhang Z, Gibson P, Clark SB, Tian G, Zanonato PL, Rao L. 2007. Lactonization and protonation of gluconic acid: A thermodynamic and kinetic study by potentiometry, NMR and ESI-MS. J Solution Chem 36:1187–1200.

Organic Process Research & Development

Article

pubs.acs.org/OPRD

Process Requirements of Galactose Oxidase Catalyzed Oxidation of Alcohols

Asbjørn Toftgaard Pedersen,[†] William R. Birmingham,[‡] Gustav Rehn,[†] Simon J. Charnock,[§] Nicholas J. Turner,[‡] and John M. Woodley*[,†]

[†]Department of Chemical and Biochemical Engineering, Technical University of Denmark, DK-2800 Kgs. Lyngby, Denmark

[‡]School of Chemistry, University of Manchester, Manchester Institute of Biotechnology, 131 Princess Street, Manchester, M1 7DN, United Kingdom

[§]Prozomix Ltd, Station Court, Haltwhistle, Northumberland NE49 9HN, United Kingdom

ABSTRACT: Biocatalytic oxidation reactions have the potential to substitute many chemically catalyzed oxidations in the pharmaceutical and fine chemical industry due to their superior regio- and stereoselectivity and low environmental impact. Galactose oxidase (GOase) has been shown to be a promising biocatalyst for the oxidation of primary and secondary alcohols to their corresponding aldehydes and ketones, respectively. However, GOase requires a number of additives to sustain its catalytic function, such as the enzyme catalase for degradation of the byproduct hydrogen peroxide as well as single-electron oxidants to reactivate the enzyme upon loss of the amino acid radical in its active site. In this work, the addition of catalase, single-electron oxidants, and copper ions was investigated systematically in order to find the minimum concentrations required to obtain a fully active GOase. Furthermore, it was found that the concentration and type of buffer is essential for the activity of GOase, which was significantly more active in sodium phosphate buffer than in other buffers investigated. Enzyme stability and oxygen requirements are of crucial importance for the implementation of oxidase based processes. GOase was shown to be completely stable for 120 h in buffer with stirring at 25 °C, and the activity even increased 30% if the enzyme solution was also aerated in a similar experiment. The high K_m for oxygen of GOase (>5 mM) relative to the solubility of oxygen in water reveals a trade-off between supplying oxygen at a sufficiently high rate and ensuring a high degree of enzyme utilization (i.e., ensuring the highest possible specific rate of reaction). Nevertheless, the good stability and high activity of GOase bode well for its future application as an industrial biocatalyst.

INTRODUCTION

Oxidation reactions are one of the most important types of reactions in industrial chemistry. Bulk industrial scale oxidations are frequently conducted using noble metal catalysts and readily available oxidants such as molecular oxygen or hydrogen peroxide.[1] In contrast, the pharmaceutical and fine chemical industry mainly employs stoichiometric amounts of inorganic oxidants to supply the required redox equivalents. However, these reactions typically have poor selectivity and a large environmental impact due to extensive waste generation, the use of solvents with a poor environmental profile, and the requirements for additional synthetic steps for protection and deprotection of labile functional groups.[2,3] Biocatalysis may help to overcome many of the limitations experienced in the fine chemical industry, as a result of the regio- and stereoselective nature of enzymatic reactions and their environmentally benign operating conditions.[4,5] In nature, redox reactions are catalyzed by oxidoreductases (EC 1), such as dehydrogenases, oxygenases, oxidases, and peroxidases, and include several reaction types of high industrial importance.

The copper-dependent enzyme galactose oxidase (GOase, EC 1.1.3.9) is an example of an industrially relevant oxidase that naturally catalyzes the oxidation of the C6 hydroxyl group of D-galactose to the corresponding aldehyde, while simultaneously reducing molecular oxygen to hydrogen peroxide (Figure 1a).[6−8] GOase and mutants thereof catalyze oxidations of a wide range of substrates with potential industrial application.[9,10] First, GOase can be used to modify naturally occurring polysaccharides with terminal galactose moieties (or other saccharides through GOase mutants) by oxidizing the C6 hydroxyl groups and enabling further chemical or enzymatic modifications of the aldehyde such as amination.[11−14] Second, GOase can be applied in the synthesis of a range of industrially relevant compounds containing ketones and aldehydes, such as diformylfuran obtained by selective oxidation of 5-hydroxymethylfurfural.[15,16] Finally, GOase mutants able to enantioselectively oxidize secondary alcohols enable the use of the

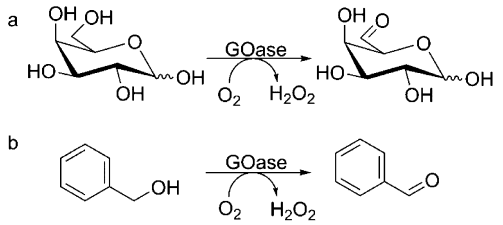

Figure 1. Examples of oxidations catalyzed by galactose oxidase (GOase). (a) Oxidation of galactose. (b) Oxidation of benzyl alcohol.

Special Issue: Oxidation and Oxidative Reactions

Received: September 6, 2015
Published: October 8, 2015

DOI: 10.1021/acs.oprd.5b00278
Org. Process Res. Dev. 2015, 19, 1580−1589

enzyme for kinetic resolution of racemic mixtures of secondary alcohols.[17]

The substrate specificity of wild-type GOase is rather restricted; it accepts galactose-containing polysaccharides and also some primary alcohols such as dihydroxyacetone and benzyl alcohol.[10,18] A great effort has therefore been put into modifying galactose oxidase via mutagenesis to broaden its substrate specificity.[17,19,20] A variety of altered substrate specificities for GOase variants have been reported in the scientific literature, such as increased galactose activity,[20] novel glucose 6-OH activity,[21] increased fructose 6-OH activity,[19] increased activity on mannose and *N*-acetylglucose,[22] and activity toward a range of secondary alcohols.[17,21] A particularly interesting GOase mutant is the M_{3-5} variant described by Escalettes and Turner,[17] which is able to selectively oxidize the *(R)*-enantiomer of secondary benzylic alcohols to the corresponding ketones. M_{3-5} GOase is capable of accepting a range of primary and secondary alcohols, and compared to the wild-type enzyme, the activity toward nonpolar substrates is significantly increased.

The GOase used in this study was produced intracellularly in *E. coli* and is therefore not loaded with copper during the fermentation and expression, due to the toxicity of copper toward E. *coli* at the concentrations required to ensure full saturation of GOase. After cell disruption and centrifugation, copper can be loaded into the apoenzyme through dialysis against copper-containing buffer or more simply by adding copper(I/II) salts to the reaction mixture.[23,24] The two-electron oxidation catalyzed by GOase is accomplished by an active site composed of a tyrosine radical coordinated to a copper(II) ion, which during oxidation of the substrate is reduced to a nonradical tyrosine copper(I) complex (Figure 2).[7,8] Subsequently, copper is reoxidized and the radical reformed by reduction of molecular oxygen to hydrogen peroxide. The tyrosine radical readily undergoes single-electron reduction to form an inactive nonradical copper(II) complex. The inactive form of GOase can be reactivated by further reduction to form the active copper(I) complex or reformation of the radical by single-electron oxidation.[7] In practice, only reoxidation, and not further reduction, of the inactive state is performed to ensure a fully active enzyme, typically using mild chemical oxidants such as potassium ferricyanide ($K_3[Fe(CN)_6]$). However, it has also been shown that protein based single-electron oxidants such as peroxidases can regenerate the active radical center.[25,26] Hydrogen peroxide formed during catalysis has been shown to inhibit and inactivate GOase,[27,28] thus removal of hydrogen peroxide is a necessity for enzymatic function. This is most effectively done using catalase, which breaks down one mole of hydrogen peroxide to one mole of water and half a mole of oxygen. This reduce the stoichiometric oxygen requirements of the overall reaction by half and hence the oxygen requirements of the process.

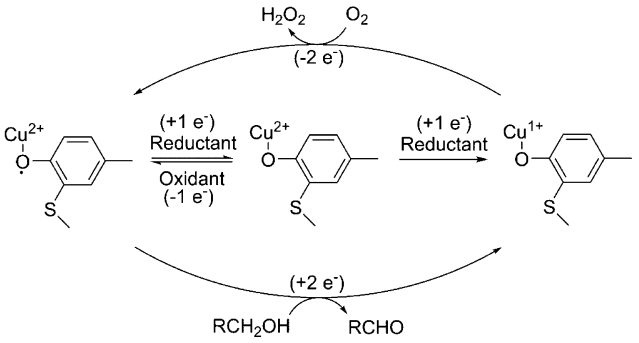

Figure 2. Catalytic cycle of GOase including the reduction to the semioxidized inactive form. The active site is simplified to only shown the copper-Tyr272 coordination. Adapted with permission from ref 8. Copyright 2003 American Chemical Society.

As more chemical and biological additives are required to ensure an effective biocatalytic process, process development and implementation becomes more complicated. Despite the complexity of the reaction system, a systematic investigation into the requirements of additives for GOase is lacking in the scientific literature. Therefore, the present study has investigated the role of additives required for a successful biooxidation reaction based on GOase, as well as the implications these have on process development and implementation. To do this, the oxidation of benzyl alcohol to benzaldehyde was used as a model system (Figure 1b), because it displays many of the challenges associated with other more industrially relevant reactions, such as low solubility of substrates/products, volatile reaction components, unnatural substrates for the enzyme, and requirements for sufficient oxygen transfer. The investigation focused on two different enzyme purity levels: one being highly purified enzyme as it normally is used in early stage protein characterization, and the second being a crude cell-free extract, which is a type of preparation more relevant for industrial scale application.

Oxygen supply is essential for oxygen-dependent enzyme catalysis and can become a limiting factor upon scale-up of biocatalytic oxidation reactions.[29] Additionally, the supply of oxygen through bubbling with air may significantly increase the deactivation rate of some enzymes.[30−32] Analysis of the enzyme stability in the presence of a gas−liquid interface and the influence of the oxygen concentration in solution on the reaction rate is therefore essential when evaluating the potential of a biooxidation process. In the present work, this analysis has been performed for GOase on the basis of experimental data for the model system studied.

RESULTS AND DISCUSSION

Purified Enzyme. *pH Optimum.* The optimum pH for GOase M_{3-5} was determined in a standard liquid phase horseradish peroxidase (HRP)/ABTS coupled assay, varying only the reaction pH from 6.0 to 8.0 in sodium phosphate buffer (NaPi). The highest activity was observed at pH 7.0−8.0 for oxidation of benzyl alcohol (Figure 3a). Given this activity range, all subsequent experiments with both purified GOase and GOase in crude lysate were performed at pH 7.4.

Activation by Horseradish Peroxidase. HRP has long been known to activate GOase.[26,33] Although the mechanism of the phenomenon is not fully understood, it can nonetheless be exploited as a means of increasing GOase activity to shorten conversion time in a biocatalytic reaction. Because a high requirement of HRP could potentially be cost prohibitive for a scaled process, it is of financial interest to identify the minimal amount of HRP required to fully activate GOase. Type IV HRP is a common form of HRP used in coupled assays with a chromogenic substrate to monitor the formation of H_2O_2. Type I HRP, an isoenzyme form of HRP, was used as a comparison for activation of the purified enzyme. Because of the low and varied amount of HRP used in the activation experiments, a typical HRP/ABTS assay could not be used to measure GOase activity. Instead, titration of GOase activation by HRP was

DOI: 10.1021/acs.oprd.5b00278
Org. Process Res. Dev. 2015, 19, 1580−1589

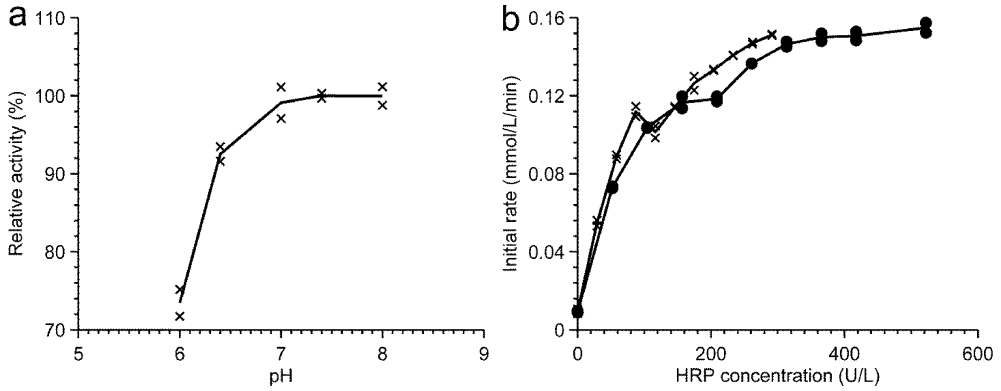

Figure 3. (a) Effect of pH on the activity of purified GOase in 50 mM NaPi. (b) Effect of two different isoenzymes of horseradish peroxidase (HRP) on the activity of purified GOase. Type I (x), Type IV (●).

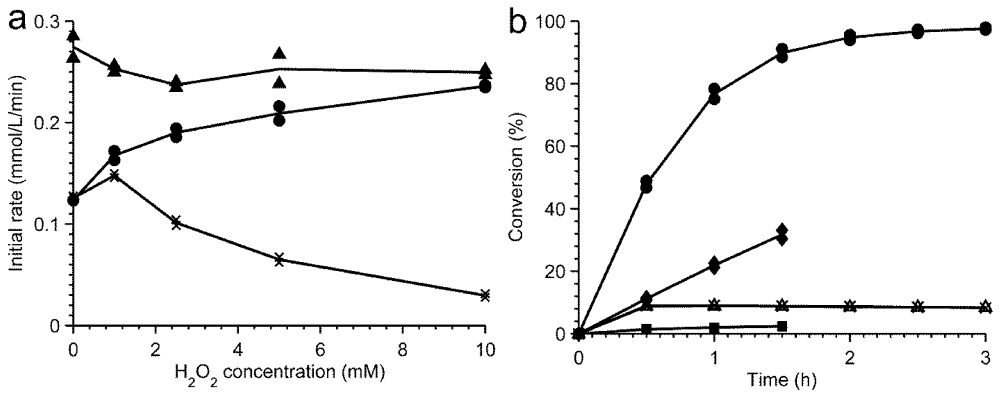

Figure 4. (a) Effect of hydrogen peroxide on the activity of purified GOase. GOase was incubated with indicated concentrations of H_2O_2 for 10 min, after which the reaction was started by addition of substrate (x), catalase (to break down all H_2O_2) and then substrate (●), catalase and additional H_2O_2 to bring the total addition up to 10 mM, and then substrate (▲). (b) Effect of catalase and horseradish peroxidase (HRP) on conversion of 25 mM benzyl alcohol. (●) HRP and catalase added, (♦) catalase but not HRP added, (■) no catalase or HRP added, (Δ) HRP but no catalase added, (x) HRP added, catalase added after 1.5 h.

performed in a cuvette-based assay measuring the formation of NADPH through oxidation of the benzaldehyde product to benzoic acid by an aldehyde dehydrogenase. Activation of 0.0078 mg/mL GOase M_{3-5} reached a maximum in the initial rate of 0.15 mmol/L/min in the presence of 365 U/L type IV HRP, whereas 291 U/L of type I HRP was needed to reach the same level of activity (Figure 3b). This is compared to an initial rate of 0.0094 mmol/L/min in the absence of HRP. In addition to demonstrating the ability of different types of HRP to activate GOase, the 16-fold increase in specific activity over the samples with no HRP present shows that activation is essential for a high rate of catalysis.

Effect of H_2O_2 and Protection by Catalase. Previous studies have demonstrated that the wild type GOase is irreversibly inactivated by H_2O_2, accumulating as a byproduct of alcohol oxidation, although inactivation only occurs during catalysis, and the enzyme is actually stable when exposed to H_2O_2 under resting conditions.[28] To confirm that these observations similarly apply to the GOase M_{3-5} construct containing a series of mutations, in which particular concern is the addition of an oxidizable active site methionine residue, the enzyme was incubated in the presence of various concentrations of H_2O_2 and then assayed either with H_2O_2 present or after removal by catalase. Specific activity measurements clearly indicate a loss in GOase activity in a concentration-dependent manner only when H_2O_2 remains in the reaction during catalysis (Figure 4a). The samples that were treated with catalase showed increasing activity with increasing concentration of H_2O_2, which initially suggested another form of activation event within this system. However, this activity increase was the result of higher concentrations of dissolved oxygen in the buffer after H_2O_2 was eliminated by catalase (Figure 4a). The effect of catalase in the biocatalytic reaction was demonstrated to be 2-fold, first providing protection against activity loss by removing H_2O_2, and second through regeneration of dissolved oxygen to continue alcohol oxidation.

Analytical Scale Biocatalytic Reaction. As a first step toward translating the above parameters to a production setting, the effect on conversion rate of several of these variables was examined in analytical scale biocatalytic reaction with purified enzyme. Oxidation of benzyl alcohol to benzaldehyde was monitored over time in small-scale reactions with, and without, HRP present to activate GOase, as well as with, and without, catalase present to remove H_2O_2 and regenerate oxygen (Figure 4b). Excluding HRP resulted in a significant loss in initial conversion rate (11% of 25 mM benzyl alcohol at 30 min point) compared to the optimized reaction with both HRP and catalase present (48% conversion at 30 min). In the absence of catalase, GOase lost all activity within 30 min, and only minimal (≈2%) conversion was observed in the samples that contained neither HRP nor catalase. Under optimized conditions (with HRP and with catalase), 95% conversion to benzaldehyde was achieved after 2 h. The conversions over time for each set of experiments verified the

DOI: 10.1021/acs.oprd.5b00278
Org. Process Res. Dev. 2015, 19, 1580−1589

results observed in the initial rate experiments, proving that GOase activation and inactivation processes are extremely important considerations for continued productive oxidation of alcohols by this biocatalyst.

Although the above experiment conclusively shows that H_2O_2 has an effect on GOase activity, it does not clearly indicate if the effect is due to GOase inhibition or deactivation. To distinguish between these two potential modes of action, samples were prepared initially without catalase so that H_2O_2 could accumulate, then catalase was added after 1.5 h of reaction to remove the detrimental compound. If H_2O_2 acts to inhibit GOase, removal by catalase would have been expected to recover benzaldehyde production. Instead, we found that no activity returned after removal, confirming that H_2O_2 directly deactivates GOase.

Cell-Free Extract. *CFE Characterization.* The activity of cell free extract was found to be 3.8 U/mg under standard assay conditions, corresponding to 4.9% of the activity obtained when using purified GOase (77.5 U/mg). This correlates well with a protein yield of 4−5% by weight from STREP-tag purification and estimations of protein content from bicinchoninic acid assay (BCA) quantification of total protein (0.45 mg/mg CFE) and SDS gel band density (data not shown). The CFE did not contain peroxidase activity when measured using ABTS and H_2O_2. However, the CFE showed some catalase activity in a simple qualitative measurement through observing bubble formation upon H_2O_2 addition. The CFE was lyophilized from NaPi buffer, pH 7.4, at a concentration corresponding to 0.17 mM at 100 mg CFE/L.

Requirements for Copper and Single-Electron Oxidants. GOase in CFE formulation was loaded with copper by adding $CuSO_4$ directly to the reaction mixture. Figure 5 shows the

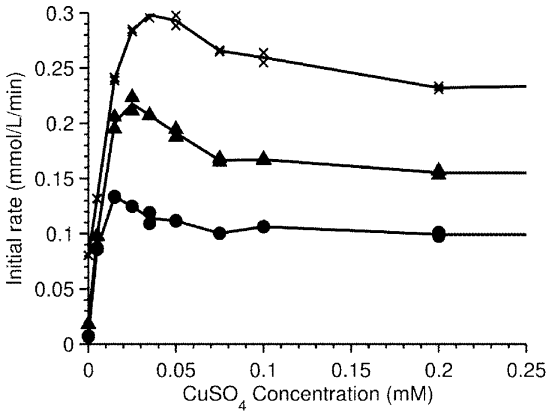

Figure 5. Effect of copper sulfate on reaction rate in 4 mL vials at 100 mg/L (●), 200 mg/L (▲), and 500 mg/L (x) of CFE GOase.

dependence of the initial rate of reaction on the amount of added $CuSO_4$. Initially the reaction rate increased almost linearly with the concentration of Cu^{2+} until an apparent optimum was reached at 15 μM (for 100 mg CFE/L), after which the initial rate dropped to reach a constant plateau at approximately 80% of the maximum rate. One would expect the profile to follow the normal binding curve, due to the equilibrium between copper in the active site and copper in solution. The observed results may be caused by interactions between other constituents of the system, such as inhibition of HRP by Cu^{2+}, which has been previously reported in the scientific literature.[34]

The apparent optimum Cu^{2+} concentration increased with increasing concentration of CFE and was found to be 15, 25, and 35 μM for 100, 200, and 500 mg CFE/L, respectively. The low concentration of GOase (≈0.35 μM enzyme at 500 mg CFE/L) will not significantly reduce the concentration of Cu^{2+} in solution by binding in the active site and hence not the concentration at which the enzyme is fully loaded. Sequestering of Cu^{2+} by cell debris and other proteins in the CFE is therefore a more likely explanation for the increase in the optimal $CuSO_4$ concentration with increasing concentration of CFE. An additional note is that the initial rates do not scale with enzyme concentration. This is likely due to the high K_m for oxygen (>3 mM)[27] relative to the solubility of oxygen (0.268 mM, air at 1 atm, 25 °C),[35] implying that even a small change in oxygen concentration will have a large effect on the reaction rate. Conversely, an increase in enzyme concentration will therefore not result in a proportional increase in reaction rate, due to oxygen transfer limitations resulting in a lower concentration of oxygen in the vial.

As shown previously, single-electron oxidants such as HRP are crucial for ensuring a fully activated GOase. Inorganic oxidants such as potassium ferricyanide are an alternative to protein-based oxidants. HRP reactivates the enzyme presumably by utilizing the hydrogen peroxide formed in the oxidation reaction and is therefore only required in catalytic amounts. On the other hand, potassium ferricyanide is required in stoichiometric amounts, and a minimum concentration is necessary to reach the redox potential required to ensure that all the GOase is fully activated. Figure 6 shows the effect of different amounts of horseradish peroxidase (HRP) or potassium ferricyanide at different CFE concentrations. By adding only small amounts of HRP, the initial rate increased several fold, until an apparent optimum was reached at a HRP concentration of 40 U/L, independent of the GOase concentration. Surprisingly, the smooth increase in activity seen when using purified GOase (Figure 3b) was not observed when CFE was applied. Additionally, the CFE requires much less HRP than the purified enzyme to reach full activation (40 U/L vs 291 U/L). This suggests that the optimum is caused by interactions between HRP and components present in the CFE and that these interactions enhance the ability of HRP to activate GOase; however, this process remains unclear. In the case of potassium ferricyanide, the activity of GOase increased with increasing ferricyanide concentration until the enzyme was fully activated in the presence of 10 mM ferricyanide. The fully activated enzyme using potassium ferricyanide displayed an initial rate of 0.17 mmol/L/min (100 mg CFE/L), which is identical to the rate observed when using the optimum HRP concentration. This indicates that the optimal value seen when using HRP for activation does in fact correspond to a fully active enzyme.

If CFE is subjected to the same HRP titration assay used to measure the activity of purified protein, no dependence on HRP concentration can be observed; that is, the enzyme appears fully activated without addition of HRP. However, after incubating CFE with $CuSO_4$ for 15 min before initiating the reaction, the initial activation effect disappears, and the reaction rate drops to zero in the absence of HRP. This is also seen in the longer assays used for CFE characterization, where linear initial rates (5−15 min) are not seen for HRP or ferricyanide concentrations below 10 U/L and 0.02 mM, respectively. These results confirm that the tyrosyl-radical is formed immediately upon copper loading to successfully generate the active

DOI: 10.1021/acs.oprd.5b00278
Org. Process Res. Dev. 2015, 19, 1580−1589

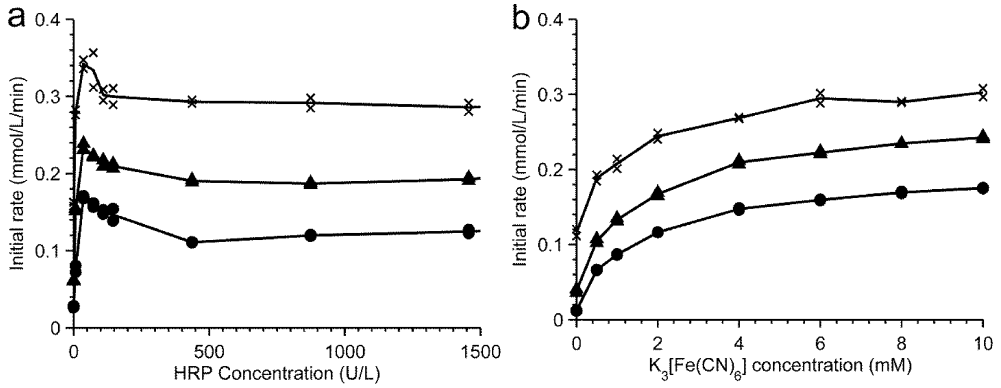

Figure 6. Effect of single-electron oxidation on the activity of GOase. (a) Effect of horseradish peroxidase (HRP) at a GOase concentration of 100 mg/L (●), 200 mg/L (▲), and 500 mg/L (x). (b) Effect of potassium ferricyanide ($K_3[Fe(CN)_6]$) at a GOase concentration of 100 mg/L (●), 200 mg/L (▲), and 500 mg/L (x).

enzyme,[24] and since this happens just prior to reaction, there is no time for the radical to decay as in the case for the copper loaded purified enzyme. However, the radical is not indefinitely stable even under conditions where substrate is available to oxidize, so the presence of an oxidant is still required to reactivate GOase to maintain activity for the full duration of the biocatalytic reaction.

Buffer System. Influence of ions and ionic strength on enzyme activity and stability is a well-established phenomenon.[36] Different salts affect the enzyme stability and activity through the interaction with charged groups on the protein and the essential water molecules surrounding the protein molecule.[37] The interaction between ions and GOase has primarily been limited to studies investigating the inhibitory effect of ions that bind to the active site, such as cyanide and azide.[18,38] In general, few observations regarding the effect of ionic strength, buffer concentration, or buffer type have been published, most likely because most ions do not affect the enzyme function of wild-type GOase. Interestingly, Saysell and co-workers[39] studied the interaction between a Trp290His GOase mutant with six different buffers. Here it was shown that buffers containing free OH groups (such as phosphate) interact with the inactive semireduced form of the Trp290His mutant, whereas no interaction was seen for the wild-type. The interaction can be ascribed to a shielding effect of the active site by Trp290, which is significantly reduced when the tryptophan is exchanged for histidine, thereby leaving the active site accessible to solvents that can interact with the copper center.[39] Despite identifying the interaction, the positive or negative effects on enzyme activity of these interacting buffers was not investigated. In an analogous way to the histidine mutant, the Trp290Phe mutation in GOase M_{3-5} may be expected to show a similar effect from buffer interactions. However, analysis of crystal structures suggest that the shielding of the active site is just as effective for the Trp290Phe mutant as for the wild type.[40] Despite this, a significant impact of the buffer identity and concentration on the activity of M_{3-5} GOase was identified in the present study (Figure 7). Ionic strength appears to be crucial for the activity of GOase, and for all investigated buffer types, the activity initially increased with increasing buffer strength. For diglycine (GlyGly)/NaOH buffer, 3-(*N*-morpholino)propanesulfonic acid (MOPS)/NaOH, and NaPi, a stable plateau was reached, whereas the activity when using *N*-ethylmorpholine (NEM)/HCl decreased at higher buffer concentrations. Interestingly, the activity in

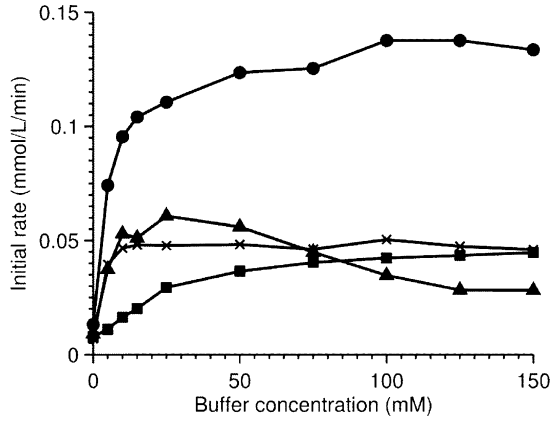

Figure 7. Effect of buffer type on initial activity of GOase at pH 7.4. Sodium phosphate (●), diglycine (GlyGly) + NaOH (x), 3-(*N*-morpholino)propanesulfonic acid (MOPS) + NaOH (□), *N*-ethylmorpholine (NEM) + HCl (▲).

NaPi increased much more than in other buffer systems, and the reason for this could be the free OH group of phosphate interacting with copper in the active site as suggested by Saysell and co-workers for the Trp290His mutant. Attempts to reach the same activation effect seen by NaPi using other inorganic salts (such as NaCl) only had a limited effect (data not shown). A buffer system using the conjugated NEM acid/base pair and using MOPS to adjust the ratio follows the same behavior as the NEM/HCl system (data not shown), which suggest that it is primarily NEM and not chloride ions that inhibits GOase. The reason for the decrease in activity could be complexation between amines and Cu^{2+}; however, according to the scientific literature, tertiary amines with substituents consisting of two or more carbon atoms are too sterically hindered to chelate.[41]

Enzyme Kinetics and Stability. The catalytic mechanism of GOase can be described by the ping-pong bi bi mechanism, where the alcohol substrate is oxidized in one catalytic half-reaction followed by reoxidation of the enzyme by reduction of oxygen to hydrogen peroxide in a second half-reaction (Figure 2).[42−45] There are only a few studies in the literature that report all kinetic constants for galactose oxidase—these being k_{cat}, $K_{m,Sub}$, and K_{mO}. In studies where only the alcohol substrate is varied, the reported k_{cat} and K_m values will only be apparent values, making it difficult to compare results obtained in different studies since the oxygen concentration is not necessarily identical. Kwiatkowski an co-workers[27] investigated

DOI: 10.1021/acs.oprd.5b00278
Org. Process Res. Dev. 2015, 19, 1580−1589

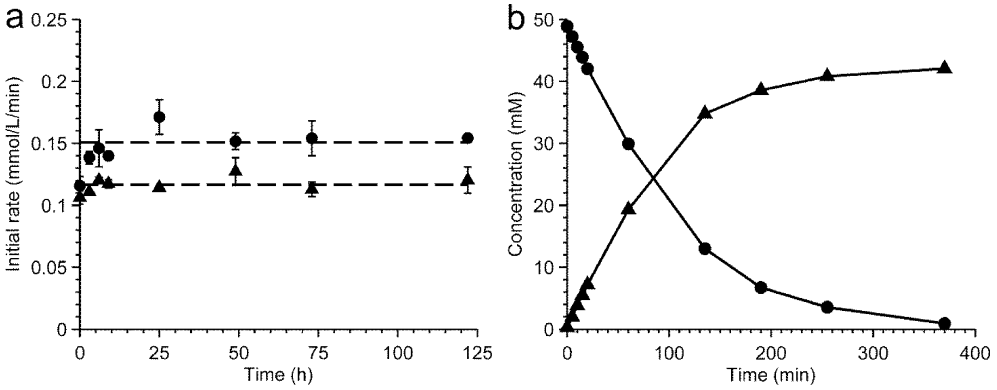

Figure 8. (a) Stability of GOase in 50 mM NaPi pH 7.4 exposed to stirring (250 rpm, two Rushton turbines) with aeration (air; 0.5 vvm) at 25 °C (●) and stirring without aeration at 25 °C (▲). (--) The average value in the interval 3−122 h. (b) Bioconversion of 50 mM benzyl alcohol (●) to benzaldehyde (▲) in a sparged bioreactor (250 rpm stirring, aeration using air at 1 vvm) using 500 mg CFE/L, 800 U HRP/L, 50 μM $CuSO_4$, and 100 mM NaPi pH 7.4.

the oxidation of galactose at 20 °C and reported a k_{cat} of 1180 s^{-1}, a K_m for galactose of 175 mM and a K_{mO} of 3 mM, the last value reported as uncertain because full saturation of the enzyme could not be achieved under the experimental conditions. Furthermore, the values are derived on the basis of the ordered bi bi mechanism, an assumption that later has been refuted.[43,44] A more precise measurement of K_{mO} was achieved by Humphreys and co-workers[45] by performing the reaction at 10 °C, hereby decreasing the reaction rate and the concentration of oxygen at which enzyme saturation was observed. At this temperature, the K_{mO} was determined to be 0.44 mM, whereas the k_{cat} and K_m for 1-*o*-methyl-α-D-galactopyranoside was 1165 s^{-1} and 144 mM, respectively. For the oxidation of benzyl alcohol using GOase M_{3-5} cell lysate, our initial investigation suggests a K_{mO} > 5 mM, a K_m for benzyl alcohol of ≈150 mM and a k_{cat} of ≈50 U/mg CFE.

The stability of GOase has not attracted much attention in the scientific literature, even though it is of great importance for the implementation of GOase in industrial processes. Sun and co-workers[20] describe a GOase mutant that shows increased thermostability and long-term stability over the wild-type. The mutant retained 80% of the initial activity after 8 days of storage at room temperature in the presence of catalase and $CuSO_4$, as opposed to the wild-type that lost 50% after 8 days under identical conditions. Figure 8a shows the stability of GOase M_{3-5} CFE during 5 days of stirring at 25 °C in 50 mM NaPi, pH 7.4. The stability of GOase was investigated both with and without bubbling with air, because gas−liquid interfaces previously have been shown to deactivate certain enzymes.[31,32,46] GOase did not lose activity during the period investigated, even when exposed to aeration rate of 0.5 vvm (volume/volume/min), a typical value employed at industrial scale. In fact, the bubbling apparently activated GOase during the first 6−9 h, after which a stable plateau was reached with an apparent activity that was 30% higher than the activity of the enzyme not exposed to bubbling. The oxygen concentration was approximately the same in the two systems, and the evaporation of water was negligible (<2%/day). The increased activity can therefore not be explained by a higher initial oxygen concentration in the assay or increased enzyme concentration due to evaporation of solvent.

Figure 8b shows a typical biocatalytic oxidation of 50 mM benzyl alcohol in a sparged bioreactor using a GOase concentration of 500 mg CFE/L. Full conversion was reached after 6 h of reaction. Due to sparging with air, the produced benzaldehyde was stripped into the gas phase and lost with the off-gas, despite the condenser attached to the bioreactor. This explains why only a concentration of 42 mM benzaldehyde was measured despite the fact that almost all of the 50 mM benzyl alcohol was converted.

Process Implications. *Requirements for Additives.* As shown in the previous sections, oxidation of alcohols using GOase requires not only the enzyme itself but also several additives to enable efficient use of the enzyme. The requirement for copper in the active site of GOase is inevitable. Copper can either be loaded prior to the reaction by applying dialysis, or copper salts can be added directly to the reaction mixture. Direct addition of copper to the reaction mixture has been shown to effectively load copper into the active site (Figure 5) and is therefore preferred in order to avoid the additional cost and processing effort involved in applying dialysis at large scale.

A single-electron oxidant required to restore the radical in the active site is also critical to obtain a fully active enzyme, because without an oxidant, the enzyme loses its activity within 15 min of reaction when GOase is applied in the form of CFE. Both inorganic oxidants and proteins capable of single-electron oxidation can be used as demonstrated in Figure 3a and Figure 6 for ferricyanide and HRP. A minimum of 40 U/L of HRP is required to fully activate GOase independent of the concentration of GOase when added as a CFE. At a GOase concentration of 500 mg CFE/L, this corresponds to a molecular ratio between the two enzymes of 59:1 (GOase:HRP), assuming a Type I HRP with a specific activity of 146 U/mg and that the formulation from Sigma-Aldrich contains only protein. However, for purified protein, approximately 300 U/L of HRP was needed to reach full activity, which corresponds to an enzyme ratio of 8:1 when transferring the result directly to a system with an enzyme concentration of 500 mg CFE/L. The difference between purified protein and CFE might be an artifact seen due to the complexity of the system, and therefore, the safest choice is to design the reaction system based on the HRP level dictated by the purified protein experiments. In this case, the requirements to HRP will be a significant cost addition to the process, since the production cost per gram protein of HRP and GOase most likely will be comparable at industrial scale. However, if a ratio of only 59:1 is required to ensure a fully active enzyme for an entire

DOI: 10.1021/acs.oprd.5b00278
Org. Process Res. Dev. 2015, 19, 1580−1589

Biocatalytic reaction, the cost contribution from HRP will be almost negligible. The ratio of GOase to HRP will of course depend on the specific activity of HRP and will increase with increasing concentration of GOase, but a high enzyme concentration implies high oxygen consumption that eventually will become a bottleneck.

The alternative to HRP is an inorganic oxidant such as ferricyanide. Ferricyanides and the reduced form, ferrocyanide, are widely applied in the production of pigments, in wine refining, as anticaking agent, and historically as a bleaching agent in photography.[47] These large scale applications imply a relatively low cost for potassium ferricyanide, combining this with the limited concentration needed to obtain a fully activated enzyme (10 mM corresponding to 3.3 g/L of potassium ferricyanide) means that ferricyanide activation most likely will be significantly cheaper than HRP activation (especially if a GOase-HRP ratio of 8:1 is required), assuming that the activation is persistent throughout the biotransformation. Ferricyanides are also applied in organic chemistry for many oxidation reactions, such as oxidation of tertiary amines,[48] oxidative coupling of phenols,[49] and oxidative hydroxylation of pyridinium salts.[50] The reactions typically require strongly alkaline pH, however most reactions also proceed at a pH close to neutral but at a much lower rate.[48] GOase substrates of industrial relevance could potentially be larger molecules with several labile functional groups, where the increased specificity compared to chemical alternatives will be the main driver for the implementation of an enzymatic process. A potential problem might therefore be byproduct formation via reactions between ferricyanide and functional groups present in the molecule, such as substituted aromatics rings. The extent of byproduct formation via ferricyanide reactions will be highly dependent on the functional groups present in the substrate molecule, and potential byproduct formation will have to be evaluated on a case-by-case basis. In the case of benzyl alcohol oxidation, no byproduct formation due to side-reactions with ferricyanide was observed.

Interestingly, we discovered that the GOase activity depends heavily not only on the ionic strength of the reaction mixture but also on the type of buffer applied. A sodium phosphate buffer turned out to result in significantly higher reaction rates than any other buffer or salt investigated. This discovery is very important to keep in mind when designing a process, because too low a buffer concentration will result in significant activity reduction. Furthermore, the cost contribution from the buffer requirements will be significant, unless an efficient recycling of the reaction medium can be established.

Oxygen Requirements. Oxidases require oxygen, which in biotechnology traditionally is supplied by bubbling air through the reactor. The transfer of oxygen from the gas phase to the liquid phase is notoriously slow due to the low solubility of oxygen in water under normal operating conditions (0.268 mM, 25 °C, 1 atm air) and hence a low driving force for mass transfer. The supply of oxygen to the reactor therefore sets an upper limit to the reaction rates that can be obtained. The maximum oxygen transfer rate in an industrial scale bioreactor is typically around 100 mmol/L/h (corresponding to a volumetric mass transfer coefficient, k_La, of approximately 500 h^{-1}) when the concentration of oxygen in solution is close to zero (i.e., maximum driving force) and air is applied for aeration.[51] Stoichiometric amounts of oxygen are required in a GOase catalyzed oxidation. However, by recycling oxygen via catalase mediated degradation of the hydrogen peroxide byproduct the requirements for oxygen can be halved. The typical industrial scale oxygen transfer rate therefore limits the maximum volumetric productivity to 200 mmol/L/h, corresponding to 21 g/L/h in the case of benzaldehyde, a value which is in range with typical requirements for industrial implementation.[52] However, since oxygen is a substrate for the enzyme the reaction rate depends on the concentration of oxygen in solution. The Michaelis−Menten constant for oxygen, K_{mO}, is ≈5 mM for GOase, which is significantly above the solubility of oxygen at normal operating conditions. This means that the reaction rate will be almost directly proportional to the dissolved oxygen concentration, when operating at, or close to, atmospheric pressure and assuming saturation of the enzyme with the alcohol substrate. This reveals a trade-off between an efficient use of the enzyme, that is, the biocatalyst yield (g product/g enzyme), and a sufficient oxygen transfer rate to sustain the desired volumetric productivity (g product/L/h). At low oxygen concentrations relative to saturation, the oxygen transfer rate will be high, whereas the specific reaction rate will be low, and vice versa, at an oxygen concentration close to saturation. This is exemplified in Figure 9, where the rate of oxygen transfer to the reactor and oxygen consumption by an enzymatic reaction is depicted as a function of the concentration of oxygen in solution. The figure shows the oxygen consumptions for two different values of K_{mO}, and the oxygen transfer rate when bubbling with air or pure oxygen at two different volumetric mass transfer coefficients. The operating points for the given examples will be the intersection of the lines. For GOase with a K_{mO} of 5 mM the operating point, when using air and a typical industrial scale k_La value of 500 h^{-1}, will be at an oxygen concentration of 0.21 mM (79% air saturation), corresponding to an oxygen consumption rate of 30 mmol/L/h and therefore a volumetric productivity of 60 mmol/L/h (or 6.4 g/L/h in the case of benzaldehyde). At this operating point, the enzyme functions at a rate corresponding to only 7% of V_{max} at the applied benzyl alcohol concentration. Hence, the enzyme is severely oxygen

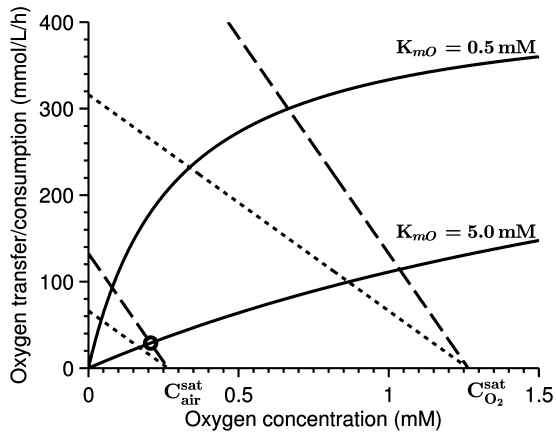

Figure 9. Rate of oxygen transfer to the reactor using air (C^{sat}_{air} = 0.265 mM) or pure oxygen (C^{sat}_{air} = 1.27 mM) at two different volumetric mass transfer coefficients (--) k_La = 250 h^{-1} (− −) k_La = 500 h^{-1}, and the enzymatic rate of oxygen consumption at two different K_{mO} as a function of oxygen concentration. The plot is based on a K_m for benzyl alcohol of 150 mM, a k_{cat} of 50 U/mg CFE, an enzyme concentration of 500 mg CFE/L and a substrate concentration of 200 mM. The operating points of the given examples will be the intersections between the lines, such as the point illustrated by a circle.

DOI: 10.1021/acs.oprd.5b00278
Org. Process Res. Dev. 2015, 19, 1580−1589

limited, or in other words, the efficiency is significantly lower than that which could have been at a higher oxygen concentration. The effect will be most severe in the beginning of the reaction, because the apparent K_{mO} will decrease as the reaction progresses and the substrate concentration approach zero.

The above analysis illustrates the importance of K_{mO} to the performance of oxygen dependent enzymes at industrial scale, a fact that is often overlooked when developing new biocatalysts. The key objective from a process engineering point of view is therefore not only to supply enough oxygen to sustain a desired productivity but also to supply it at the right oxygen concentration, which for many oxidases is the highest concentration possible due to the relatively high K_{mO}. The optimal oxygen level will depend on the cost of the biocatalyst relative to the operating and capital costs of the process.

The oxygen transfer rate can be increased by applying enriched air (i.e., air with higher oxygen content and/or increased reactor pressure), thereby increasing the driving force for oxygen transfer by increasing the oxygen saturation concentration. The incentive to implement solutions to increase oxygen transfer is 2-fold, because both higher oxygen transfer rate and dissolved oxygen concentration can be obtained, thereby potentially increasing both the volumetric productivity and biocatalyst yield. This benefit has to be weighed against the added cost from purifying air, increasing reactor strength and increased safety precautions when dealing with a higher oxygen partial pressure in combination with volatile organic compounds.

Biocatalyst Stability. The stability of enzymes may be significantly reduced when exposed to gas−liquid interfaces, due to the tendency of protein to unfold when in contact with the hydrophobic air.[30−32] Thus, supply of oxygen by bubbling with air can pose a problem for oxidase catalyzed reactions. However, in the case of GOase, deactivation at the gas−liquid interface is not an issue (Figure 8), and in fact, the enzyme appears to be activated during the first 9 h of bubbling. The stability trials were designed to mimic the reaction conditions, but since they were conducted in the absence of substrate, the observed stability may be different from the actual stability during catalysis (i.e., the operational stability). The importance of determining the stability during catalysis can also be seen from the experiment with different levels of hydrogen peroxide (Figure 4a), where it is shown that GOase is not deactivated by H_2O_2 in the absence of catalytic action. However, during catalysis, GOase is deactivated within minutes in the presence of small amounts of H_2O_2. This indicates that it is the reduced form of the enzyme that is susceptible to deactivation by H_2O_2 and not the oxidized form predominantly present in the absence of an alcohol substrate. Similarly, other deactivation mechanisms such as oxidation of amino acid side-chains in the active site by dissolved oxygen may only take place at certain stages of the catalytic cycle.

CONCLUSIONS

Benzyl alcohol oxidation catalyzed by galactose oxidase (GOase) was used as a model system for the investigation of reaction additive requirements to obtain an efficient biotransformation:

- Catalase was necessary to keep the concentration of hydrogen peroxide, formed as a byproduct, at a minimum in order to avoid enzyme deactivation. Interestingly, GOase was completely stable in the presence of H_2O_2 up to 10 mM, when not actively catalyzing an oxidation.
- Addition of a single-electron oxidant such as horseradish peroxidase (HRP) or potassium ferricyanide was required to regenerate the active site radical upon decay. 40 U/L of HRP was required to fully activate GOase added as cell-free extract (CFE), whereas approximately 300 U/L was needed to fully activate purified GOase. Potassium ferricyanide was also capable of activating GOase, and in this case, 10 mM was required for full activation.
- Copper, required in the active site, was loaded into the enzyme by adding $CuSO_4$ to the reaction mixture containing crude GOase. The optimal concentration was found to be 15, 25, and 35 μM of $CuSO_4$ for 100, 200, and 500 mg CFE/L, respectively.
- Buffer type and concentration was found to be essential for GOase activity, minimum 100 mM of preferably sodium phosphate buffer pH 7−8 resulted in the highest activity.

The process aspects of GOase-catalyzed oxidation reactions were discussed in light of the determined requirements for additives, the stability of GOase, and the trade-off between sufficient oxygen transfer and full utilization of the enzyme due to the high K_m for oxygen relative to the solubility of oxygen at normal process conditions. The resulting reaction parameters are critical for implementation of GOase in an industrial scale biocatalytic oxidation process.

EXPERIMENTAL SECTION

Materials. All reagents used were of the highest grade available from Sigma-Aldrich (St. Louis, Missouri, U.S.A.). Catalase with an activity of 3172 U/mg (one unit (U) corresponds to the amount of enzyme which decomposes 1 μmol H_2O_2 per min at pH 7.0 and 25 °C) and horseradish peroxidase (HRP) with an activity of 145.7 U/mg (Type I) or 261 U/mg (Type IV) (1 U corresponds to the amount of enzyme that forms 1 mg purpurogallin from pyrogalin in 20 s. at pH 6.0 and 20 °C) was acquired from Sigma-Aldrich. Galactose oxidase mutant M_{3-5} from *Fusarium* NRLL 2903[17] as a cell-free extract (CFE), $NADP^+$, and aldehyde dehydrogenase (ALDH(003)) were acquired from Prozomix (Haltwhistle, U.K.). GOase M_{3-5} was purified as previously described.[14] Solutions were made using deionized water and fresh enzyme solutions were made every day.

Purified Enzyme. *Liquid-Phase Determination of pH Optimum.* The pH optimum for purified GOase M_{3-5} was determined in a liquid phase HRP/ABTS coupled assay at 420 nm as previously described.[17,22] Activity was measured on a 96-well plate in triplicate at 30 °C with 10 μL GOase M_{3-5} dilution in 90 μL reaction mix (containing 0.23 mg/mL HRP and 0.4 mg/mL ABTS in 100 mM sodium phosphate buffer (NaPi) at the indicated pH levels) and initiated by addition of 100 μL 50 mM benzyl alcohol in water. Initial rates were normalized by protein concentration to calculate specific activities for each assay condition. 1U corresponds to the amount of enzyme which converts 1 μmol of substrate per min at pH 7.4 and 30 °C.

Activation of GOase M_{3-5} by HRP. Purified GOase M_{3-5} specific activity for benzyl alcohol was measured in a cuvette at 340 nm by following the production of NADPH from subsequent oxidation of benzaldehyde to benzoic acid by

DOI: 10.1021/acs.oprd.5b00278
Org. Process Res. Dev. 2015, 19, 1580−1589

aldehyde dehydrogenase (ALDH(003), Prozomix). The 1 mL reaction contained 2.5 mg/mL $NADP^+$, 25 mM benzyl alcohol, 0.5 mg/mL ALDH(003), 0.0078 mg/mL GOase M_{3-5}, and between 0 and 522 U/L HRP in 50 mM NaPi, pH 7.4. The reaction was initiated by addition of GOase (10 μL of 0.78 mg/mL stock) before measuring at 340 nm. Reactions were performed in duplicate.

Deactivation of GOase M_{3-5} by H_2O_2 and Protection by Catalase. The effect of H_2O_2 on the specific activity of purified GOase M_{3-5} for benzyl alcohol oxidation was measured similar to the activation by HRP. GOase was incubated at room temperature in 50 mM NaPi, pH 7.4 in the presence of H_2O_2 for 10 min in a cuvette. H_2O_2 was either degraded prior to assay by addition of catalase or allowed to remain in the sample during the assay. In a third sample series, catalase was added to remove H_2O_2, and then additional H_2O_2 was added to bring the final assay concentration to 10 mM H_2O_2. This experiment was performed to equally oxygenate the reaction mix prior to the assay. The remaining reaction components were added to give a 1 mL reaction containing 2.5 mg/mL $NADP^+$, 25 mM benzyl alcohol, 0.5 mg/mL ALDH(003), 0.0039 mg/mL GOase M_{3-5}, 522 U/L HRP (Type IV), 0 or 220 U/mL catalase, and 0−10 mM H_2O_2. The reaction was initiated by addition of benzyl alcohol before measuring at 340 nm. Reactions were performed in duplicate.

Biocatalytic Reactions Comparing GOase Deactivation versus Inhibition by H_2O_2. The effect of H_2O_2 on GOase conversion of benzyl alcohol was measured over time. Duplicate reactions were performed in 50 mM NaPi, pH 7.4 with 0.01 mg/mL purified GOase M_{3-5}, 25 mM benzyl alcohol, 10% dimethyl sulfoxide, with or without 330 U/L HRP (Type IV), and with or without 440 U/mL catalase. After 1.5 h, catalase (to 440 U/mL) was added to two samples that contained no catalase initially. Aliquots of 25 μL were removed from each sample in 30 min intervals and extracted into 500 μL dichloromethane by vortexing. The samples were centrifuged, and the organic layer was dried over magnesium sulfate. Filtered samples were analyzed on an Agilent (Santa Clara, California, U.S.A.) 6850 gas chromatograph system equipped with an FID. Analytes were separated on an HP-1MS column (Agilent) using a temperature gradient held initially at 50 °C for 4 min, and then ramped up by 25 °C/min to 225 °C. The retention times for benzyl alcohol and benzaldehyde were 7.46 and 6.67 min, respectively.

Cell-Free Extract. *Characterization.* GOase content in the cell-free extract powder was approximated in several experiments. Protein content in the CFE powder was determined using the Pierce BCA Protein Assay Kit (Life Technologies) following the manufacturer's protocol. Band density corresponding to GOase M_{3-5} on SDS-PAGE was estimated to be 10% of the soluble protein fraction. Purification of GOase M_{3-5} from 5 g of CFE using previously published methods[14] yielded 200 mg of isolated enzyme. Specific activity of the cell-free extract was measured in the liquid-phase HRP/ABTS assay described above, and it was normalized to the concentration of CFE powder. Peroxidase activity in the CFE was also tested with this assay by addition of 1, 2.5, or 5 mM H_2O_2 and ABTS to the lysate solution (0.25 mg/mL final); however, no activity was observed. The presence of catalase activity was confirmed in the CFE by the appearance of bubbles after addition of H_2O_2 (5 mM final) to a solution of 0.05 mg/mL CFE.

Investigation of Reaction Conditions. Experiments with systematic variation in the concentration of copper sulfate, horseradish peroxidase, potassium ferricyanide, and buffers were carried out in 4 mL vials that were heated to 25 °C and mixing at 800 min^{-1} in a HLC BioTech thermoshaker (Bovenden, Germany). The standard reaction conditions were 50 mM NaPi buffer at pH 7.4, 0.05 mM $CuSO_4$, 875 U/L HRP, 20000 U/L catalase, 100 mg/L CFE GOase, and 25 mM benzyl alcohol, unless otherwise stated. The working volume was 3 mL in all experiments, thereby leaving 1 mL of headspace to enable oxygen transfer to the liquid phase. Samples were taken after 5, 10, and 15 min of reaction by removing the cap, thereby allowing air to enter the headspace and hence avoiding complete oxygen depletion. The experiments were performed in duplicate.

Biocatalytic Reaction in an Aerated Reactor. A complete biooxidation reaction was conducted in a 250 mL reactor (MiniBio with my-Control) from Applikon Biotechnology (Delft, Netherlands). The reactor was equipped with a sintered metal sparger to ensure efficient oxygen supply and two Rushton turbines for mixing. The reaction conditions were as follows: 100 mM NaPi buffer at pH 7.4, 50 mM benzyl alcohol, 800 U/L HRP, 50 μM $CuSO_4$, 20000 U/L catalase, 500 mg/L CFE GOase, 25 °C, 250 min^{-1} stirring, and 1 vvm air sparging. At regular time intervals samples were withdrawn for analysis.

Stability Experiments. Stability experiments were carried out in the 250 mL reactors described above with a working volume of 150 mL. CFE (300 mg/L) was solubilized in 50 mM NaPi buffer at pH 7.4 and stirred at 250 rpm with or without aeration, 0.5 vvm air. Samples were withdrawn from the reactor at regular time intervals, and the residual activity was determined in 4 mL vials as described above. The residual activity was determined as the average of three assays.

Analysis. The reaction was stopped by addition of 800 μL 1 M HCl to a 200 μL reaction aliquot. Samples were analyzed on a Thermo Fisher Scientific (Waltham, Massachusetts, U.S.A.) Dionex Ultimate 3000 HPLC equipped with a Diode Array Detector. Analytes were separated at 30 °C on a Phenomex (Torrance, California, U.S.A.) Kinetex C18 column (5 μm, 100 Å, 250 × 4.6 mm) using 30% acetonitrile in water with 0.1% trifluoroacetic acid as mobile phase. Benzyl alcohol, benzaldehyde, and benzoic acid were analyzed at 254 nm, and the retention times were 2.8, 5.4 and 3.6 min, respectively.

AUTHOR INFORMATION

Corresponding Author

*E-mail: jw@kt.dtu.dk.

Notes

The authors declare no competing financial interest.

ACKNOWLEDGMENTS

The research leading to these results has received funding from the European Union's Seventh Framework Programme for research, technological development and demonstration under grant agreement no. 613849 supporting the project BIOOX.

REFERENCES

(1) Punniyamurthy, T.; Velusamy, S.; Iqbal, J. *Chem. Rev.* **2005**, *105*, 2329.

(2) Sheldon, R. A.; Arends, I. W. C. E.; Ten Brink, G.-J.; Dijksman, A. *Acc. Chem. Res.* **2002**, *35*, 774.

(3) Sheldon, R. A. *Green Chem.* **2007**, *9*, 1273.

(4) Turner, N. J. *Chem. Rev.* **2011**, *111*, 4073.

(5) Hollmann, F.; Arends, I. W. C. E.; Buehler, K.; Schallmey, A.; Bühler, B. *Green Chem.* **2011**, *13*, 226.

DOI: 10.1021/acs.oprd.5b00278
Org. Process Res. Dev. 2015, 19, 1580−1589

(6) Avigad, G.; Amaral, D.; Asensio, C.; Horecker, B. L. *J. Biol. Chem.* **1962**, *237*, 2736.
(7) Whittaker, J. W. *Arch. Biochem. Biophys.* **2005**, *433*, 227.
(8) Whittaker, J. W. *Chem. Rev.* **2003**, *103*, 2347.
(9) Pickl, M.; Fuchs, M.; Glueck, S. M.; Faber, K. *Appl. Microbiol. Biotechnol.* **2015**, *99*, 6617.
(10) Siebum, A.; van Wijk, A.; Schoevaart, R.; Kieboom, T. *J. Mol. Catal. B: Enzym.* **2006**, *41*, 141.
(11) Parikka, K.; Tenkanen, M. *Carbohydr. Res.* **2009**, *344*, 14.
(12) Yalpani, M.; Hall, L. *J. Polym. Sci., Polym. Chem. Ed.* **1982**, *20*, 3399.
(13) Schoevaart, R.; Kieboom, T. *Top. Catal.* **2004**, *27*, 3.
(14) Bechi, B.; Herter, S.; Mckenna, S.; Riley, C.; Leimkühler, S.; Turner, N. J.; Carnell, A. J. *Green Chem.* **2014**, *16*, 4524.
(15) McKenna, S.; Leimkühler, S.; Herter, S.; Turner, N. J.; Carnell, A. *Green Chem.* **2015**, *17*, 3271.
(16) Qin, Y.-Z.; Li, Y.-M.; Zong, M.-H.; Wu, H.; Li, N. *Green Chem.* **2015**, *17*, 3718.
(17) Escalettes, F.; Turner, N. J. *ChemBioChem* **2008**, *9*, 857.
(18) Mendonça, M. H.; Zancan, G. T. *Arch. Biochem. Biophys.* **1987**, *252*, 507.
(19) Deacon, S. E.; Mahmoud, K.; Spooner, R. K.; Firbank, S. J.; Knowles, P. F.; Phillips, S. E. V; McPherson, M. J. *ChemBioChem* **2004**, *5*, 972.
(20) Sun, L.; Petrounia, I. P.; Yagasaki, M.; Bandara, G.; Arnold, F. H. *Protein Eng., Des. Sel.* **2001**, *14*, 699.
(21) Sun, L.; Bulter, T.; Alcalde, M.; Petrounia, I. P.; Arnold, F. H. *ChemBioChem* **2002**, *3*, 781.
(22) Rannes, J. B.; Ioannou, A.; Willies, S. C.; Grogan, G.; Behrens, C.; Flitsch, S. L.; Turner, N. J. *J. Am. Chem. Soc.* **2011**, *133*, 8436.
(23) Whittaker, M. M.; Whittaker, J. W. *J. Biol. Chem.* **2003**, *278*, 22090.
(24) Rogers, M. S.; Hurtado-Guerrero, R.; Firbank, S. J.; Halcrow, M. A.; Dooley, D. M.; Phillips, S. E. V; Knowles, P. F.; McPherson, M. J. *Biochemistry* **2008**, *47*, 10428.
(25) Kersten, P. J. *Proc. Natl. Acad. Sci. U. S. A.* **1990**, *87*, 2936.
(26) Kwiatkowski, L. D.; Kosman, D. J. *Biochem. Biophys. Res. Commun.* **1973**, *53*, 715.
(27) Kwiatkowski, L. D.; Adelman, M.; Pennelly, R.; Kosman, D. J. *J. Inorg. Biochem.* **1981**, *14*, 209.
(28) Hamilton, G. A.; Adolf, P. K.; De Jersey, J.; DuBois, G. C.; Dyrkacz, G. R.; Libby, R. D. *J. Am. Chem. Soc.* **1978**, *100*, 1899.
(29) Law, H. E. M.; Baldwin, C. V. F.; Chen, B. H.; Woodley, J. M. *Chem. Eng. Sci.* **2006**, *61*, 6646.
(30) Van Hecke, W.; Ludwig, R.; Dewulf, J.; Auly, M.; Messiaen, T.; Haltrich, D.; Van Langenhove, H. *Biotechnol. Bioeng.* **2009**, *102*, 122.
(31) Bommarius, A. S.; Karau, A. *Biotechnol. Prog.* **2005**, *21*, 1663.
(32) Thomas, C. R.; Geer, D. *Biotechnol. Lett.* **2011**, *33*, 443.
(33) Cleveland, L.; Coffman, R. E.; Coon, P.; Davis, L. *Biochemistry* **1975**, *14*, 1108.
(34) Guilbault, G. G.; Brignac, P., Jr; Zimmer, M. *Anal. Chem.* **1968**, *40*, 190.
(35) Wilhelm, E.; Battino, R.; Wilcock, R. J. *Chem. Rev.* **1977**, *77*, 219.
(36) Zhao, H. *J. Mol. Catal. B: Enzym.* **2005**, *37*, 16.
(37) Zhang, Y.; Cremer, P. S. *Curr. Opin. Chem. Biol.* **2006**, *10*, 658.
(38) Paukner, R.; Staudigl, P.; Choosri, W.; Haltrich, D.; Leitner, C. *Protein Expression Purif.* **2015**, *108*, 73.
(39) Saysell, C. G.; Barna, T.; Borman, C. D.; Baron, A. J.; McPherson, M. J.; Sykes, A. G. *JBIC, J. Biol. Inorg. Chem.* **1997**, *2*, 702.
(40) Rogers, M. S.; Tyler, E. M.; Akyumani, N.; Kurtis, C. R.; Spooner, R. K.; Deacon, S. E.; Tamber, S.; Firbank, S. J.; Mahmoud, K.; Knowles, P. F.; Phillips, S. E. V; McPherson, M. J.; Dooley, D. M. *Biochemistry* **2007**, *46*, 4606.
(41) Kandegedara, A.; Rorabacher, D. B. *Anal. Chem.* **1999**, *71*, 3140.
(42) Whittaker, M. M.; Whittaker, J. W. *Biochemistry* **2001**, *40*, 7140.
(43) Whittaker, M. M.; Ballou, D. P.; Whittaker, J. W. *Biochemistry* **1998**, *37*, 8426.
(44) Borman, C. D.; Saysell, C. G.; Sykes, A. G. *JBIC, J. Biol. Inorg. Chem.* **1997**, *2*, 480.
(45) Humphreys, K. J.; Mirica, L. M.; Wang, Y.; Klinman, J. P. *J. Am. Chem. Soc.* **2009**, *131*, 4657.
(46) Ganesh, K.; Joshi, J. B.; Sawant, S. B. *Biochem. Eng. J.* **2000**, *4*, 137.
(47) Gail, E.; Gos, S.; Kulzer, R.; Lorösch, J.; Rubo, A.; Sauer, M.; Kellens, R.; Reddy, J.; Steier, N.; Hasenpusch, W. In *Ullmanns Encyclopedia of Industrial chemistry*; Wiley-VCH Verlag GmbH & Co. KGaA: Weinheim, 2012; pp 673−710.
(48) Hull, L. A.; Davis, G. T.; Rosenblatt, D. H. *J. Am. Chem. Soc.* **1969**, *91*, 6247.
(49) Küenburg, B.; Czollner, L.; Fröhlich, J.; Jordis, U. *Org. Process Res. Dev.* **1999**, *3*, 425.
(50) Gnecco, D.; Marazano, C.; Enriquez, R. G.; Teran, J. L.; Del Rayo Sanchez, M.; Galindo, S. A. *Tetrahedron: Asymmetry* **1998**, *9*, 2027.
(51) Charles, M. *Trends Biotechnol.* **1985**, *3*, 134.
(52) Straathof, A.; Panke, S.; Schmid, A. *Curr. Opin. Biotechnol.* **2002**, *13*, 548.

DOI: 10.1021/acs.oprd.5b00278
Org. Process Res. Dev. 2015, 19, 1580−1589